# Light-Responsive Azobenzene-Based Architectures: From Large Macromolecular Aggregates to Small Zwitterions

## Dissertation

zur Erlangung des akademischen Grades

**doctor rerum naturalium**

**(Dr. rer. nat.)**

im Fach Chemie

eingereicht an der

Mathematisch-Naturwissenschaftlichen Fakultät der

Humboldt-Universität zu Berlin

von

**M. Sc. Christopher Knie**

geboren am [redacted] in [redacted]

Präsidentin der Humboldt-Universität zu Berlin

Prof. Dr.-Ing. Dr. Sabine Kunst

Dekan der Mathematisch-Naturwissenschaftlichen Fakultät

Prof. Dr. Elmar Kulke

---

| | |
|---|---|
| Gutachter: | 1. Prof. Stefan Hecht, Ph.D. |
| | 2. Prof. Dr. Matthias Ballauff |
| | 3. Prof. Dr. Helmut Schlaad |
| Tag der mündlichen Prüfung: | 09. April 2019 |

Die vorliegende Arbeit wurde in der Zeit von Dezember 2014 bis September 2018 am Institut für Chemie der Humboldt-Universität zu Berlin unter Anleitung von Prof. Stefan Hecht, Ph.D. angefertigt.

# Danksagung

Zuerst möchte ich mich bei Dr. David Bléger und Prof. Stefan Hecht für das Ermöglichen dieser Arbeit bedanken. Die zahlreichen Gespräche und Diskussionen, Hinweise und Denkanstöße, sowie kritischen Nachfragen und konstruktive Kritik haben mich nicht nur aus wissenschaftlicher Sicht sondern auch auf persönlicher Ebene weitergebracht.

Ich möchte außerdem dem gesamten AK Hecht für die große Hilfsbereitschaft, vielen nützlichen Tipps und Kommentare sowie auch allen Gesprächen darüber hinaus danken. Besonders hervorheben möchte ich hier meine Laborkollegin Fangli Zhao, die mich mit ihrer einzigartigen Sichtweise oft zum Staunen gebracht hat und mir damit immer eine willkommene Ablenkung vom Arbeitsalltag war. Weiterhin möchte ich Virginia Valderrey, Dennis Chung-Yang Huang, Sebastian Fredrich, Anna Grafl für die gute Zeit im Labor aber auch außerhalb der Universität danken. Ich hoffe (zumindest mit den meisten von euch) noch lange in Kontakt bleiben zu können.

Ebenso möchte ich meiner Bachelorstudentin Julia Giesinger, meinem Forschnungspraktikanten Nils Pfister und Jutta Schwarz für die synthetische Zuarbeit danken.
Darüber hinaus möchte ich den technischen Mitarbeitern des Instituts für Chemie danken, für die vielen, aufgenommenen NMR-Spektren, die Kristallstrukturanalyse sowie für die unerschöpfliche Hilfsbereitschaft im Gefahrenstofflager.

Abschließend möchte ich meiner Familie für die fortwährende Unterstützung und den beständigen Rückhalt danken, ohne den diese Arbeit nicht möglich gewesen wäre. Meine Freunde als Quelle neuer Motivation sowie eine ganz besondere Person sollen dabei nicht unerwähnt bleiben. Besonders letzterer danke ich für die Geduld und das Verständnis während der zeitintensiven Phasen und dem Ertragen meiner „Labormüdigkeit“. Danke, TD.

# Abstract

The present thesis is separated into two main sections, both employing azobenzene photoswitches to control (macro)molecular processes. As a light-responsive molecule that undergoes a large geometrical change upon *E*/*Z* photoisomerization, azobenzenes have found their way into multiples areas of life and material sciences. Advantages such as high stability, good addressability, and well-established synthesis methods are accompanied by a large variety of derivatives that offer adjustable properties through specific substitution patterns. Being one of the most popular photochromic compounds, azobenzenes provide a reliable basis for the development of new responsive systems that use light as a clean and readily accessible energy source.

The first part of this work is aimed at the amplification of the switching dimensions by incorporating azobenzene into rigid macromolecules and macromolecular aggregates. Based on the polymer architecture, the motion of the small responsive repeating units is transferred to the entire macromolecule, which ideally helps to increase the conversion of consumed energy into mechanical work. Following a small overview about the basics of photochromism and azobenzene photochemistry, general strategies to increase geometrical changes in molecular systems are presented. Furthermore, the design and synthesis as well as the characterization of a light-responsive polymer aggregate that exhibits a large geometrical change upon isomerization is described.

The second part of this work deals with the reversible formation of ions. Besides their great importance for vital functions in living organisms, adsorption characteristics as well as bactericidal properties can be regulated by ionic modifications on surfaces. Based on the model of spiropyran, the theoretical background for the preparation of an azobenzene equivalent is presented. The computational data is converted into model compounds that were investigated by means of NMR analysis. Based on these combined theoretical and experimental data, a promising target structure for a light-responsive dynamic covalent zwitterion is described.

# Kurzzusammenfassung

Beide thematischen Abschnitte der vorliegenden Arbeit beschäftigen sich mit Azobenzol-Photoschaltern zur Steuerung (makro)molekularer Prozesse. Aufgrund der ausgeprägten geometrischen Strukturänderung, die mit der lichtinduzierten *E*/*Z*-Photoisomerisierung von Azobenzolen einhergeht, hat diese Substanzklasse als Steuereinheit Einzug in mehrere Bereiche der Lebens- und Materialwissenschaften gehalten. Vorteile wie die hohe Stabilität, gute Ansprechbarkeit und etablierte Synthesemethoden werden von einer großen Vielfalt an Derivaten vervollständigt, die durch spezifische Substitutionsmuster zielgerichtet in ihren Eigenschaften angepasst werden können. Als eines der populärsten photochromen Systeme bieten Azobenzole eine zuverlässige Grundlage für die Entwicklung neuer molekularer Maschinen, die durch Licht als saubere und leicht zugängliche Energiequelle angetrieben werden können.

Der erste Teil dieser Arbeit hat die Vergrößerung der geometrischen Änderung des Schaltvorgangs zum Ziel. Dafür werden Azobenzole in starre Makromoleküle und makromolekulare Aggregate eingebaut, die der Bewegung der kleinen Wiederholungseinheiten aufgrund der gewählten Architektur folgen und somit idealerweise die Umwandlung der aufgenommenen Energie in mechanische Arbeit erhöhen. Nach einem kurzen Überblick zu den Grundlagen der Photochromie und der Azobenzol-Photochemie werden allgemeine Strategien zur Steigerung geometrischer Änderungen in molekularen Systemen vorgestellt. Des Weiteren wird das Design und die Synthese sowie die Charakterisierung eines durch Licht ansprechbaren Polymeraggregats beschrieben, das bei der Isomerisierung eine große geometrische Änderung durchläuft.

Der zweite Teil dieser Arbeit beschäftigt sich mit der reversiblen Bildung von ionischen Substanzen. Geladene Spezies sind von großer Wichtigkeit für die Aufrechterhaltung verschiedener Körperfunktionen in Lebewesen, können jedoch auch Adsorptions- und bakterizide Eigenschaften auf Oberflächen regulieren. Basierend auf dem Modell des Photoschalters Spiropyran wird der theoretische Hintergrund für die Herstellung eines entsprechenden Azobenzol-Äquivalents vorgestellt. Theoretische Daten aus DFT-Rechnungen werden in Modellverbindungen umgewandelt, die mittels NMR-Analyse untersucht werden. Auf Grundlage der theoretischen und experimentellen Daten wird eine vielversprechende Zielstruktur eines durch Licht steuerbaren dynamisch kovalenten Zwitterions vorgestellt.

# Table of Contents

Part I – Light-Responsive Cylindrical Micelles

Part II – Light-Responsive Zwitterions

Part I

# Light-Responsive Cylindrical Micelles

## Increasing Change of Size and Shape of Azobenzene Photoisomerization

# 1 Introduction

The reversible change of structures and properties as a result of external stimuli is an omnipresent event in the everyday life on our planet. Similar to the growth of a tree which is continuously adapting its shape, height, and even the color of the leaves to the direction and intensity of the sun, many processes in nature can only fulfill their purposes by undergoing repeated alterations and modifications. Over time and by trial and error, evolution created highly efficient systems that enable organisms to perceive the features of their environment in multiple ways and to react accordingly. Vital functions of plants and animals such as phototropism, perspiration, or digestion are triggered by addressable units within the cells that flexibly respond to different levels of light, temperature, or the pH value, among others, and allow adaptability as a crucial skill of every living organism. Many of these processes are based on reversible conformational changes of proteins where, for instance, even a single photon of appropriate energy can trigger a complex molecular amplification process, that is providing vision by triggering the isomerization of the photoresponsive retinal molecule in our eyes.[1]

Taking these structures as models, scientist try to copy the responsive units and their basic function from nature and transfer them into small artificial workers that can be fully controlled by the according stimulus. A broad spectrum of possible applications in the areas of life and material sciences based on switchable molecules like the retinal cofactor is conceivable. Turning to the medical field for instance, drugs benefit from a controlled release or later activation of a dormant species in specific areas of the body limiting side effects and reducing the overall amount needed for a successful treatment.[2] Similarly, novel storage devices require efficient release mechanisms for the enclosed compounds[3] or, in case of data memories, the feasibility of several deletion and writing cycles without loss of information and capacity.[4] Self-healing materials are another example for the necessity of stimuli-responsive systems providing an easy and economical way of repairing damages on surfaces like walls and finishes.[5]

However, in order to gain full control over the processes reliable stimuli are essential. Most commonly, temperature changes,[6] irradiation by light of different wavelengths,[7] pH value adjustments,[8] application of electric fields,[9] or magnetic actuation,[10] among others are exploited. In this regard, light as a clean and renewable energy source must be pointed out due to its very high spatiotemporal resolution. The easily controllable intensity and penetration depth, the possibility of remote and non-invasive application, as well as the simple way of turning on and off complete the series of advantages and are reasons why light is a favored trigger.

Therefore, photoswitchable molecules with at least two (temporary) stable and independently addressable states are perfect candidates as basis for the development of novel responsive materials. Considering the efficiency of such systems as well, a dramatic change of size and shape after exposure to light is desirable increasing the direct conversion of consumed energy into mechanical work.[11] Additionally, the differentiation and potential read-out is easier as well as a stronger overall effect is achieved due to the larger difference of the occupied states. Several photochromic molecules performing significant changes of their geometrical structure upon isomerization are known with azobenzenes as one of the most investigated and popular examples.[12] Their high stability and low fatigue, the good addressability of the *E* and *Z* configuration with high ratios of the corresponding isomer in the photostationary state, as well as the easy and reliable synthesis methods turn these photoswitches into a good basis for new light-responsive systems.

In the first part of this thesis the development of a light-responsive system is presented that is aiming to maximize the difference of size and shape between the addressable states. In this context, the principles of photochromism and some examples of photoswitches are briefly discussed. After a more detailed elaboration on the properties and characteristics of azobenzenes as the responsive moiety in this project, several ways of increasing reversible geometrical changes of molecules and literature examples of already existing systems are shown. Considerations regarding design and synthesis as well as the achieved results complete the first subject area.

# 2 Theoretical Background

## 2.1 Light-responsive Molecules and Photochromism

The first report of a photochromic molecule dates back to 1867 when Fritzsche observed the decoloration of orange tetracene in daylight and its recoloring at night. It, however, took another 83 years until the word photochromism was first applied by Hirshberg in 1950 to address a system that reversibly changes colors after irradiation with light of a specific wavelength.[13]

Today photochromism defines a reversible transformation of a chemical species between two forms, A and B, exhibiting different UV/vis spectra by absorption of electromagnetic radiation in one or both ways (Figure 1).[14]

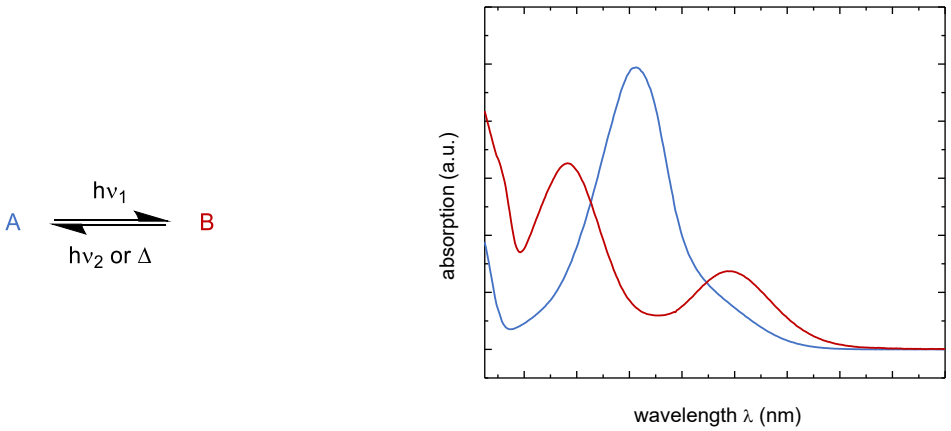


**Figure 1.** Photochromism: reversible interconversion of a single chemical species existing in two states, A and B, by irradiation with light of a specific wavelength in one or both directions exhibiting different absorption spectra (and different properties), the return to the initial state can be triggered by another stimulus like temperature.

There are several classes of photochromic systems differentiated by the stimulus employed to trigger the return to the initial state and the nature of the shift in the absorption spectra that occurs upon transformation from one state to the other, i.e. photoreversible, thermoreversible, inverse photochromic, and multiphotochromic systems.[13] In the first case the reversion from state B to A can be performed by irradiation only, while in the second case the process is thermally induced. A combination of both pathways is likewise possible, however, independent of photo- or thermoreversibility, the absorption spectrum of B is supposed to be bathochromically shifted in comparison to one of A. On the contrary, for negative (or inverse) photochromic molecules and materials a hypsochromic shift of the spectrum is observed. The last case defines a condition where more than two states are converted into each other which can be photochemically and/or thermochemically addressed.

Since the time of Fritzsche, numerous compounds were discovered that respond to irradiation with light of a specific wavelength by not only reversibly changing their absorption spectra but also properties like geometry, polarity, conjugation, refractive index, or conductance, among others. Typical reactions providing the basis for photochromic moieties are *E*/*Z* isomerizations as well as electrocyclic ring closure and opening. Selected examples of commonly applied photoswitches are depicted in Figure 2. In this context, T-type molecules exhibit thermoreversible characteristics while P-Type molecules are thermally stable in both forms (photoreversible).

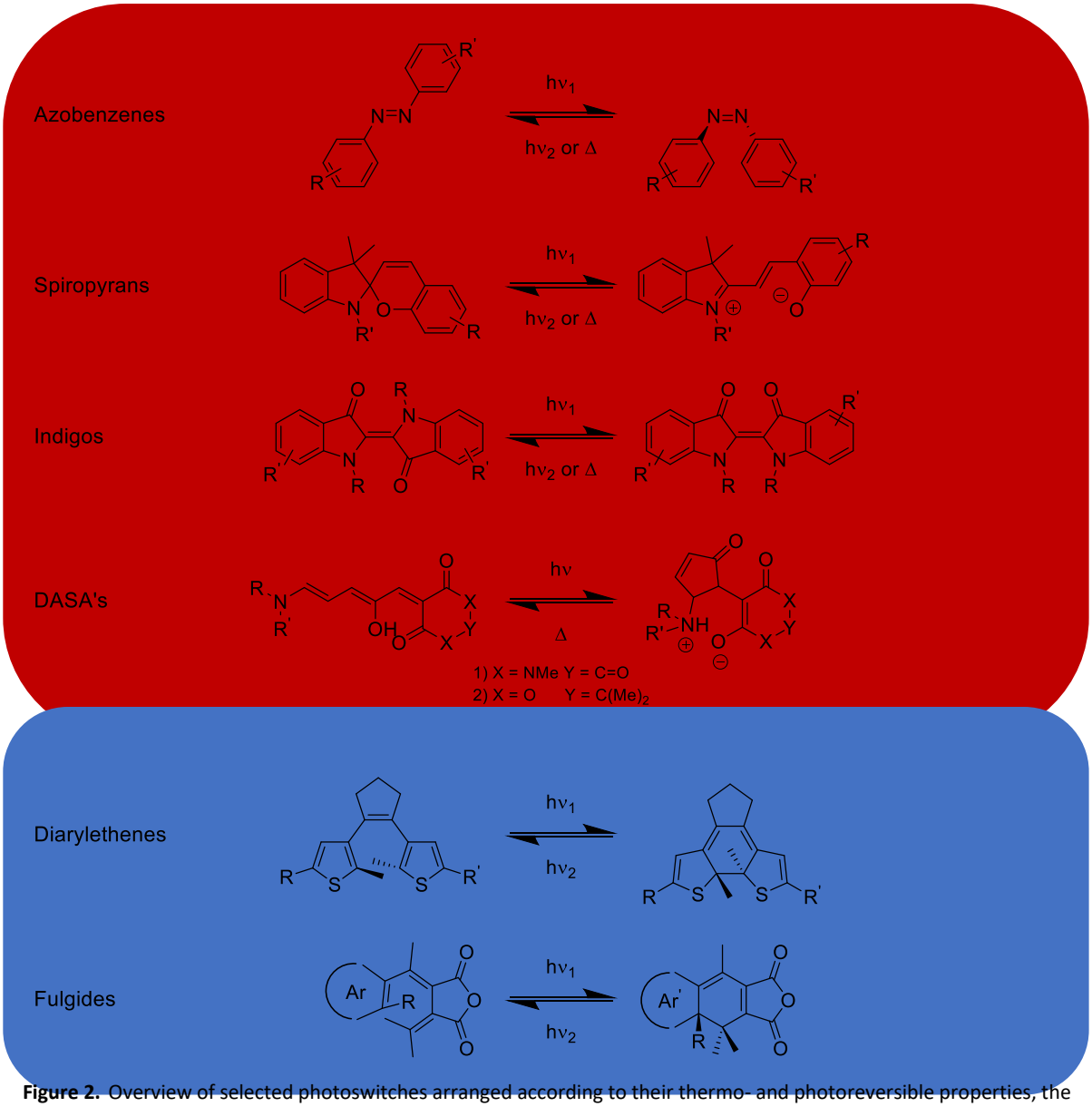


**Figure 2.** Overview of selected photoswitches arranged according to their thermo- and photoreversible properties, the re-isomerization of T-type photochromic systems can be thermally triggered while both states of P-type compounds are thermally stable; typical representatives for the former class are DASA's (donor-acceptor Stenhouse adduct), indigos, azobenzenes, and spiropyrans (red); diarylethenes and fulgides (blue) are counted to the latter class.

Each photochromic compound has distinct features giving access to a specific kind of control that can be chosen according to the needs of the investigated system. Starting with indigo, its photochromic properties are based on the *E*/*Z*-isomerization about the central carbon double bond, addressable for derivatives where R ≠ H.[12c] Due to the relative planarity of both isomers a large geometrical change is achieved separating or combining the substituents attached to the nitrogen atoms. In a similar way, azobenzenes exhibit a significant structural difference of both occupied states, which are covered in the upcoming chapter more in detail.

Another molecule undergoing a relatively large geometrical change from an extended to a more compact structure are the negative photochromic donor-acceptor Stenhouse adducts (DASA's).[12b, 15] After isomerization about the enol double bond, ring closure occurs that is accompanied by the formation of a zwitterion and thereby converting the original hydrophobic nature into hydrophilicity. A similar polarity change is observed for spiropyrans after ring opening to the likewise zwitterionic merocyanine.[16] Accordingly, both photochromic systems are apt to control solubility and aggregation behavior due to the reversible formation and disappearance of charges.

In contrast, diarylethenes show minor geometrical changes upon 6π electrocyclization.[17] However, the more rigid ring-closed structure connects the substituents R and R' by direct conjugation while in the open form a cross-conjugated system is limiting the interaction of both groups. Fulgides provide a similar function by creating a $sp^3$ center at the carbon bearing the R group that was incorporated in a conjugated system before ring closure.[18] A major advantage of both switches is their thermal irreversibility rendering them good candidates for storage applications.

## 2.2 Azobenzenes

### 2.2.1 General Properties and Classes[12a, 19]

Azobenzenes are structurally based on the diazene group that comprises two nitrogen atoms connected by a double bond. Additional aromatic substituents (Figure 3a) establish a fully conjugated system that in combination with the nitrogen lone pairs gives rise to two major absorption bands in the UV/vis region, i.e. the ππ* (intensive, symmetry allowed) and the nπ* (weak, symmetry forbidden) bands. Spectra of unsubstituted *E* and *Z* azobenzenes as the most simple representatives are depicted in Figure 3b. Irradiation with light of higher energy leads to excitation of the $S_0 \rightarrow S_2$ transition while light of lower power induces the $S_0 \rightarrow S_1$ conversion. Either processes can eventually trigger isomerization about the double bond in both directions,

however, different quantum yields are observed violating Kasha's rule.[20] Typical ratios of isomerizations per photon absorbed range from 0.10 – 0.15 for $\phi_{E\rightarrow Z}$ in the UV region and are twice as high in the visible area. Furthermore, they are dependent on variables such as temperature, solvent polarity and viscosity. The conversion from the *Z* form to *E* form can also occur thermally since the former is energetically more stable by approximately 58 kJ/mol exhibiting a thermal activation barrier of about 90-100 kJ/mol. The half-life of the unsubstituted photoswitch is about 2 d which can be strongly influenced by differently functionalized aromatics. The isomerization about the nitrogen double bond of azobenzene is accompanied by a hypsochromic shift of the maxima in the absorption spectrum. In contrast to the ππ* band, which decreases in intensity after conversion to the *Z* isomer, the nπ* band shows hyperchromic behavior.

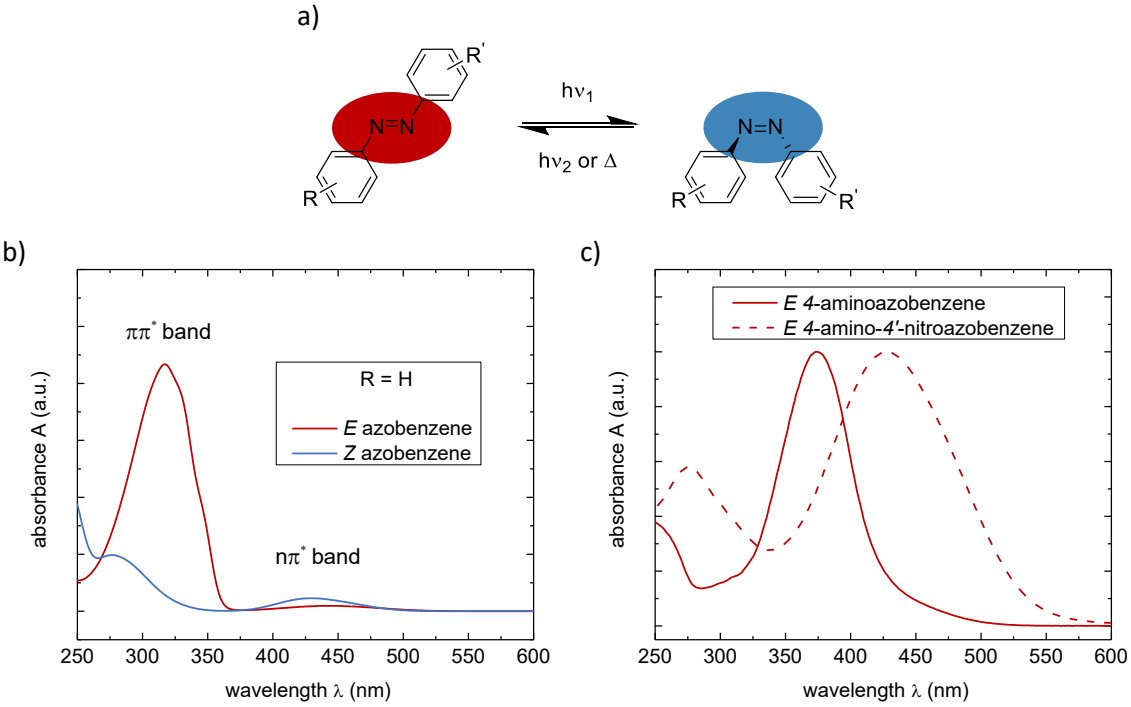


**Figure 3.** a) Structure of parent azobenzene in both isomeric forms, the aromatic units can be substituted with various functional groups resulting in different spectral properties and thermal stabilities, the switching process brings the *4* and *4'* position in close proximity or separates them, while the *E* configuration is entirely planar the phenyl rings of the *Z* form are twisted by ca. 90° relative to the C-N=N-C plane; b) absorption spectra of *E* and *Z* azobenzene showing the intensive ππ* band in the UV region and weak nπ* band in the visible area; c) spectra of *4*-aminoazobenzene (solid line) and *4*-amino-*4'*-nitroazobenzene (dashed line) as representatives of the aminoazobenzene and pseudo-stilbene type, due to a bathochromic shift of the ππ* transition both bands are gradually overlapping.

The most interesting feature of the configurational change is the large geometrical difference of both isomers. The distance between the *4* and *4'* positions of the parent molecule decreased from 10 Å for the planar *E* form to 5.5 Å for the non-planar *Z* form. A polarity change as well as a different refractive index is also observed after isomerization.

Other deactivation processes besides a change of configuration or vibrational relaxation and release of heat are usually not observed due to their high fatigue resistance and very weak emission properties. Fluorescence yields vary in the range of $10^{-7}$ – $10^{-5}$ while phosphorescence has not been observed yet. Isomerization, however, can occur from the triplet state of *Z* azobenzene by employing aromatic sensitizers.

Azobenzenes are differentiated in three classes according to the substituents attached to the aromatic rings and their resultant electronic properties, i.e. the azobenzene, the aminoazobenzene, and the pseudo-stilbene type.[12a] The former type exhibits properties similar to non-substituted azobenzene. The two featureless absorption bands are completely separated, and their maxima exhibit only minor shifts in different solvents. Common groups attached to the aromatic rings are aryl, alkyl, halogen, as well as electron-withdrawing moieties in general such as cyano, carbonyl, and nitro. Electron-donating groups, however, are limited to the *meta* positions to avoid conjugation with the diazene group.

In contrast, derivatives of the aminoazobenzene type are functionalized with electron-donating groups, e.g. alkoxy and amino substituents, in conjugation to the azo bond. As a result, the ππ* band is bathochromically shifted leading to a partial overlap with the nπ* transition (Figure 3c, solid line, *4*-aminoazobenzene), though, the overall extent highly depends on the solvent polarity. The quantum yields are generally higher and the thermal half-lifes shorter in comparison to the parent molecule. Especially hydroxy-substituted derivatives show rapid thermal *Z* → *E* isomerization due to the formation of intramolecular hydrogen bonds and tautomerism.

Pseudo-stilbenes comprise donor-acceptor substituted (push-pull) and protonated azobenzenes. In these cases, the two absorption bands are almost degenerated rendering independent addressability no longer possible (Figure 3c, dashed line, *4*-amino-*4'*-nitroazobenzene). The very low thermal stability (half-lifes of ms to s) that is dependent on solvent polarity poses a challenge when determining quantum yields. However, protonation only occurs under strongly acidic conditions ($pK_{a,E}$ = -2.6, $pK_{a,Z}$ = -1.6 determined in 10% ethanolic sulfuric acid) and, therefore, is of minor importance. In addition, cyclization to cyclo[c]cinnoline occurs as an irreversible side reaction in acidic medium.

Several mechanisms of azobenzene photoisomerization in solution are discussed based on quantum chemical calculations and ultrafast spectroscopy, though, no definite decision for one or the other has been made so far. Unlike stilbene, azobenzene's carbon counterpart, the quantum yields for *E* and *Z* isomerization do not add up to unity and change upon excitation of different

bands implying multiple pathways from one configuration to the other. An overview of proposed mechanisms is depicted in Figure 4, i.e. rotation, inversion, a combination of both, and the hula-twist.[12a, 21]

In the first case, the N-N π-bond must be broken allowing the alteration of the C-N-N-C dihedral angle whereas the N-N-C angle remains at the same value. The opposite trend is followed under inversion where no change of the C-N-N-C dihedral angle occurs but one or both N-N-C angles become 180° depending on considering a simple or concerted pathway, respectively, giving rise to a partially or fully linear transition state. Furthermore, the latter carries no dipole moment leading to a non-polar intermediate. The combination of rotation and inversion leads to significant changes of all angles around the nitrogen double bond. A more recent publication suggests a hula-twist mechanism where the phenyl rings and nitrogen atoms undergo a pedal-like concerted motion rotating the $C_1$-$N_1$-$N_2$ plane angle about the $C_1$-$N_2$ axis by 180°.

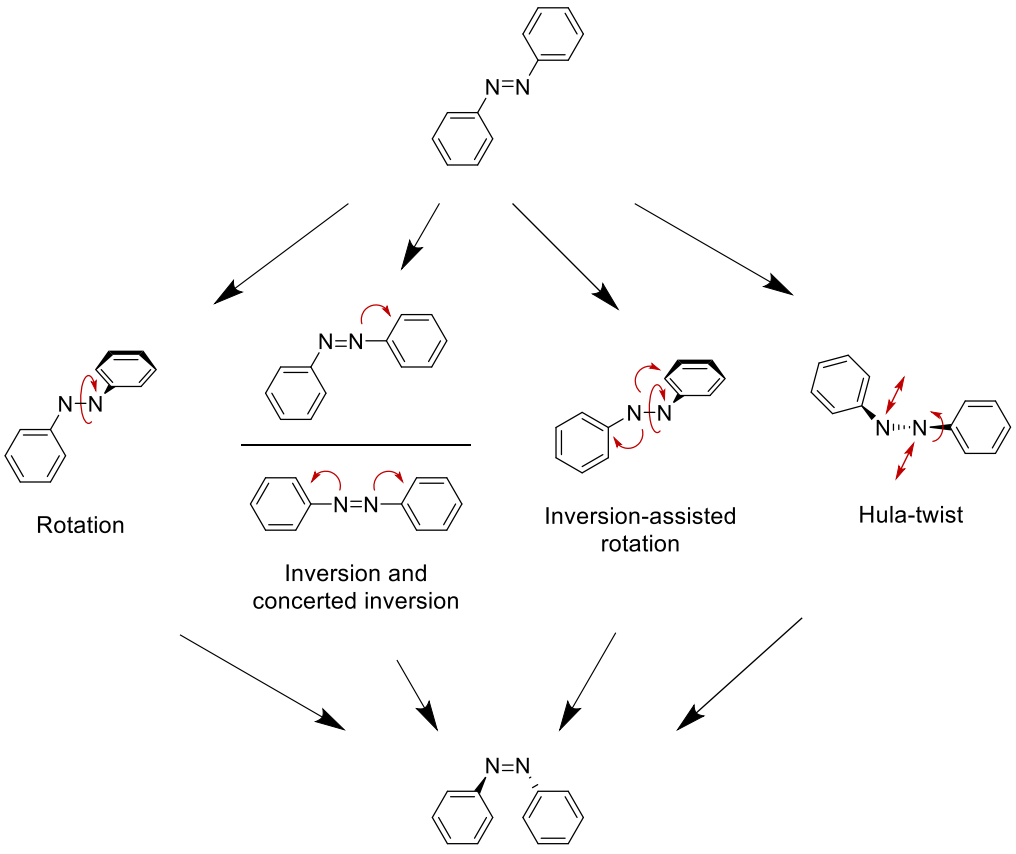


**Figure 4.** Proposed pathways for azobenzene isomerization, i.e. rotation, (concerted) inversion, inversion-assisted rotation, and hula-twist; most recent results suggest the latter one where the phenyl rings and nitrogen atoms conduct a pedal-like concerted motion.

However, regardless of the mechanism, all theories agree on the fact that excitation of the *E* isomer to the $S_2$ state followed by relaxation gives partial access to a region of the $S_1$ state that cannot be reached by direct irradiation of the nπ* band and solely results in formation of the

*E* isomer. Besides the most recent spectroscopic data, the difference in quantum yields by a factor of two depending on the irradiated band further supports that idea.
Similarly, the mechanism for thermal *Z* to *E* isomerization has been discussed, though, also in this case none of the theories was proven by now. In this context, mostly the rotation, inversion, and combination of both pathways are taken into consideration.[22]

A major drawback of all sufficiently thermally stable classes of azobenzene is the requirement for UV light to induce isomerization from the *E* to the *Z* form. Especially for applications in biological environments high-energy radiation is undesirable due to its toxic and carcinogenic nature. Facing this issue, several derivatives have been developed that can be switched in both ways by visible light exclusively. The basic concept comprises the modification of the energetic level of the HOMO which is usually located at the nitrogen lone pairs by introduction of *ortho* substituents or coordination, thus, causing a shift of the nπ* band in one or both isomers. The resultant separation of the lower energy transition of both configurations provides addressability of the two states via nπ* excitation. Four derivatives following this strategy (including one spectrum to exemplify the effect), i.e. tetra *ortho* methoxy-[23] and tetra *ortho* fluoroazobenzene,[24] an azobenzene bridged in *ortho* position by an ethylene linker,[25] and a $BF_2$ coordinated azo compound,[26] are depicted in Figure 5.

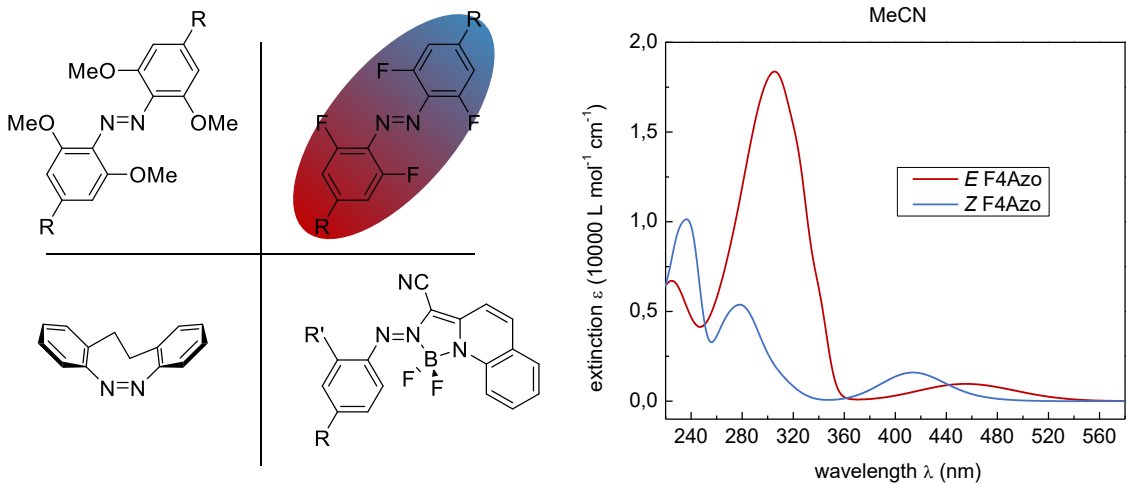


**Figure 5.** Azobenzene derivatives fully addressable with visible light in both directions and spectra of *E* and *Z* tetra *ortho* fluoroazobenzene (F4Azo), substitution in *ortho* position influences the energetic level of the HOMO located at the nitrogen lone pairs or causes a structural distortion that leads to a splitting of the nπ* bands of both isomers; in case of the $BF_2$ derivative, coordination to the azo bond causes a significant bathochromic shift of the ππ* band which can be exploited for excitation instead of the nπ* transition.

In case of the methoxy derivative (Figure 5, top left), the bulky *ortho* groups distort the planar structure of the *E* isomer which leads to a blueshift of the ππ* band. Furthermore, the electron-

rich oxygen atoms interact with the nitrogen lone pairs raising their energy and causing a bathochromic shift of the nπ* transition which is not operative in the *Z* isomer ($\Delta\lambda_{n\pi^*}$ = 36 nm, R = NHAc).[23] A similar effect is observed for the *ortho* fluorinated azobenzene (Figure 5, top right and spectrum). However, the electron-withdrawing effect of the fluorine atoms stabilize the n orbital of the *Z* form as well as the π* orbital in general leading to a hypsochromic and bathochromic shift of the visible band for the *Z* and *E* isomer, respectively ($\Delta\lambda_{n\pi^*}$ = 42 nm, R = H).[24] An unexpected side effect of the fluorination is the relatively long thermal half-life of these derivatives going up to ca. 700 d at room temperature (R = F).

The bridge azo derivate (Figure 5, bottom left), one of the few examples where the *Z* form is the thermally stable isomer, exhibits an nπ* shift of about 86 nm, one of the largest ever observed. The effect is reasoned in terms of geometrical constraints caused by the ethylene linker.[25] Turning to the $BF_2$-coordinated azo compound (Figure 5, bottom right), a significant shift of the ππ* transition to the visible range similar to pseudo-stilbenes is observed which shifts by 28 nm (R = R' = H) upon isomerization. In contrast to push-pull azobenzene, the ππ* and nπ* transition do not overlap and the thermal half-life (12.5 h) is substantially higher.[26]

### 2.2.2 Synthesis

Numerous methods are available for the formation of symmetrical and non-symmetrical azobenzene.[27] An overview of the main techniques is presented in Figure 6, i.e. the oxidative and reductive coupling procedures of anilines and nitrobenzenes, respectively, the Mills reaction, the Azo coupling via diazonium salts, and metal-catalyzed cross-couplings starting from hydrazine derivatives.

Besides the direct electrolytic approach, typical oxidizing agents to transfer anilines into azobenzenes range from peroxides and hypoiodites[28] to metal salts and oxides such as HgO, $KMnO_4$, $Pb(OAc)_4$, and $K_3[Fe(CN)_6]$.[29] Since at least stoichiometric amounts of the oxidant are necessary, substitution of the latter by more environmentally friendly compounds is desirable. A method employing oxygen from the air and a copper(I)-pyridine complex as catalyst poses a good alternative in this context.[30] Turning to the reductive side, mostly elemental metals like Mg, Zn, or Al[31] and agents such as $LiAlH_4$, $NaBH_4$, and silanes are employed. Basic conditions are usually necessary since complete reduction to the corresponding aniline is favored in acid medium. Both methods are limited by the accessibility of only symmetrical azobenzene. Furthermore, functional groups at the aromatic rings sensitive to oxidation or reduction and the electronic properties of

the targeted azo derivative must be taken into consideration to avoid side reactions and formation of hydrazos, azoxys, or other oxidation state of nitrogen.

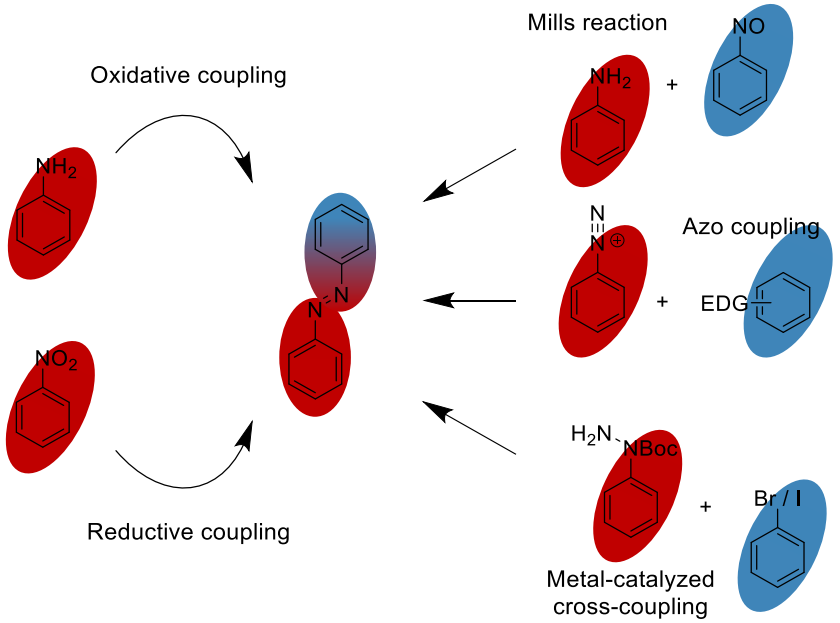


**Figure 6.** General strategies for the synthesis of azobenzenes; the oxidative and reductive pathway starting from aniline or nitro derivatives, respectively, provide access to symmetrical azobenzene; the Mills reaction, the azo coupling, and metal-catalyzed cross-couplings are methods for the formation of non-symmetrical azo compounds.

Turning to the synthesis of non-symmetrical azobenzenes, several methods are available, though, the Mills reaction must be pointed out as one of the most powerful in the field.[27c] The procedure couples an aniline and nitroso derivative under acidic conditions in which the former should be electron-rich and the latter electron-poor to increase nucleophilicity and electrophilicity, respectively. Limiting factors are the possibly challenging formation of the nitroso compounds and the low reactivity of anilines bearing electron-withdrawing substituents. Another approach to azo compounds with different aromatic rings is the azo coupling employing diazonium salts.[27c] Since these substances are highly unstable, low temperatures (< 5 °C) must be kept at any time of the reaction to avoid nitrogen elimination. Due to their relatively low electrophilicity only electron-rich aromatic groups such as anilines, anisoles, and phenoxides can be converted and substitution usually occurs in the *para* position to the donor for steric reasons. Furthermore, the pH value is of great importance since diazonium salts are only reactive in acidic or neutral medium otherwise forming inactive diazoates. A common side reaction with free amines is the formation of triazenes which, however, is reversible at low pH values. A last procedure for the synthesis of non-symmetrical azobenzenes are metal-catalyzed cross-coupling reactions similar to Buchwald-Hartwig.[32] A partially Boc-protected hydrazine derivative is coupled to an aryl halide employing

typical Pd catalysts such as $Pd(dppf)Cl_2$ or $Pd(OAc)_2$ in combination with phosphine ligands. The obtained stable Boc-protected hydrazo compound must still be deprotected and oxidized to the final photochromic molecule in the last step.

Besides these general methods, several other approaches to specific azobenzene designs are available that are not discussed in this chapter. The scope ranges from the Wallach reaction that converts azoxy derivatives into the corresponding *4*-hydroxyazobenzenes, thermolysis of azides in the presence of anilines, and the opening of benzotriazoles as source for diazonium salts, to the reaction of arylhydrazines with quinones, and the triazene rearrangement, among others.[27c]

### 2.2.3 Applications

Historically, azobenzenes were employed as dyes owing to the bright, intensive colors of certain derivatives and their high fatigue resistance with little to no photodegradation. Since their spectral features, however, are dependent on the electronic characteristics of the attached functional groups, an application as colorimetric pH sensors by modification with substituents responding to acids and bases is equally obvious. Well-known examples are methyl yellow/orange/red, Congo red, and Alizarine yellow R providing sulfonate, amine, or carboxyl groups as pH responsive moieties.

More advanced applications rely on the configurational change of azobenzene caused by photoisomerization that directly converts light into mechanical work, or the difference in polarity of both forms that can change solvation and aggregation behavior. As basis for light-driven molecular machines or as simple on-off switches these photochromic molecules made their way into various fields of life and material sciences such as cytology,[33] pharmacology,[34] self-assembly processes,[35] and polymer networks,[36] among others. Chosen examples are presented in the upcoming paragraph to give an impression of the diversity of possible azobenzene applications.

Turning to the field of biochemistry, the activity of proteins and enzymes highly relies on their 3D structure and accurate folding. Taking advantage of the conformational change of azobenzene, the photochromic molecules can be connected to subunits of complex organic macromolecules, reversibly change motifs by isomerization, and, thus, enable or disable accessibility of substrates or receptors. An example is depicted in Figure 7a where the photoswitch controls the association of a protein with DNA by altering an α-helix structure essential for proper interaction of both units.[33c]

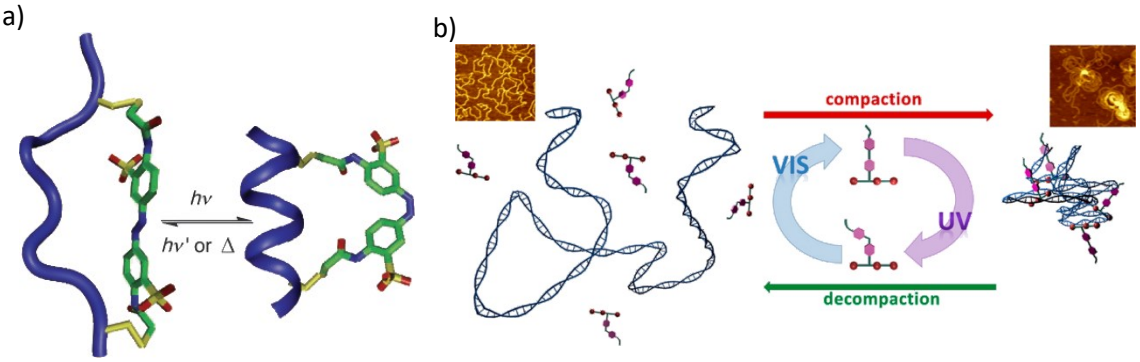


**Figure 7.** Reversible binding of azobenzene-substituted proteins to DNA controlled by light; a) isomerization to the *Z* configuration causes the formation of an α-helical structure that can bind in the major groove of DNA, the *E* state cannot adopt this structure and, therefore, does not associate;[33c] b) isomerization changes the polarity of the peptidomimetic causing aggregation accompanied by compaction of the genetic material.[37]

In this way, the activity of transcription factors (proteins that bind to DNA and initiate the RNA synthesis as the primal step of the expression of genetic information) can be influenced. Furthermore, due to specific binding to DNA these peptides can be exploited as carriers for therapeutics or for blocking gene sequences still providing the option for later disassembly. In another work, a photoresponsive peptidomimetic was synthesized that similarly binds with DNA in one switching state but does not in the other (Figure 7b).[37] In this case however, the process is not a result of geometrical alterations but a polarity change that triggers the binding event leading to a reversible compaction of the genetic material. Densely packed DNA is desirable for gene delivery into cells where the cargo could be spread again by irradiation with light once the target is reached.

In material sciences, azobenzenes are blended in polymer matrices or covalently integrated in their main or side chains aiming to control properties such as tensile strength, elasticity, or glass transition temperature. Due to the macromolecular environment, the geometrical or polarity change as a result of isomerization requires a response of the whole polymeric surrounding leading to an amplification of the single switching event and, thus, a possible macroscopic effect. An example for the latter is depicted in Figure 8 where a self-oscillating soft actuator was prepared by incorporating fluorinated azobenzene in polymer films with liquid-crystalline properties.[38] A continuous chaotic motion was observed under exposure to normal sunlight which could be reproduce by irradiation with green and blue light, the usual wavelengths to address the nπ* bands of both isomers. While the effect has not been completely rationalized yet, one important contribution is the iterative change of the isomer ratio. In this case, however, the light source is not considered a stimulus but rather a constant energy source. Applications in self-cleaning surfaces and coatings are conceivable that are activated and driven automatically when the sun is shining.

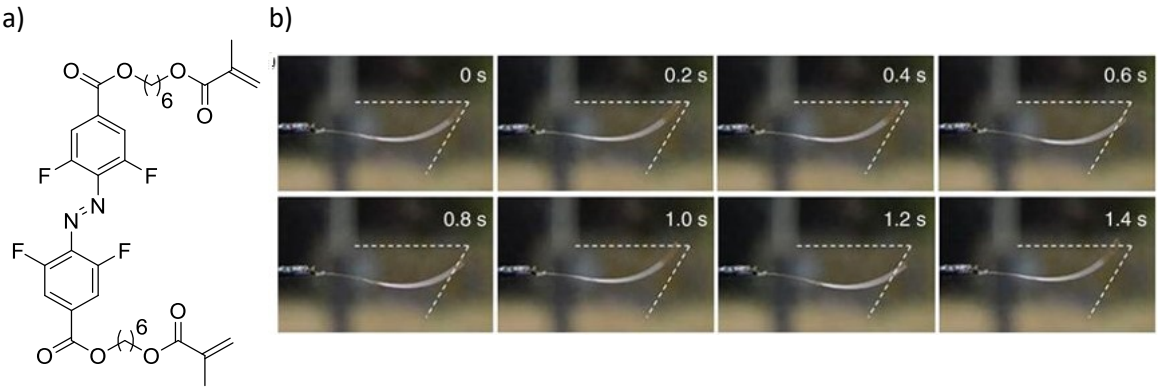


**Figure 8.** a) Fluorinated azobenzene-based crosslinker providing methacrylates for covalent incorporation in the polymer network; b) liquid-crystalline film containing the azo crosslinker, produced by photopolymerization, a continuous chaotic motion is observed by exposure to normal sunlight, the pictures show snapshots within a short period of the oscillation.[38]

Covering the medical field, the administration of most pharmaceuticals is not conducted in a directed fashion, but compounds are spread out all over the body, thus, causing possibly serious side effects at locations they are not meant to act. In this context, photoswitches are exploited to control the activity of drugs and therapeutics enabling activation only in the body parts of interest. The challenge in that process is the modification of the molecular structure of existing pharmaceuticals by exchanging subunits for azobenzene or attaching them without loss of activity in one isomeric form but a significant decrease in activity in the other.

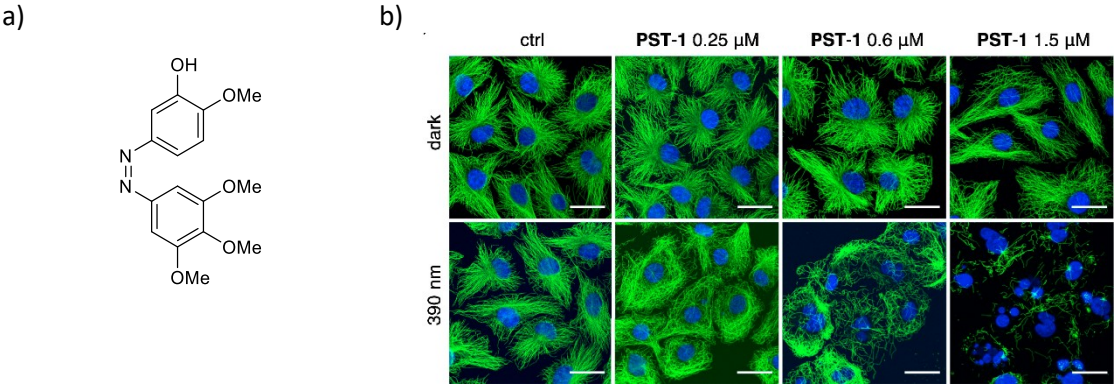


**Figure 9**. a) Photoresponsive microtubule inhibitor Photostatin-1 obtained by modification of stilbene derivative Combretastatin A-4; b) pictures of cells exposed to different concentrations of Photostatin-1 in the dark (top) or after irradiation at 390 nm (bottom), in the higher concentrated, irradiated samples the destruction of the microtubules is observed while the non-irradiated samples remain intact.[33b]

One elegant example is depicted in Figure 9 where the stilbene double bond of Combretastatin A-4, a microtubule inhibitor, is exchanged for a nitrogen double bond creating an azobenzene analogue.[33b] Depending on the concentration, the destruction of the microtubules is observed under irradiation with 390 nm light. Since only the *Z* isomer is active the non-irradiated cells

remain intact. An application in cancer therapy is conceivable as only tumor cells are affected when precisely targeted by light, thus, preserving healthy tissue.

Numerous other possible applications of photoswitches and azobenzenes in particular are reported ranging from modified surfaces that enable directed motion on them,[39] reversible ion channel blockers in cells,[33a] and generation of anisotropy in polymeric material,[40] to the controlled release of small molecules,[36d, 36e, 41] and self-healing materials.[42]

## 2.3 Light Scattering

When aiming to create a system that undergoes a reversible geometrical change induced by an external stimulus, an analytical method is required which is able to detect alterations in size and shape. Besides direct imaging techniques based on electron microscopy, the specific scattering characteristics of molecules and larger objects hit by electromagnetic radiation provide insight on their architecture and dimension in the range of a few nanometers to micrometer size. In this context, the combination of dynamic and static light scattering is especially convenient since relevant quantities such as molecular weight, diffusion coefficient, hydrodynamic radius, radius of gyration, as well as morphological information are accessible with high precision. The theoretical background of both methods as well as the most important formulas necessary for data treatment are discussed in the upcoming two chapters.[43] Furthermore, a real data set obtained during the work on this thesis is used to exemplify the analysis procedure.

The basis for light scattering is the ability of electromagnetic radiation to change the spatial charge distribution within molecules, whose extent is dependent on the polarizability of the specific species. The irradiated objects turn into oscillating dipoles that follow the same time modulation as the incident light and, in case of an elastic scattering process, emit isotropically at the same wavelength perpendicular to the oscillator. However, for particles larger than 20 nm several scattering centers are generated simultaneously giving rise to areas of constructive and destructive interferences of the emitted waves. In these cases, the scattered light intensity is dependent on the observation angle and the overall interference pattern characteristic for the shape and size of the investigated objects (referred to as the particle form factor). An exception are particles of sizes smaller than $\lambda/20$ where interferences occur at a negligible degree.

Generally, samples concentrations in light scattering experiments have to be kept as low as possible to avoid interactions between the particles and multiple scattering events.

For evaluation, the scattering angle θ is substituted by the scattering vector q (Equation 1) which is an inverse length scale of the scattering process, dependent on the wavelength of the incident light λ and the refractive index of the solvent $n_D$. The vector represents the level of details achievable by the scattering experiment and is comparable to the zoom factor of an optical microscope. Besides information on mass, size, and topology of the whole object, conformational details as well as density distributions of the particle's subunits and interior are accessible under proper conditions.

$$q = \frac{4\pi n_D \sin(\theta/2)}{\lambda} \quad (1)$$

### 2.3.1 Dynamic Light Scattering (DLS)

Dynamic light scattering detects the mobility of particles in solution by measuring fluctuations of the scattering intensity I after several different correlation times τ at a single observation angle. These fluctuations are attributed to changing interference patterns of the electromagnetic waves that are emitted by objects continuously changing their relative position in space. An example of a scattering intensity variation in the course of 30 s is depicted in Figure 10a which can be used to derive the corresponding intensity correlation function $g_2$ (Equation 2, Figure 10b).

$$g_2(q,\tau) = \frac{\langle I(q,t) I(q,t+\tau)\rangle}{\langle I(q,t)^2\rangle} \quad (2)$$

$$g_1(q,\tau) = F_s(q,\tau) = \exp\left(-q^2 \langle \Delta R^2(\tau)\rangle \frac{\tau}{6}\right) \quad (3)$$

$$g_2(q,\tau) = 1 + g_1(q,\tau)^2 \quad (4)$$

The intensity correlation function can be converted into the amplitude correlation function $g_1$ (also referred to as dynamic structure factor $F_s$, Equation 3) by means of the Siegert relation (Equation 4). In this context, ΔR denotes the average distance that a particles moves within the correlation time, which is directly related to the translational self-diffusion coefficient $D_s$ (Equation 5). Substitution of ΔR in Equation 3 provides access to $D_s$ via the measured scattering intensity fluctuations (Equation 6).

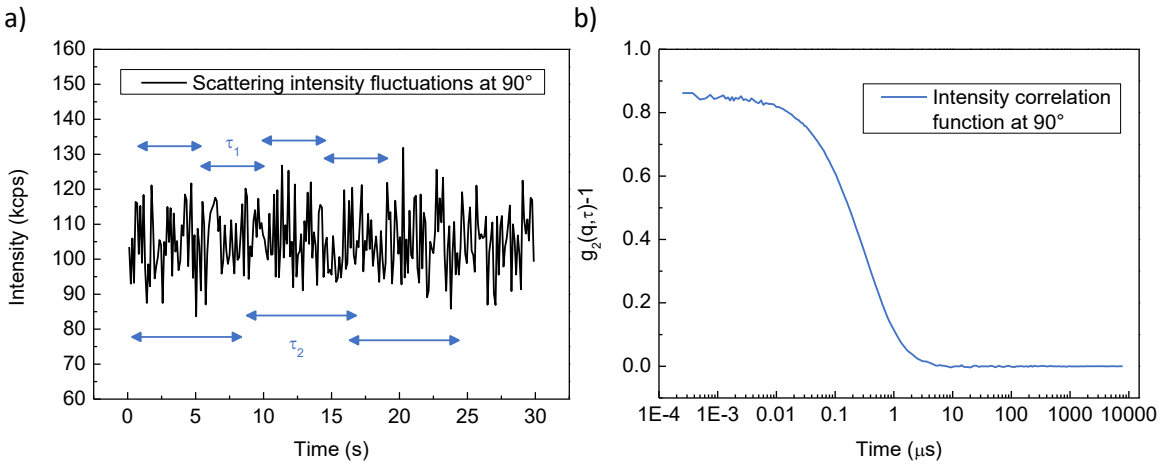


**Figure 10.** Dynamic light scattering data obtained for an aqueous solution of a linear amphiphilic polymer forming cylindrical micelles (c = 0.5 mg/mL), a) scattering intensity fluctuations in the course of 30 s measured at an observation angle of 90° and two example correlation times $\tau_1$ and $\tau_2$ illustrated by blue arrows, b) derived intensity correlation function $g_2$ subtracted by 1 which can be converted into the amplitude correlation function $g_1$ according to the Siegert relation.

$$\langle \Delta R(\tau)^2 \rangle = 6 D_s \tau \tag{5}$$

$$F_s(q,\tau) = \exp(-D_s q^2 \tau) = \sqrt{\frac{\langle I(q,t) I(q,t+\tau) \rangle}{\langle I(q,t)^2 \rangle} - 1} \tag{6}$$

$$D_s = \frac{kT}{6\pi\eta R_h} \tag{7}$$

Eventually, the diffusion coefficient can be translated into the hydrodynamic radius $R_h$ employing the Stokes-Einstein relation in Equation 7, where k denotes the Boltzmann constant, T the temperature, and η the viscosity of the solvent.

For a monodisperse sample, $F_s$ decays single-exponentially. However, in case of polydisperse samples, the dynamic structure factor is constituted by a superposition of several exponentials that are weighted according to the corresponding distribution function $P(D_s)$ (Equation 8).

$$F_s(q,\tau) = \int P(D_s) \exp(-q^2 D_s \tau) dD_s \tag{8}$$

$$F_s(q,\tau) = \exp\left(-\kappa_1 \tau + \frac{1}{2!}\kappa_2 \tau^2 - \frac{1}{3!}\kappa_3 \tau^3 + \ldots\right) \tag{9}$$

$$\kappa_1 = \langle D_s \rangle q^2 \qquad \kappa_2 = \left(\langle {D_s}^2 \rangle - \langle D_s \rangle^2\right) q^4$$

In this work, the Cumulant analysis, a common procedure to treat the DLS data of polydisperse samples, is employed. The dynamic structure factor is evolved by a Taylor series (Equation 9) where the first cumulant $\kappa_1$ represents the average (angle-dependent) diffusion coefficient and the second cumulant $\kappa_2$ provides information about the polydispersity of the system. Three

cumulants are sufficient to obtain an appropriate fit for the current data as depicted in Figure 11a. The corresponding hydrodynamic radius at 90° scattering angle is 51 nm and the polydispersity about 0.83 (very broad distribution).

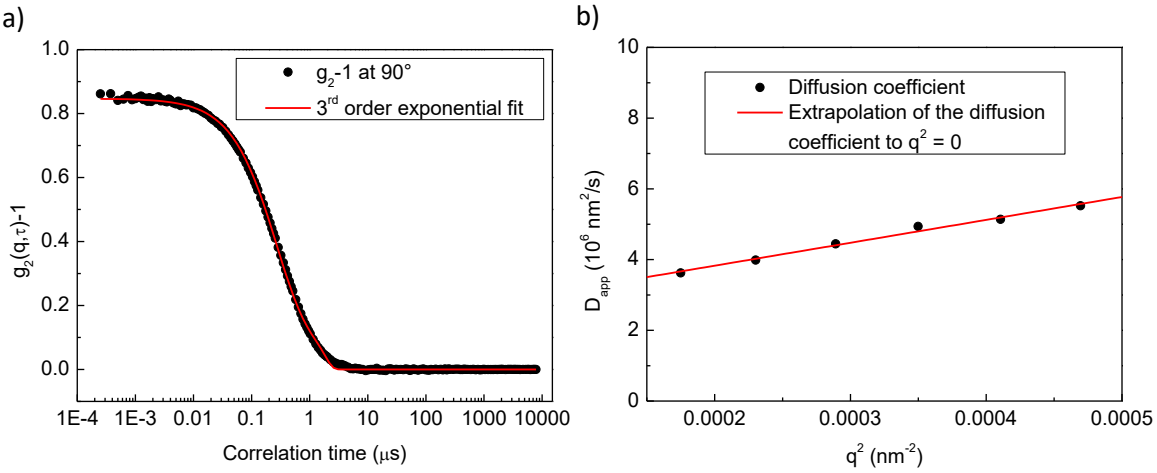


**Figure 11.** Evaluation of dynamic light scattering data obtained at a 90° scattering angle by 3rd order Cumulant analysis, a) exponential fit to the intensity correlation function $g_2$ according to Equation 4 and 9 (adj. $R^2$ = 0.99972, RMSE = 0.00598) providing access to the apparent diffusion coefficient $D_{app}$, b) linear extrapolation of $D_{app}(q)$ to zero scattering angle according to Equation 10 yielding the average diffusion coefficient at the intercept, the average hydrodynamic radius can be obtained by means of the Stokes-Einstein equation.

$$D_{app}(q) = \langle D_s \rangle \left(1 + K \langle {R_g}^2 \rangle q^2\right) \qquad 10$$

However, due to a stronger contribution of smaller objects to the scattering signal with increasing q, a dependency of the diffusion coefficient on the observation angle is observed. Hence, a linear extrapolation of the apparent diffusion coefficient $D_{app}$ to zero scattering angle according to Equation 10 is required, which eliminates contributions of the particle form factor and non-diffusional processes to the correlation function (Figure 11b). In this context, K denotes a constant that depends on the polydispersity as well as the topology of the objects, while $R_g$ represents the radius of gyration. Eventually, the average $R_h$ can be calculated from the intercept of $D_{app}(q)$ by means of the Stokes-Einstein equation (97 nm for the current sample).

### 2.3.2 Static Light Scattering (SLS)

In contrast to DLS where scattering intensity fluctuations are measured, for SLS the average scattering intensity is basis for the determination of quantities such as the radius of gyration ($R_g$) and the weight-average molecular mass ($M_w$). Depending on the size of the analytes, two cases have to be differentiated, i.e. samples containing objects either smaller or larger than λ/20. In the

first case, the particles exhibit scattering properties independent of the detection angle and the corresponding absolute scattering intensity R (also referred to as Rayleigh ratio) is represented by Equation 11.

$$R = Kc\left(\frac{1}{M} + 2A_2c + \ldots\right)^{-1} = (I_{solu} - I_{solv})\frac{I_{std,abs}}{I_{std}} \quad 11$$

$$K = \frac{4\pi^2}{\lambda^4 N_A} {n_s}^2 \left(\frac{\partial n_a}{\partial c}\right)^2 \quad 12$$

The Rayleigh ratio depends on the contrast factor K (also referred to as scattering power, Equation 12) with λ denotes the wavelength of the incident light, $N_A$ the Avogadro constant, $n_s$ and $n_a$ the refractive indices of the solvent and analyte, respectively, and c and M the mass concentration and molar mass of the analyte. The second Virial coefficient $A_2$ represents the deviation of the real system in comparison to the ideal one by including the interactions of solvent and analyte. Experimentally, R is obtained by measuring the scattering intensities $I_{solu}$ and $I_{solv}$ of the solution and solvent, respectively, and the (absolute) intensity $I_{std}$ ($I_{std,abs}$) of a standard. Eventually, the basic equation of static light scattering for small particles is obtained by converting Equation 11 into Equation 13.

$$\frac{Kc}{R} = \frac{1}{M} + 2A_2c + \ldots \quad 13$$

For larger objects exhibiting multiple scattering centers (up to 50 nm where $R_g^2q^2 << 1$), the scattering intensity is dependent on the scattering angle. Therefore, the particle form factor P(q), which represents the normalized scattering of a single particle and includes contributions of the objects size and shape, has to be taken into account. Considering homogeneous isotropic objects, P(q) can be represented by a series expansion as depicted in Equation 14.

$$P(q) = \frac{1}{N^2Z^2K} I(q) = 1 - \frac{1}{3}{R_g}^2q^2 + \ldots \quad 14$$

$$\left(\frac{1}{P(q)} \approx 1 + \frac{1}{3}{R_g}^2q^2 \quad for \quad {R_g}^2q^2 \ll 1\right)$$

$$\frac{Kc}{R} = \frac{1}{MP(q)} + 2A_2c = \frac{1}{M}\left(1 + \frac{1}{3}{R_g}^2q^2\right) + 2A_2c \quad 15$$

The combination of Equation 13 and 14 gives rise to the Zimm equation which provides access to the (average) radius of gyration and (weight-average) molar mass of the analyte (in case of polydisperse and/or anisotropic objects).

An example data set is depicted in Figure 12 illustrating the average scattering intensity obtained from the intensity fluctuations (a) and the extrapolation of the reduced scattering intensities at multiple angles to q = 0 (b).

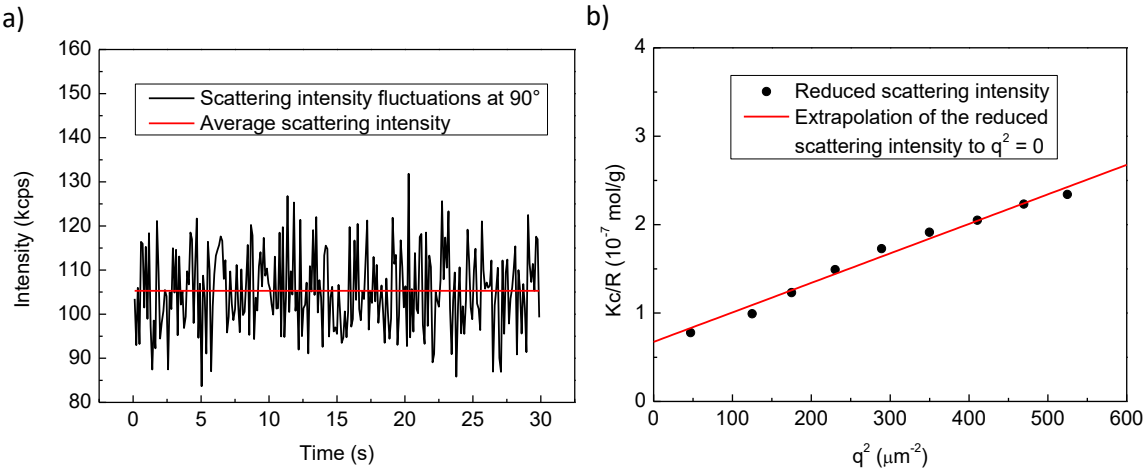


**Figure 12**. Evaluation of static light scattering data, a) illustration of the average scattering intensity (red line) obtained from the intensity fluctuation within a 30 s period, b) extrapolation of the reduced scattering intensity Kc/R to q = 0 according to the Zimm equation, the average radius of gyration is accessible via the slope of the linear fit, the weight-average molar mass can be derived from the intercept in case the refractive index increment (Equation 12) is known.

From the intercept and slope the molar mass and the radius of gyration, respectively, can be derived. However, in case the refractive index increment (Equation 12) is unknown, only $R_g$ is accessible via this route.

For objects of sizes greater than 50 nm, the series expansion of the form factor might not be sufficient. In these cases, P(q) is represented by different formulas dependent on the particle morphology as shown in Equation 16 and 17 for homogeneous spheres of radius r and thin cylinders of length l.

$$P(q) = \frac{9}{(qr)^6}(\sin(qr) - qr\cos(qr))^2 \qquad 16$$

$$P(q) = \frac{2}{ql}Si(ql) - \frac{\sin^2\left(\frac{ql}{2}\right)}{\left(\frac{ql}{2}\right)^2} \qquad 17$$

## 2.4 Amplification of Geometrical Changes for Molecular Processes

### 2.4.2 Reasons and Targets

The major goal of increasing the change of size, shape, and other properties of synthetic systems as a result of stimuli-responsive reversible molecular processes such as *E-Z* photoisomerization is the accompanied boost of efficiency for the conversion of an energy source (light) into mechanical work. In the appropriate scaffold or matrix, the actuation of single or multiple responsive moieties can be combined and amplified, enabling the creation of materials that elevate work at the nanoscale to the macroscopic level. These materials provide basis for various applications ranging from adaptive systems and new actuators to artificial muscles.

Regarding artificial muscles, one example was already described in chapter 2.2.3 where a polymer film containing fluorinated azobenzene-based crosslinkers is showing a continuous chaotic motion in sunlight.[38] Two other cases of materials exhibiting a macroscopic response and muscle-like behavior are depicted in Figure 13 and Figure 14, i.e. an artificial spring by the group of Katsonis[44] and an artificial muscle-like string from the Feringa lab[45], respectively.

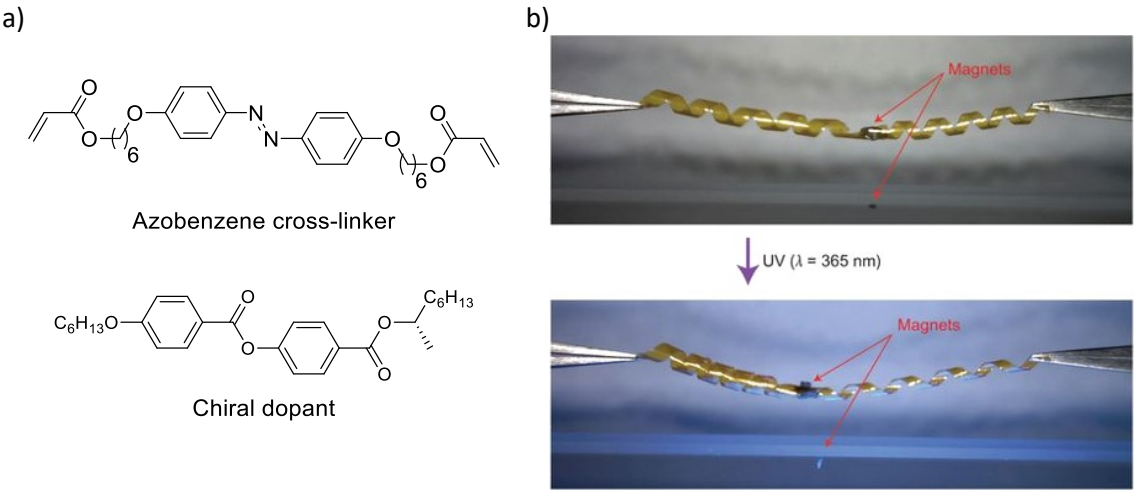


**Figure 13.** Liquid-crystalline polymer film in ribbon shape containing an azobenzene cross-linker as photo-responsive unit and a chiral dopant (a); depending the sense of the ribbon, a contraction or expansion is observed upon irradiation with UV-light for a left- and right-handed structures, respectively; b) combining ribbons of opposite sense and attachment of a magnet at the transition point enables light-induced motion of magnetic material.[44]

Katsonis' spring is made of a liquid-crystalline polymer film containing azobenzene cross-linkers and a chiral dopant. Depending on the preparation technique of the ribbons, their sense can be either left- or right-handed. This results in a decrease or increase of the macroscopic pitch, respectively, after irradiation with UV-light which is reversible by excitation in the visible range. Connecting ribbons of opposite senses amplifies their strength by combining motions in the same direction, one side expands while the other contracts. After attachment of a magnet at the

transition point of both ribbons, another small piece of magnetic material can be moved from distance, following the light-induced motion of the magnet attached to the springs.

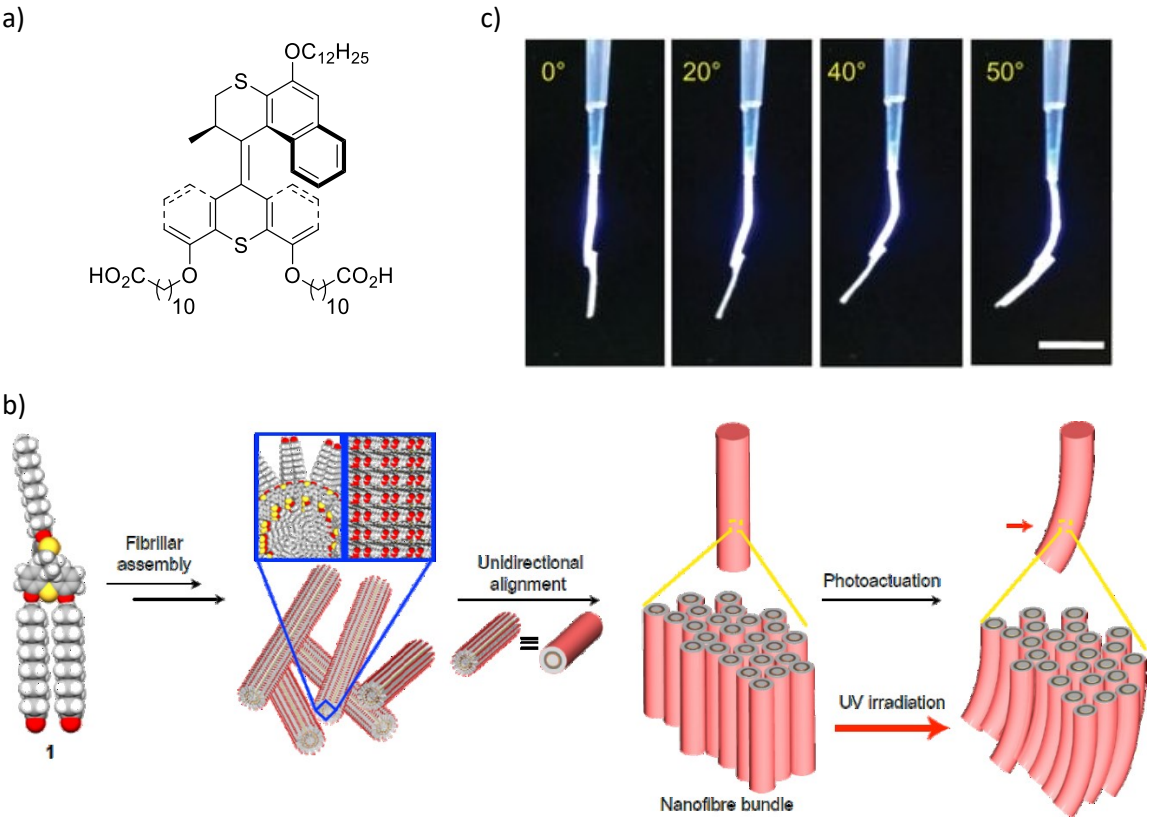


**Figure 14.** Artificial muscle-like string based on self-assembly of the depicted stilbene derivative (a) undergoing a directed rotation about the carbon double bond that is stimulated by irradiation with UV-light and subsequent thermal relaxation, b) upon exposure to $Ca^{2+}$ the cylindrical fibers formed in basic water align unidirectionally and aggregate into light-responsive bundles that can be drawn from solution, c) the light-responsive string bends under UV excitation performing work of about 0.05 µJ when attaching a small piece of paper at the end.[45]

Feringas system is based on an amphiphilic molecule derived from stilbene that performs a directed rotation about the carbon double bond triggered by excitation with UV-light and subsequent thermal relaxation. Due to the amphiphilic properties, self-assembly in basic aqueous medium is observed forming cylindrical fibers with high aspect ratios (diameter: 5-6 nm, length: several µm). $Ca^{2+}$-ions induce a unidirectional alignment of the fibers and formation of bundles that can be drawn from solution in the form of strings. Application of UV-light triggers bending of the string in water and air performing work of about 0.05 µJ when weight is attached, e.g. a small piece of paper. Besides the ability to conduct motion at macroscopic scale, the combination of single fibers in bundles and the accompanied amplification of their actuation clearly reminds of naturally occurring muscle structures.

### 2.4.1 Basic Considerations

Several requirements for the development of stimuli-responsive materials that exhibit a large change of size and shape upon excitation must be considered, i.e. the responsive moiety to be employed, the appropriate number of addressable units, and the overall size and architecture of the targeted system.[11] As can be concluded from the previous chapter, azobenzenes are perfect candidates for the development of scaffolds that amplify geometrical changes, due to their high stability, reliable isomerization properties, and the already featured large geometrical change of the single molecule triggered by photoisomerization. Nonetheless, there are other light-responsive compounds that perform better regarding structural alterations, e.g. indigo derivatives enabling a nearly 180° isomerization about the carbon-carbon double bond. However, the availability of numerous azo derivatives, their known characteristics, as well as their many applications provide a reliable and easily accessible basis for the current project, which is of greater benefit than a less-investigated photoswitch that undergoes slightly larger geometrical changes upon isomerization.

Aiming to boost the extent of the structural transformation after switching, the responsive units should be incorporated in systems of greater dimension, such as polymers, that are able to reproduce the changes induced by photoisomerization of the single responsive moiety. In this regard, these systems must provide a certain level of rigidity since too flexible designs will adapt to minor geometrical disturbances within short range not causing a response of the whole macromolecule. Confirming this assumption, several dendrimer generations of flexible (benzyl-linkers) and rigid (alkyne-linkers) design were synthesized in the group of McGrath to compare the effect of isomerization on the change of the hydrodynamic volume ($V_h$). They found that dendrimers of the same generation undergo a much larger shift of V upon irradiation when following a rigid architecture as depicted for the third generation in Figure 15, left side ($\Delta V_{h\text{-flexible}} \approx 5\%$, $\Delta V_{h\text{-rigid}} \approx 23\%$).[46] Besides rigid polymers, reversible aggregation processes exploiting non-covalent interactions allow the creation of greater structures. In this regard, switching does not only occur between a larger and smaller version of the same molecule but a transformation between the aggregate and its single components is conceivable. Depending on the substituents of the photochromic molecules, possible non-covalent interactions comprise van-der-Waals and dipole-dipole interactions, hydrogen bonds, ππ interactions, and solvophobic effects. Especially the last three examples hold potential because they require certain geometrical features or polarity characteristics that can be changed by azobenzene isomerization.

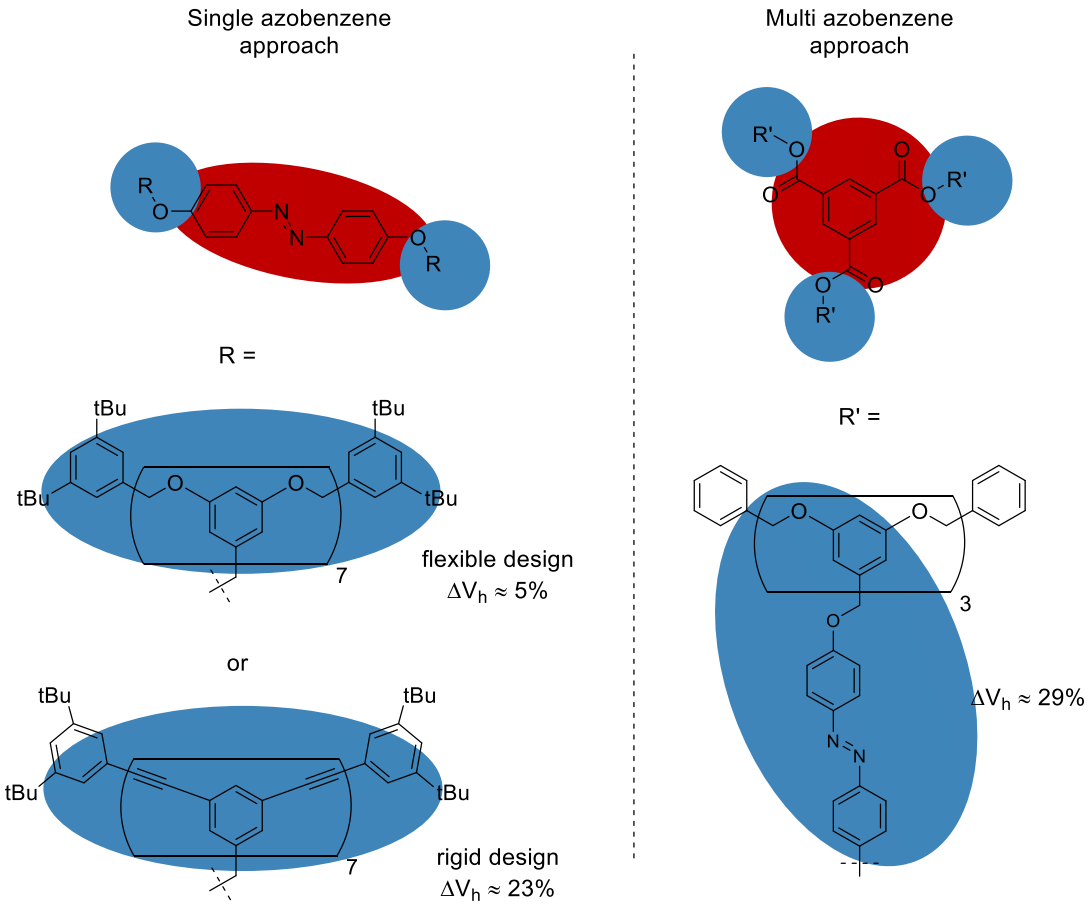


**Figure 15.** Comparison of flexible and rigid dendrimer architectures containing variable numbers of azobenzene according to their change of hydrodynamic volume ($\Delta V_h$) upon isomerization, the rigid design as well as the multi azobenzene approach exhibits a significantly higher $\Delta V_h$ of about 23% and 29%, respectively, in contrast to the flexible single azobenzene strategy ($\Delta V_h \approx 5\%$), the core units are highlighted in red while the dendrimer arms are colored blue, the numbers at the boxes (x) represent the total quantity of the enclosed unit in the final dendrimer, the corresponding generation (g) can be calculated according to $g = \log_2(x+1)$.[46-47]

In this context, the formation of anisotropic structures such as fibers and helices would be particularly advantageous as their existence relies on highly ordered components that might be disturbed even by minor geometrical changes holding potential for large deformations by cooperative effects. However, the transformation from one configuration to the other must be envisioned as a motion through space that requires enough void to operate. Hence, too constricted architecture or too densely packed materials must be avoided as they might limit efficient photoswitching and do not allow repeated dynamic contraction and expansion cycles.

Subsequent to the choice of an appropriate photo-responsive basis, the incorporation of a high number of azobenzenes in the targeted system is desirable for increasing the amount of contractile elements which contribute to the overall geometry change. In Figure 15, top left and right, two dendrimer designs of similar structure and hydrodynamic radius containing either one[46] or three[47c] azobenzene units in their core are shown. While for the former V varied by

about 5%, in the latter case the change was about six times as high ($\Delta V_h \approx 29\%$, Figure 15). However, when striving for high PSS compositions, it is important to note that the close association of several excitable moieties can have a detrimental impact on the switching efficiency, namely if the overall extinction becomes too high rendering excitation of the whole material impossible or due to distribution of the excitation energy among responsive units in conjugation. While the former point can be easily controlled by carefully selecting the concentration of absorbing groups during preparation of the final system, the latter must be respected in the early stages of synthesis. Efficient decoupling strategies for polyazobenzenes were developed by breaking the conjugation via either connections of aliphatic nature,[48] substitution in *meta* position,[49] or introduction of large twist angles between the aromatic units.[50] Therefore, although a maximized number of photoswitches is pursued, the optical density of the final material as well as rigorous decoupling of the photo-responsive units must be taken into consideration.

Respecting the aforementioned points, a system undergoing a large change of the hydrodynamic volume after isomerization was developed by synthesizing linear rigid-rod azobenzene polymers as depicted in Figure 16.[51]

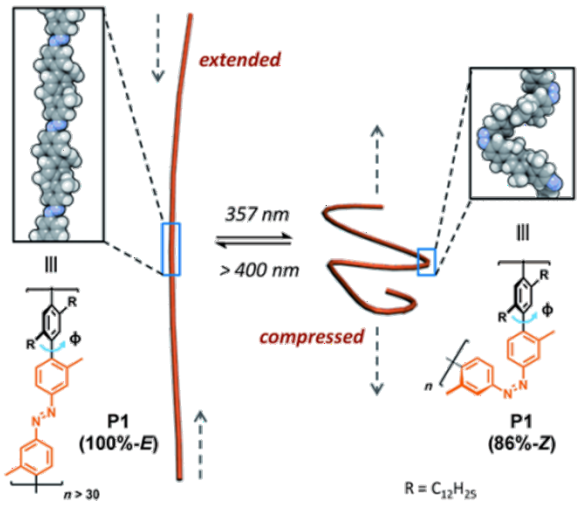


**Figure 16.** Linear rigid-rod azobenzene polymer exhibiting a large change of hydrodynamic volume ($\Delta V_h = 72\%$) upon isomerization, the high PSS composition is a result of a strict decoupling strategy by introduction of large twist angles between the aromatic rings.

The rigid backbone contains on average more than 30 repeating units and exhibits a high aspect ratio. The decoupled azobenzene moieties efficiently isomerize from an extended to a compressed structure (PSS composition of about 86% *Z* isomer) accompanied by a $\Delta V_h$ of 72%.

# 3 Conceptual Thoughts and Molecular Design

## 3.1 Basic Concept

Summarizing the previous chapters, the following main conditions must be met when creating a new system based on azobenzene that undergoes a dramatic geometrical change upon photoisomerization.

- Incorporation of the responsive moiety in macromolecular scaffolds
- Integration of a high number of switchable elements
- Construction of rigid architectures
- Integration of anisotropic characteristics

The rigid-rod polymers depicted in Figure 16 offer an excellent starting point for the new light-responsive system since all the aforementioned requirements are already met.[51] Furthermore, for a similar polymer design exhibiting less solubilizing groups, the publication describes the formation of spherical aggregates in non-polar organic solution. Aiming to gain full control over the assembly process, exchanging the hydrophobic design for an amphiphilic one should allow the formation of cylindrical micelles in aqueous medium (Figure 17).

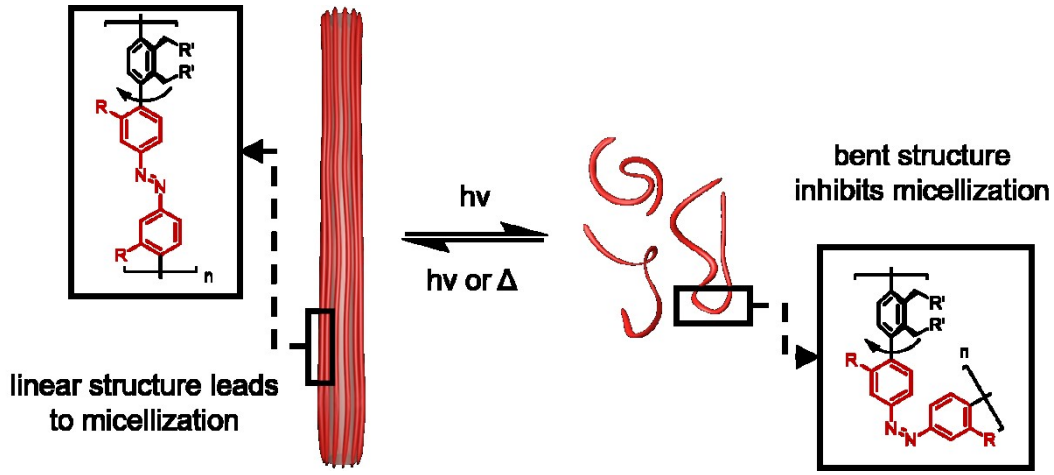


**Figure 17.** Conceptual illustration of the targeted light-responsive system based on an amphiphilic rigid-rod polymer that dramatically changes size and shape upon photoisomerization of the azobenzene units, the formation of cylindrical micelles is disturbed by the bended structure of the polymers *Z* state leading to a complete disappearance of the aggregates at best, R and R' denote hydrophilic and hydrophobic groups, respectively.

In this case, photoinduced shrinking of the single polymer chains upon $E \rightarrow Z$ isomerization should efficiently disassemble the micelles. Assuming that the linear structure of the rigid polymers would

be necessary to form micelles of cylindrical shape, a potential cooperative effect might be observed as soon as the number of straight polymer chains is below the critical micelle concentration (CMC). Additionally, the CMC should rise upon isomerization due to the higher polarity of *Z* azobenzene and the accompanied better solubility in water.

## 3.2 Molecular Design and Retrosynthesis

The targeted polymer comprises an aromatic backbone with side chains of hydrophilic (head group) and hydrophobic (tail) nature. Normally, the size of these substituents and their occupied volume is highly important when striving for specific micelle geometries. The rigid linear structure of the azo macromolecule, however, determines a cylindrical aggregation shape since assembling into spherical objects would require unfavored bending of the rods under the assumption that polar and non-polar groups can only aggregate among similar moieties. Nonetheless, the hydrophilic outer shell of micellar aggregates is larger in comparison to the lipophilic interior space when considering the circular cross section of the cylinder. Hence, the hydrophilic groups should be attached to the azobenzene aromatic rings which occupy more space than the single phenyl linker.

Typical lipophilic substituents for the formation of micelles and vesicles are alkyl chains of different size in which especially dodecyl chains have been proven suitable in numerous publications. Furthermore, this group is already present in the original polymer design providing a starting point for synthetic considerations. However, modifications are required in order for both $C_{12}$-chains to point in the same direction, hence facilitating the aggregation. On the polar side, many water solubilizing moieties are available with glyme chains, ammonium ions, and sulfonates being the most popular. The former holds the advantage of no charge which simplifies synthesis and avoids influence of counter ions on micelle formation. The hydrophilic and hydrophobic groups are attached in *ortho* position with respect to the bond between the azobenzene and the phenyl linker inducing a twist angle necessary for electronic decoupling and thus efficient photoisomerization leading to high PSS compositions.

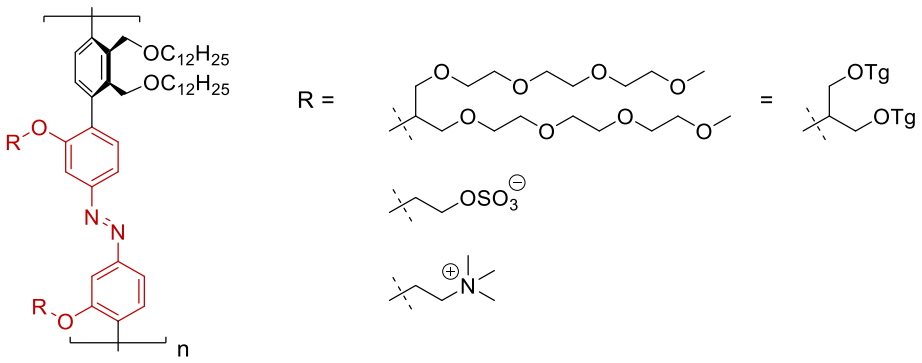


**Figure 18.** Final design of the polymer potentially forming cylindrical micelles in aqueous medium, two dodecyl chains at the phenyl linker and two polar groups, i.e. triglyme derivative, sulfate, ammonium ion, at the azobenzene constitute the amphiphilic properties, the triglyme derivative is the first target since there is no charge involved facilitating the synthesis and the micelle formation due to the absence of counter ions.

The final design is depicted in Figure 18. The phenyl linker bears two dodecyl chains pointing in the same direction that are attached in the form of alkoxides at benzylic position. The azobenzene unit has oxygens in two *meta* positions that can be easily substituted by different polar groups via etherification. The triglyme derivative is the first target due to the reasons mentioned above.

Two pathways can be followed for the synthesis of the polymer, i.e. the Suzuki polycondensation approach and the polyazo coupling approach (Figure 19).

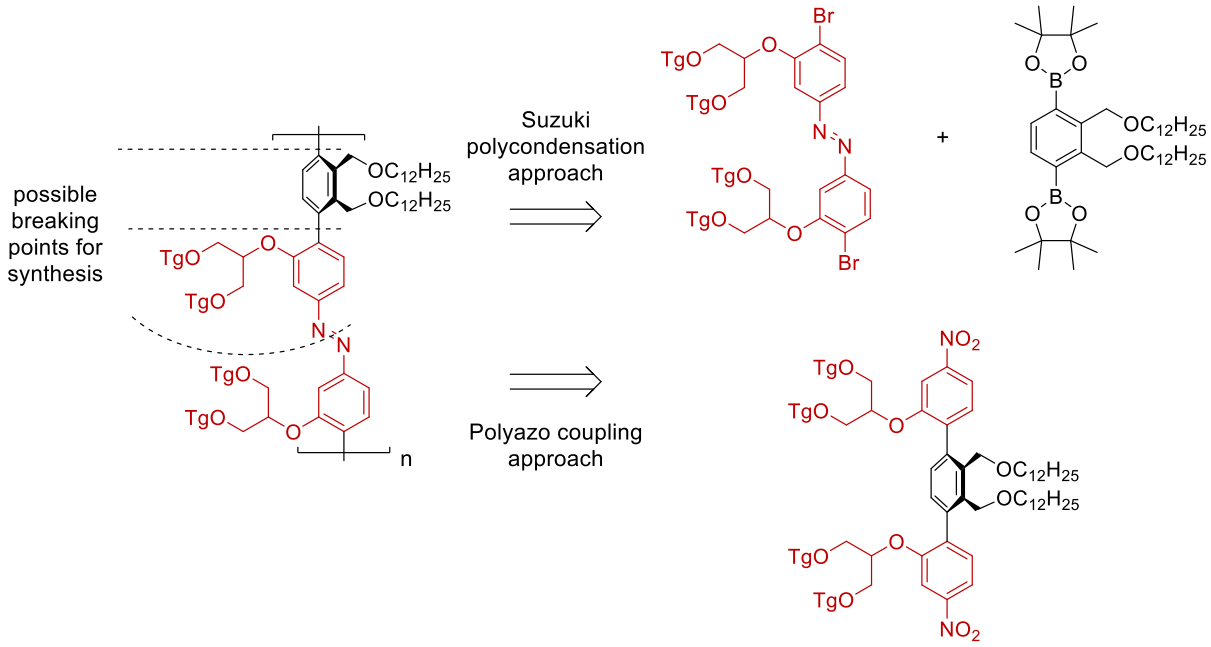


**Figure 19**. Two retrosynthetic pathways can be followed towards the amphiphilic polymer, i.e. the Suzuki polycondensation approach (top) and the polyazo coupling approach (bottom); while synthesis of both monomers for the Suzuki reaction is easier, material of high purity is needed to meet the exact 1:1 stoichiometry; the azo coupling require only one monomer which is more difficult to make due to a higher degree of functionalization.

In the former case, the polymer backbone is dissected between the aromatic rings yielding two synthetic equivalents that are cross-coupled by a Suzuki reaction. The advantage of that method is the usually easier accessibility of the monomers since they are not as highly functionalized as a monomer exhibiting all substituents at once. The drawback, however, is the requirement of ultrapure materials because exact stoichiometry is of great importance when striving for products of high molecular weight in an $A_2 + B_2$ polymerization. Even slight deviations from a 1:1 ratio can result in significantly smaller macromolecules. In contrast, the second approach displays opposite characteristics, i.e. stoichiometry is negligible as only one monomer exists, however, the combination of all functional groups in one molecule renders synthesis more difficult. The strategy of the polyazo coupling was followed already by Wiktorowicz et al. with good results employing Red-Al as reductive agent.[52]

First, the Suzuki polycondensation approach is followed since the easier synthesis gives potentially faster access to polymeric material.

# 4 Results and Discussion

## 4.1 Rigid Rods by Suzuki Polycondensation

### 4.1.1 Synthesis and Compound Characterization

The synthesis of triglyme substituted azobenzene monomer **5** and bisboronic ester monomer **11** is depicted in Scheme 1 and Scheme 2, respectively.

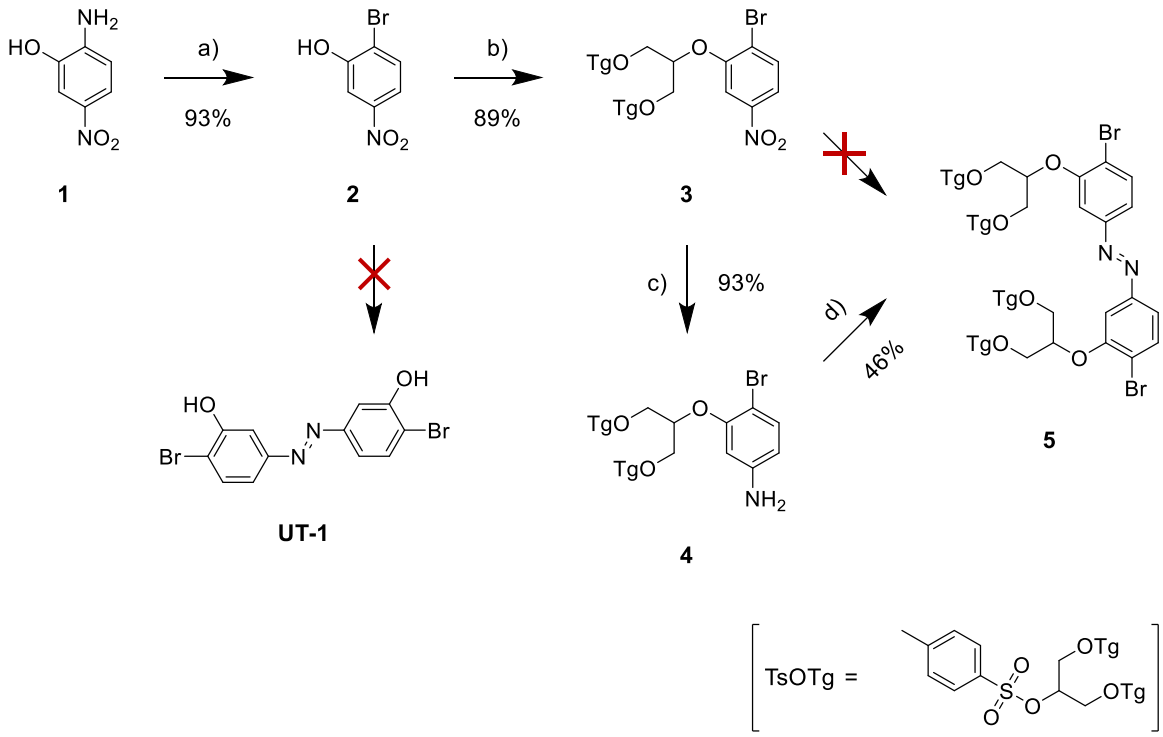


**Scheme 1.** Synthesis of triglyme substituted azobenzene monomer **5**, a) 1) aqueous HBr (24% w/w), $NaNO_2$, 0 °C, 20 min 2) CuBr, RT → reflux, 2 h, b) argon atmosphere, $K_2CO_3$, TsOTg, dry DMF, 80 °C, 24 h, c) argon atmosphere, Fe, $NH_4Cl$, EtOH, $H_2O$, 80 °C, o/n, d) air ($O_2$), CuBr, pyridine, toluene, 60 °C, 20 h.

The preparation of monomer **5** was started from commercially available *2*-amino-*5*-nitrophenol (**1**) that was subjected to a Sandmeyer reaction according to standard procedures. In this process, the aniline derivative is converted into the corresponding diazonium salt by means of $NaNO_2$ in acid medium carefully maintaining temperatures below 5 °C to avoid elimination of nitrogen gas. Subsequent addition of CuBr as redox catalyst accompanied by a gradual rise of the reaction temperature triggers the replacement of nitrogen by bromide via formation of an aromatic radical intermediate.

Several attempts to form azobenzene derivative **UT-1**, an easily modifiable monomer precursor exhibiting free phenols, by reductive coupling of *2*-bromo-*5*-nitrophenol (**2**) remained unsuccessful. Neither Al or Zn in basic solution nor the Mg/triethylammonium formate reductive

system by Pamar et al.[31b] or hydrosilane in combination with an indium catalyst developed by Sakai et al.[53] yielded the target structure but complete reduction to the aniline or, in the latter cases, slow decomposition of the starting material was observed. Preparation of **UT-1** by Mills reaction equally failed because the corresponding nitroso derivative of **2** was synthetically not accessible. Given that free phenols usually render reductive and oxidative azo couplings difficult, the synthetic route was successfully continued by introduction of the triglyme substituent via Williamson etherification. In this regard, the triglyme tosylate derivative TsOTg should be employed stoichiometrically and not in excess since separation of both starting materials is highly difficult due to their very similar properties that are mainly governed by the polarity of the triglyme chains. In contrast to compound **2**, the reductive coupling of nitro derivative **3** by means of Al or Zn under basic conditions yielded the corresponding azobenzene **5**, however, only in combination with the singly and doubly de-halogenated species that were impossible to remove from the final product. Alternatively, nitro benzene **3** was converted into aniline **4** employing Fe/$NH_4Cl$ as reductive agent. The conversion of **4** by a Cu(I)/pyridine-catalyzed oxidative coupling procedure and $O_2$ from the air as oxidant provided monomer **5** as an orange oil.

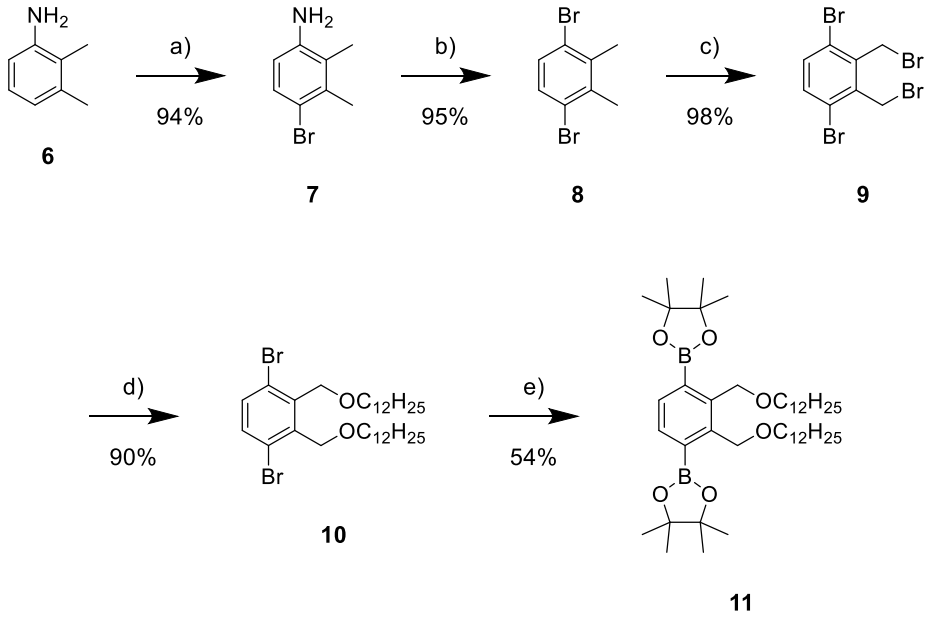


**Scheme 2.** Synthesis of bisboronic ester monomer **11**, a) NBS, DMF, 0 °C, 5 h, b) *p*TSA, $N(Bu)_4Br$, $CuBr_2$, $^tBuONO$, MeCN, RT, o/n, c) NBS, DBPO, MeCN, reflux + hν (500 W), 3 h, d) 1) argon atmosphere, *n*-$C_{12}H_{25}OH$, NaH, dry THF, RT, 2 h, 2) **9**, RT, o/n, e) argon atmosphere, bis(pinacolato)diboron, KOAc, $Pd(dppf)Cl_2$, dioxane, 80 °C, o/n.

The first synthetic step towards monomer **11** was the bromination of commercially available *2*,*3*-dimethylaniline (**6**) which, due to the electron donating nature of the amino group, can equally occur in *ortho* and/or *para* position. The selected reaction conditions, however, yielded exclusively the desired *para* product, which was proven by $^1$H-NMR analysis of the subsequent step

(Sandmeyer reaction) in which a symmetrical benzene derivative **8** was obtained. In this case, the standard Sandmeyer procedure had to be changed as only low yields of compound **8** were obtained and the formation of a significant amount of the corresponding phenolic species was observed. Accordingly, the reaction was conducted employing water-free reagents in acetonitrile solution which improved the yield from about 30% to over 90%. The radical bromination of **8** was first conducted in chloroform, however, only low yields of compound **9** and the formation of several byproducts were observed. These results could be dramatically improved by exchanging the solvent for acetonitrile and the use of fresh *N*-bromosuccinimde providing an NMR-clean material without further purification. The subsequent Williamson etherification employing in-situ prepared sodium dodecane oxide as nucleophile introduces the hydrophobic substituents for the final polymer. Eventually, monomer **11** was obtained by Miyaura borylation of compound **10**. Several attempts to increase the moderate yields were made, i.e. employment of another boron source (pinacolborane), another catalytic system (Ni), and borylation via halogen-metal exchange ($^{n}$BuLi, $^{t}$BuLi, Grignard). However, no improvement was accomplished and the corresponding monoboronic ester as well as dehalogenated species remained as typical byproducts.

Highly pure materials as well as a strict 1:1 stoichiometry of both monomers are essential for a successful $A_2 + B_2$ polymerization when targeting a product of high molecular weight.

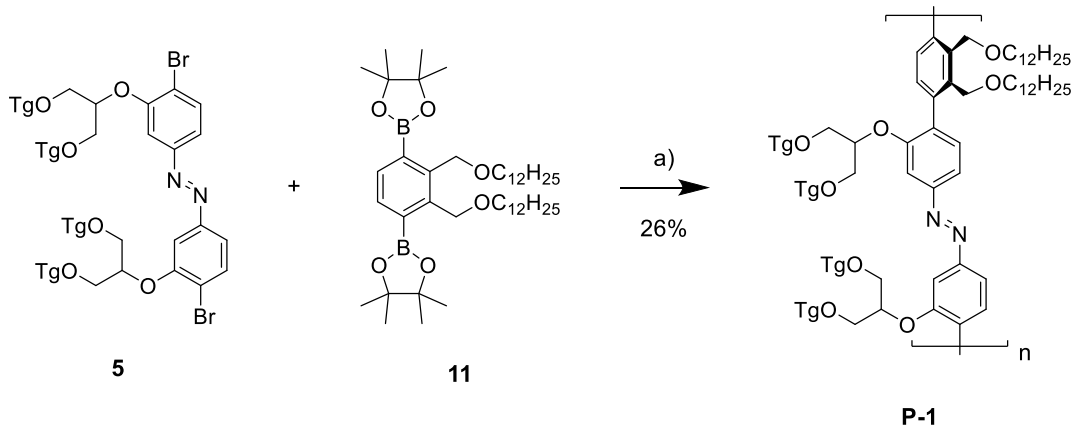


**Scheme 3.** Polymerization of azobenzene monomer **5** and boronic ester monomer **11** by Suzuki cross-coupling yielding amphiphilic polymer **P-1**, the linear polyaromatic backbones provides rigidity while *ortho* substituents at the bond between azobenzene and phenyl linker induce twist angles to decouple the photochromic units, a) the 1:1 stoichiometry of both monomers is strictly respected, argon atmosphere, the mixture was degassed by three freeze-pump-thaw cycles, $K_3PO_4$, $Pd(OAc)_2$, SPhos, toluene/water, 100 °C, 3 d.

However, even at low temperatures (-20 °C) azobenzene monomer **5** as well as boronic ester monomer **11** are viscous liquids rendering repeated recrystallization, the typical final purification step for monomers, impossible in this context.

In order to compensate for the inapplicability of the standard procedure, each compound was purified by flash column chromatography three times and only the middle fractions were combined. After the high purity of the starting materials was certified by NMR analysis, both monomers were subjected to a Suzuki polycondensation as depicted in Scheme 3. The exact stoichiometry was ensured by preparation of stock solutions in toluene and weighting out the appropriate mass of these solutions into a sealed tube. Palladium in combination with the SPhos ligand was employed as catalytic system, which facilitates coupling of sterically demanding molecules.

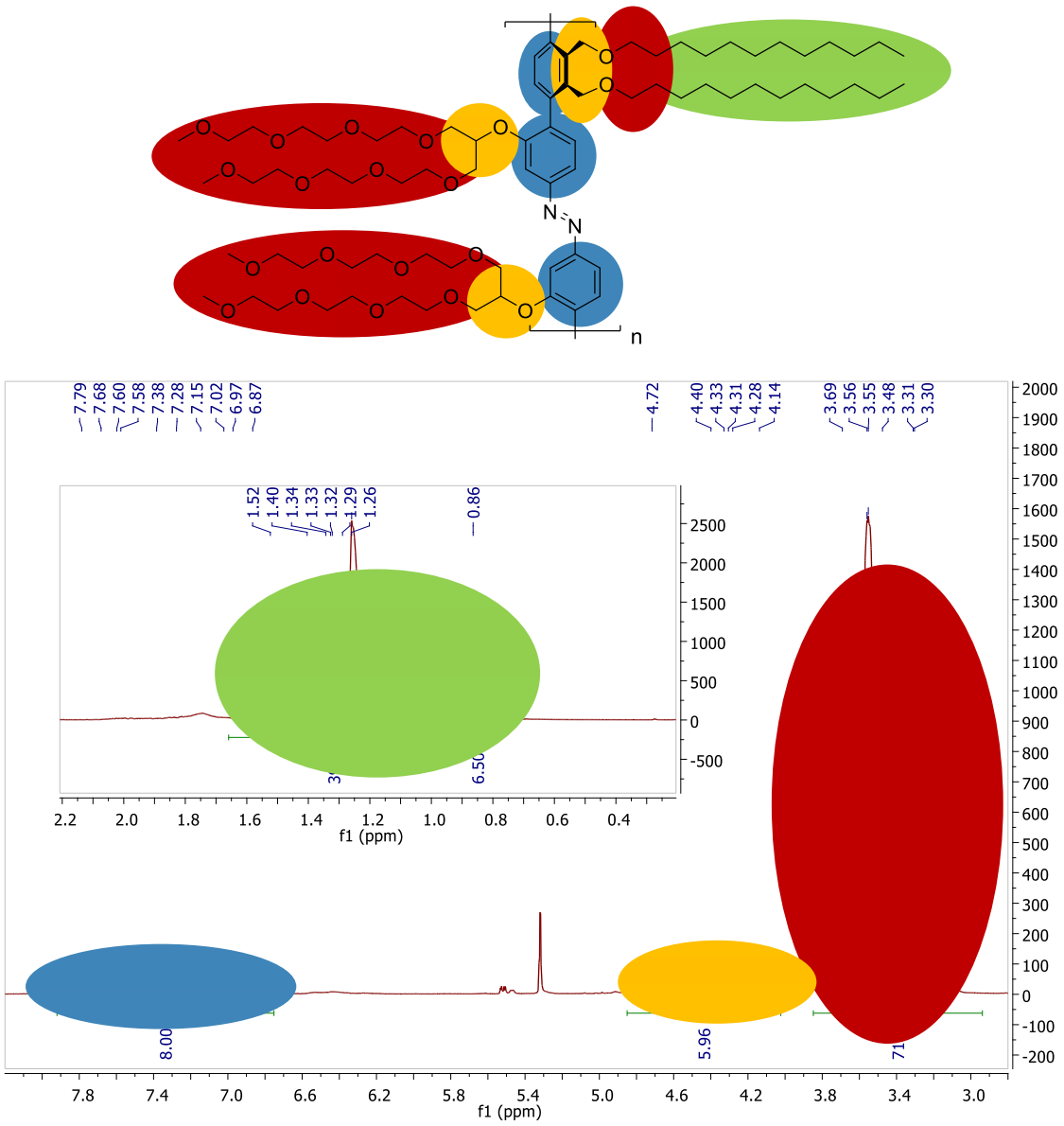


**Figure 20.** $^{1}$H-NMR (300 MHz) spectrum of polymer **P-1** in DCM-$d_2$, the broad signals can be distinguished in four major areas each representing multiple protons, slight impurities originating from THF (GPC eluent) are obvious, blue: aromatic protons, yellow: benzylic and tertiary protons, red: triglyme and ether protons, green: dodecyl protons.

The reaction was run for three days, the crude product purified by preparative GPC, and the final material analyzed by NMR spectroscopy (Figure 20), UV/vis spectroscopy, and GPC.

The NMR spectrum exhibits broad signals typical of polymeric species rendering the assignment of specific protons difficult. Four major areas can be differentiated representing the aromatic region (blue), the benzylic and tertiary protons (yellow), the triglyme and ether protons (red), and the remaining dodecyl protons (green). All integrals match the expected number of hydrogen atoms, however, a determination of the degree of polymerization by integration is not feasible due to the lack of distinct end groups. Slight impurities originating from THF (GPC eluent) are detected as well but will not interfere with further analysis as they do not absorb in same wavelength area.

Subsequently, the UV/vis spectroscopic properties and the molecular mass of the polymeric material were investigated giving information about if and how many of the photoresponsive elements had been incorporated in the polymer backbone. The UV/vis absorption spectra before and after irradiation as well as the corresponding GPC traces are depicted in Figure 21a and b, respectively.

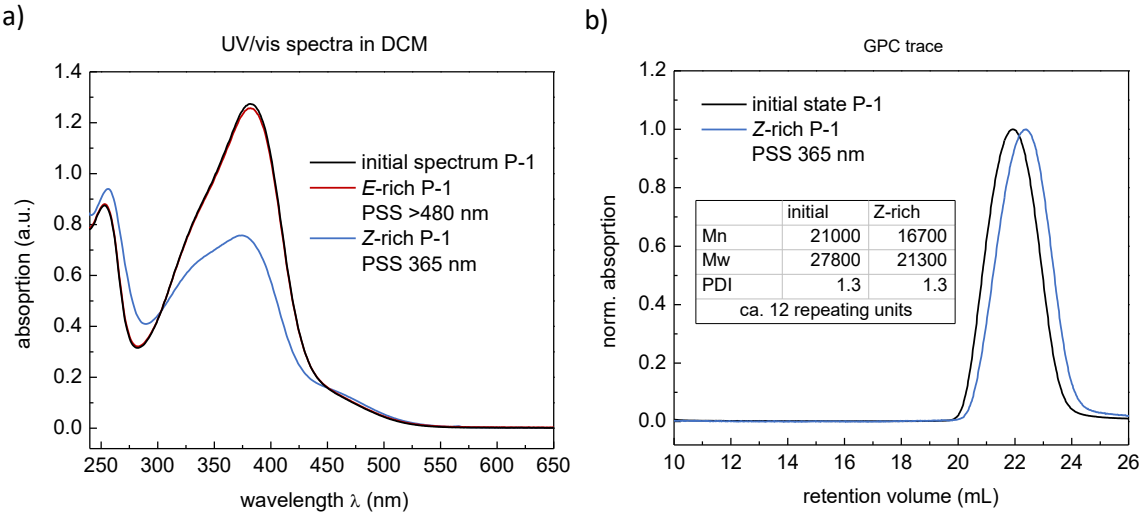


**Figure 21.** a) UV/vis absorption spectra of polymer **P-1** in DCM exhibiting varying *Z* isomer content, the initial spectrum of the freshly prepared solution (black), the Z-rich spectrum obtained after irradiation at 365 nm (blue), and the spectrum related to the PSS at > 480 nm (red), b) GPC traces vs. PS standards of the freshly prepared solution of **P-1** in THF and after irradiation at 365 nm until PSS was reached, the average molecular weight decreases by approximately 20%, with respect to $M_n$ of the *Z*-rich state the polymer contains 12 repeating units on average (M(repeating unit) = 1418 g/mol).

Irradiation of the polymer at 365 nm in DCM solution induces isomerization to a *Z*-rich photostationary state while light > 480 nm triggers the reverse process. However, precise determination of the corresponding *E*/*Z* compositions by NMR analysis was unsuccessful due to the strong overlap of the signals belonging to both isomers. Considering the shape and relative

intensity of the blue spectrum in comparison to the data obtained for monomer **5**, an estimation of about 40% of *Z* isomer appears reasonable (azobenzene **5** reaches 90% *Z* isomer under the same conditions). In contrast, excitation in the visible region almost completely restores the initial spectrum indicating nearly quantitative conversion to the all-*E* configuration. A reason for the low yield of *Z* isomer might be insufficient decoupling of the azobenzene moieties. DFT computations indicate a higher energy difference between the planar (highest steric interaction) and perpendicular (lowest steric interaction) structure of biphenyls bearing methyl or methylene-linked groups in comparison to derivatives bearing oxygen substituents in *ortho* position to the connecting bond (Figure 22). An energy difference of $\Delta E_h$ = 192.52 kJ/mol was calculated for the *tetra*-ethyl-substituted biphenyl while $\Delta E_h$ = 119.19 kJ/mol was obtained for the *tetra*-methoxy derivative.

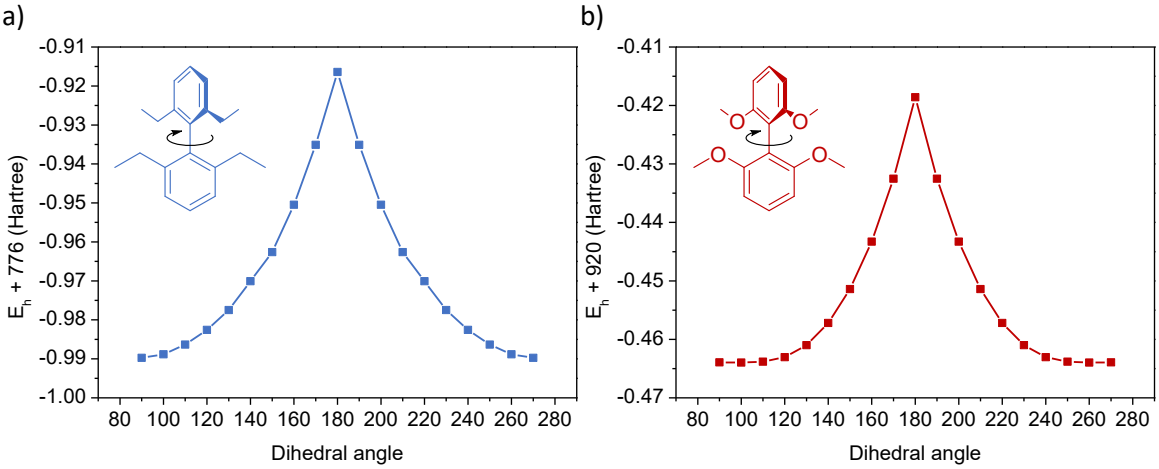


**Figure 22.** DFT scans of the total energy $E_h$ of a) *2,2',4,4'*-tetraethylbiphenyl (blue) and b) *2,2',4,4'*-tetra-methoxybiphenyl (red) in vacuum, the energy difference between the planar and perpendicular structure is larger for the ethyl derivative suggesting a larger dihedral angle between the phenyl rings, $\Delta E_h$ (ethyl) = 192.52 kJ/mol and $\Delta E_h$ (methoxy) = 119.19 kJ/mol, for the computations the dihedral angles were fixed at the given values (90° - 180°, 10° per step), all other parameters were optimized (HSEH1PBE/6-31+g(d,p)), the mirror image of the data is depicted, too, for better clarity (dihedral angles >180° were not calculated as they equal the corresponding dihedral angles subtracted by 90°).

Albeit a high PSS is desirable when aiming to control micellization processes, cooperative effects might compensate for the lower conversion to the bended state. Nonetheless, the photochromic behavior of the polymer was verified indicating that azobenzene units remain intact after polymerization.

The size of the macromolecules was determined by GPC analysis before and after irradiation with 365 nm light. In this process, a change of the number average molecular weight $M_n$ by approximately 20% from 21000 to 16700 g/mol for the *E* and *Z* configuration, respectively, is induced. These values, however, are based on a polystyrene calibration which highly overestimates the real molecular size in case of rigid linear architectures. Nonetheless,

considering the relative shortness of the chains and the folded structure of the *Z* configuration, sufficient similarity with the polystyrene standard can be assumed. Hence, a number of 12 repeating units on average appears to be a reasonable approximate value which was obtained by dividing the molar mass of the *Z*-rich species from GPC analysis by the mass of the repeating unit.

### 4.1.2 Scattering Experiments and Formation of Micelles

Even though the molecular weight of the polymeric material is relatively low, the formation of micelles in aqueous medium was tested. However, all attempts to obtain aqueous solutions of higher concentrations than those used for UV/vis spectroscopy failed. Neither elevated temperatures, exposure to ultrasound, or the combination of both, nor the addition of THF or DCM solutions of **P-1** into rapidly stirred water or vice versa provided a stable aqueous sample. Instead, precipitation and sedimentation occurred within seconds to minutes. Even in small spectroscopy concentrations, the samples remained slightly turbid indicating the formation of aggregates, which was independent of the switching state. The corresponding spectra are depicted in Figure 23a, the spectra in DCM are presented again for better comparability.

The major difference in spectroscopic properties is the lower amount of *Z* isomers in water reached upon excitation at 365 nm supporting the assumption that larger aggregates are forming in aqueous medium. However, no shift of the absorption maxima and no broadening of the excitation bands is observed implying the assembly of the macromolecules into undefined aggregates without well-defined π interactions.

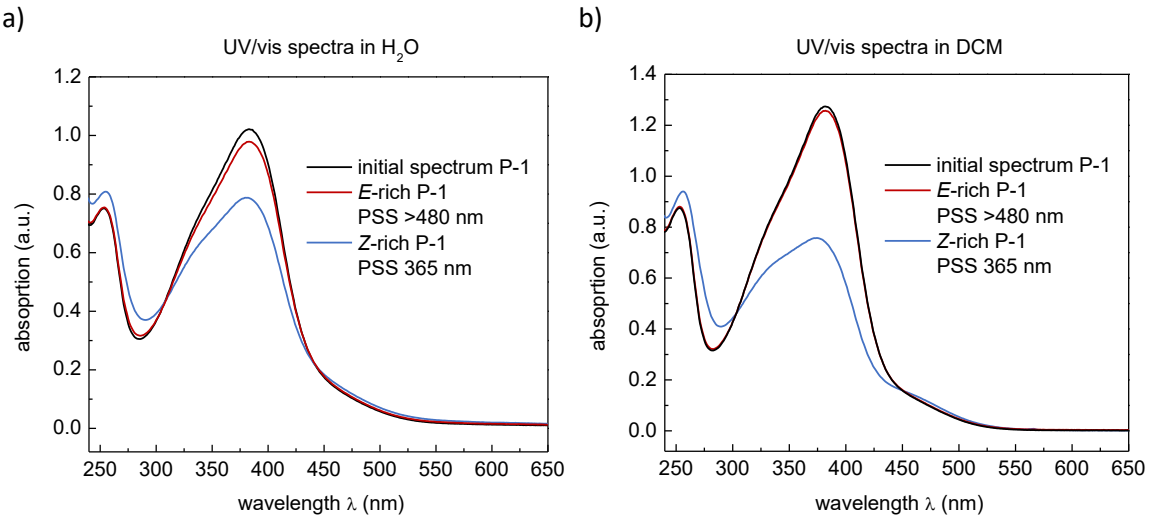


**Figure 23.** Spectra of polymer **P-1** in a) water and b) DCM, the initial spectrum of the freshly prepared solution (black), the Z-rich spectrum obtained after irradiation at 365 nm (blue), and the spectrum related to the PSS at > 480 nm (red), the PSS composition obtained after irradiation at 365 nm in water yields less *Z* isomer than in DCM possibly related to the formation of rigid aggregates of undefined nature.

Subsequently, the preparation of samples of **P-1** in water/THF mixtures was tested. A maximum of 25% (v/v) water in THF allowed the formation of clear polymer solutions that were analyzed by small-angle X-ray scattering (SAXS, Figure 24) as well as static and dynamic light scattering (SLS and DLS, respectively). For comparison, the pure THF solutions were investigated, too.

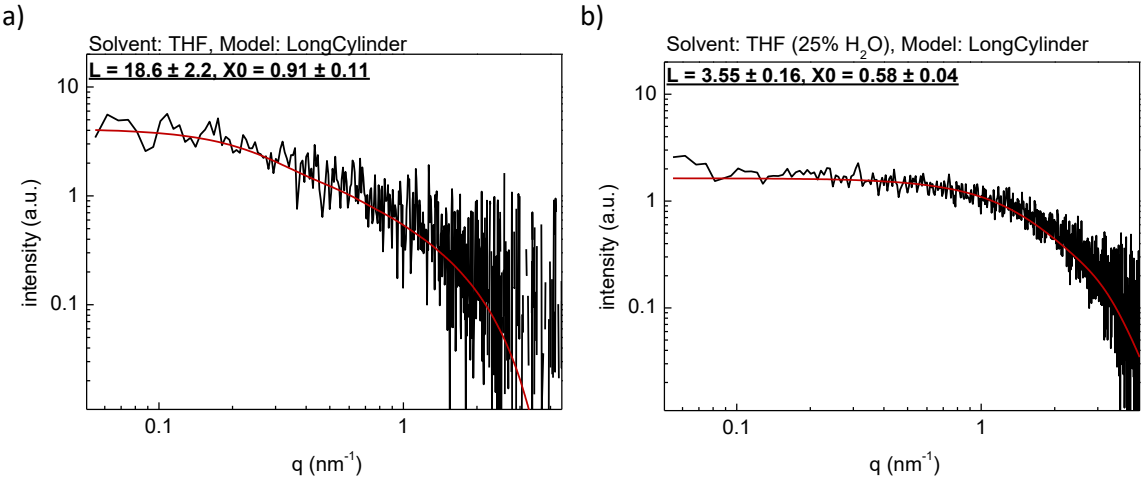


**Figure 24.** Small-angle X-ray scattering of solution of **P-1** (20 mg/mL) in a) THF and b) THF containing 25% (v/v) of water, the addition of water causes shrinking of the cylindrical objects from approximately 19 nm to 4 nm in length, this unexpected finding can be rationalized by the formation of aggregates that are too big to be detected by SAXS (> 70 nm) while objects of small molecular weight remain.

The SAXS experiment in THF (c = 20 mg/mL) revealed the presence of cylinder-shaped objects that exhibit a high persistence length supporting the polymers rigid nature. On average, the cylinders possess a length of 18.6 nm corresponding to 13 repeating units by assuming 1.4 nm per repeating unit, which is in good agreement with the degree of polymerization of 12 obtained by GPC analysis. Turning to the aqueous mixture, however, shrinking of the rod-like objects by about 80% is observed. Assuming that the addition of water must induce the aggregation of the polymer chains, this finding can be explained by the formation of assemblies that are too big for SAXS analysis (objects > 70 nm) and, thus, only the remaining species of low molecular weight are detected. Further investigation by SAXS was not possible due to the narrow size window of this method and the significant amount of material required that, in addition, prevented switching experiments because of the solution's high optical density.

Lower concentrated solution can be employed for light scattering experiments that also allow the coverage of a broader size window ranging from several nanometers to micrometer regime. Primarily, polymer samples in pure THF at a concentration of 1 mg/mL before and after irradiation at 365 nm were measured (Figure 25). The data points highlighted in red are spikes and, therefore, not included in the evaluation process.

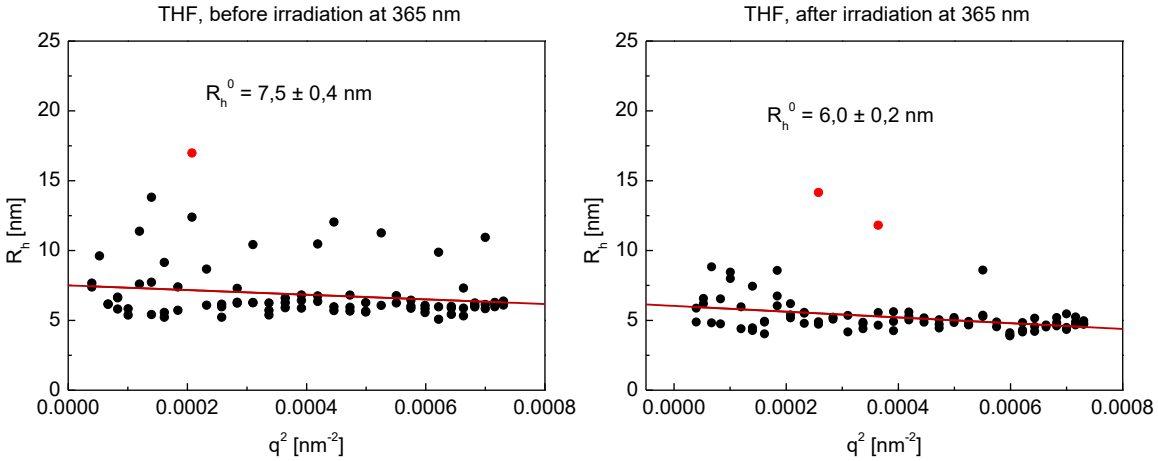


**Figure 25.** Dynamic light scattering experiments of polymer **P-1** in THF solution a) before and b) after irradiation at 365 nm and extrapolation of the hydrodynamic radius to zero scattering vector (q), a decrease of the $R_h$ of about 20% upon isomerization from the *E*-rich to the *Z*-rich configuration is observed, the relatively low polydispersity of the sample is confirmed by the low dependency of the scattering vector on the diffusion coefficient, red data points are excluded for evaluation.

Similar to the SAXS experiment, DLS displays small objects with an average hydrodynamic radius ($R_h$) of 7.5 nm obtained by extrapolation to zero scattering vector. After photoisomerization, $R_h$ decreases by approximately 20% which equals a shrinkage of the hydrodynamic volume of about 49%. Moreover, no strong dependency of the diffusion coefficient on the scattering vector is observed confirming the relatively low polydispersity of the sample as indicated by GPC. In order to gain further information on the geometry as well as the molecular weight of the polymer a SLS analysis would be require. However, the macromolecules are too small to conduct static light scattering which requires a minimum hydrodynamic radius of about 10 nm.

The same experiments were attempted in THF/water mixtures, yet, no reproducible results were obtained. Numerous high spikes occurred during the measurements indicating the existence of large particles with a significant scattering cross section. Neither filtration or dilution nor irradiation of the samples provided results of acceptable quality, rendering the further analysis of the polymer in aqueous environment impossible.

### 4.1.3 Summary and Conclusion

The linear rigid-rod polymer obtained by the Suzuki polycondensation approach has a number-average molecular weight of about 16700 g/mol and approximately 12 repeating units as concluded from GPC analysis of the *Z*-rich configuration. These results were confirmed by SAXS (cylinder length = 19 nm) and DLS ($R_h$ = 8 nm) experiments. The polymer can be reversibly isomerized in water, DCM, and THF solution leading to a change in the hydrodynamic radius of about 20% in the latter case. However, the preparation of micelles in aqueous medium was

unsuccessful due to the low solubility of **P-1** in water. SAXS and DLS experiments in THF containing 25% (v/v) of water indicate the formation of large aggregates of undefined nature.

Given the fact that the analyzed material represents the fraction of highest molecular weight after purification by preparative GPC as well as the low yield, optimizations of the Suzuki polycondensation approach would be necessary when continuing to follow this route. Furthermore, both monomers are oily liquids which complicates purification to the required high level and precise adjustment of stoichiometry. The low water solubility additionally necessitates a change of the molecular design. Hence, turning to the one monomer approach by polyazo coupling which is insensitive to small impurities and stoichiometric deviations is obvious considering that only minor changes of the previous synthetic route are required.

## 4.2 Rigid Rods by Reductive Polyazo Coupling

### 4.2.1 Monomer Synthesis

Bearing the low water solubility of the previous design in mind, charged groups such as ammonium ions, sulfonates, and sulfates are good alternatives to triglyme chains providing stronger water-solubilizing characteristics. The charged substituents, however, must be integrated after the polymerization step since they are prone to reduction by Red-Al, the agent employed for conversion of the dinitro monomers into polyazobenzene. In contrast to $LiAlH_4$ which is more frequently exploited for the reductive coupling to azo compounds, Red-Al is perfectly soluble in common organic solvents. Polymerizations are usually accompanied by a gradual increase of viscosity potentially hindering proper stirring and mixing of the reaction system that would be highly detrimental for a heterogenous synthesis.

The synthesis of the first generation of dinitro terphenyl monomers is depicted in Scheme 4. In the initial step, *2*-Bromo-*5*-nitrophenol (**2**) is protected by conversion into the tetrahydropyranyl ether **12** which is stable under the basic conditions of the subsequent Suzuki coupling. In this regard, diboronic ester **11** can be re-used as coupling component yielding terphenyl derivative **13** in high yields which is facilitated by the use of SPhos, a typical ligand for sterically demanding cross-coupling reactions.

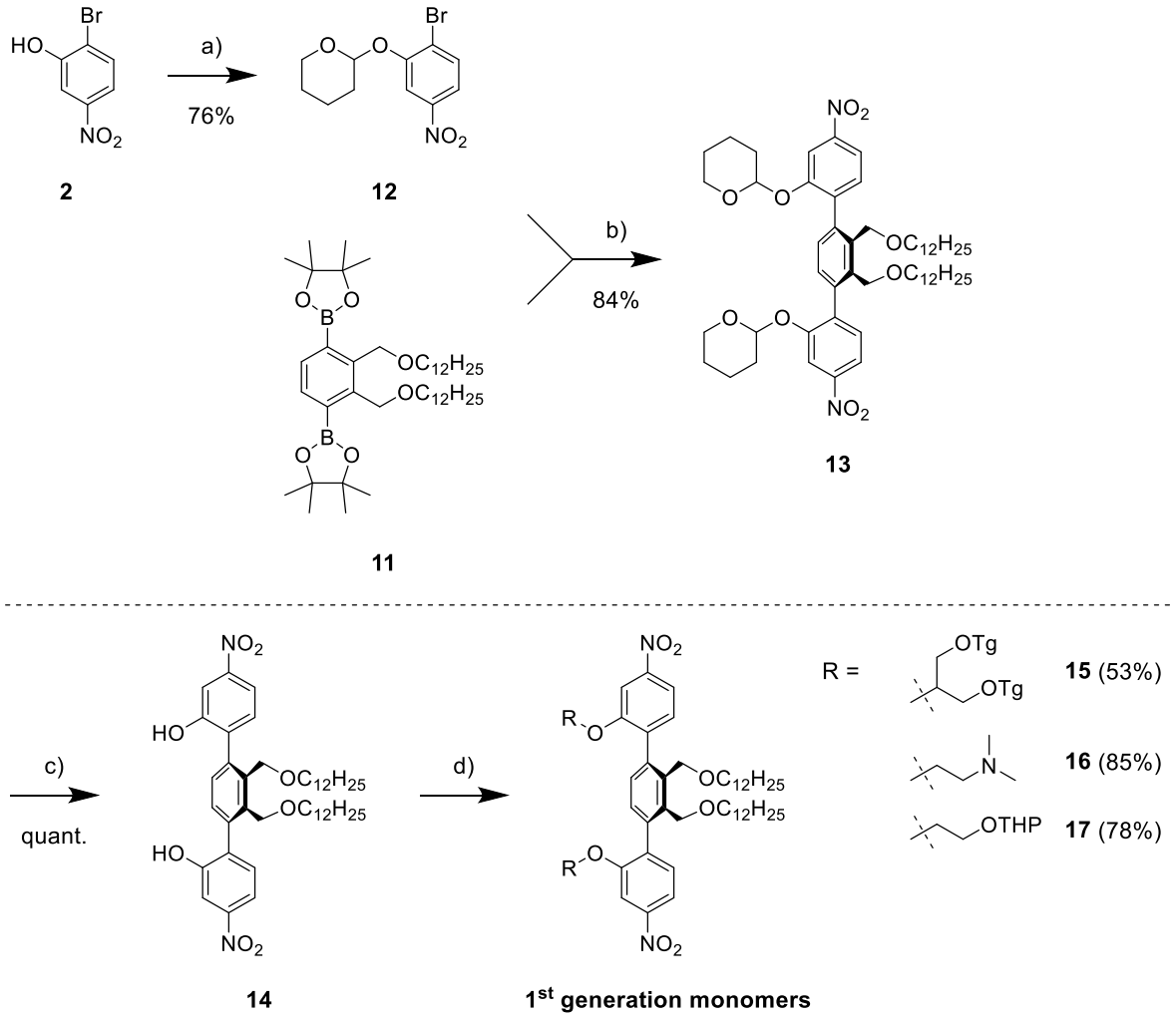


**Scheme 4.** Synthesis of the 1st generation monomers **15**-**17** to be employed in the reductive polyazo coupling, the triglyme substituted monomer **15** is additionally prepared for comparison of the polyazo coupling to the Suzuki polycondensation approach, a) *3,4*-dihydro-*2H*-pyran, *p*TSA, 0 °C, 2 h, b) $K_3PO_4$, $Pd(OAc)_2$, SPhos, toluene/water, 90 °C, o/n, c) *p*TSA, MeOH/DCM, RT, o/n, d) appropriate organic halide or tosylate, $K_2CO_3$ or $Cs_2CO_3$, acetone, reflux, o/n.

Successively, compound **13** is deprotected under acidic conditions and etherified with branched triglyme chains as well as the appropriate charged group precursors, i.e. a tertiary amine and a protected alcohol to be converted into ammonium ions and sulfates, respectively. Despite the low solubility of **P-1** in water, the triglyme substituted monomer **15** is also prepared for comparison of the reductive polymerization to the Suzuki polycondensation approach.

Two more generations of monomers were synthesized each slightly varying the structure of the phenyl linker in between the azobenzene units. The corresponding synthetic routes are depicted in Scheme 5. The preparation of diboronic ester **21** is started by double aromatic and benzylic bromination of commercially available *4*-methylbenzyl alcohol (**18**). In this process, the in-situ formed hydrogen bromide, side product of the aromatic substitution, triggers the conversion of the benzyl alcohol into the halide under cleavage of water.

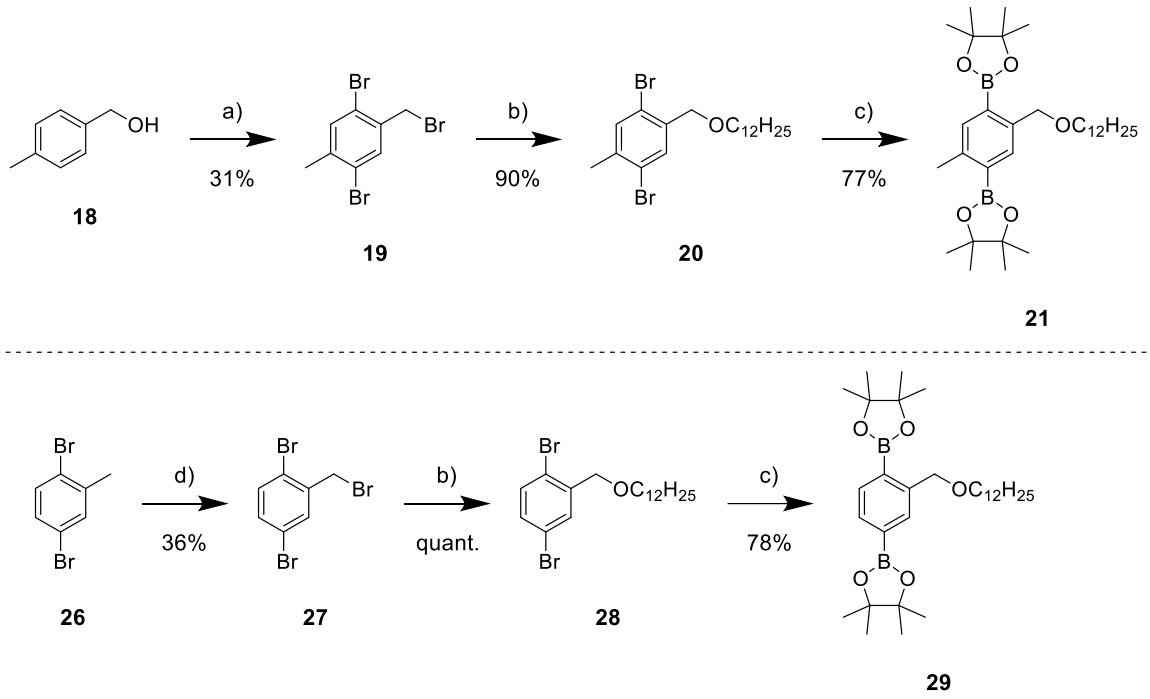


**Scheme 5.** Synthetic route towards diboronic ester **21** and **29** which exhibit only one dodecyl chain in contrast to the first design, compound **29** lacks the additional methyl group partially removing the large twist angles in the final monomer, a) $Br_2$, $I_2$, DCM, reflux, o/n, b) 1) argon atmosphere, *n*-$C_{12}H_{25}OH$, NaH, dry THF, RT, 2 h, 2) **19** or **27**, RT, o/n, c) argon atmosphere, bis(pinacolato)diboron, KOAc, Pd(dppf)$Cl_2$, dioxane, 80 °C, o/n, d) NBS, DBPO, MeCN, reflux + hν (500 W), 3 h.

However, due to the volatile nature of HBr the gas can also leave the reaction mixture under reflux conditions explaining the relatively low yield and *2*,*5*-dibromo-*4*-methylbenzyl alcohol as major side product. In contrast, the synthesis of linker **29** is started by a radical benzylic bromination of *2*,*5*-dibromotoluene (**26**) according to standard conditions. The procedures for the subsequent steps towards compound **21** and **29**, the etherification with dodecanol and Miyaura borylation, are already described for compound **11** and were performed equally.

In comparison to the first design, diboronic ester **21** and **29** bear only one dodecyl side chain which should further boost the water solubility of the final polymer. A side effect of this substitution pattern is the asymmetry of the resultant 2nd and 3rd generation monomers (Figure 26), which are synthesized by the same route as the 1st generation in Scheme 6. Since there is no obvious preference of one nitro group to specifically couple with itself or the other during the polymerization step the resultant macromolecules have an undefined and potentially not reproducible architecture. However, these very slight variations attributed to the position of the dodecyl chains within the polymer should not cause any significant difference in the properties of the final material. Furthermore, in the 3rd generation the additional methyl group at the phenyl linker is missing which removes the large twist angle about one of the bonds between the aromatic rings. While the twist angle about the other bond remains to maintain the decoupling of the

repeating units, the overall twist of the polymer backbone is thus reduced potentially facilitating aggregation and assembly into cylindrical micelles.

Furthermore, due to the lower hydrophobicity of the 2nd generation in comparison to the 1st one the triglyme substituents might be sufficient as water solubilizing groups and, therefore, are included in the monomer selection (derivative **24**).

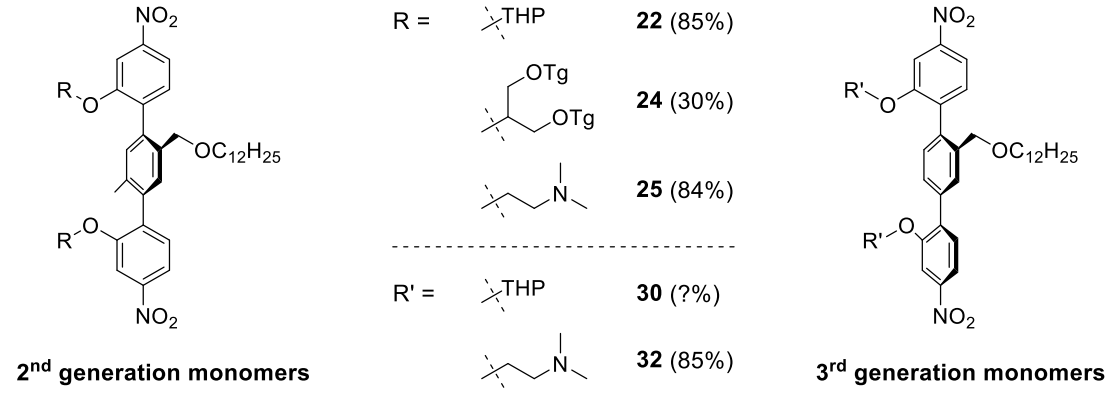


**Figure 26.** Overview of the 2nd and 3rd generation monomers, in comparison to the first design the second dodecyl chain was removed to increase the water solubility of the final polymer, the introduction of an additional methyl group in the middle ring of generation 2 is required to maintain the large twist angles, in the 3rd generation no methyl group is present reducing the overall twist of the resultant polymer which potentially facilitates aggregation and, thus, the formation of cyclindrical micelles, the yields are given in the brackets.

### 4.2.2 Reductive Polymerization

The major problem of the polyazo coupling approach is the rapid gelation of the reaction mixture during or shortly after the addition of Red-Al that renders proper stirring of the batch and further polymer growth very difficult. It is known that macromolecular solutions exhibit higher viscosities than mixtures containing small molecules, however, the polymers in the present case are only of small to medium size and do not show the same behavior when pure polymer solution are prepared. Furthermore, the observed gelation effect is reproducible for all monomers presented in the previous chapter independent of their side chain characteristics. These observations indicate a great contribution of the generated aluminum species such as aluminum hydroxide that are known to form gels and might form larger networks by coordination with Lewis acidic substituents like amines and tetrahydropyranyl ethers.

A typical polyazo coupling experiment employing 1st generation monomers is depicted in Scheme 6 providing a starting point for further optimizations. The terphenyl derivative is dissolved in dry toluene in a Schenk flask under argon and a solution of Red-Al (10 eq.) in toluene is slowly added at room temperature. The overall concentration of the monomer is adjusted to be 0.5 M. Before the addition was completed rapid gelation of the reaction mixture occurred. After

complete addition, a sample was taken from the batch, subjected to a small-scale work-up, and the same process repeated 24 h later. Both samples were analyzed by GPC, however, no significant difference was observed indicating no further polymer growth after formation of the gel.

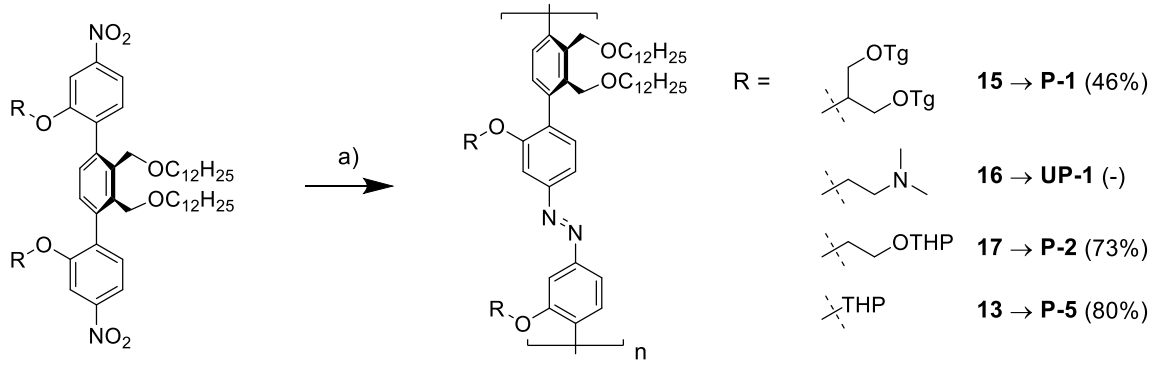


**Scheme 6**. Polymerization of the first generation dinitro terphenyl monomers **13**, **15**-**16**, the proper conditions must be carefully met to avoid gelation and to obtain polymers of high molecular weight, polymer **UP-1** exhibiting amine terminated side-chains could not be synthesized as gelation was inevitable regardless of the chosen reaction parameters, polymerization of the 2nd and 3rd generation monomers was conducted under the same conditions, a) argon atmosphere, Red-Al, dry toluene, 0 °C, 3 d.

Several reaction parameters were investigated with the objective of avoiding gelation and the accompanied end of the polymer growth, i.e. monomer concentration, temperature, Red-Al® equivalents, solvent, and the addition order as well as the addition speed of the reactants. All experiments were conducted employing monomer **17**. At this point it must be noted that despite all optimization polymer **UP-1** could not be made, since gelation occurred under all tested conditions. This result supports the theory of potential aluminum coordinated networks considering that the amine-terminated ethylene moiety is the strongest Lewis acid among the polymer side chains.

The first obvious parameter that influences the formation of gels is the amount of the gelation agent in solution where a higher number usually relates to a higher probability of gelling at a certain temperature. While a high concentration of monomers is usually beneficial for the growth of large macromolecules by bringing the reactive moieties closer together, it is detrimental in the current case as it results in similarly high polymer concentrations. It must be noted that at temperatures > 60 °C irreversible bleaching of the product mixture occurred implying complete reduction of the azobenzene nitrogen double bond and, thus, decomposition of the polymeric product. A summary of the investigated monomer concentrations at a specific temperature is presented in Table 1. In this regard, “no gel” denotes a reaction mixture that can still be stirred

one hour after complete addition of the reductive agent. Apparently, gelation is inevitable at low solvent levels with a maximum concentration of about 0.1 M at 0 °C that still yields a manageable mixture viscosity.

**Table 1.** Gelation behavior within the first hour after addition of 10 eq. of the reducing agent dependent on the monomer concentration (c) and the reaction temperature while Red-Al addition (T), high concentrations > 0.1 mol/L always induce gelation (red) while at lower concentrations and the appropriate temperature viscous liquids were obtained permitting further polymer growth (green), all experiments were conducted employing monomer **17**.

| T (°C) (mol/L) \ c | **0.05** | **0.10** | **0.25** | **0.50** |
|---|---|---|---|---|
| **0** | no gel | no gel | gel | gel |
| **20** | no gel | gel | gel | gel |
| **60** | no gel | gel | gel | gel |

Subsequently, attempts to reduce the amount of Red-Al were conducted (6 and 8 eq. instead of 10 eq.) assuming that the removal of metal ions inhibits the sufficient formation of the network. However, the same trend as shown in Table 1 was observed for lower concentrations (equivalents) of reducing agent. At 6 eq. of Red-Al and monomer levels of 0.25 M gelation occurred independent of temperature whereas a monomer concentration of 0.10 M at 0 °C yielded a viscous mixture that still could be stirred. Furthermore, the average molecular weight of the obtained polymers after 24 h of reaction time decreased by approximately 25% when lowering the equivalents of Red-Al from 8 to 6 indicating no beneficial but a rather detrimental effect of decreasing reductive agent levels (Table 2).

**Table 2**. Effect of different equivalents of Red-Al on the number average molecular weight of the polymer product after 24 h of reaction time while keeping all other parameter constant, increasing the number of equivalents beyond 8 does not result in significantly bigger macromolecules, all experiments were conducted employing monomer **17**.

| **Equivalents (Red-Al)** | **$M_n$ (g/mol)** |
|---|---|
| 6 | 12300 |
| 8 | 16500 |
| 10 | 17200 |

Finally, the effect of a different solvent on the reaction outcome was investigated by substituting toluene for THF, a common medium for reductions employing comparable lithium aluminum hydride. In this case, gelation did not occur even at higher concentrations, yet only small oligomers

and partial decomposition of the starting material was observed. It remains unclear whether the disappearance of gelation can be attributed to the absence of larger macromolecules or the additional coordinating properties of THF that inhibit the binding of aluminum to the polymer side chains. However, a combination of both effects seems to be the most reasonable.

In summary, the best conditions to obtain a high molecular weight product by reductive polymerization of the dinitro terphenyl monomers of all generations are:

- Solvent: toluene, temperature during addition of Red-Al: 0 °C
- Slow addition of the monomer solution to 8-10 eq. of Red-Al
- Final monomer concentration: 0.10 M

Following these optimizations, the triglyme substituted monomer **15** could be efficiently converted into polymer **P-1** improving the yield and number-average molecular weight by about 75% (from 26% to 46%) and 71% (from 21000 g/mol to 36000 g/mol), respectively.
However, even when taking these precautions gelation could not be completely excluded in all cases and batches. Besides the characteristic rise in viscosity during the formation of macromolecules, the previous experiments imply a contribution of certain aluminum species to explain the observed extreme gelation effect. In this context, aluminum hydroxide, a typical side product of reduction reactions employing LAH or Red-Al, is known to form gels. This assumption is further supported by the fast dissolution of the gel after addition of methanol which is used to quench the polymerization and a common dehydrating agent for aluminum hydroxide gels. In combination with polymers bearing Lewis acidic side chains, such as amines and THP ethers, the formation of complex networks is conceivable that also depend on traces of water limiting this polymerization approach.

### 4.3.3 Post-Functionalization and Final Polymers

Employing the optimized polyazo coupling conditions, several macromolecular compounds exhibiting different side chains were synthesized. However, except for the triglyme designs post-functionalization is required to introduce charges that provide sufficient water-solubility. An overview of the modifications performed directly on the polymeric material independent of the phenyl linker's substitution pattern is depicted in Scheme 7.

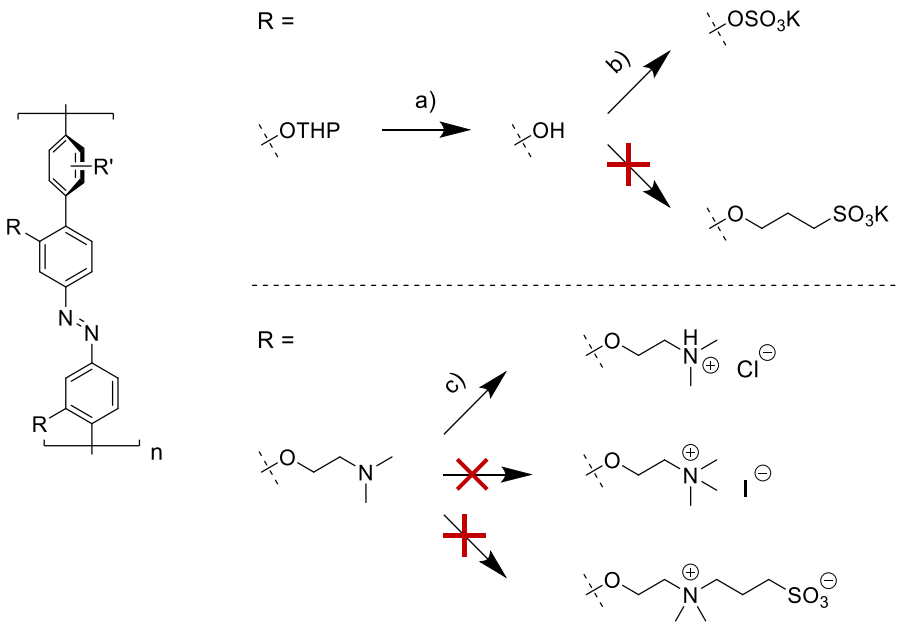


**Scheme 7**. Attempted post-functionalizations of polymers obtained by the polyazo coupling approach independent of generation; starting points are tetrahydropyranyl ethers, which are deprotected and converted into sulfates or sulfonates, and amines as basis for ammonium ions and zwitterionic structures; crossed arrows indicate highly incomplete reactions or insoluble products, a) *p*TSA, DCM/MeOH, RT, o/n, b) 1) argon atmosphere, pyridine $SO_3$ complex, pyridine, dry DMF, RT, 24 h, 2) $K_2CO_3$, $H_2O$, c) HCl, THF, RT, 1 h.

Starting from the free phenol that is obtained by facile deprotection of the tetrahydropyranyl ethers in acidic medium two routes were followed targeting their conversion into sulfates or the formation of sulfonate-terminated propyl ethers. Common reagents to convert an ROH group into an $ROSO_3^-$ group are chlorosulfuric acid and complexes of sulfur trioxides with pyridine, triethyl amine, or DMF. For the first sulfatation attempt chlorosulfonic acid was employed leading to complete decomposition of the polymers, which was proven by the disappearance of the azobenzene absorption bands in the UV/vis spectrum. Moreover, the excellent water-solubility of the product material implies extensive sulfonation on the phenyl rings rendering this method inappropriate for further investigation. In contrast, utilization of a $SO_3$ pyridine complex enabled quantitative conversion of the phenols into the corresponding sulfates confirmed by NMR analysis (examples of the spectra of polymer **P-11** and **P-12** shown in Figure 27).

The more downfield shifted signal at 10.27 ppm corresponding to the two phenolic protons (red) vanishes and a new signal at 8.64 ppm (blue) appears representing one aromatic hydrogen according to integration. Albeit the assignment of the latter signal is unclear without further 2D-NMR analysis, it might belong to the proton of the phenyl linker in *ortho* position relative to the connecting bond of the aromatic rings that forms a hydrogen bond with the sulfate group in close proximity.

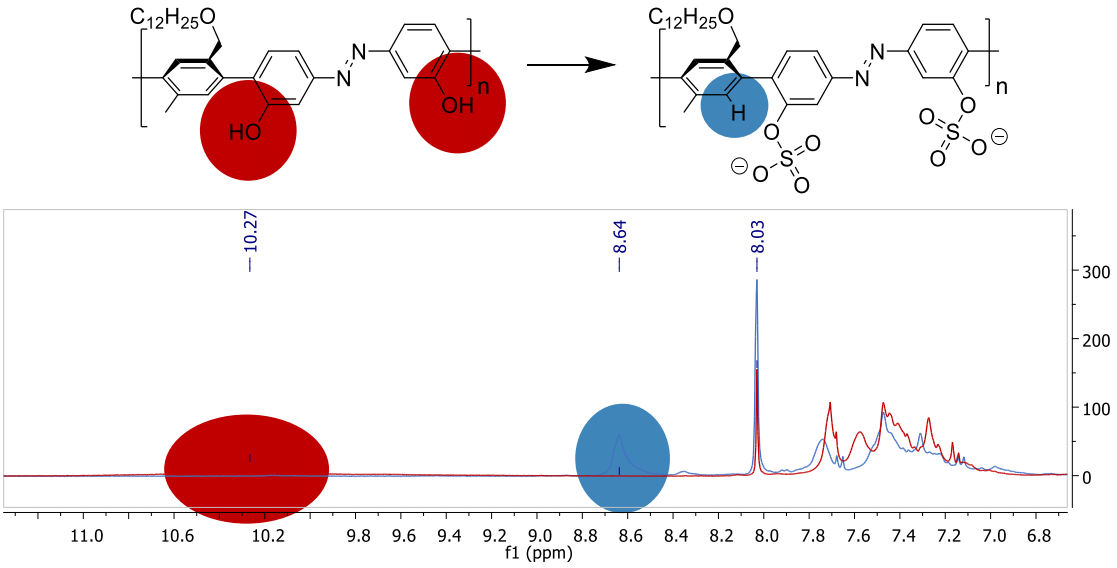


**Figure 27**. NMR spectra in deuterated DMF representing phenolic polymer **P-11** and sulfate substituted polymer **P-12**, the red signals belongs to the phenolic protons that vanish upon conversion into sulfates, the blue signal might be assigned to the phenyl linker which forms a hydrogen bond with sulfates in close proximity.

The preparation of the sulfonate-terminated propyl ether (**UP-4** and **UP-7**) could not be accomplished due to the rather low ratio of converted hydroxy groups to free phenols even though a high excess of reagents was applied.

The second type of post-functionalization covers amine-bearing polymers that can be converted into ammonium ions by either protonation or methylation and zwitterionic structures by reaction with *1,3*-propane sultone. With respect to the protonation approach, the amine-substituted polymers are first dissolved in THF and, subsequently, a 1 M HCl solution is added. The solvent as well as the excess acid is evaporated yielding the final material that exhibits a dramatically increased water-solubility. Direct protonation of the macromolecules in acidic water was not feasible due to the insolubility of the starting material in pure aqueous medium even at high temperatures. However, the formation of permanent charges is preferable due to pH independent solution properties. In this regard, methylation of the amine side-chains was conducted by means of methyl iodide and dimethyl sulfate. In both cases, rapid precipitation of an orange solid was observed in THF and DCM likewise after addition of the methylating agent, which could not be re-dissolved in any of the following liquids: $H_2O$, DMSO, DMF, MeOH, EtOH, *2,2,2*-trifluoroethanol, toluene. Similar behavior was observed after the addition of *1,3*-propane sultone to a solution of the amine polymers in *2,2,2*-trifluoroethanol. Precipitation of the presumably zwitterionic material occurred yielding an orange solid that was completely insoluble in the liquids mentioned above. No further experiments following amine functionalization were attempted considering

that most derivatives do not provide the required level of water solubility for the formation of micelles.

An overview of all final polymer designs is depicted in Figure 28 including all successfully synthesized derivatives (P-series) and the yields of the final synthetic step as well as the inaccessible compounds (UP-series). The solubility in pure water or mixture of water and a small amount of organic solvent (DMF or THF, organic content < 1% v/v) was investigated to determine the best candidates for the formation of micelles in aqueous medium. All polymers meeting this requirement at a concentration of $c_{polymer}$ = 1 mg/mL are highlighted in green.

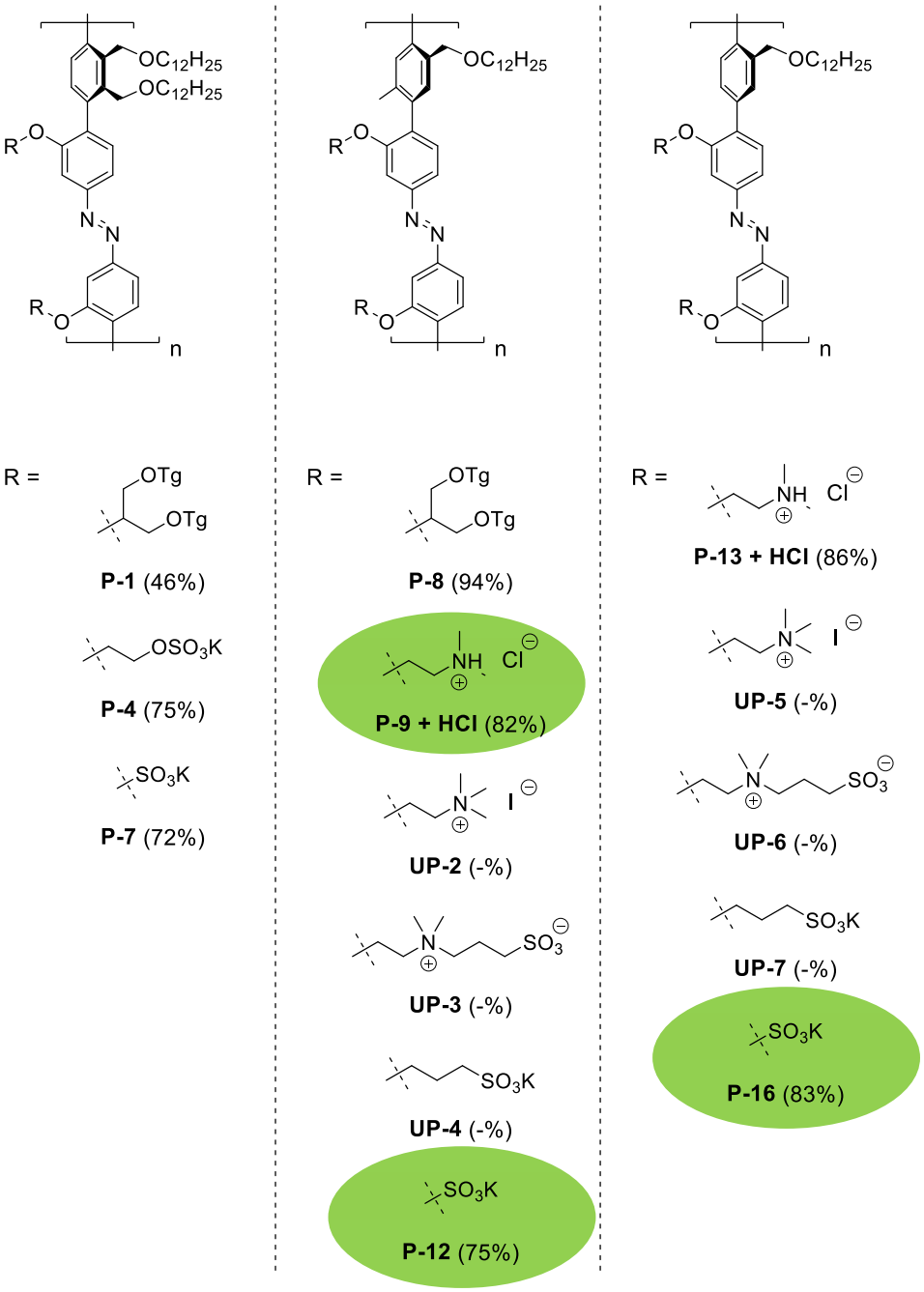


**Figure 28.** Overview of all final polymer architectures, the P-series was successfully synthesized and the corresponding yield of the final step is given in parentheses, the UP-series was not accessible after multiple synthetic attempts or exhibits drastically low solubility in multiple solvents rendering the analysis of the material difficult, the highlighted (green) derivatives are sufficiently soluble in pure water or mixture of water and an organic solvent (organic solvent content < 1% v/v).

## 4.3 Light-Responsive Micelles

### 4.3.1 Polymer Characteristics and Preparation of Micelles

The polymers exhibiting the highest water-solubility as well as the simplest procedure for the preparation of micellar solutions are the sulfated derivatives **P-12** and **P-16** of the 2nd and 3rd generation, respectively. The basic characteristics of these compounds such as the number- and weight-average molecular weight $M_n$ and $M_w$, respectively, the polydispersity (PDI) as well as the number of repeating units (Đ) are depicted in Figure 29. The theoretical Đ is calculated by dividing $M_n$ by the mass of the repeating unit. However, due to the linear rigid architecture of the polymers the average molecular mass obtained by GPC is highly overestimated requiring an additional correction factor of typically 0.5.

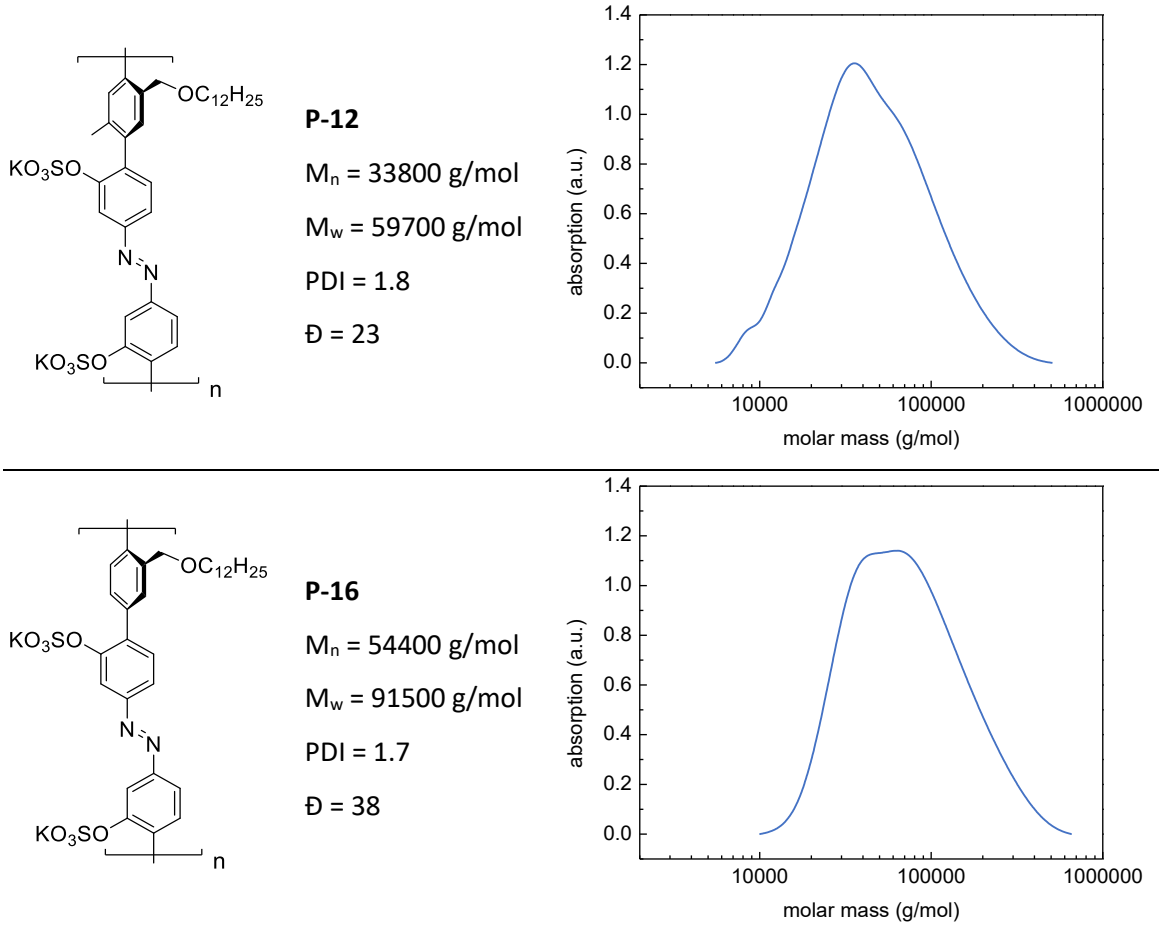


**Figure 29.** Overview of the basic characteristics of the linear rigid azobenzene polymers **P-12** (top) and **P-16** (bottom), $M_n$ = number-average molecular weight, $M_w$ = weight-average molecular weight, PDI = polydispersity index, Đ = number of repeating units, the diagrams present the molar mass distribution obtained by GPC analysis in DMAc vs. PS standards.

The preparation of micelles can be accomplished in several ways depending on the solubility of the amphiphilic material in water. In the easiest case, the amphiphile is mixed with pure water at

a certain temperature and stirred until complete dissolution which can take minutes, hours, or even days depending on the nature of the compound. Due to the absence of additional solvents or detergents potentially detrimental interactions of the additives and the micelle forming agent can be excluded. However, some amphiphilic compounds in solid state do not dissolved in pure water but their polar and non-polar groups need to be pre-arranged for proper assembly. This arrangement takes place at interfaces of liquids of different polarity where polar and non-polar groups are pointing towards the corresponding phase. Subsequent slow evaporation of one solvent releases the pre-arranged molecules into the remaining phase under formation of micelles. The same procedure can be followed in case of two mixable liquids where the same process occurs, yet, with significantly higher rate.

According to the first method, both polymers were mixed with Milli-Q water at a concentration of 1 mg/mL and stirred for 3 d at RT. However, the absence of color in the liquid layer indicated no dissolution of the solid material. Hence, a temperature of 60 °C was applied providing a clear yellow solution of **P-12** that was stable for several days at room temperature. In contrast, **P-16** remained undissolved which can be attributed to less twisting of the polymer backbone due to the absence of the additional methyl group and, therefore, stronger aggregation in solid state. This problem could be solved by preparation of a highly concentrated solution of **P-16** in DMF and subsequent dilution with water yielding a mixture containing a negligible amount of the organic solvent (< 1% v/v). Both samples were analyzed by static and dynamic light scattering as well as cryo-TEM imaging.

### 4.3.2 Light scattering of Micellar Solutions

First, the effect of different treatments and polymer concentrations on the micelle size of the freshly prepared aqueous solutions of **P-12** and **P-16** were investigated. In this regard, the samples were subjected to heat and ultrasound as well as repeated freezing-thawing cycles. The latter is known to break micelles due to the formation of ice crystals while the subsequent melting process triggers re-assembly. This procedure is usually employed to incorporate a cargo in pre-formed micelles and vesicles, however, it might as well have a homogenization effect which decreases the polydispersity of the sample. Furthermore, the effect of a small amount of DMF in the solvent was examined with respect to the standard preparation method of **P-16** solutions. The average hydrodynamic radius ($R_h$) and the average radius of gyration ($R_g$) obtained by dynamic and static light scattering, respectively, are given in Figure 30 (left table).

No clear trend of the micelle size is observed when subjecting the standard polymer solutions to the different treatments. In the case of polymer **P-12** for instance, three freeze-thaw cycles increase the average $R_h$ by about 40%. However, the same treatment on polymer **P-16** causes the opposite effect decreasing the same quantity by about 15%. Only the application of ultrasound induces the same effect on both samples dramatically lowering the size of the assemblies, which is a known observation for micellar solutions. In this context it must be noted that the preparation of two or more samples under precisely same conditions and at the same concentration yield micelles that can differ in size by about 100% and more. A representation of that behavior is depicted in Figure 30 (right diagram) where a total number of eleven **P-12** solutions were prepared according to the standard procedure. Subsequent determination of the average $R_h$ revealed highly polydisperse objects in the range of 60 nm up to 175 nm when turning from one sample to the other. Furthermore, considering that the ρ-value (ratio of $R_g$ and $R_h$) does not equal two (typical for cylindrical objects) as long as $R_h$ > 50 nm, this effect might arise from the formation of micellar aggregates, common among polyelectrolytes.

| Treatment | P-12 $R_h/R_g$ (nm) | P-16 $R_h/R_g$ (nm) |
|---|---|---|
| - | 95/108 | 123/166 |
| **60 °C for 14 h** | - | 27/73 |
| **3 freeze-thaw cycles** | 136/200 | 108/139 |
| **polymer pre-dissolved in DMF** | 38/77 | - |
| **pre-dissolved in DMF + 3 freeze-thaw cycles** | 44/97 | 108/139 |
| **ultrasound** | 19/38 | 22/38 |

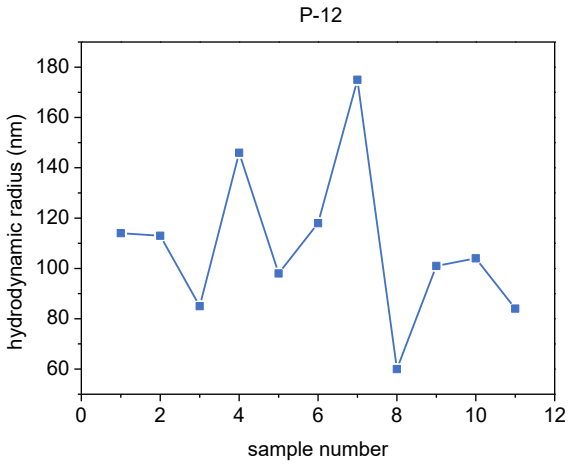


**Figure 30.** Table (left): effect of different treatments on the size of the micelles prepared according to the standard procedure of the respective polymer, **P-12** standard procedure: 60 °C, o/n, **P-16** standard procedure: pre-dissolved in DMF and subsequent addition of water, $c_{polymer}$ = 0.5 mg/mL; diagram (right): $R_h$ of eleven **P-12** solution prepared according to the standard procedure at the same concentration, large deviation in size are observed implying a potential contribution micellar aggregates.

Two strategies are available to confirm and counter the aggregation of polyelectrolytes, i.e. dilution and addition of salts to shield the charges on the surface. Both processes should decrease the size of the objects in solution. In this regard, a concentration profile for both polymers in pure water and aqueous sodium chloride solution was prepared, the data is shown in Figure 31. However, neither the overall size nor the ρ-ratio undergoes a significant shift towards smaller or

higher values, respectively, at lower polymer levels but the same chaotic distribution similar to the previous samples is observed (Figure 31a). Likewise, the addition of sodium chloride in a 1:1 ratio (2 equivalents of sodium chloride per repeating unit) for c(polymer) = 1 mg/mL up to a 1:20 ratio for c(polymer) = 0.05 mg/mL did not alter the hydrodynamic radius (Figure 31b). Only in one case (c(**P-16**) = 0.1 mg/mL) a significant decrease of $R_h$ was observed after the addition of salt. However, considering the overall trend of the data, this point represents rather a statistical spike.

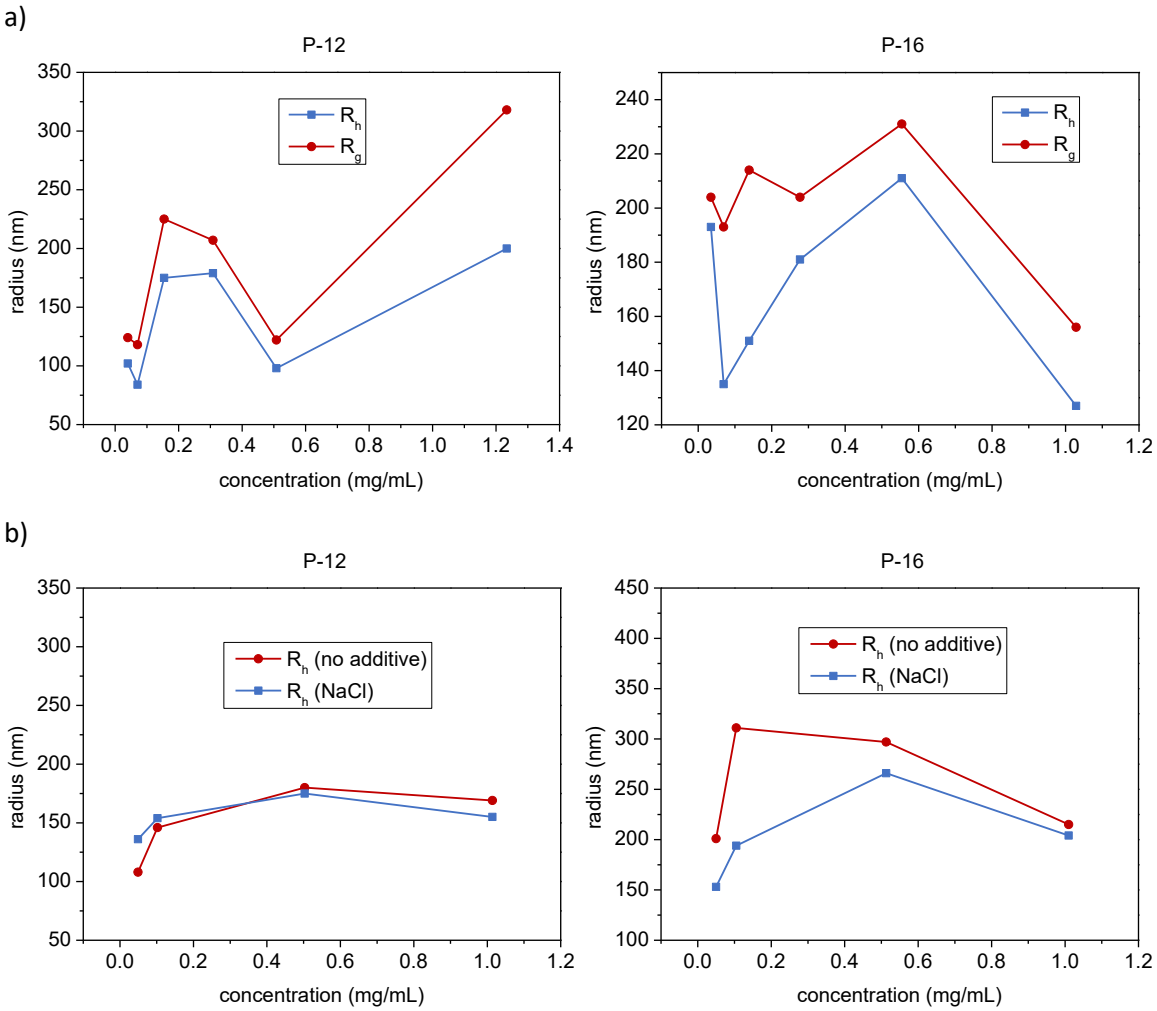


**Figure 31.** a) Hydrodynamic radius $R_h$ and radius of gyration $R_g$ of objects in solution depending on the polymer concentration, neither a trend towards smaller or larger objects nor a change of the ρ-ratio is observed when decreasing the concentration of **P-12** or **P-16** but the same deviation similar to samples of higher concentrations is observed, b) no change of $R_h$ in pure water and sodium chloride solution is observed which indicates no aggregation of the potential micelles, for c(**P-16**) = 0.1 mg/mL a significant decrease of the hydrodynamic radius in NaCl solution is observed, however, following the general trend of the data, this value is rather a statistical spike, the molar ratio of repeating unit to NaCl is 1:1, 1:2, 1:10, and 1:20 from the solution of the highest to the lowest polymer concentration, respectively.

In contrast, di- or multivalent ions are known to facilitate aggregation of multi-charged objects. This could be confirmed by addition of $Mg^{2+}$, $Ca^{2+}$, and $Ba^{2+}$ which induces slow precipitation of the polymeric material.

In conclusion, the formation of micellar aggregates was not confirmed but a high polydispersity of the polymer assemblies appears reasonable when trying to explain the broad range of object sizes. The observed strong dependency of the diffusion coefficient on the scattering vector is supporting this assumption.

### 4.3.3 Irradiation Experiments

The photochromic behavior of polymers **P-12** (Figure 32) and **P-16** (Figure 33) in aqueous solutions was investigated by means of UV/vis spectroscopy, light scattering, and cryo-TEM imaging. The 2$^{nd}$ generation polymer exhibits similar switching properties as the triglyme derivative obtained by Suzuki polycondensation (Figure 32a). Upon irradiation at 365 nm the ππ* band, which is overlapping with the nπ* transition, decreases due to photoisomerization to the *Z* state. The switching efficiency in water is lower than in organic solvents (DMSO and DMF) indicating aggregation of the macromolecules that is restricting the isomerization about the nitrogen double bond. The precise PSS composition, however, could not be determined since sufficiently high concentrations for an NMR analysis in water are not accessible.

Subsequently, the switching process was followed by dynamic light scattering to investigate its effect on the micelle size (Figure 32b). In this regard, the hydrodynamic radius was recorded at a detector angle of 100° which does not represent the average value of the whole system (average $R_h$ = 118 nm) but is sufficient to analyze the percental change. An overall decrease of 48% from 48 nm to 25 nm was observed relating to an alternation of the hydrodynamic volume by about 86%. A cooperative effect triggered by the large geometrical deformation of the linear rigid polymers was not observed during the process indicated by the absence of a sigmoidal curve. The return to the *E*-rich state can be trigger photochemically, however, no full or partial recovery to objects of the initial size was observed. In contrast, thermal recovery at RT was successfully performed yielding assemblies of 40 nm at a detector angle of 100° and 129 nm on average.

In order to further prove the switching event and to gain insight on the nature of the geometrical changes upon photoisomerization cryo-TEM image before (Figure 32c) and after irradiation at 365 nm (Figure 32d) were recorded.

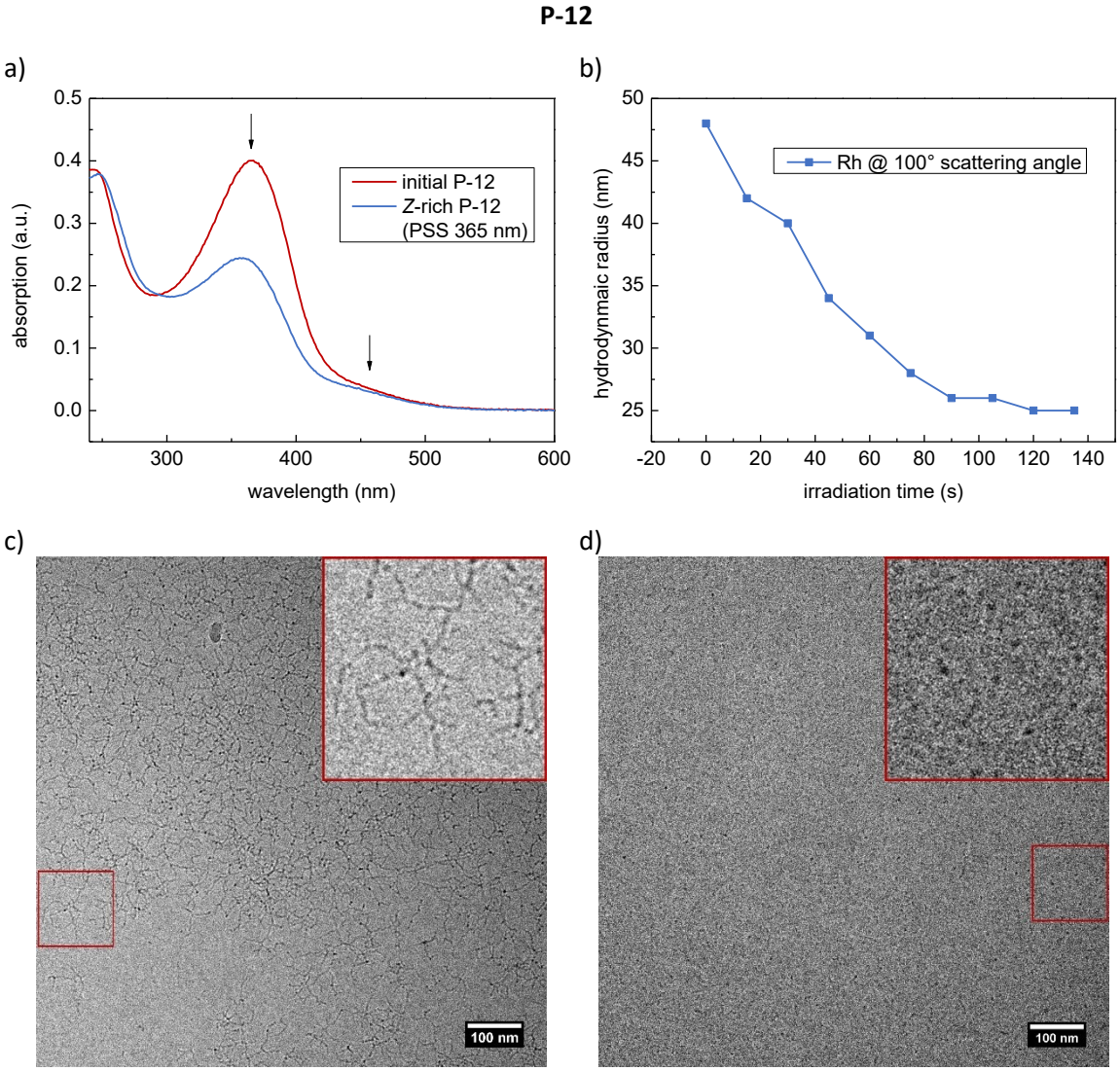


**Figure 32.** a) UV/vis absorption spectra of **P-12** in water, red: initial state of the freshly prepared solution, blue: PSS after irradiation at 365 nm, the composition is estimated to be about 40% *Z* isomer, b) evolution of $R_h$ during irradiation at 365 nm until a stationary state is reached, the measurement was conducted at a fixed angle of 100° and, therefore, does not represent the average $R_h$ of the system, c) cryo-TEM image of an aqueous solution of **P-12** before and d) after irradiation at 365 nm, the worm-like objects disappear after isomerization, the details in the upper right corner represent a 3 x magnification of the area within the red square.

The former image shows highly entangled worm-like micelles that take all orientations in space. Due to the close proximity of the objects to each other a precise measurement of the length is impossible, however, an average length of 100 nm seems to be a reasonable assumption. Moreover, the formation of branched objects cannot be excluded which would require a 3D view on the sample (by electron cryotomography for instance). After irradiation the worm-like objects disappear and mostly spheres below 10 nm remain, an even smaller size than indicated by the light scattering measurements. However, a precise determination of dimensions is again not feasible as the objects are beyond the limits of this method.

**P-16**

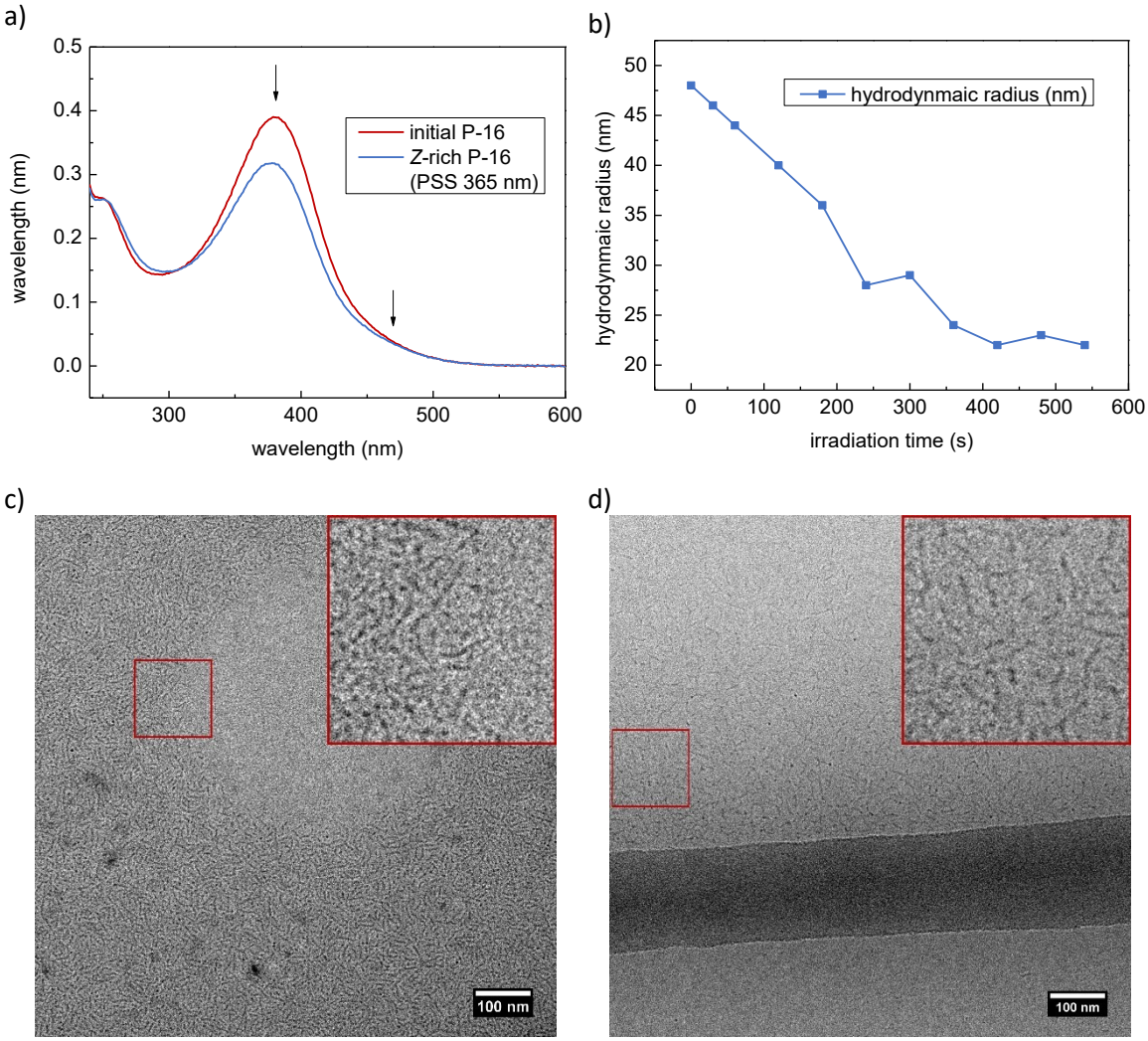


**Figure 33.** a) UV/vis absorption spectra of **P-16** in water, red: initial state of the freshly prepared solution, blue: PSS after irradiation at 365 nm, the composition is estimated to be about 20% *Z* isomer, b) evolution of $R_h$ during irradiation at 365 nm until a stationary state is reached, the measurement was conducted at a fixed angle of 100° and, therefore, does not represent the average $R_h$ of the system, c) cryo-TEM image of an aqueous solution of **P-16** before and d) after irradiation at 365 nm, the worm-like objects remain after isomerization, though, their overall number decreases, the details in the upper right corner represent a 3 x magnification of the area within the red square.

Polymer **P-16** (Figure 33) exhibits a rather similar behavior in comparison to the previous design. Although the switching efficiency is significantly lower as a result of the lower twist of the aromatic backbone (20% *Z* isomer estimated by the decrease of the ππ* band, Figure 33a) and more time is required to reach the stationary state, the hydrodynamic radius changes from 48 nm to 22 nm by 54% ($\Delta V_h$ = 90%, Figure 33b). Surprisingly, the cryo-TEM images do not support this observation. Before irradiation (Figure 33c) worm-like micelles with an estimated length of 80 nm are visible that do not undergo a geometrical change upon photoexcitation but merely decrease their overall number (Figure 33d). In this regard, the number of wormlike objects was counted in four randomly chosen square details of the images, each of 200 px edge length (the details can be

found in the experimental part in section 5.4, Table 3). Regions of high object density were preferred. Before irradiation, an average number of about 25 objects per detail was found. After irradiation, the same number decreased by over 60% to 8.5 objects per detail. It must be noted that most of the cryo-TEM images after irradiation did not show any objects suggesting that successful dissolution of the micelles by isomerization took place. Considering the observed tendency of these objects to stick together, the present image might be a “lucky shot” of the few remaining species.

## 4.4 Summary, Conclusion, and Outlook

All in all, the synthesis of 15 polymer designs was attempted following a Suzuki polycondensation and a reductive polyazo coupling approach, of which eight derivatives could be successfully made. In this context, the second strategy employing one monomer instead of two has distinct advantages and yielded products of medium to high molecular weight after optimization of the reaction conditions. However, only three of these polymers exhibited sufficient water solubility. The two most promising candidates (**P-12** and **P-16** with an aryl sulfate design) where investigated with respect to their switching and micellization properties. Although the photoisomerization ability of both polymers is worse in water than in organic solvents, the dissolution of cylindrical micelles could be controlled by irradiation with light at 365 nm. The reversible process failed to be triggered by visible light but was accomplished by thermal relaxation. Hence, the conceptual illustration must be somewhat updated (Figure 34).

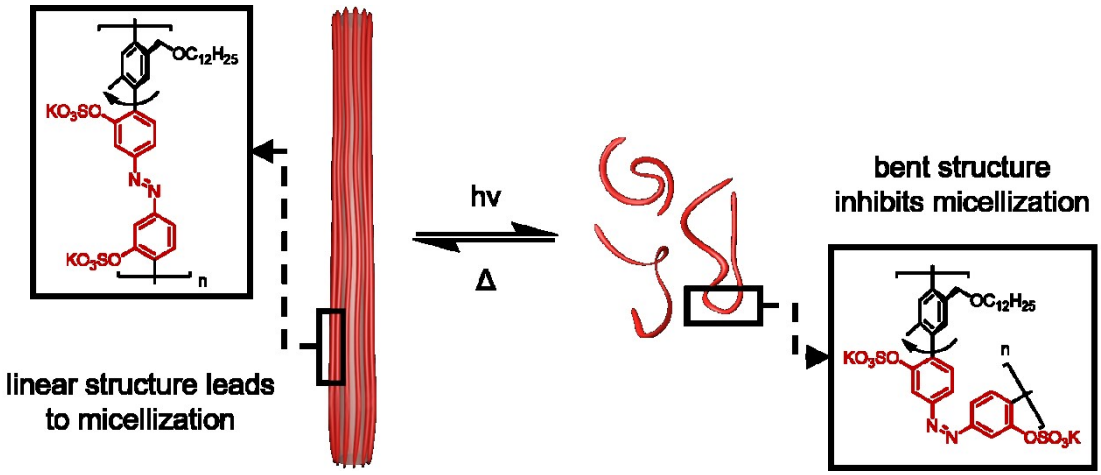


**Figure 34.** Updated conceptual illustration of the light-responsive system based on the amphiphilic rigid-rod polymer **P-12** that dramatically changes size and shape upon photoisomerization of the azobenzene units, the formation of cylindrical micelles is disturbed by the bended structure of the polymers *Z* state leading to a complete disappearance of the worm-like assemblies, the linear *E* state can be recovered by thermal relaxation also re-forming the micelles.

The major drawback of the system is the slow recovery of the initially assembled state by thermal relaxation. A possible improvement might be the formation of permanent micelles by integration of polymerizable moieties on the aliphatic side chains, thus providing the possibility of a covalent connection between the polymer chains. Similar to the earlier presented publication from the group of Feringa,[45] a controlled alignment of these nanofibers mimicking the composition of biological muscles might amplify their individual strength and allow the direct transfer of light energy into mechanical work on a macroscopic scale.

# 5 Experimental Part

## 5.1 Materials and Instrumentation

Commercial chemicals were used as received without further purification. Solvents were distilled prior to use. Dry solvents were taken from an Innovative Technologies solvent purification system. Toluene was additionally dried by storage over activated molecular sieves (4 Å) for a minimum period of two weeks. All reactions were monitored by thin layer chromatography (TLC) on Merck 60F-254 silica gel plates using UV light for visualization. Merck 60 silica gel (VWR, particle size 0.040–0.063 mm) was used for flash column chromatography.

Ultraperformance liquid chromatography coupled to mass spectrometry (UPLC-TOF) was performed on a Waters Alliance system (eluent: gradient mixtures of acetonitrile/water) equipped with Acquity UPLC columns. The Waters system consisted of a Waters Separations Module 2695, a Waters Diode Array Detector 996, a LCT Premier XE mass spectrometer, and a Waters Mass Detector ZQ 2000. Recycling gel permeation chromatography (GPC) was performed on a JAI LC-9210NEXT (eluent: DCM).

UV/Vis absorption spectra were recorded using quartz cuvettes on a Cary 60 or a Cary 50 spectrophotometer equipped with a Peltier-thermostate cell holder (25 °C, temperature accuracy ± 0.1 °C). The solvents were of spectrophotometric grade.

NMR spectra were recorded on a Bruker Avance II 300 ($^{1}$H at 300.13 MHz and $^{13}$C at 75.47 MHz) and a Bruker Avance II 500 ($^{1}$H at 500.13 MHz and $^{13}$C at 125.76 MHz) at ambient temperatures. All spectra are referenced to the solvent residual signal ($^{1}$H: δ($CHCl_3$) = 7.26 ppm, δ($CHDCl_2$) = 5.32 ppm, δ(DMSO-$d_5$) = 2.50 ppm, δ(benzene-$d_5$) = 7.16 ppm, δ(DMF-$d_6$) = 8.03 ppm; $^{13}$C: δ($CDCl_3$) = 77.16 ppm, δ($CD_2Cl_2$) = 53.84 ppm, δ(DMSO-$d_6$) = 39.52 ppm, δ(benzene-$d_6$) = 128.06 ppm, δ(DMF-$d_7$) = 163.15 ppm). Deuterated solvents were purchased from EurisoTOP and used without further purification unless indicated differently. Multiplicities are abbreviated as follows: singlet (s), doublet (d), triplet (t), doublet of doublets (dd), quintet (q) and multiplet (m). Coupling constants (J) are given in Hz. Chemical shifts (δ) are given in ppm.

Light scattering experiments (DLS and SLS) were performed on an ALV-4000 instrument in combination with a He-Ne-laser (18 mW, 633 nm) and an avalanche photodiode detector system. SAXS measurements were performed with a Kratky-type instrument (SAXSess) from Anton Paar, Austria, in a quartz capillary (diameter 1 mm) at 294 ± 1 K. The device exhibits a low sample-to-detector distance of 0.309 m, which is appropriate for low scattering intensities.[54]

## 5.2 Light Scattering – General Procedure

The light scattering system was tested for proper operation by measuring a nanoparticle standard (25 nm).

All sample solutions were transferred through syringe filters (Nylon, 450 nm pore size) directly into disposable glass cells, while carefully avoiding contact of the solutions with the wall of the glass cells. The cells were sealed with a rubber stopper. The glass cells were washed with distilled acetone and dried in an airflow prior to use. The outside of the glass cells was cleaned with acetone and the sample transferred into a bath of toluene tempered at 25 °C. The measurement chamber was closed to avoid interferences with ambient light. The samples were allowed to adjust to the temperature of the toluene bath for 5 min.

For DLS measurements, the scattering intensity fluctuations were recorded for 30 s per angle. For SLS measurements, the average scattering intensity was recorded for 10 s, three times per angle.

## 5.3 Small-Angle X-Ray Scattering – General Procedure

The measurements were performed at the Federal Institute for Materials Research and Testing (BAM), Unter den Eichen 87, 12205 Berlin, in the group of Andreas F. Thünemann.

Two samples were prepared for SAXS investigation, i.e. a THF solution of polymer **P-1** and a solution of polymer **P-1** in a THF/water mixture. In the former case, 20 mg of polymer **P-1** were dissolved in 1 mL of pure THF. In the latter case, 20 mg of polymer **P-1** were dissolved in 0.75 mL of pure THF followed by slow addition of 0.25 mL of pure water. The clear solutions were filled in the quartz capillary without filtration and measured for 180 x 10 s. The solutions were allowed to equilibrate inside the capillary for 3 min before measurements were started. Before samples were changed, the capillary was carefully flushed with pure THF to remove all material from the previous sample.

The scattering vector q is calculated according to equation 18, where λ denotes the wavelength of the radiation (0.154 nm) and θ the scattering angle.

$$q = \frac{4\pi}{\lambda} \sin\theta \qquad 18$$

The SAXS-Quant software was employed for deconvolution (slit length desmearing) of the SAXS curves. The data was evaluated employing the SASfit tool[55] by fitting the curves according to the Porod cylinder model.[56]

## 5.4 Synthetic Procedures

**General procedure for the etherification of benzyl bromides with dodecanol**

Dodecanol is dissolved in dry THF under argon followed by careful addition of sodium hydride. The suspension is stirred until the evolution of gas stops (2 h) and, subsequently, the benzyl bromide derivative is added slowly. The mixture is stirred overnight at room temperature, remaining NaH quenched by slow addition of methanol, diluted with water, and extracted with DCM two times. The combined organic layers are washed with water and brine, dried over $MgSO_4$, filtered, and evaporated. The crude material is purified by flash column chromatography.

**General procedure for the etherification of OH-Terphenyls**

The Terphenyl derivative and the corresponding alkyl halide are dissolved/suspended in acetone and ground $K_2CO_3$ or $Cs_2CO_3$ is added. The mixture is heated at reflux overnight. After cooling down, water and ethyl acetate are added, the layers separated, and the organic layer washed with 1 M NaOH, water, and brine. Subsequently, the organic layer is dried over $MgSO_4$, filtered, and evaporated. The crude material is purified by flash column chromatography.

**General procedure for the Miyaura borylation of dibromobenzenes:**

The dibromobenzene derivative, bis(pinacolato)diboron, KOAc, and $Pd(dppf)Cl_2$ are transferred into a Schlenk flask. The flask is evacuated for 5 min and filled with argon, both is repeated three times. Dioxane is added and the mixture heated at 80°C under argon until TLC indicates complete conversion of the starting material. After cooling down, the mixture is filtered through celite and the solvent evaporated. The crude material is purified by flash column chromatography.

**General procedures for the Suzuki coupling to terphenyls:**

The bromobenzene, diboronic ester, and $K_3PO_4$ are dissolved in a mixture of toluene and water (5:2). The biphasic system is degassed by three freeze-pump-thaw cycles, $Pd(OAc)_2$ and SPhos are added, and the mixture heated at 90°C overnight. After cooling down, water and ethyl acetate are added, the layers separated, and the organic layer washed with saturated $NaHCO_3$ solution, water, and brine, dried over $MgSO_4$, filtered, and evaporated. The crude material is purified by flash column chromatography.

**General procedure for the deprotection of tetrahydropyranyl ethers:**

The tetrahydropyranyl ether is dissolved in a mixture of methanol and DCM (1:1, 1:2 for polymers) and *p*-toluenesulfonic acid is added. The solution is stirred at room temperature overnight. Water

and ethyl acetate are added, the layers separated, and the organic layer washed with 1 M HCl, water, and brine, dried over $MgSO_4$, filtered, and evaporated. The crude material is purified by flash column chromatography. In case of a polymer, the dichloromethane is evaporated, the precipitate filtered, washed with methanol, and dried under vacuum.

**General procedure for the reductive polymerization of Dinitro-Terphenyls:**

The Terphenyl derivative was dissolved in dry toluene (the volume of toluene was adjusted so that the concentration of terphenyl of the final mixture is 0.1 M) under argon and cooled down to 0°C. A solution of Red-Al in toluene (60%) was added very slowly dropwise. If the mixture got too viscous, the addition was stopped for some minutes until stirring could be maintained properly. After complete addition, the mixture was stirred for 3 d at room temperature (sometimes gelification occurred so that stirring was not possible anymore, in that case more toluene was added until stirring could be maintained, otherwise the reaction was stopped earlier). The remaining Red-Al was quenched by addition of MeOH and the solution stirred for 1 h under air to re-oxidize possibly formed hydrazo groups. More methanol was added until the orange polymer precipitated. The polymer was filtered, washed with methanol, and dried under vacuum. In case a narrower polydispersity is needed, the material can be dissolved in dichloromethane and precipitated by adding the solution into cold methanol.

**General procedure for the sulfatation of OH-polymers:**

The polymer is dissolved in dry DMF under argon and pyridine and sulfur trioxide pyridine complex is added. The solution is stirred for 24 h at room temperature. Ground $K_2CO_3$ and an amount of water enough to quench the remaining sulfur trioxide complex is added. The mixture stirred for 1 h. The resulting suspension is centrifuged, the liquid decanted, and the polymer solution added to cold toluene. The thin jelly-like precipitate is separated by centrifugation, washed with toluene 4 times, and dried under vacuum.

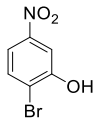


***2*-Bromo-*5*-nitrophenol (2)**: *2*-Amino-*5*-nitrophenol (**1**) (40.2 mmol, 6.20 g, 1 eq.) was suspended in half concentrated HBr and the mixture cooled down to 0°C. A solution of $NaNO_2$ (40.2 mmol, 2.77 g, 1 eq.) in water was added slowly so that no evolution of gas occurred. After stirring for 10 min the diazonium salt solution was added slowly to a solution of CuBr (52.3 mmol, 7.50 g, 1.3 eq.) in concentrated HBr and stirred for 1 h at room temperature and 1 h at reflux. After cooling down

the mixture was diluted with water and extracted with DCM three times. The combined organic layers were washed with water and brine, dried over $MgSO_4$, filtered, and evaporated. The crude material was purified by flash column chromatography (hexanes/EA) yielding *2*-bromo-*5*-nitrophenol (**2**) as an off-white solid (8.14 g, 93%).

**$^1$H-NMR** (500 MHz, DMSO-$d_6$): δ (ppm) = 11.36 (s, 1H), 7.79 (d, J = 8.7 Hz, 1H), 7.71 (d, J = 2.7 Hz, 1H), 7.58 (dd, J = 8.7, 2.7 Hz, 1H). **$^{13}$C-NMR** (125 MHz, DMSO-$d_6$): δ (ppm) = 154.9, 147.5, 133.8, 117.5, 114.9, 110.1. **MS-ESI**: m/z = 215.9326 (calc. for [M - $H^+$]: 215.9296).

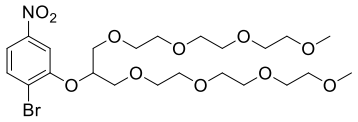

***2*-Bromo-*5*-nitrophenyl glyme ether 3:** *2*-Bromo-*5*-nitrophenol (**2**) (5 mmol, 1.09 g, 1 eq.) was dissolved in dry DMF under argon. Bis(tri(ethylene glycol) monomethyl ether) tosylate (TsOTg) (5 mmol, 2.69 g, 1 eq.) and ground $K_2CO_3$ (9 mmol, 1.24 g, 1.8 eq.) were added and the mixture stirred at 80°C for 24 h. After cooling down the suspension was diluted with 1 M NaOH and extracted with ethyl acetate three times. The combined organic layers were washed with brine, dried over $MgSO_4$, filtered, and evaporated. The crude material was purified by flash column chromatography (DCM/MeOH) yielding *2*-Bromo-*5*-nitrophenyl glyme ether **3** as a slightly yellow oil (2.61 g, 89%, contains traces of TsOTg according to NMR).

**$^1$H-NMR** (300 MHz, $CDCl_3$): δ (ppm) = 8.04 (d, J = 2.2 Hz, 1H), 7.70 – 7.59 (m, 2H), 4.71 – 4.59 (m, 1H), 3.81 – 3.44 (m, 28H), 3.32 (s, 6H). **$^{13}$C-NMR** (75 MHz, $CDCl_3$): δ (ppm) = 156.1, 147.9, 133.4, 121.0, 116.9, 111.2, 80.5, 71.9, 71.3, 71.0, 70.63, 70.60, 70.57, 70.5, 59.0. **MS-ESI**: m/z = 584.1776 (calc. for [M + $H^+$]: 584.1706), 606.1624 (calc. for [M + $Na^+$]: 606.1526).

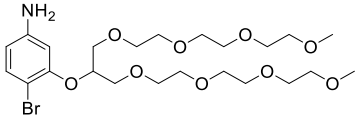

***2*-Bromo-*5*-aminophenyl glyme ether 4:** *2*-Bromo-*5*-nitrophenyl glyme ether **3** (4.8 mmol, 2.81 g, 1 eq.) was dissolved in EtOH (25 mL) under argon. Water (5 mL), Fe (12.5 mmol, 0.70 g, 2.6 eq.) and saturated $NH_4Cl$ (5 mL) were added and the mixture stirred at 80°C overnight. After cooling down the suspension was diluted with water and DCM, the layers separated, and the aqueous layer extracted with DCM two times. The combined organic layers were dried over $MgSO_4$, filtered, and evaporated. The crude material was purified by flash column chromatography (DCM/MeOH) yielding *2*-Bromo-*5*-aminophenyl glyme ether **4** as a slightly brown oil (2.48 g, 93%).

**$^{1}$H-NMR** (300 MHz, $CDCl_3$): δ (ppm) = 7.17 (d, J = 8.5 Hz, 1H), 6.52 (d, J = 2.5 Hz, 1H), 6.16 (dd, J = 8.4, 2.5 Hz, 1H), 4.43 (p, J = 5.1 Hz, 1H), 3.84 (s, br, 2H), 3.78 – 3.45 (m, 28H), 3.34 (s, 6H). **$^{13}$C-NMR** (75 MHz, $CDCl_3$): δ (ppm) = 155.6, 147.6, 133.2, 109.6, 104.1, 101.0, 79.3, 72.0, 71.1, 70.7, 70.64, 70.62, 70.5, 59.1. **MS-ESI**: m/z = 554.1935 (calc. for [M + $H^+$]: 554.1965), 576.1819 (calc. for [M + $Na^+$]: 576.1784).

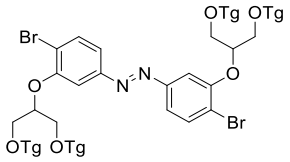


**Dibromo-DiglymeAzo 5:** *2*-Bromo-*5*-aminophenyl glyme ether **4** (2.5 mmol, 1.40 g, 1 eq.) was dissolved in toluene (10 mL) and a mixture of CuBr (0.1 mmol, 0.01 g, 0.03 eq.) and pyridine (0.2 mmol, 0.02 g, 0.09 eq.) in toluene (0.5 mL) was added. The solution was stirred vigorously under air and heated at 60°C for 7 h. Another portion of catalyst was added, and the reaction continued overnight. Water and DCM was added, the layers separated, and the aqueous layers extracted with DCM two times. The combined organic layers were dried over $MgSO_4$, filtered, and evaporated. The crude material was purified by repeated flash column chromatography (DCM/acetone/MeOH and DCM/MeOH) yielding Dibromo-DiglymeAzo **5** as a red oil (0.64 g, 46%). **$^{1}$H-NMR** (300 MHz, $CDCl_3$): δ (ppm) = 7.64 (d, J = 8.4 Hz, 2H), 7.61 (d, J = 2.1 Hz, 2H), 7.41 (dd, J = 8.4, 2.1 Hz, 2H), 4.69 (p, J = 5.0 Hz, 2H), 3.86 – 3.42 (m, 56H), 3.32 (s, 12H). **$^{13}$C-NMR** (75 MHz, $CDCl_3$): δ (ppm) = 155.7, 152.5, 133.6, 118.5, 117.0, 108.5, 79.1, 71.9, 71.3, 70.6, 70.5, 59.0. **MS-ESI**: m/z = 1103.3630 (calc. for [M + $H^+$]: 1103.3538), 1125.3457 (calc. for [M + $Na^+$]: 1125.3358), 552.1768 (calc. for [M + 2$H^+$]: 552.1803), 575.1641 (calc. for [M + 2$Na^+$]: 575.1612).

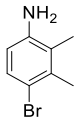


***4*-Bromo-*2,3*-dimethylaniline (7):** *2,3*-Dimethylaniline (**6**) (10.3 mmol, 1.25 g, 1 eq.) was dissolved in DMF (20 mL) and cooled down to 0°C. A solution of NBS (10.3 mmol, 1.83 g, 1 eq.) in DMF (10 mL) was added dropwise (dropping funnel) under vigorous stirring and exclusion of light. After complete addition stirring was continued for 5 h. The solution was diluted with water and extracted with DCM three times. The combined organic layers were washed with 1 M NaOH and brine, dried over $MgSO_4$, filtered, and evaporated yielding a violet oil that was pure according to NMR (1.94 g, 94%).

**$^1$H-NMR** (300 MHz, $CD_2Cl_2$): δ (ppm) 7.16 (d, J = 8.5 Hz, 1H), 6.44 (d, J = 8.5 Hz, 1H), 3.63 (s, br, 2H), 2.36 (s, 3H), 2.12 (s, 3H). **$^{13}$C-NMR** (75 MHz, $CD_2Cl_2$): δ (ppm) = 144.7, 136.5, 130.3, 123.2, 114.7, 114.2, 20.4, 14.5. **MS-ESI**: m/z = 199.9938 (calc. for [M + $H^+$]: 200.0075), 241.0253 (calc. for [M + MeCN + $H^+$]: 241.0340).

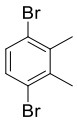


***1,4*-Dibromo-*2,3*-dimethylbenzene (8):** *4*-Bromo-*2,3*-dimethylaniline (**7**) (30.1 mmol, 6.01 g, 1 eq.) was dissolved in acetonitrile and *p*-toluenesulfonic acid (36.1 mmol, 6.86 g, 1.2 eq.), tetrabutylammonium bromide (60.1 mmol, 19.38 g, 2 eq.), and $CuBr_2$ (0.3 mmol, 0.07 g, 0.01 eq.) were added. Under vigorous stirring $^t$butyl nitrite (36.1 mmol, 3.72 g, 1.2 eq.) was added dropwise and the obtained suspension was stirred overnight. The mixture was diluted with water and extracted with hexanes three times. The combined organic layers were washed with 1 M NaOH, 1 M HCl, and brine, dried over $MgSO_4$, filtered, and evaporated yielding a brown solid that was pure according to NMR (7.57 g, 95%).

**$^1$H-NMR** (300 MHz, $CDCl_3$): δ (ppm) 7.25 (s, 2H), 2.45 (s, 6H). **$^{13}$C-NMR** (75 MHz, $CDCl_3$): δ (ppm) = 138.1, 131.1, 124.5, 21.2.

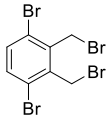


***1,4*-Dibromo-*2,3*-bis(bromomethyl)benzene (9):** *1,4*-Dibromo-*2,3*-dimethylbenzene (**8**) (17.8 mmol, 4.71 g, 1 eq.) was dissolved in acetonitrile (100 mL) and *N*-bromosuccinimide (36.6 mmol, 6.51 g, 2.05 eq.) as well as dibenzoyl peroxide (0.5 mmol, 0.13 g, 0.03 eq.) were added. The solution was heated at reflux and illuminated with a 500 W lamp for 3 h. hexanes and aqueous $Na_2S_2O_3$ (10%) was added the layers separated and the aqueous layer extracted with hexanes twice. The combined organic layers were dried over $MgSO_4$, filtered, and evaporated. The crude material was dissolved in DCM and the solution slowly dropped into cold EtOH. The precipitate was filtered and dried under vacuum yielding the title compound as a white solid (7.48 g, 98%).

**$^1$H-NMR** (300 MHz, $CD_2Cl_2$): δ (ppm) = 7.45 (s, 2H), 4.83 (s, 4H). **$^{13}$C-NMR** (75 MHz, $CDCl_3$): δ (ppm) = 138.1, 134.6, 125.3, 29.8.

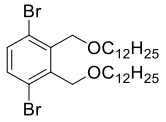


***1,4*-Dibromo-*2,3*-bis((dodecoxy)methyl)benzene (10):** Following the general procedure for the etherification of benzyl bromides with dodecanol, dodecanol (53.3 mmol, 9.92 g, 3 eq.), NaH (44.4 mmol, 1.07 g, 2.5 eq.), *1,4*-Dibromo-*2,3*-bis(bromomethyl)benzene (**9**) (17.8 mmol, 7.49 g, 1.0 eq.), column chromatography eluent: hexanes/DCM, yield: 10.06 g (90%).

**$^1$H-NMR** (300 MHz, $CDCl_3$): δ (ppm) = 7.39 (s, 2H), 4.75 (s, 4H), 3.55 (t, J = 6.5 Hz, 4H), 1.72 – 1.53 (m, 4H), 1.44 – 1.13 (m, 36H), 0.88 (t, J = 6.7 Hz, 6H). **$^{13}$C-NMR** (75 MHz, $CDCl_3$): δ (ppm) = 139.1, 134.1, 125.9, 71.3, 69.4, 32.1, 29.9, 29.82, 29.79, 29.6, 29.5, 26.3, 22.8, 14.3.

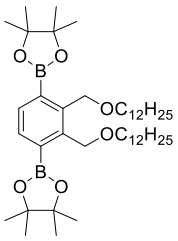


**Didodecoxy-Diboronic ester 11:** Following the general procedure for the Miyaura borylation of dibromobenzenes, *1,4*-Dibromo-*2,3*-bis((dodecoxy)methyl)benzene (**10**) (14.2 mmol, 9.00 g, 1 eq.), Bis(pinacolato)diboron (32.7 mmol, 8.31 g, 2.3 eq.), KOAc (85.4 mmol, 8.38 g, 6 eq.), Pd(dppf)$Cl_2$ (0.4 mmol, 0.31 g, 0.03 eq.), column chromatography eluent: hexanes/EA, yield: 5.62 g (54%).

**$^1$H-NMR** (300 MHz, $CDCl_3$): δ (ppm) = 7.61 (s, 2H), 4.81 (s, 4H), 3.39 (t, J = 6.8 Hz, 4H), 1.61 – 1.44 (m, 4H), 1.42 – 1.15 (m, 60H), 0.88 (t, J = 6.7 Hz, 6H). **$^{13}$C-NMR** (75 MHz, $CDCl_3$): δ (ppm) = 142.6, 133.8, 83.7, 70.2, 68.3, 32.1, 30.0, 29.83, 29.80, 29.7, 29.5, 26.4, 25.0, 22.8, 14.3. **MS-ESI**: (the free boronic acid was observed) m/z = 585.4470 (calc. for [M + $Na^+$]: 585.4474), 545.4555 (calc. for [M - $H_3O^+$]: 545.4549).

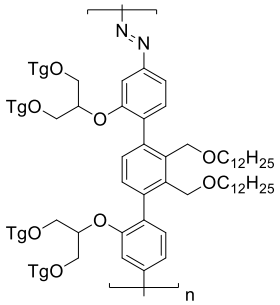


**AzoPolymer P-1: P-1** was prepared in two different ways following the Suzuki polycondensation and the polyazo coupling approach.

Suzuki polycondensation: Dibromo-DiglymeAzo **6** (0.2 mmol, 0.18 g, 1 eq.), Didodecoxy-Diboronic ester **9** (0.2 mmol, 0.12 g, 1 eq.), and $K_3PO_4$ (0.5 mmol, 0.10 g, 3 eq.) were filled in a sealed tube and dissolved in toluene (0.7 mL) and water (0.3 mL) carefully respecting the stoichiometry of the monomers. The mixture was degassed by three freeze-pump-thaw cycles. $Pd(OAc)_2$ (0.01 mmol, 1.0 mg, 0.04 eq.) and SPhos (0.02 mmol, 7.0 mg, 0.1 eq.) were added and the mixture heated at 100°C under argon for 3 d. After cooling down DCM and water were added, the layers separated, and the aqueous layer extracted with DCM three time. The combined organic layers were washed with brine, dried over $MgSO_4$, filtered, and evaporated. The crude material was purified by preparative GPC with THF as eluent yielding polymer **P-1** as a red sticky paste (0.03 g, 26%).

Polyazo coupling: Following the general procedure for the reductive polymerization of Dinitro-Terphenyls, Terphenyl **23** (0.2 mmol, 0.30 g, 1 eq.), Red-Al (2.0 mmol, 0.41 g, 10 eq.), yield: 0.25 g (46% after preparative GPC). This polymer could not be precipitated by adding its solution to cold methanol. Alternatively, compound **31** was dissolved in THF and the solution added to cold water. The precipitate was further purified by preparative GPC.

**$^1$H-NMR** (300 MHz, $CD_2Cl_2$): δ (ppm) = 7.93 – 6.75 (m, 8H), 4.84 – 4.02 (m, 6H), 3.85 – 2.93 (m, 72H), 1.62 – 0.99 (m, 40H), 0.86 (s, 6H).

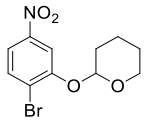


***2*-Bromo-*5*-nitrophenyl tetrahydropyranyl ether 12:** *2*-Bromo-*5*-nitrophenol (**2**) (30.0 mmol, 6.54 g, 1 eq.) was dissolved in *3,4*-dihydro-*2H*-pyran (20 mL) and cooled down to 0°C. *p*-Toluenesulfonic acid (1.5 mmol, 0.29 g, 0.05 eq.) was added and the mixture stirred for 2 h. The solution was diluted with ethyl acetate, washed with 1 M NaOH, water, and brine, dried over $MgSO_4$, filtered, and evaporated. The crude material was purified by flash column chromatography (hexanes/DCM) yielding the title compound as an off-white solid (6.88 g, 76%).

**$^1$H-NMR** (300 MHz, $CDCl_3$): δ (ppm) = 7.99 (d, J = 2.3 Hz, 1H), 7.74 (dd, J = 8.7, 2.3 Hz, 1H), 7.69 (d, J = 8.7 Hz, 1H), 5.64 (t, J = 2.7 Hz, 1H), 3.89 – 3.56 (m, 2H), 2.20 – 1.54 (m, 6H). **$^{13}$C-NMR** (75 MHz, $CDCl_3$): δ (ppm) = 154.0, 148.1, 133.6, 120.8, 117.3, 111.0, 97.2, 62.1, 30.0, 25.1, 18.2. **MS-ESI**: m/z = 323.9860 (calc. for $[M + Na^+]$: 323.9842).

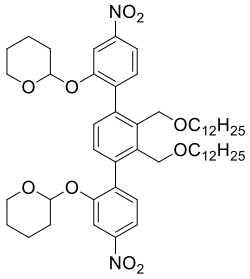

**2THP-2C12-Terphenyl 13:** Following the general procedure for the Suzuki coupling to Terphenyls, *2*-Bromo-*5*-nitrophenyl ether **12** (19.3 mmol, 5.83 g, 1 eq.), Didodecoxy-Diboronic ester **11** (7.7 mmol, 5.61 g, 0.4 eq.), $K_3PO_4$ (57.9 mmol, 12.29 g, 3 eq.), $Pd(OAc)_2$ (1.0 mmol, 0.22 g, 0.05 eq.), SPhos (1.9 mmol, 0.79 g, 0.1 eq.), column chromatography eluent: hexanes/EA, yield: 5.98 g (84%).

**$^1$H-NMR** (300 MHz, $CD_2Cl_2$): δ (ppm) = 8.15 – 8.02 (m, 2H), 7.98 – 7.86 (m, 2H), 7.64 – 7.41 (m, 2H), 7.39 – 7.15 (m, 2H), 5.66 – 5.42 (m, 2H), 4.83 – 3.99 (m, 4H), 3.85 – 3.54 (m, 4H), 3.37 – 3.11 (m, 4H), 1.87 – 1.07 (m, 52H), 0.99 – 0.80 (m, 6H). **$^{13}$C-NMR** (75 MHz, $CDCl_3$): δ (ppm) = 155.3, 148.9, 138.6, 137.1, 132.2, 129.7, 116.6, 110.3, 98.3, 97.1, 71.2, 68.1, 62.3, 32.5, 30.5, 30.4, 30.3, 30.2, 30.1, 29.9, 26.8, 25.6, 24.2, 23.3, 18.8, 14.5. **MS-ESI**: m/z = 939.5759 (calc. for $[M + Na^+]$: 939.5711).

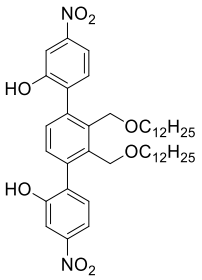

**2OH-2C12-Terphenyl 14:** Following the general procedure for the deprotection of tetrahydropyranyl ethers, terphenyl **13** (6.5 mmol, 5.98 g, 1 eq.), *p*-toluenesulfonic acid (0.7 mmol, 0.124 g, 0.1 eq.), column chromatography eluent: hexanes/EA/methanol, yield: 4.88 g (quant.).

**$^1$H-NMR** (300 MHz, $CD_2Cl_2$): δ (ppm) = 7.95 – 7.81 (m, 4H), 7.45 – 7.32 (m, 4H), 4.78 – 4.14 (m, 4H), 3.60 – 3.39 (m, 4H), 1.70 – 1.49 (m, 4H), 1.43 – 1.19 (m, 36H), 0.96 – 0.81 (m, 6H). **$^{13}$C-NMR** (75 MHz, $CD_2Cl_2$): δ (ppm) = 155.6, 149.5, 139.0, 136.5, 135.9, 132.5, 132.2, 116.4, 114.0, 72.8, 68.4, 32.5, 30.2, 30.2, 30.0, 29.9, 29.8, 26.5, 23.3, 14.5 (only major signals corresponding to the main atropisomer are given). **MS-ESI**: m/z = 747.4576 (calc. for $[M - H^+]$: 747.4584).

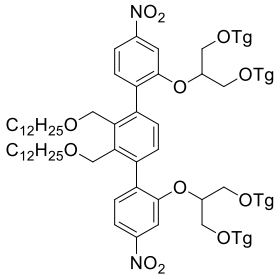

**2OTg-2C12-Terphenyl 15:** Following the general procedure for the etherification of OH-Terphenyls, Terphenyl **14** (0.8 mmol, 0.60 g, 1 eq.), $(triglyme)_2$ tosylate (2.0 mmol, 1.08 g, 2.5 eq.), $Cs_2CO_3$ (2.0 mmol, 0.65 g, 2.5 eq.), solvent: *N*,*N*-dimethylformamide, chromatography eluent DCM : acetone : MeOH and DCM : MeOH, yield: 0.62 g (53%).

**$^1$H-NMR** (500 MHz, $CD_2Cl_2$): δ (ppm) 8.18 – 8.11 (m, 2H), 7.92 – 7.85 (m, 2H), 7.57 – 7.43 (m, 2H), 7.32 (s, 2H), 4.76 – 3.97 (m, 6H), 3.69 – 3.42 (m, 60H), 3.36 – 3.28 (m, 12H), 1.46 (m, 4H), 1.34 – 1.17 (m, 40H), 0.87 (t, J = 7.0 Hz, 6H) (the given signals belong to all atropisomers, separation not possible due to strong overlapping). **$^{13}$C-NMR** (125 MHz, $CD_2Cl_2$): δ (ppm) 156.9, 148.8, 138.6, 138.0, 136.9, 132.6, 130.3, 116.0, 110.3, 79.7, 72.4, 72.4, 71.7, 71.6, 71.5, 71.2, 71.14, 71.11, 71.02, 71.00, 70.97, 70.91, 70.9, 67.9, 59.13, 59.11, 32.5, 30.3, 30.24, 30.20, 30.1, 29.9, 26.9, 23.2, 14.4 (only major signals corresponding to the main atropisomer are given). **MS-ESI**: m/z = 771.3668 (calc. for $[M + Na^+ + K^+]$: 741.4347).

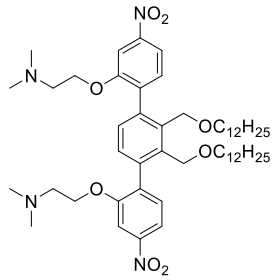

**2NMe$_2$-2C12-Terphenyl 16:** Following the general procedure for the etherification of OH-Terphenyls, Terphenyl **14** (0.25 mmol, 0.19 g, 1 eq.), *2*-chloro-*N*,*N*-dimethylethylamine hydrochloride (1.0 mmol, 0.14 g, 4 eq.), $Cs_2CO_3$ (1.5 mmol, 0.49 g, 6 eq.), chromatography eluent: ethyl acetate/hexanes/triethylamine, yield: 0.19 g (85%).

**$^1$H-NMR** (300 MHz, $CD_2Cl_2$): δ (ppm) = 7.98 – 7.80 (m, 4H), 7.49 (dd, J = 26.0, 8.2 Hz, 2H), 7.25 (d, J = 12.5 Hz, 2H), 4.57 (dd, J = 45.9, 10.5 Hz, 2H), 4.32 – 3.95 (m, 6H), 3.38 – 3.12 (m, 4H), 2.62 (t, J = 5.9 Hz, 4H), 2.20 (d, J = 7.0 Hz, 12H), 1.57 – 1.14 (m, 40H), 0.88 (t, J = 6.7 Hz, 6H) (the big coupling constants belong to a separate sets of signals of another atropisomer). **$^{13}$C-NMR** (75 MHz, $CD_2Cl_2$): δ (ppm) 157.0, 148.9, 138.4, 137.6, 137.0, 132.5, 130.1, 115.8, 107.2, 71.3, 68.3, 68.0, 58.2, 46.3, 32.5, 30.4, 30.3, 30.1, 29.9, 26.9, 23.3, 14.5 (only major signals corresponding to the main

atropisomer are given). **MS-ESI**: m/z = 891.6287 (calc. for [M + $H^+$]: 891.6211), 446.3147 (calc. for [M + $2H^+$]: 446.3139).

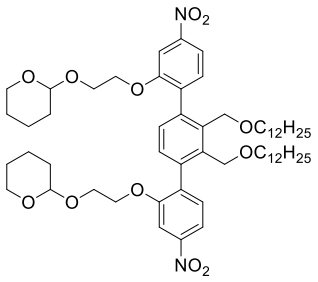

**2EtOTHP-2C12-Terphenyl 17:** Following the general procedure for the etherification of OH-Terphenyls, Terphenyl **14** (0.5 mmol, 0.38 g, 1 eq.), THP-protected *2*-bromoethanol (4.0 mmol, 0.84 g, 8 eq.), $K_2CO_3$ (2.0 mmol, 0.28 g, 4 eq.), chromatography eluent: hexanes/ethyl acetate, yield: 0.39 g (78%).

**$^1$H-NMR** (300 MHz, $CD_2Cl_2$): δ (ppm) = 8.05 – 7.83 (m, 4H), 7.62 – 7.40 (m, 2H), 7.34 – 7.20 (m, 2H), 4.70 – 4.43 (m, 4H), 4.36 – 4.18 (m, 4H), 4.12 – 3.10 (m, 14H), 1.93 – 1.11 (m, 52H), 0.87 (t, J = 6.7 Hz, 6H) (the given signals belong to all atropisomers, separation not possible due to strong overlapping). **$^{13}$C-NMR** (75 MHz, $CD_2Cl_2$): δ (ppm) 157.1, 148.9, 138.4, 137.0, 132.6, 130.2, 115.8, 107.6, 99.3, 99.1, 71.5, 69.3, 67.9, 65.8, 62.2, 32.5, 30.3, 30.3, 30.2, 30.1, 29.9, 23.3, 14.5. (only major signals corresponding to the main atropisomer are given). **MS-ESI**: (both THP protecting groups were cleaved under the acidic conditions in the UPLC) m/z = 859.5167 (calc. for [M - 2THP + $Na^+$]: 859.5085).

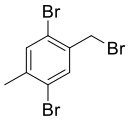

***2,5*-Dibromo-*4*-(bromomethyl)-toluene (19):** Bromine (250.0 mmol, 39.95 g, 3.1 eq.) and iodine (0.8 mmol, 0.20 g, 0.01 eq.) were dissolved in dichloromethane (8 mL) and *4*-methylbenzyl alcohol (**18**) (80.0 mmol, 9.77 g, 1 eq.) in dichloromethane (10 mL) was added slowly. The solution was heated at reflux overnight. After cooling down, the mixture was diluted with dichloromethane, washed with aqueous $Na_2S_2O_3$ (10%), water, and brine, dried over $MgSO_4$, filtered, and evaporated. The crude material was recrystallized from ethanol yielding 8.38 g (31%) of the title compound as white needles.

**$^1$H-NMR** (300 MHz, $CDCl_3$): δ (ppm) 7.60 (s, 1H), 7.44 (s, 1H), 4.51 (s, 2H), 2.36 (s, 3H). **$^{13}$C-NMR** (75 MHz, $CDCl_3$): δ ppm 140.5, 136.2, 135.0, 134.5, 124.0, 123.0, 32.3, 22.6.

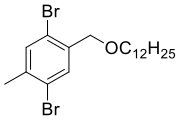


***1,4*-dibromo-*2*-((dodecyloxy)methyl)-*5*-methylbenzene (20):** Following the general procedure for the etherification of benzyl bromides with dodecanol, dodecanol (1.8 mmol, 0.33 g, 1.5 eq.), NaH (1.8 mmol, 0.04 g, 1.5 eq.), *2,5*-Dibromo-*4*-(bromomethyl)-toluene (**19**) (1.2 mmol, 0.40 g, 1.0 eq.), column chromatography eluent: hexanes/DCM, yield: 10.06 g (90%).

**$^{1}$H-NMR** (300 MHz, $CDCl_3$): δ (ppm) = 7.62 (s, 1H), 7.39 (s, 1H), 4.47 (s, 2H), 3.53 (t, J = 6.6 Hz, 2H), 2.35 (s, 3H), 1.71 – 1.58 (m, 2H), 1.45 – 1.16 (m, 18H), 0.88 (t, J = 6.7 Hz, 3H). **$^{13}$C-NMR** (75 MHz, $CDCl_3$): δ (ppm) = 138.7, 137.4, 134.2, 132.4, 124.0, 120.9, 77.2, 71.4, 71.3, 32.1, 29.83, 29.80, 29.77, 29.6, 29.5, 26.3, 22.9, 22.5, 14.3.

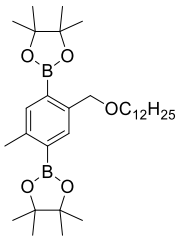


**Dodecoxy-Me-Diboronic Ester 21:** Following the general procedure for the Miyaura borylation of dibromobenzenes, *1,4*-dibromo-*2*-((dodecyloxy)methyl)-*5*-methylbenzene (**20**) (0.5 mmol, 0.22 g, 1 eq.), Bis(pinacolato)diboron (1.1 mmol, 0.28 g, 2.2 eq.), KOAc (3.0 mmol, 0.29 g, 6 eq.), $Pd(dppf)Cl_2$ (0.03 mmol, 0.02 g, 0.06 eq.), column chromatography eluent: hexanes/EA, yield: 0.21 g (77%).

**$^{1}$H-NMR** (300 MHz, $CDCl_3$): δ (ppm) = 7.76 (s, 1H), 7.55 (s, 1H), 4.67 (s, 2H), 3.43 (t, J = 6.8 Hz, 2H), 2.51 (s, 3H), 1.65 – 1.51 (m, 2H), 1.43 – 1.21 (m, 42H), 0.88 (t, J = 6.8 Hz, 3H). **$^{13}$C-NMR** (75 MHz, $CDCl_3$): δ (ppm) = 143.1, 140.6, 136.8, 135.9, 83.6, 83.5, 72.1, 70.5, 32.1, 30.0, 29.8, 29.77, 29.74, 29.5, 26.4, 25.02, 24.99, 22.8, 21.8, 14.3. **MS-ESI**: (the free boronic acid was observed) m/z = 361.2749 (calc. for [M - $H_3O^+$]: 361.2716).

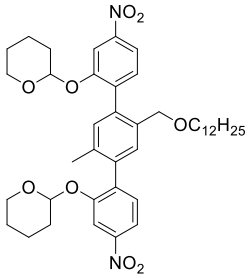

**2THP-1C12-1Me-Terphenyl 22:** Following the general procedure for the Suzuki coupling to Terphenyls, Dodecoxy-Me-Diboronic Ester **21** (1.0 mmol, 0.54 g, 1 eq.), *2*-Bromo-*5*-nitrophenyl ether **12** (2.1 mmol, 0.63 g, 2.1 eq.), $K_3PO_4$ (6.0 mmol, 1.27 g, 3 eq.), $Pd(OAc)_2$ (0.1 mmol, 0.02 g, 0.1 eq.), SPhos (0.2 mmol, 0.08 g, 0.2 eq.), column chromatography eluent: hexanes/ethyl acetate, yield: 0.62 g (85%).

**$^1$H-NMR** (500 MHz, $CD_2Cl_2$): δ (ppm) = 8.07 (d, br, J = 4.7 Hz, 2H), 7.93 (ddd, J = 8.3, 4.7, 2.2 Hz, 2H), 7.42 (dd, J = 11.8, 8.3 Hz, 2H), 7.25 (d, br, J = 56.2 Hz, 2H), 5.53 (s, br, 2H), 4.29 (s, br, 2H), 3.93 – 3.50 (m, br, J = 18.2 Hz, 4H), 3.27 (t, J = 6.4 Hz, 2H), 2.20 (s, br, 3H), 1.85 – 1.36 (m, 14H), 1.35 – 1.14 (m, 18H), 0.87 (t, J = 6.9 Hz, 3H). **$^{13}$C-NMR** (125 MHz, $CD_2Cl_2$): δ (ppm) = 148.9, 138.9, 138.0, 137.2, 136.3, 135.8, 134.8, 132.1, 132.0, 131.8, 130.2, 116.9, 71.1, 70.9, 62.6, 60.8, 32.5, 30.59, 30.55, 30.3, 30.22, 30.19, 30.18, 30.16, 30.0, 29.9, 26.8, 25.6, 23.3, 20.0, 18.9, 14.4. **MS-ESI**: (one THP protecting group was cleaved under the acidic conditions in the UPLC) m/z = 647.3392 (calc. for [M - THP - $H^+$]: 647.3338).

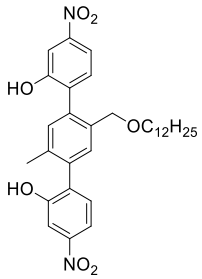

**2OH-1C12-1Me-Terphenyl 23:** Following the general procedure for the deprotection of tetrahydropyranyl ethers, terphenyl **22** (1.9 mmol, 1.41 g, 1 eq.), *p*-toluenesulfonic acid (0.2 mmol, 0.04 g, 0.1 eq.), column chromatography eluent: hexanes/EA, yield: 1.08 g (quant.).

**$^1$H-NMR** (500 MHz, DMSO-$d_6$): δ (ppm) = 10.60 (d, J = 5.7 Hz, 2H), 7.86 – 7.65 (m, 4H), 7.44 – 7.31 (m, 2H), 7.24 (s, 1H), 7.10 (s, 1H), 4.27 (s, 2H), 3.22 (t, J = 6.3 Hz, 2H), 2.13 (s, 3H), 1.42 – 1.02 (m, 18H), 0.83 (t, J = 6.9 Hz, 3H). **$^{13}$C-NMR** (125 MHz, DMSO-$d_6$): δ (ppm) = 155.3, 155.2, 147.5, 147.5, 136.5, 135.6, 135.5, 134.9, 134.7, 134.2, 131.8, 131.7, 131.1, 129.1, 113.8, 113.7, 109.7, 109.6, 69.7, 69.6, 31.3, 29.0, 28.98, 28.8, 28.7, 25.6, 22.1, 19.1, 13.9. **MS-ESI**: m/z = 563.2751 (calc. for [M - $H^+$]: 563.2757), 609.2797 (calc. for [M + $HCOO^-$]: 609.2812).

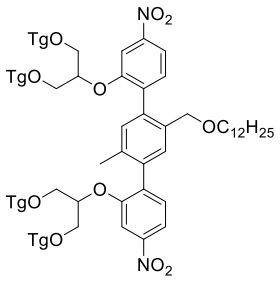


**2OTg-1C12-1Me-Terphenyl 24:** Following the general procedure for the etherification of OH-Terphenyls, Terphenyl **23** (0.8 mmol, 0.45 g, 1 eq.), $(triglyme)_2$ tosylate (2.0 mmol, 1.08 g, 2.5 eq.), $Cs_2CO_3$ (2.0 mmol, 0.65 g, 2.5 eq.), solvent: *N*,*N*-dimethylformamide (5 mL), chromatography eluent DCM/acetone/MeOH and DCM/MeOH, yield: 0.31 g (30%).

**$^1$H-NMR** (300 MHz, $CD_2Cl_2$): δ (ppm) 8.11 (dd, J = 4.1, 2.2 Hz, 2H), 7.90 (ddd, J = 8.3, 4.4, 2.2 Hz, 2H), 7.40 (dd, J = 17.2, 8.3 Hz, 2H), 7.24 (d, J = 47.2 Hz, 2H), 4.74 – 4.58 (m, 2H), 4.28 (s, br, 2H), 3.74 – 3.41 (m, 58H), 3.35 – 3.28 (m, 12H), 2.15 (s, br, 3H), 1.51 – 1.35 (m, 2H), 1.25 (m, 18H), 0.87 (t, J = 6.7 Hz, 3H) (the given signals belong to all atropisomers, separation not possible due to strong overlapping). **$^{13}$C-NMR** (75 MHz, $CD_2Cl_2$): δ (ppm) 156.8, 156.7, 148.8, 138.8, 138.0, 137.3, 136.4, 136.0, 134.9, 132.3, 132.1, 131.9, 130.3, 116.4, 116.3, 110.2, 110.1, 79.4, 79.1, 72.4, 71.6, 71.2, 71.1, 71.0, 70.93, 70.87, 59.1, 32.4, 30.24, 30.17, 30.1, 30.0, 29.9, 26.8, 23.2, 19.9, 14.4 (only major signals corresponding to the main atropisomer are given). **MS-ESI**: m/z = 688.4125 (calc. for $[M + H_2O + Na^+ + K^+]$: 688.3486), 1314.7419 (calc. for $[M + H_2O]$: 1314.7449).

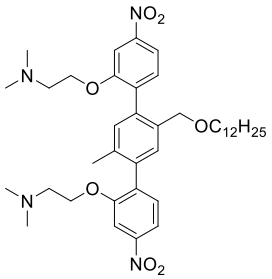


**2NMe$_2$-1C12-1Me-Terphenyl 25:** Following the general procedure for the etherification of OH-Terphenyls, Terphenyl **23** (0.7 mmol, 0.42 g, 1 eq.), *2*-chloro-*N*,*N*-dimethylethylamine hydrochloride (3.0 mmol, 0.43 g, 4 eq.), $Cs_2CO_3$ (4.4 mmol, 1.45 g, 6 eq.), chromatography eluent: ethyl acetate : hexanes : triethylamine, yield: 0.44 g (84%).

**$^1$H-NMR** (300 MHz, $CD_2Cl_2$): δ (ppm) = 7.91 (ddd, J = 8.2, 4.3, 2.2 Hz, 2H), 7.86 (dd, J = 4.5, 2.1 Hz, 2H), 7.40 (dd, J = 13.3, 8.2 Hz, 2H), 7.22 (d, J = 55.3 Hz, 2H), 4.46 – 4.02 (m, 6H), 3.31 – 3.21 (m, 2H), 2.64 (dd, J = 10.1, 5.7 Hz, 4H), 2.18 (d, J = 12.0 Hz, 12H), 1.51 – 1.36 (m, 2H), 1.34 – 1.15 (m, 18H), 0.87 (t, J = 6.7 Hz, 3H) (the given signals belong to all atropisomers, separation not possible due to strong overlapping). **$^{13}$C-NMR** (75 MHz, $CD_2Cl_2$): δ (ppm) = 157.1, 157.0, 148.9, 138.2, 137.4,

137.2, 136.2, 136.1, 135.1, 132.2, 132.0, 131.9, 130.2, 116.2, 116.1, 107.2, 107.1, 71.2, 70.8, 68.2, 58.2, 58.2, 46.3, 46.3, 32.5, 30.3, 30.22, 30.17, 30.0, 29.9, 26.8, 23.3, 19.8, 14.5 (only major signals corresponding to the main atropisomer are given). **MS-ESI**: m/z = 354.2233 (calc. for [M + $2H^+$]: 354.2226), 707.4440 (calc. for [M + $H^+$]: 707.4384).

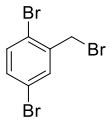


***1,4*-Dibromo-*2*-(bromomethyl)benzene 27:** *1,4*-Dibromo-*2*-methylbenzene (**26**) (60.0 mmol, 15.00 g, 1 eq.) was dissolved in acetonitrile (400 mL) and *N*-bromosuccinimide (90.0 mmol, 16.02 g, 1.5 eq.) as well as dibenzoyl peroxide (1.8 mmol, 0.44 g, 0.03 eq.) were added. The solution was heated at reflux and illuminated with a 500 W lamp for 3 h. DCM and aqueous $Na_2S_2O_3$ (10%) was added the layers separated and the aqueous layer extracted with DCM twice. The combined organic layers were dried over $MgSO_4$, filtered, and evaporated. The crude material was purified by flash column chromatography (hexanes) yielding the title compound as a white solid (7.14 g, 36%).

**$^1$H-NMR** (300 MHz, $CDCl_3$): δ (ppm) = 7.59 (d, J = 2.4 Hz, 1H), 7.44 (d, J = 8.5 Hz, 1H), 7.29 (dd, J = 8.5, 2.4 Hz, 1H), 4.53 (s, 2H). **$^{13}$C-NMR** (75 MHz, $CDCl_3$): δ ppm 139.4, 135.1, 135.0, 133.8, 123.4, 123.0, 32.9.

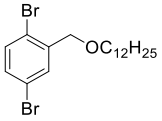


***1,4*-Dibromo-*2*-((dodecoxy)methyl)benzene 28:** Following the general procedure for the etherification of benzyl bromides with dodecanol, dodecanol (31.9 mmol, 5.95 g, 1.5 eq.), NaH (31.9 mmol, 0.78 g, 1.5 eq.), *1,4*-Dibromo-*2*-(bromomethyl)benzene (**27**) (21.3 mmol, 7.00 g, 1.0 eq.), column chromatography eluent: hexanes, yield: 9.16 g (99%).

**$^1$H-NMR** (300 MHz, $CDCl_3$): δ (ppm) = 7.60 (d, J = 2.4 Hz, 1H), 7.40 (d, J = 8.5 Hz, 1H), 7.30 (dd, J = 8.5, 2.4 Hz, 1H), 4.49 (s, 2H), 3.51 (t, J = 6.6 Hz, 2H), 2.37 (s, 3H), 1.72 – 1.56 (m, 2H), 1.43 – 1.14 (m, 18H), 0.89 (t, J = 6.7 Hz, 3H). **$^{13}$C-NMR** (75 MHz, $CDCl_3$): δ (ppm) = 137.6, 137.1, 133.5, 132.2, 123.8, 120.7, 77.1, 71.7, 71.4, 31.9, 29.84, 29.80, 29.76, 29.6, 29.5, 26.3, 14.3.

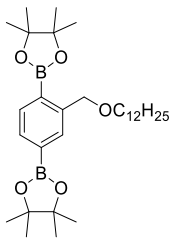


**Dodecoxy-Diboronic ester 29:** Following the general procedure for the Miyaura borylation of dibromobenzenes, *1*,*4*-dibromo-*2*-((dodecyloxy)methyl)benzene (**28**) (20.7 mmol, 9.00 g, 1 eq.), Bis(pinacolato)diboron (45.6 mmol, 11.58 g, 2.2 eq.), KOAc (124.3 mmol, 12.2 g, 6 eq.), Pd(dppf)$Cl_2$ (1.2 mmol, 0.91 g, 0.06 eq.), column chromatography eluent: hexanes/EA, yield: 8.51 g (78%).

**$^1$H-NMR** (500 MHz, $CD_2Cl_2$): δ (ppm) = 7.77 (s, 1H), 7.72 (d, J = 7.3 Hz, 1H), 7.64 (d, J = 7.3 Hz, 1H), 4.68 (s, 2H), 3.48 (t, J = 6.8 Hz, 2H), 1.65 – 1.55 (m, 2H), 1.32 (m, 42H), 0.89 (t, J = 6.9 Hz, 3H). **$^{13}$C-NMR** (125 MHz, $CDCl_3$): δ (ppm) = 144.5, 135.1, 134.5, 133.2, 84.4, 84.3, 72.6, 71.3, 32.5, 30.5, 30.3, 30.2, 30.2, 30.0, 26.9, 25.3, 25.2, 23.3, 14.5. **MS-ESI**: m/z = 529.4206 (calc. for [M + $H^+$]: 529.4230).

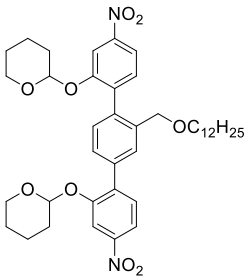


**2OTHP-1C12-Terphenyl 30:** Following the general procedure for the Suzuki coupling to terphenyls, Dodecoxy-Diboronic Ester **29** (15.8 mmol, 8.34 g, 0.5 eq.), *2*-Bromo-*5*-nitrophenyl ether **12** (33.6 mmol, 10.15 g, 1.0 eq.), $K_3PO_4$ (94.7 mmol, 20.14 g, 2.8 eq.), $Pd(OAc)_2$ (1.7 mmol, 0.38 g, 0.05 eq.), SPhos (3.2 mmol, 1.30 g, 0.09 eq.), column chromatography eluent: hexanes/ethyl acetate, yield: 8.12 g (72%)

**$^1$H-NMR** (500 MHz, $CD_2Cl_2$): δ (ppm) = 8.10 (d, J = 2.2 Hz, 1H), 8.06 (s, br, 1H), 7.94 (td, J = 8.4, 2.2 Hz, 2H), 7.81 (s, br, 1H), 7.58 (dd, J = 8.4, 0.6 Hz, 2H), 7.45 (dd, J = 8.3, 0.9 Hz, 1H), 7.32 (s, br, 1H), 5.67 – 5.39 (m, 2H), 4.53 – 4.20 (m, 2H), 3.87 – 3.51 (m, 4H), 3.32 (s, br, 2H), 1.92 – 1.40 (m, 14H), 1.34 – 1.15 (m, 18H), 0.87 (t, J = 7.0 Hz, 3H). **$^{13}$C-NMR** (125 MHz, $CD_2Cl_2$): δ (ppm) = 154.9, 149.0, 148.6, 138.0, 137.7, 137.6, 137.0, 132.0, 131.5, 130.2, 129.9, 128.6, 117.2, 111.0, 97.6, 71.4, 71.1, 62.5, 32.5, 30.53, 30.49, 30.3, 30.22, 30.18, 30.18, 30.17, 30.0, 29.9, 26.8, 25.6, 25.5, 23.3, 18.8, 14.4. **MS-ESI**: (one THP protecting group was cleaved under the acidic conditions in the UPLC) m/z = 633.3202 (calc. for [M - $H^+$]: 633.3181).

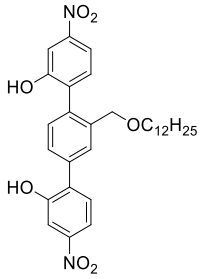

**2OH-1C12-Terphenyl 31:** Following the general procedure for the deprotection of tetrahydropyranyl ethers, terphenyl **30** (2.0 mmol, 1.41 g, 1 eq.), *p*-toluenesulfonic acid (0.2 mmol, 0.04 g, 0.1 eq.), column chromatography eluent: hexanes/EA, yield: 0.97 g (90%).

**$^1$H-NMR** (500 MHz, DMSO-$d_6$): δ (ppm) 10.68 (d, J = 44.6 Hz, 2H), 7.79 (dd, J = 19.8, 2.3 Hz, 2H), 7.76 – 7.68 (m, 3H), 7.59 (dd, J = 7.9, 1.8 Hz, 1H), 7.56 (d, J = 8.4 Hz, 1H), 7.38 (d, J = 8.3 Hz, 1H), 7.26 (d, J = 7.9 Hz, 1H), 4.33 (s, br, 2H), 3.24 (t, J = 6.3 Hz, 2H), 1.41 – 1.31 (m, 2H), 1.27 – 1.06 (m, 18H), 0.81 (t, J = 7.0 Hz, 3H) (the given signals belong to all atropisomers). **$^{13}$C-NMR** (125 MHz, DMSO-$d_6$): δ (ppm) = 155.3, 155.2, 147.6, 147.2, 136.8, 136.1, 135.7, 134.5, 134.4, 131.7, 131.1, 129.7, 128.5, 127.9, 114.3, 113.7, 110.4, 109.6, 69.8, 69.7, 31.3, 29.1, 29.0, 28.9, 28.8, 25.7, 22.1, 13.9 (the given signals belong to all atropisomers). **MS-ESI**: m/z = 549.2314 (calc. for [M - $H^+$]: 549.2601), 595.2314 (calc. for [M + $HCOO^-$]: 595.2656).

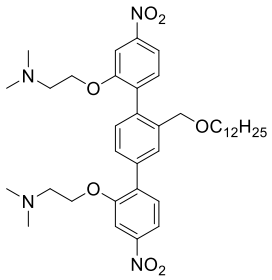

**2NMe$_2$-1C12-Terphenyl 32:** Following the general procedure for the etherification of OH-Terphenyls, Terphenyl **31** (0.8 mmol, 0.44 g, 1 eq.), *2*-chloro-*N*,*N*-dimethylethylamine hydrochloride (3.2 mmol, 0.46 g, 4 eq.), $Cs_2CO_3$ (4.8 mmol, 1.56 g, 6 eq.), chromatography eluent: DCM/triethylamine, yield: 0.47 g (85%).

**$^1$H-NMR** (500 MHz, $CD_2Cl_2$): δ (ppm) = 7.91 (ddd, J = 8.3, 6.2, 2.2 Hz, 2H), 7.87 (dd, J = 9.9, 2.1 Hz, 2H), 7.79 (s, 1H), 7.61 (dd, J = 7.9, 1.8 Hz, 1H), 7.56 (d, J = 8.3 Hz, 1H), 7.43 (d, J = 8.2 Hz, 1H), 7.30 (d, J = 7.9 Hz, 1H), 4.51 – 4.13 (m, 6H), 3.32 (t, J = 5.9 Hz, 2H), 2.79 – 2.56 (m, 4H), 2.23 (d, J = 49.2 Hz, 12H), 1.55 – 1.41 (m, 2H), 1.33 – 1.17 (m, 18H), 0.87 (t, J = 7.0 Hz, 3H) (the given signals belong to all atropisomers). **$^{13}$C-NMR** (125 MHz, $CD_2Cl_2$): δ (ppm) = 157.0, 156.9, 149.0, 148.6, 137.8, 137.4, 137.2, 136.9, 136.3, 132.1, 131.6, 130.3, 130.0, 128.8, 116.5, 116.1, 107.8, 107.1, 71.3, 71.1, 68.3, 68.2, 58.4, 58.2, 32.5, 30.3, 30.2, 30.19, 30.0, 29.9, 26.8, 23.3, 14.5 (the given signals belong

to all atropisomers). **MS-ESI**: m/z = 347.2096 (calc. for [M + 2H$^+$]: 347.2147), 693.4157 (calc. for [M + H$^+$]: 693.4227).

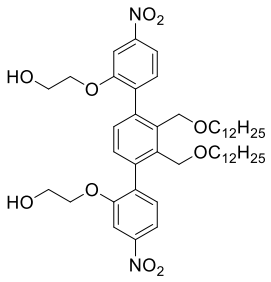

**2EtOH-2C12-Terphenyl 33:** Following the general procedure for the etherification of OH-Terphenyls, Terphenyl **17** (0.5 mmol, 0.38 g, 1 eq.), *2*-bromoethanol (8.0 mmol, 1.0 g, 16 eq.), $K_2CO_3$ (4.0 mmol, 0.55 g, 8 eq.), chromatography eluent: hexanes/üethyl acetate, yield: 0.40 g (95%).

**$^1$H-NMR** (300 MHz, $CD_2Cl_2$): δ (ppm) = 8.03 – 7.90 (m, 2H), 7.84 (d, J = 2.2 Hz, 2H), 7.56 – 7.43 (m, 2H), 7.26 (s, 2H), 4.52 – 4.28 (m, 4H), 4.22 – 3.61 (m, 10H), 3.39 – 3.19 (m, 4H), 1.68 – 1.13 (m, 40H), 0.99 – 0.80 (m, 6H). (the given signals belong to all atropisomers, separation not possible due to strong overlapping) **$^{13}$C-NMR** (75 MHz, $CD_2Cl_2$): δ (ppm) 157.0, 149.1, 138.7, 138.5, 136.9, 131.7, 130.1, 117.0, 108.6, 71.9, 68.4, 64.7, 61.1, 32.5, 30.2, 30.2, 30.2, 30.0, 29.96, 29.93, 26.7, 23.3, 14.5. (only major signals corresponding to the main atropisomer are given). **MS-ESI**: m/z = 859.5052 (calc. for [M + Na$^+$]: 859.5085).

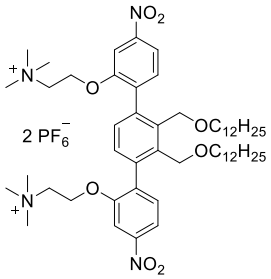

**2NMe$_3$-2C12-Terphenyl 34:** Terphenyl **16** (0.2 mmol, 0.19 g, 1 eq.) was dissolved in tetrahydrofuran and methyl iodide (2.1 mmol, 0.30 g, 10 eq.) was added. The mixture was stirred at room temperature overnight, the solvent evaporated, and the remaining solid suspended in acetone. Ammonium hexafluorophosphate (1.0 mmol, 0.17 g, 5 eq.) was added and the clear solution diluted with water. The aqueous mixture was extracted with ethyl acetate, the organic layers washed with water (3x) and brine, dried over $MgSO_4$, filtered, and evaporated yielding 0.24 g (95%) of the title compound as a yellow solid.

**$^1$H-NMR** (300 MHz, $CD_2Cl_2$): δ (ppm) 8.06 – 7.87 (m, 4H), 7.67 – 7.30 (m, 4H), 4.85 – 3.85 (m, 12H), 3.63 – 3.09 (m, 22H), 1.54 – 1.09 (m, 40H), 0.86 (t, J = 6.5 Hz, 6H) (the given signals belong to all atropisomers, separation not possible due to strong overlapping). **$^{13}$C-NMR** (125 MHz, $CD_2Cl_2$): δ ppm = 155.5, 149.0, 138.6, 137.5, 137.2, 132.3, 130.3, 117.6, 107.5, 72.0, 67.7, 65.7, 63.4, 55.0, 32.5, 30.3, 30.2, 30.15, 30.0, 29.9, 26.8, 26.7, 23.3, 14.4. **MS-ESI**: m/z = 460.3274 (calc. for [$M^{2+}$]: 460.3296), 965.6624 (calc. for [$M^{2+}$ + $HCOO^-$]: 965.6579).

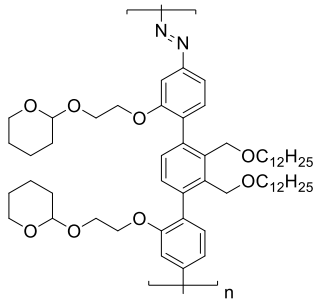


**2EtOTHP-2C12-Polyazo P-2:** Following the general procedure for the reductive polymerization of Dinitro-Terphenyls, Terphenyl **15** (0.7 mmol, 0.67 g, 1 eq.), Red-Al (6.7 mmol, 1.35 g, 10 eq.), yield: 0.47 g (73%).

**$^1$H-NMR** (300 MHz, $CD_2Cl_2$): δ (ppm) = 8.00 – 6.24 (m, br, 8H), 4.87 – 3.14 (m, br, 22H), 1.99 – 1.12 (m, br, 52H), 0.87 (m, br, 6H).

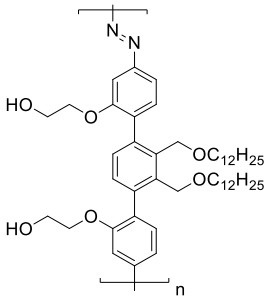


**2EtOH-2C12-Polyazo P-3:** Following the general procedure for the deprotection of tetrahydropyranyl ethers, polymer **16** (0.5 mmol, 0.47 g, 1 eq.), *p*-toluenesulfonic acid (0.05 mmol, 0.01 g, 0.1 eq.), yield: 0.31 g (79%).

**$^1$H-NMR** (300 MHz, $CD_2Cl_2$): δ (ppm) = 8.04 – 6.25 (m, br, 8H), 3.85 (m, br, 16H), 1.38 (m, br, 40H), 0.88 (s, br, 6H).

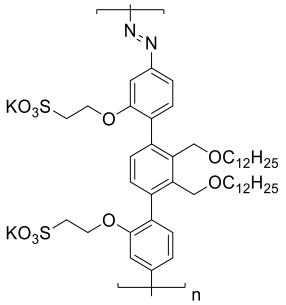

**2EtOSO3-2C12-Polyazo P-4:** Following the general procedure for the sulfatation of OH-polymers, polymer **17** (0.06 mmol, 0.05 g, 1 eq.), pyridine (0.2 mmol, 0.01 g, 3 eq.), sulfur trioxide pyridine complex (0.24 mmol, 0.04 g, 4.0 eq.), $K_2CO_3$ (0.24 mmol, 0.03 g, 4 eq.), yield: 0.05 g (75%).

**$^1$H-NMR** (300 MHz, DMSO-$d_6$): δ (ppm) = 7.82 – 6.71 (m, br, 8H), 4.77 – 3.07 (m, br, 16H), 1.54 – 0.98 (m, br, 40H), 0.85 (s, br, 6H).

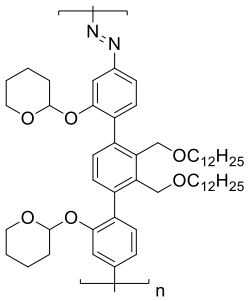

**2THP-2C12-Polyazo P-5:** Following the general procedure for the reductive polymerization of Dinitro-Terphenyls, Terphenyl **11** (0.5 mmol, 0.47g, 1 eq.), Red-Al (5.1 mmol, 1.03 g, 10 eq.), yield: 0.35 g (80%).

**$^1$H-NMR** (300 MHz, $CD_2Cl_2$): δ (ppm) 8.27 – 6.47 (m, br, 8H), 6.03 – 5.08 (m, br, 3H), 5.06 – 2.88 (m, br, 11H), 1.98 – 1.10 (m, br, 52H), 0.87 (t, br, J = 6.0 Hz, 6H).

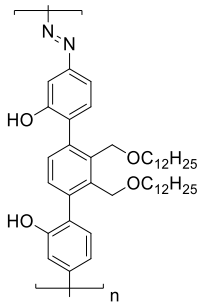

**2OH-2C12-Polyazo P-6:** Following the general procedure for the deprotection of tetrahydropyranyl ethers, polymer **20** (0.2 mmol, 0.15 g, 1 eq.), *p*-toluenesulfonic acid (0.09 mmol, 0.02 g, 0.5 eq.), yield: 0.09 g (73%).

**$^1$H-NMR** (300 MHz, THF-$d_8$): δ (ppm) = 8.31 – 6.84 (m, 10H), 4.46 (s, 4H), 3.38 (s, 4H), 1.64 – 1.11 (m, 40H), 0.87 (s, 6H).

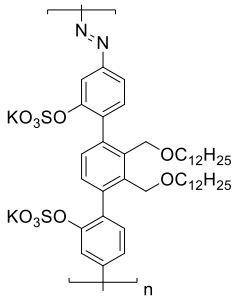


**2OSO3-2C12-Polyazo P-7:** Following the general procedure for the sulfatation of OH-polymers, polyazo **21** (0.05 mmol, 0.03 g, 1 eq.), pyridine (0.1 mmol, 0.01 g, 3 eq.), sulfur trioxide pyridine complex (0.3 mmol, 0.05 g, 6.0 eq.), $K_2CO_3$ (0.5 mmol, 0.08 g, 12 eq.), yield: 0.03 g (72%).

**$^1$H-NMR** (300 MHz, DMSO-$d_6$): δ (ppm) = 7.87 – 6.77 (m, br, 8H), 5.08 – 3.61 (m, br, 4H), 3.35 – 2.95 (m, br, 4H), 1.68 – 0.91 (m, br, J = 77.6 Hz, 40H), 0.81 (s, br, 6H).

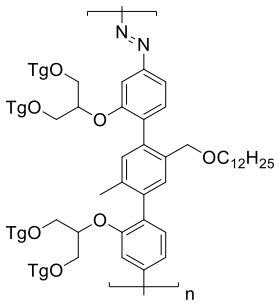


**2OTg-1C12-1Me-Polyazo P-8:** Following the general procedure for the reductive polymerization of Dinitro-Terphenyls, Terphenyl **30** (0.2 mmol, 0.31 g, 1 eq.), Red-Al (2.4 mmol, 0.49 g, 10 eq.), yield: 0.28 g (94%).

This polymer could not be precipitated by adding its solution to cold methanol. Alternatively, compound **31** was dissolved in THF and the solution added to cold water.

**$^1$H-NMR** (300 MHz, $CD_2Cl_2$): δ (ppm) = 8.59 – 6.39 (m, 8H), 4.90 – 4.08 (m, J = 114.7 Hz, 4H), 3.90 – 3.39 (m, 58H), 3.33 (s, 12H), 2.26 (s, 3H), 1.83 – 1.07 (m, 20H), 0.86 (t, J = 5.2 Hz, 3H).

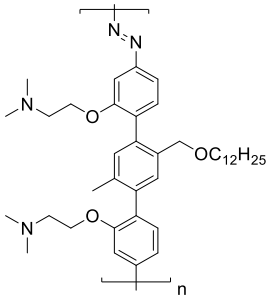

**2NMe$_2$-1C12-1Me-Polyazo P-9:** Following the general procedure for the reductive polymerization of Dinitro-Terphenyls, Terphenyl **32** (0.4 mmol, 0.30 g, 1 eq.), Red-Al (4.3 mmol, 0.87 g, 10 eq.), yield: 0.23 g (82%).

**$^1$H-NMR** (300 MHz, $CD_2Cl_2$): δ (ppm) 7.85 – 6.27 (m, 8H), 4.64 – 3.73 (m, br, 6H), 3.35 (s, br, 2H), 2.83 – 2.46 (m, br, 4H), 2.23 (s, br, 12H), 1.50 (s, br 2H), 1.25 (s, br, 18H), 0.88 (t, J = 6.0 Hz, 3H).

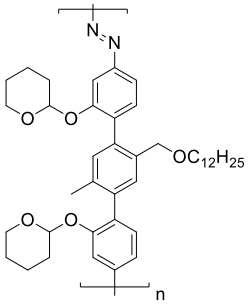

**2THP-1C12-1Me-Polyazo P-10:** Following the general procedure for the reductive polymerization of Dinitro-Terphenyls, Terphenyl **25** (0.3 mmol, 0.24 g, 1 eq.), Red-Al (3.3 mmol, 0.66 g, 10 eq.), yield: 0.17 g (78%).

**$^1$H-NMR** (300 MHz, $CD_2Cl_2$): δ (ppm) = 7.93 – 6.25 (m, 8H), 6.04 – 4.65 (m, 4H), 4.58 – 3.12 (m, 8H), 2.25 (t, J = 12.7 Hz, 3H), 1.96 – 1.07 (m, 30H), 0.86 (t, J = 5.8 Hz, 3H).

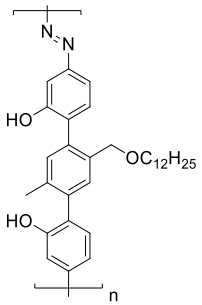

**2OH-1C12-1Me-Polyazo P-11:** Following the general procedure for the deprotection of tetrahydropyranyl ethers, polyazo **26** (2.1 mmol, 1.43 g, 1 eq.), *p*-toluenesulfonic acid (1.1 mmol, 0.20 g, 0.5 eq.), yield: 1.01 g (95%).

**$^1$H-NMR** (300 MHz, DMF-$d_7$): δ (ppm) = 10.26 (s, br, 2H), 7.86 – 6.91 (m, 8H), 4.65 – 4.30 (m, 2H), 3.47 – 3.23 (m, 2H), 2.48 – 2.05 (m, 3H), 1.50 (d, J = 5.7 Hz, 2H), 1.24 (s, 18H), 0.86 (s, 3H).

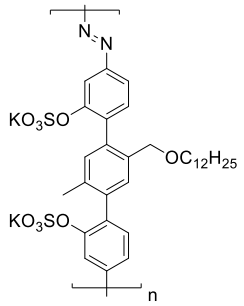


**2OSO3-1C12-1Me-Polyazo P-12:** Following the general procedure for the sulfatation of OH-polymers, polyazo **27** (0.2 mmol, 0.10 g, 1 eq.), sulfur trioxide pyridine complex (1.6 mmol, 0.26 g, 8.0 eq.), pyridine (0.6 mmol, 0.05 g, 3 eq.), $K_2CO_3$ (2.8 mmol, 0.39 g, 14 eq.), yield: 0.11 g (75%).
**$^1$H-NMR** (300 MHz, DMF-$d_7$): δ (ppm) = 8.64 (s, br, 1H), 7.89 – 6.81 (m, br, 7H), 4.50 (s, br, 2H), 3.41 (s, br, 2H), 2.31 (m, br, 3H), 1.50 (s, br, 2H), 1.25 (s, 19H), 0.86 (s, br, 3H).

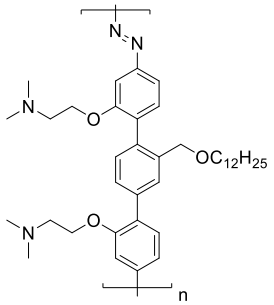


**2NMe$_2$-1C12-Polyazo P-13:** Following the general procedure for the reductive polymerization of Dinitro-Terphenyls, Terphenyl **32** (0.3 mmol, 0.21 g, 1 eq.), Red-Al (3.0 mmol, 0.61 g, 10 eq.), yield: 0.16 g (86%).
**$^1$H-NMR** (300 MHz, $CD_2Cl_2$): δ (ppm) = 8.01 – 6.43 (m, 9H), 4.69 – 3.70 (m, 6H), 3.38 (s, 2H), 2.89 – 2.41 (m, 4H), 2.38 – 2.01 (m, 12H), 1.54 (s, 2H), 1.25 (s, 18H), 0.87 (t, J = 5.9 Hz, 3H).

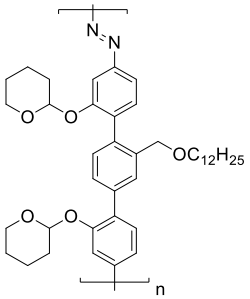

**2OTHP-1C12-Polyazo P-14:** Following the general procedure for the reductive polymerization of Dinitro-Terphenyls, Terphenyl **38** (0.5 mmol, 0.34 g, 1 eq.), Red-Al (5.4 mmol, 1.09 g, 10 eq.), yield: 0.35 g (quant.).

**$^1$H-NMR** (300 MHz, $CD_2Cl_2$): δ (ppm) = 8.20 – 6.29 (m, 9H), 6.04 – 4.77 (m, 4H), 3.86 (m, 8H), 2.16 – 1.05 (m, 30H), 0.87 (t, J = 6.2 Hz, 3H).

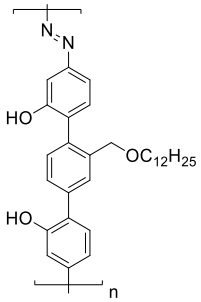

**2OH-1C12-Polyazo P-15:** Following the general procedure for the deprotection of tetrahydropyranyl ethers, polyazo **39** (0.3 mmol, 0.22 g, 1 eq.), *p*-toluenesulfonic acid (0.2 mmol, 0.03 g, 0.5 eq.), yield: 0.15 g (91%).

**$^1$H-NMR** (300 MHz, DMF-$d_7$): δ (ppm) 10.44 (s, br, 2H), 8.01 – 6.36 (m, br, 9H), 4.57 (s, br, 2H), 3.52 – 3.31 (m, br, 2H), 1.53 (s, br, 2H), 1.17 (s, br, 18H), 0.93 – 0.74 (m, 3H).

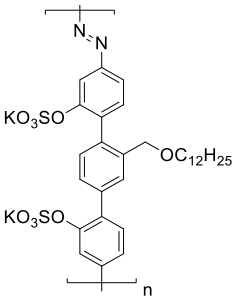

**2OSO3-1C12-Polyazo P-16:** Following the general procedure for the sulfatation of OH-polymers, polyazo **40** (0.2 mmol, 0.10 g, 1 eq.), sulfur trioxide pyridine complex (1.6 mmol, 0.26 g, 8.0 eq.), pyridine (0.6 mmol, 0.05 g, 3 eq.), $K_2CO_3$ (3.2 mmol, 0.44 g, 16 eq.), yield: 0.12 g (83%).

**$^1$H-NMR** (300 MHz, DMF-$d_7$): δ (ppm) = 8.65 (s, br, 1H), 8.15 – 6.34 (m, br, 8H), 4.56 (s, br, 2H), 3.44 (s, br, 2H), 1.54 (s, br, 2H), 1.26 (s, br, 18H), 0.85 (s, br, 3H).

## 5.5 Polymers – Analytical Data

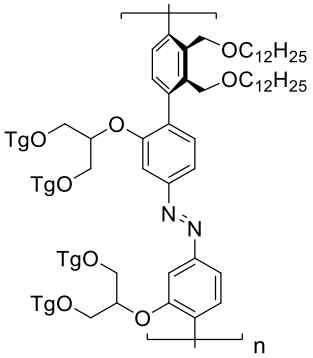


**P-1**

$M_n$ = 36000 g/mol

$M_w$ = 58800 g/mol

PDI = 1.6

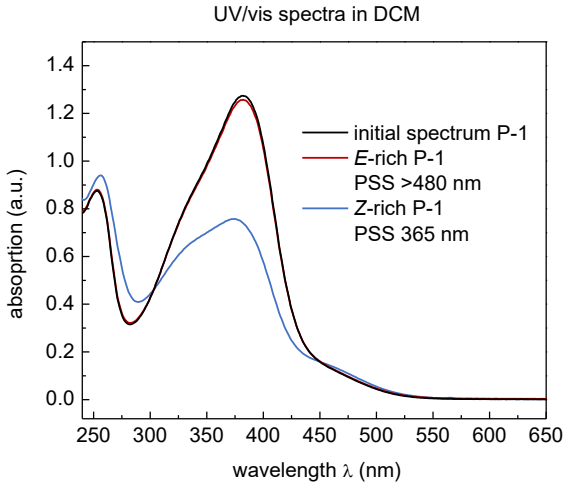


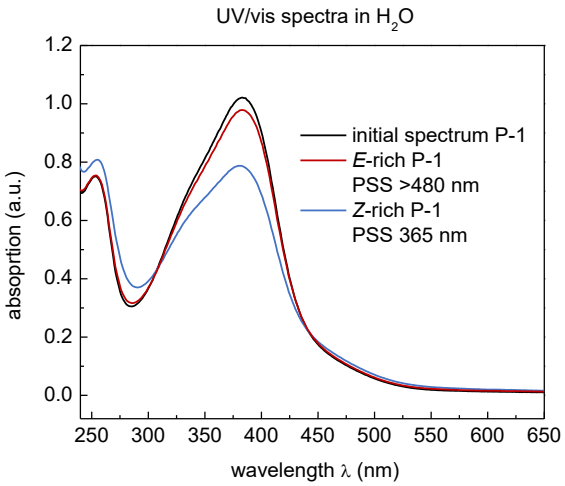

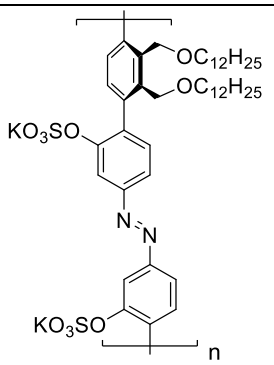


**P-7**

$M_n$ = 51000 g/mol

$M_w$ = 147900 g/mol

PDI = 2.9

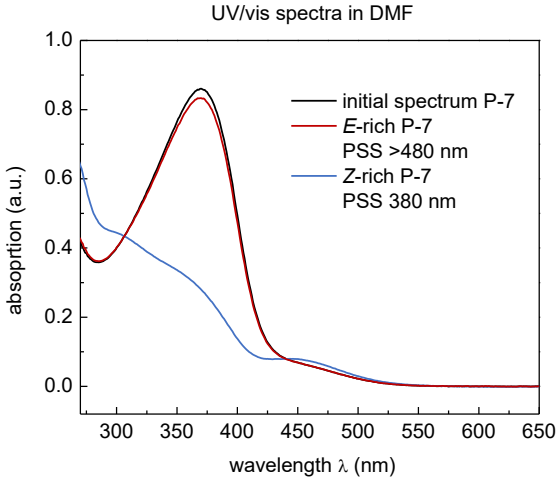


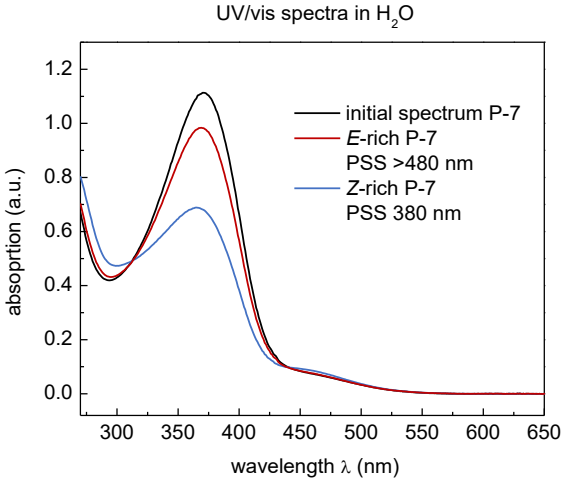


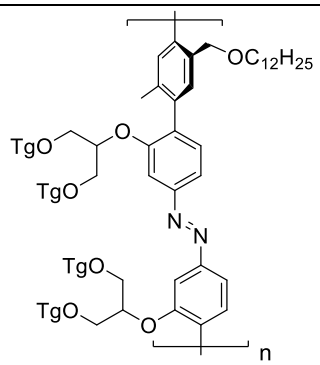


**P-8**

$M_n$ = 10600 g/mol

$M_w$ = 61600 g/mol

PDI = 5.8

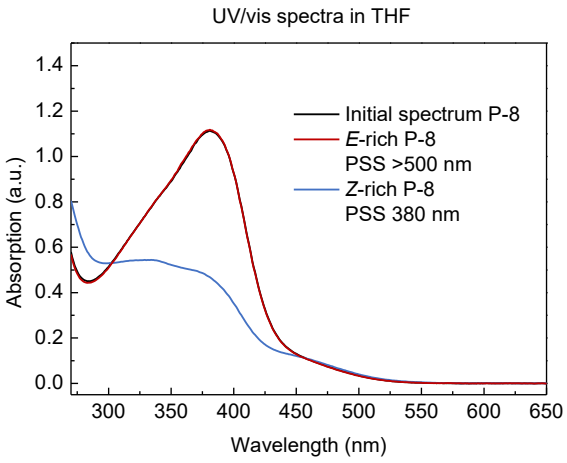


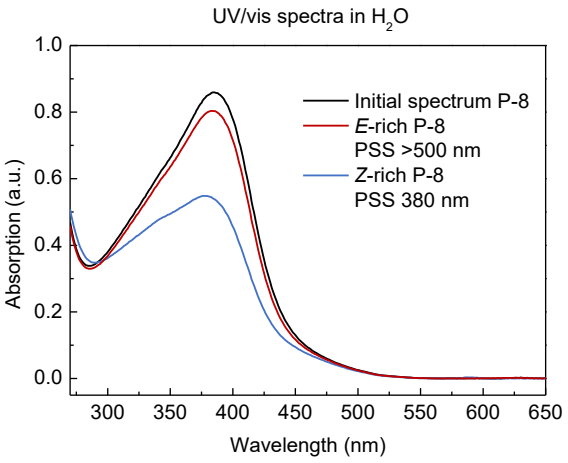

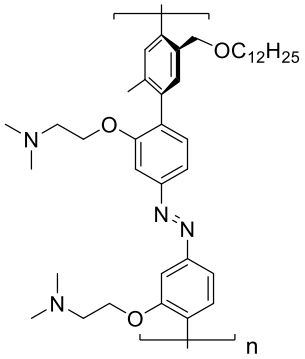


**P-9**

$M_n$, $M_w$, and PDI could not be determined by GPC as the polymer is stuck on the column (eluent: THF or DMAc).

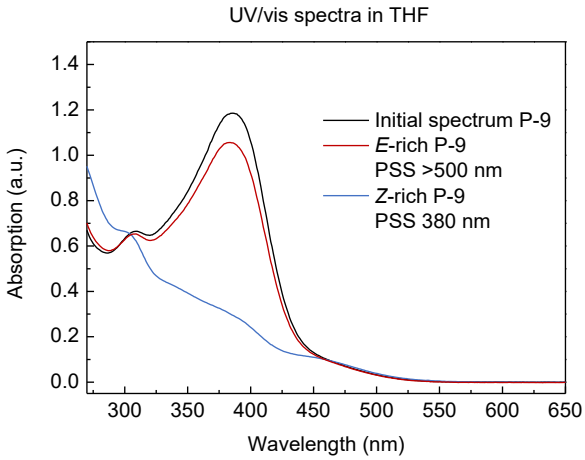


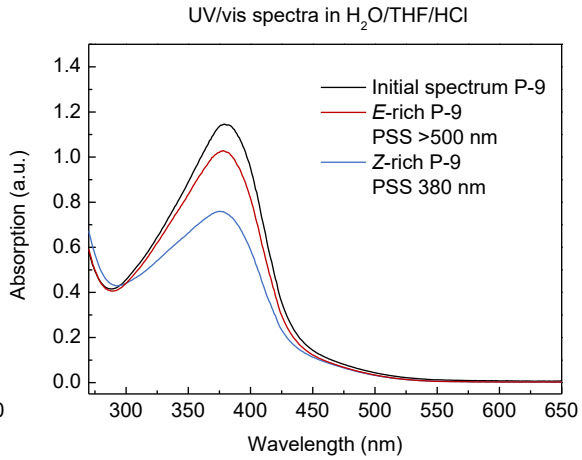


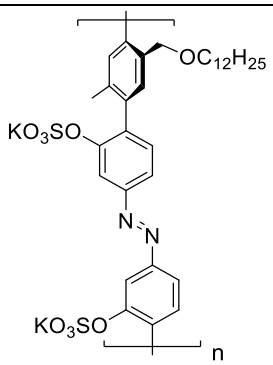


**P-12**

$M_n$ = 33800 g/mol

$M_w$ = 59700 g/mol

PDI = 1.8

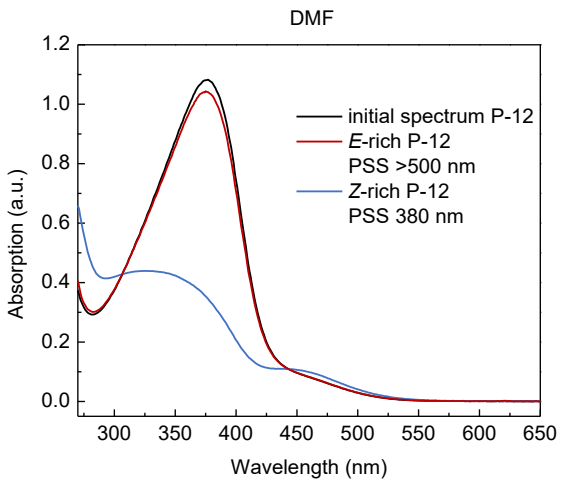


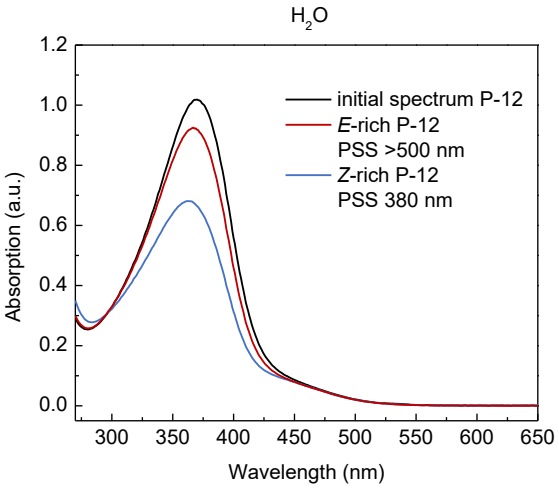

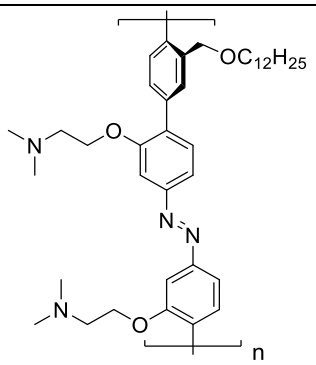


**P-13**

$M_n$, $M_w$, and PDI could not be determined by GPC as the polymer is stuck on the column (eluent: THF or DMAc).

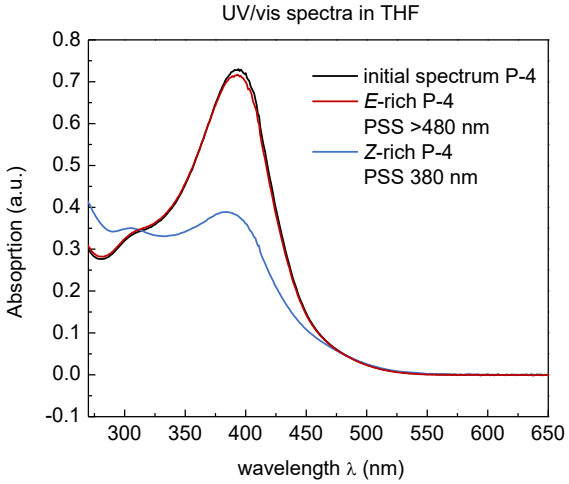


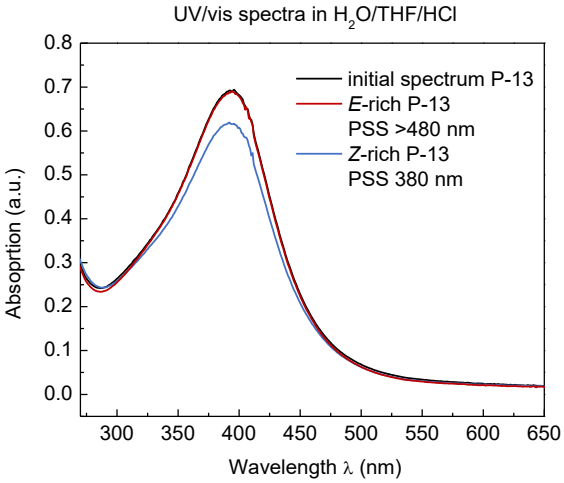


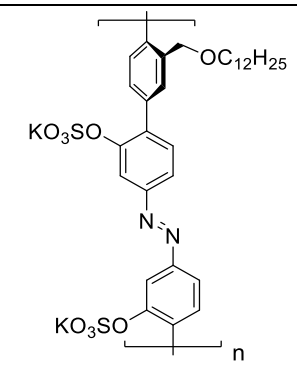


**P-16**

$M_n$ = 54400 g/mol

$M_w$ = 91500 g/mol

PDI = 1.7

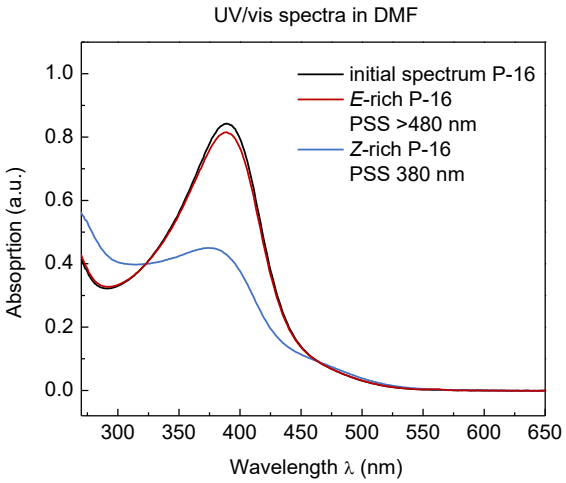


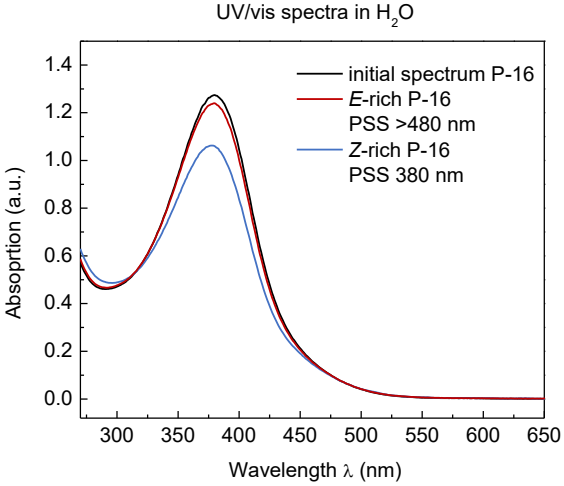

## Image details for the cryo-TEM images of polymer P-16

**Table 3.** Details of two cryo-TEM images of a solution of polymer **P-16** in water before (left) and after (right) irradiation at 365 nm, the detail is shown with and without highlighted wormlike objects, the number of objects in every detail is given next to it, regions of high object density were randomly chosen from the original cryo-TEM image, a significant decrease of the total object number is observed upon photoisomerization of the azobenzene polymers.

| Before irradiation | Number of objects | After irradiation at 365 nm | Number of objects |
|---|---|---|---|
| 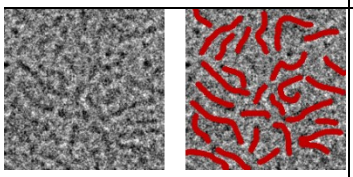 | 28 | 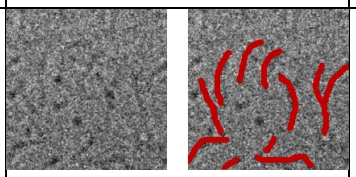 | 11 |
| 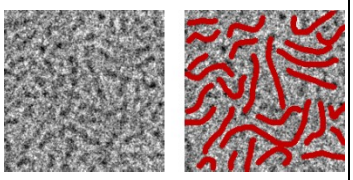 | 27 | 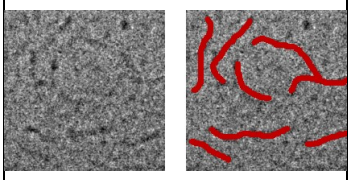 | 8 |
| 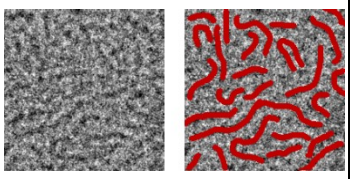 | 26 | 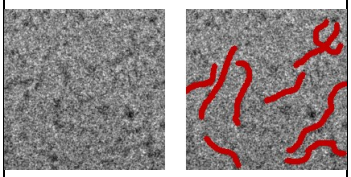 | 9 |
| 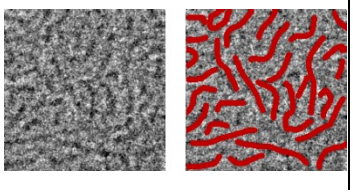 | 30 | 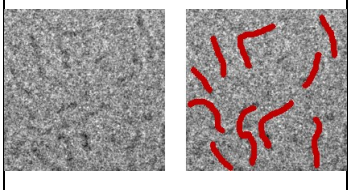 | 10 |

Part II

# Light-Responsive Zwitterions

## Control over the Formation of Charges

# 1 Introduction

Charged species and pH gradients are of great importance for the biological processes that provide the basis for every living organism. Their influence ranges from most simple effects like water solubilization, which is a critical parameter for the evolution of life, to more advanced regulatory systems within the human body, e.g. blood pressure and hydration, that are controlled by appropriate electrolyte levels, among others. Furthermore, inorganic salts dispersed in soil supply plants with essential elements for the amino acid synthesis, which represents the starting point on the way to functional organic macromolecules. Exceptionally important is their contribution to the transmission of electrical signals between cells, that enables the control of all body functions from a single central nervous system, as well as to the contraction and relaxation of muscles that convert the transferred information into action. In this context, especially sodium, potassium, and calcium ions are involved, yet also organic molecules such as the neurotransmitter acetylcholine are particularly relevant.[57]

A special role is taken by protons which form the basis for multiple biological energy storage and conversion systems. Proton gradients and areas of different pH values separated by membranes function as small organic batteries, that can be addressed on demand to power molecular machines or biosynthesis. Adenosine triphosphate (ATP) for instance, the most important biological energy currency, is continuously prepared from adenosine diphosphate in the mitochondria.[58] In this process, a continuous flow of protons induces a rotary motion in the corresponding transmembrane protein, which allocates kinetic energy for the endothermic ATP synthesis. Another fundamental energy conversion process in nature is photosynthesis, that equally relies on different levels of protons and charge separation.[59] However, in both of the latter processes, energy rich chemical species serve as temporary storage media. The direct conversion of chemical potential into macroscopic motion is performed by certain bacteria, that actively change locations by means of their flagellum.[60] Similar to the ATP synthesis, the impulse is created by a flow of protons through a membrane protein that induces a directed rotary motion of the organelle.

In view of the broad occurrence of charged species in multiple biological fields, the controlled formation of ions appears generally desirable. However, applications are not limited to the area of energy storage or the influence and regulation of biological processes. Their detrimental effect on bacteria provides a potential basis for self-sterilizing and self-cleaning surfaces in healthcare and industry, where the formation of biofilms poses risks for patients and production.[61] Positive charges usually cause bacterial death, whereas zwitterionic structures exhibit non-fouling

properties. In this context, the ability to control the formation of the respective charged species is highly desirable since both strategies, killing and repelling, cannot operate simultaneously. While bactericides require close proximity to the target to be effective, anti-fouling surfaces prevent the approach of bacteria but lack the bactericidal characteristics. As a consequence, dead bacteria are stuck to positively charged surfaces, thus protecting further microorganism from the active moieties. Hence, the combination of both strategies in one system without independent addressability of both states would significantly lower their overall efficiency. However, the introduction of a stimulus that triggers the formation of the respective species and provides the ability to reversibly change from killing to repelling conditions, would give rise to a surface that combines both strategies without the antagonizing effect.

In the second part of this thesis, the development of a light-responsive molecule that enables the reversible formation of opposite charges and thus zwitterions is targeted. The advantages of light as stimulus to control molecular processes have already been presented in part one. Based on the example of the spiropyran-merocyanine equilibrium, an azobenzene-derived molecule is developed that exhibits a zwitterionic structure in one state and no charges in the other (Scheme 8).

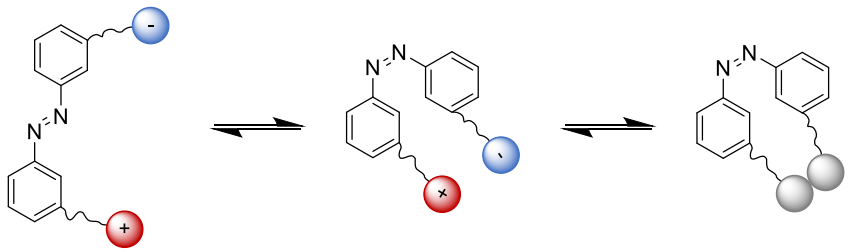

**Scheme 8.** Schematic representation of the zwitterion switch based on the model of the spiropyran-merocyanine pair, the charges are not in conjugation which should significantly increase the overall effect in comparison to merocyanine.

In contrast to spiropyran, these charges are not connected by conjugation, which should significantly increase the overall effect. Moreover, a dynamic covalent approach for the reversible generation of charges is desirable. The formation of a temporary covalent bond between the ionic moieties in the sense of a nucleophile-electrophile pair provides stability for the neutral state while maintaining reversibility due to dynamic covalent characteristics. Potential molecular structures are screened by computational analysis and the most promising results converted into model compounds. The synthesis of two model systems is described followed by the evaluation of the charged and non-charged species. The integration into a photoswitchable molecule is presented from a theoretical point of view in the final section.

# 2 Theoretical Background

## 2.1 Dynamic Covalent Chemistry – Overview and Examples

Thermodynamic equilibria are known since the end of the 19th century when van't Hoff developed his homonymous equation that relates the equilibrium constant K of a chemical reaction to the reaction temperature T, depending on the change of the standard enthalpy ΔH (Figure 35b, Equation 20, where $K_1$ and $K_2$ are the equilibrium constants of a reaction at temperatures $T_1$ and $T_2$, respectively). This correlation is a specific example for the general principle of Le Chatelier and Braun which expands the variables of reversible processes to quantities such as concentration, pressure, and volume. Accordingly, adjustment of these parameters allows influence and, to a certain extent, control over the formation and composition of dynamic systems and provides the basis for supramolecular and dynamic covalent chemistry (DCC).[62] While in the former case the dynamic nature of the chemical transformations relies on relatively weak and labile non-covalent interactions, the advantage of the latter is the higher robustness and stability of covalent bonds. However, higher stability is usually accompanied by a slower conversion rate from one state to the other making the careful adjustment of the systems equilibration properties necessary.

a)

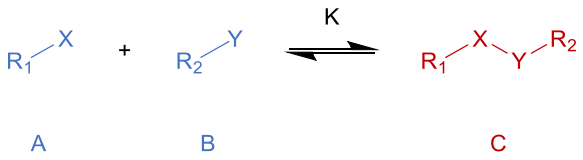


b)

$$K = \frac{[C]^c}{[A]^a[B]^b} \qquad 19$$

$$\ln\left(\frac{K_2}{K_1}\right) = \frac{-\Delta H}{R}\left(\frac{1}{T_2} - \frac{1}{T_1}\right) \qquad 20$$

**Figure 35.** a) Equilibrium of three chemical species A, B, C and their stoichiometric numbers a, b, c, respectively, X and Y are functional groups that can undergo a reversible bond formation, blue letters are considered starting materials while red letters refer to the product, the equilibrium constant K describes the characteristics of the stationary state, b) Equation 19: equilibrium constant K derived from the concentrations of the chemical species at the stationary state (d[A] = d[B] = d[C] = 0), Equation 20: van't Hoff equation describing the dependence of the equilibrium constant K of a reaction under thermodynamic control on the reaction temperature T, ΔH denotes the change of the standard enthalpy and R the gas constant, assuming a constant ΔH, the equilibrium constant $K_2$ at a given temperature $T_2$ can be calculated from a known equilibrium constant $K_1$ and the corresponding temperature $T_1$.

Generally, lifetimes of dynamic bonds range between milliseconds to minutes in order to allow the formation of stable isolable species and characterization by standard analytical methods, while still maintaining a fast response to stimuli. Furthermore, efficient equilibration should proceed under mild reaction conditions and in preferably aqueous environment to provide compatibility with a broad range of functional groups and biological systems. As a last attribute of dynamic covalent processes, the possibility to stop the equilibration after a certain period of time

is desirable to facilitate the isolation and analysis of specific species in the potentially complex mixtures.

A typical equilibrium of three components is depicted in Figure 35a, where A and B denote starting materials that are converted into the product C under formation and/or break of covalent bonds. The stationary state of the reversible reaction is described by the equilibrium constant K according to Equation 19 (Figure 35b).

Three classes of dynamic exchange processes can be differentiated according to the symmetry of the dynamic bond, i.e. symmetric, non-symmetric, and trans-symmetric.[62a] In the first case, X and Y are the same functionals groups (e.g. thiols forming a disulfide), while in the second case X and Y are different functionals groups (e.g. a carboxylic acid and thiol forming a thioester). The last case represents a system where the functional groups X and Y can be converted into each other by the dynamic reaction, e.g. an aldehyde and amine forming an imine. Hence, the imine double bond position can change from the $R_1$ side to the $R_2$ side or vice versa in the course of the equilibration or a mixture of both species is observed. The major difference of all systems is the complexity of the resultant dynamic mixture and the number of species that can be investigated at the same time.

When generating a dynamic covalent system, the analysis of the equilibrium state regarding composition and stability is pursued. However, the confirmation about reaching the stationary state must be obtained beforehand. A good indication for a complete process is provided by monitoring the temporal evolution of the system's components until no further change occurs. The disadvantage of that procedure is that processes slower than the timeframe of analysis cannot be detected. A more reliable way is provided by the dual entry-point analysis which relies on the feature of an equilibrium to be reached independent of the pathway. In this case, two different starting points are chosen that exhibit the same composition of dynamic subunits. Subsequently, both mixtures are subjected to equilibration until the same product distribution is observed which is attributed to the final equilibrium state.

Multiple molecular structures are known to perform reversible association and dissociation cycles depending on environmental parameters. A wide range of examples for dynamic covalent chemistry can be found in nature where they enable essential biochemical processes in living organism. For instance, the correct folding of proteins into their tertiary or quaternary structures, which is mandatory for proper functioning, is partially stabilized by dynamic disulfide bridges.[63] Moreover, the retinal cofactor, indispensable for the process of vision, is bound to the corresponding protein via an imine moiety that allows replacement of the photo-responsive unit

after fatigue.[1] Another representative for DCC is Coenzyme A, which reversibly forms active thioesters with fatty acids and thereby contributes to the fat metabolism and energy production in cells.[64] Several other dynamic covalent systems were discovered, an overview of the most common examples is depicted in Figure 36.[62a]

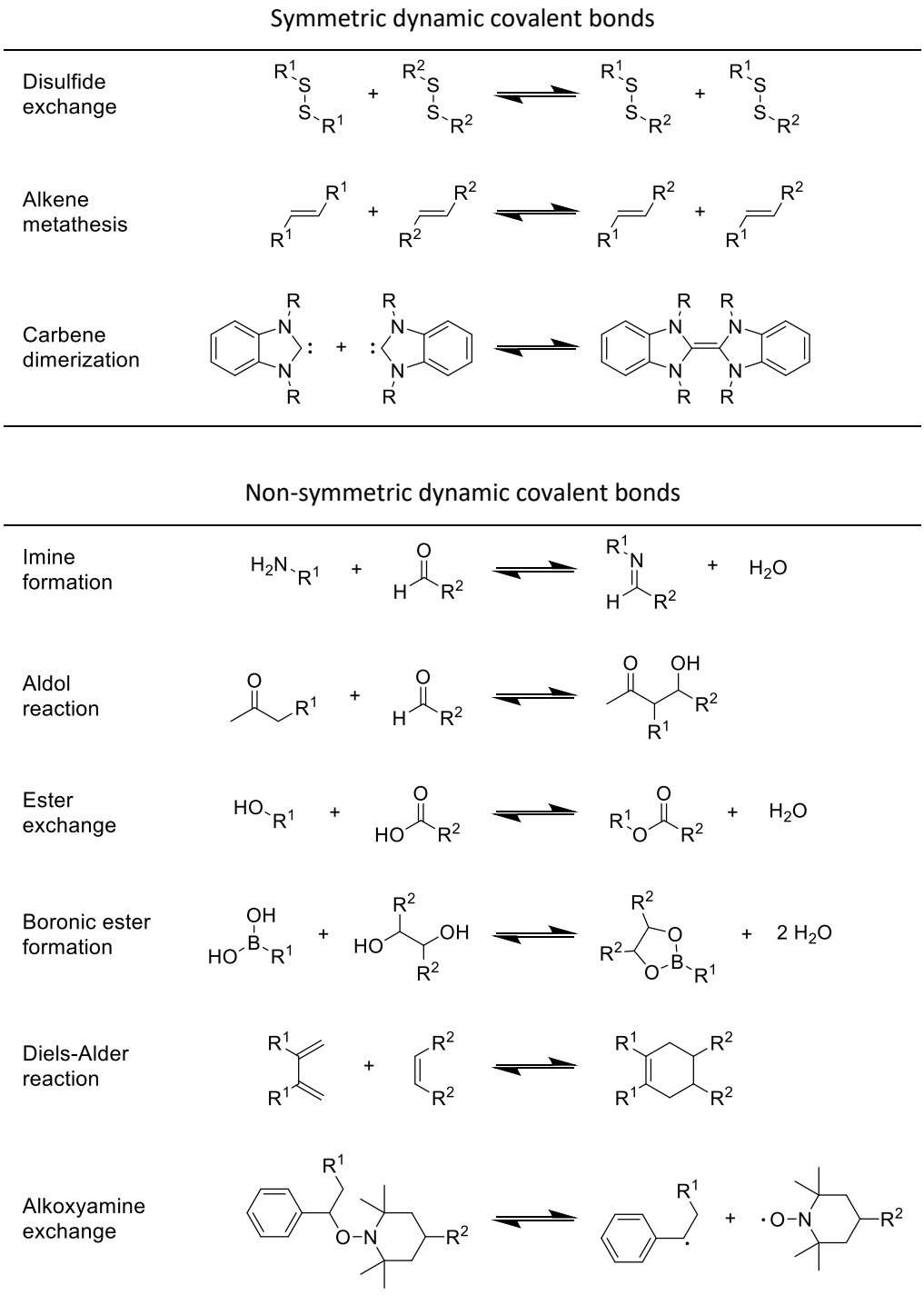


**Figure 36**. Overview of common dynamic covalent systems classified according to the symmetry of the dynamic bond, symmetric bonds constituted by the same functional groups are formed during disulfide exchange, alkene metathesis, and carbene dimerization reactions, non-symmetric bonds formed by reaction of different functional groups comprise imine formations, aldol reactions, ester formations and exchanges, Diels-Alder reactions, and alkoxyamine exchanges.[62a, 65]

One of the best-investigated DCC systems relies on C-N bond formations comprising the condensation of carbonyls with amines into imines and imine exchange reactions. In this process, water occurs as a byproduct/reagent which initiates hydrolysis and, thus, enables subsequent re-condensation. However, in case of imine exchange reactions, hydrous conditions are not required since both transamination and imine metathesis are also observed in water-free environment. Although the reaction and equilibration process take place under neutral conditions, a significant acceleration is achieved when applying Brønsted or Lewis acidic catalysts. An important property that influences the stationary state is the basicity of the amine unit. The stronger basic the amine, the more stable is the corresponding imine, and the slower is the equilibration rate. Related imine structures such as oximes, hydrazones, and nitrones, among others, exhibit similar dynamic behavior.

Another well-established class of dynamic covalent structures is based upon C-C bond formation, a core reaction in organic synthesis. In this context, the Aldol reaction is a classic example, although applications benefitting from the dynamic nature are rare due to the frequent occurrence of by-products and lack of appropriate catalysts. The nitroaldol (Henry) reaction as a special case in the Aldol family, however, exhibits clean dynamic exchange behavior under basic conditions. Moreover, the formation of a stereogenic center provides further structural information for potential screening, recognition, and selection purposes. The addition of cyanides to carbonyls and imines giving rise to cyanohydrins and $\alpha$-amino nitriles is equally reversible in basic and Lewis acidic environment, respectively. An additional pathway towards reversible C-C bond formation is represented by the dimerization of *N*-heterocyclic carbenes. In this case, the equilibrium composition highly depends on the size of the substituents and the properties of the heterocyclic ring. One of the most useful DCC reactions to build up connections between carbon atoms is olefin metathesis. The mechanism proceeds via sequential [2+2] cycloaddition under transition metal catalysis for which typically Grubbs and Schrock carbenes are employed. Great advantages of olefin metathesis are mild reaction conditions, commercially available catalysts, wide tolerance of functional groups, high equilibration rates, and orthogonality to many other dynamic covalent systems. However, the method is limited by large differences in reactivity of terminal and internal or sterically demanding double bonds and functional groups that coordinate to the catalyst.

The formation of C-O bonds provides further means of creating dynamic covalent systems. Transesterifications occur in strongly basic or acidic environment; however, potential decomposition of the components might be problematic under too harsh conditions. Alternatively, Lewis acids such as titanium alkoxides can be employed as catalysts. Other

structures, i.e. hemiacetals, acetals, and orthoesters, also exhibit dynamic exchange properties but are often limited by the requirement of anhydrous conditions or equilibria that favor the single components. The same effects are observed for the corresponding sulfur derivatives, though the higher polarizability of sulfur in comparison to oxygen causes higher nucleophilicity, better leaving group characteristics, and thus more dynamic behavior. For instance, transesterifications of thioesters can be conducted without catalyst in aqueous environments, and thia-Michael additions exhibit fast equilibration rates under mildly basic conditions. Furthermore, disulfides are among the most utilized dynamic covalent systems due to their vast occurrence in nature. The exchange proceeds via nucleophilic attack of a thiolate at the disulfide in basic medium but can also be triggered by reducing a fraction of a disulfide mixture in order to form a catalytic amount of thiol initiator. Accordingly, partial oxidation of a thiol mixture under air also provides the necessary components for the dynamic covalent system.

Numerous other DCC classes exist, i.e. boronic esters, pericyclic reactions such as the Diels-Alder type, and reversible formations of radical species, among others. Regarding boronic esters, especially diol derivatives are of interest due to their higher stability, which are formed under dehydrating conditions. However, since boron compounds exhibit Lewis acidic properties, dynamic systems are not restricted to esters but the formation of boronates provides an alternative starting point. The Diels-Alder reaction, in contrast to most of the other DCC structures, can be efficiently controlled without an additional catalyst but under temperature control. However, in order to avoid harsh conditions, systematic substitution of the diene and dienophile with electron donating and electron withdrawing substituents, respectively, is necessary to allow equilibration at lower temperatures. A special characteristic of the Diels-Alder reaction is its self-contained nature; all atoms are present in the starting materials and in the product. A final example is the reversible formation of radicals which, similar to the Diels-Alder reaction, does not rely on catalysis but on stability of the radical species and the applied temperature. Drawbacks are typical side reactions of radicals such as recombination and disproportionation.

## 2.2 Dynamic Covalent Chemistry – Control

The distinctive feature of dynamic covalent chemistry is the continuous reversible formation and breakage of covalent bonds, which changes the overall composition of the system until the thermodynamic minimum is reached. However, the position of a thermodynamic equilibrium depends on environmental parameters according to the principle of Le Chatelier and Brown. Hence, the application of external stimuli such as mechanical stress, irradiation, temperature, and

electric fields, among others, the introduction of templates, or a change of solvent are able to adjust the distribution of species in the final state. In order to quantify the extent of the realized perturbation for a given member A of the dynamic covalent system, the normalized amplification factor $AF_n$ was introduced.

$$[A]_x \xrightarrow{perturbation} [A]_y \qquad AF_n = \frac{[A]_y - [A]_x}{[A]_{max} - [A]_x} \qquad 21$$

In this context, $[A]_x$, $[A]_y$, and $[A]_{max}$ denote the concentrations of species A (including complexes with non-dynamic additives such as templates) before the change of an environmental parameter, after perturbation, and the maximum possible concentration, respectively. The amplification factor ranges from 0 to 1 for which 0 represents no effect of the applied stimulus and 1 indicates full conversion to the most A-rich state. A negative $AF_n$ occurs for events that decrease the concentration of A. However, this is not an amplification but a reduction and is therefore not covered by this approach.

An example of a thermally controllable Diels-Alder reaction operating in the range of room to moderate temperatures is depicted in Scheme 9.[66] While the equilibrium constant at room temperature is about 63 $M^{-1}$, the same quantity significantly decreases to 11 $M^{-1}$ at 50 °C. The corresponding yields regarding the Diels-Alder adduct are 67% and 39% at 25 °C and 50 °C, respectively.

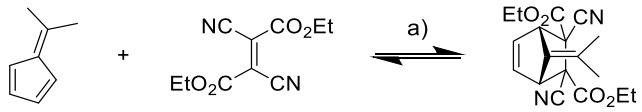


**Scheme 9.** Diels-Alder reaction of *6,6*-dimethylfulvene and diethyl 2,3-dicyanofumerate, a) $CHCl_3$, 25 °C or 50 °C; the equilibrium constant decreases from 63 $M^{-1}$ to 11 $M^{-1}$ for the lower and higher reaction temperature, respectively, which drives the position of the equilibrium from the product side to the reactants (adduct yield of 67% and 39% at 25 °C and 50 °C, respectively).[66]

Another method to modify the composition of a dynamic covalent system towards less stable and hence less developed species is the template approach (Figure 37).[62a] In this case, a selector, e.g. an ion, ligand, or protein, which preferentially binds a specific structure, is added to the equilibrating system. Two strategies can be followed, i.e. the molding and the casting strategy. In the former case, the dynamic subunits assemble around a guest molecule, while in the latter case the dynamic structures are the guest of a host molecule.

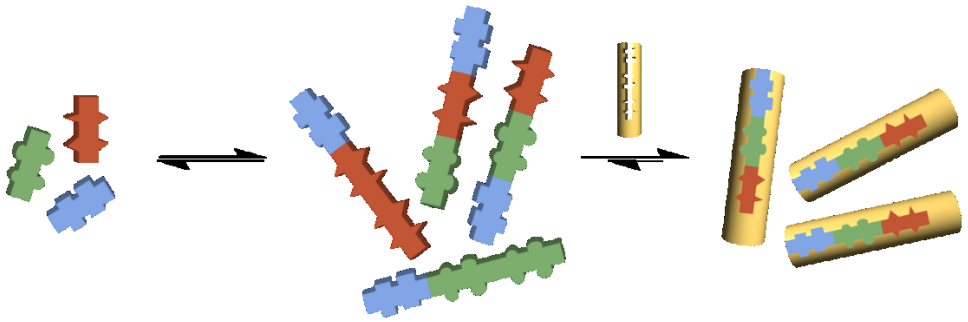

**Figure 37.** Dynamic covalent system constituted by three molecular subunits, the blue one exhibits a single functional group while the green and red ones exhibit two reactive moieties, after equilibration no preference for a specific structure but an equal distribution of all possible combinations is observed; the addition of a selector following the casting strategy, which preferentially binds one structure and thus stabilizes it, causes a shift of the equilibrium towards the appropriate combination, in this way, the selective preparation of one specific compound in a dynamic mixture or the simultaneous screening of several potential guests for a given host is feasible.

Due to stabilization of a less-favored species by coordination to the selector a new thermodynamic minimum is created, and the binding structure eventually removed from the initial equilibrium. Besides favorable interactions of selector and final product, the stabilizing effect can equally occur in the reaction's transition state. Furthermore, intermolecular interactions among the same species can give rise to auto-amplification.

The influence of a template on a dynamic covalent system based on orthoesters is depicted in Scheme 10.[67] Under anhydrous acidic conditions, the authors converted diethylene glycol and trimethyl orthoformate into the corresponding 1+1 octacycle. However, the addition of metal ions such as $Li^+$, $Na^+$, and $K^+$ gives rise to the formation of larger cycles with 2+2 stoichiometry similar to crown ethers. A special behavior is observed after prolonged exposure to sodium ions where the formation of a bicyclic species as the major product is observed. The cryptand could not be detected before the addition of $Na^+$ which highlights the amplification effect of a template in dynamic covalent chemistry.

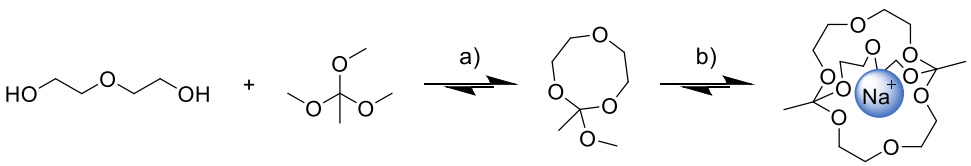


**Scheme 10.** Dynamic covalent system based on orthoester exchange, a) cat. TFA, molecular sieves 4 Å, $CDCl_3$, RT b) sodium tetrakis[*3*,*5*-bis(trifluoromethyl)phenyl]borate, in water-free acidic environment an octacycle with 1:1 stoichiometry of the starting materials is the major product, by addition of sodium ions as a template the equilibrium is shifted towards a bicyclic cryptand.[67]

Besides the control over the position of a thermodynamic equilibrium, also the rate of equilibration can be influenced. Especially considering the relative strength of covalent bonds in comparison to supramolecular interactions, the application of a catalyst can be required to reach

the final state in a reasonable period of time. However, the lower activation barrier of a chemical reaction as a result of catalysis can not only speed up its progress, but also enable the formation of bonds under mild conditions and thus potential dynamic behavior in the first place. Most importantly, the catalyst must exhibit a high turnover number in order to maintain the dynamic characteristics of the system until the stationary state is reached.

An example is presented in Scheme 11 where the reversible formation of acylhydrazones was investigated.[68] The cleavage of the relatively stable C-N double bond usually occurs at low pH values (< 4) that results in slow or no equilibration in biologically relevant environments.

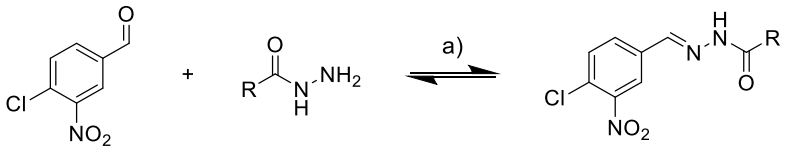


**Scheme 11**. Dynamic covalent system composed of *4*-chloro-*3*-nitrobenzaldehyde, 10 differently substituted hydrazides, and the corresponding acylhydrazones, under non-catalytic conditions, the equilibration was finished after 5 d, the addition of aniline dramatically increased the reaction rate lowering the equilibration time to 6 h, a) (aniline), DMSO, ammonium acetate buffer, RT.[68]

Accordingly, several days were required to reach the steady state for the conversion of *4*-chloro-*3*-nitrobenzaldehyde with a total number of 10 different hydrazides at a pH value of 6.2. However, the addition of a nucleophilic catalyst, i.e. aniline, to the reaction mixture allowed equilibration within several hours under the same conditions. Due to the dramatically increased reaction rate, screening for a potential glutathione S-transferase inhibitor was successfully accomplished.

## 2.3 Dynamic Covalent Chemistry – Applications

Applications for dynamic covalent systems cover multiple areas of life and material sciences. Their responsiveness to external stimuli as well as the continuous formation and cleavage of covalent bonds provide the basis for smart adaptive materials that are able to respond to environmental changes and to self-correct damages and errors. The systems inherent information is efficiently stored or, if needed, reproduced by the thermodynamic driving force towards the equilibrium state. These characteristics can be exploited in the fields of self-healing, catalysis, sensing, pattern recognition, molecular motors, and for the preparation of complex molecular architectures, among others.[62b]

The first example is taken from the area of molecular motors and walkers where the major purpose is to drive systems away from equilibrium and to perform work in a directed fashion.

Inspired by kinesin, a motor protein in cells capable of transporting cargo such as membrane components, vesicles, or other proteins, many systems have been developed that are striving to copy the features of nature's molecular carrier. Besides directionality, important characteristics of walking molecular systems comprise the abilities of repetitive, progressive, and processive motion; i.e. the walker should be able to perform several operating cycles, it should exhibit the possibility for re-initialization at the end of one cycle without loss of the performed work, and it should remain attached to its path during operation. In this context, dynamic covalent systems are especially suited as they combine the robustness of covalent bonds with the ability to reversibly connect and disconnect to and from an anchor point, the basis for a stepwise motion.

An imine-based walker developed in the group of Lehn is depicted in Scheme 12.[69] In the presence of acid, the imine is converted into a cyclic aminal and subsequently ring-opened to yield the iminium salt of the adjacent secondary amine.

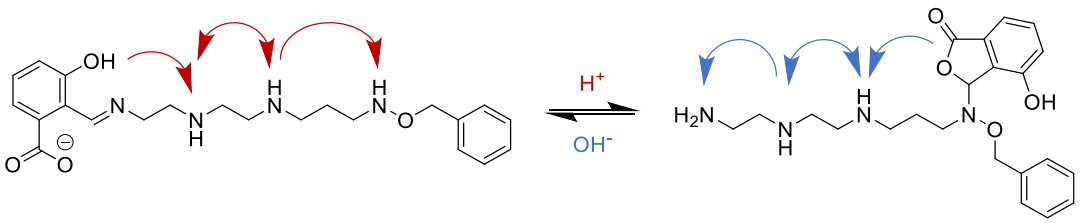


**Scheme 12**. Directional motion of a dynamic covalent system based on the formation of imines, the driving force of the process is the higher thermal stability of the imine structure in basic medium while the lactone derivative is energetically favored in acidic environment, the intermediate steps involving the formation of aminals, iminium ions, and lactones (attached to secondary amines), display random motion in both directions.[69]

This iminium salt, which is in equilibrium with the corresponding lactone, can be re-attacked by amines in close proximity until the end of the chain is reached. Eventually, a thermodynamically stable lactone is formed at the position of the hydroxylamine derivative which is favored in comparison to the similar cyclic ester attached to one of the secondary amines. The reverse process is induced under basic conditions where the initial imine exhibits higher thermal stability than the lactone. While the intermediate steps perform motion randomly in both directions, directionality is solely achieved by the different thermal stabilities of both final structures in basic and acid medium.

Another example is taken from the field of medical research and drug discovery. The usual strategy necessitates the synthesis of large libraries of molecules that are subsequently tested for their individual binding properties with the target. This very time-consuming approach can be simplified by means of dynamic covalent chemistry. Depending on the number of components, multiple species are present at the same time in dynamic covalent systems. In the presence of the target

receptor, the best fitting structure is automatically amplified according to the template approach rendering the stepwise analysis of single molecules unnecessary. The process represents an elegant self-screening method; however, four conditions have to be met to ensure a sufficiently high chance of success. First, one of the components must exhibit a motif that is already known for its good binding characteristics. Second, the reaction conditions must be compatible with the requirements of the protein and allow equilibration within an acceptable period of time. Third, the reactivity and stability of all components must be similar in order to allow a reliable correlation of the binding strength with the observed amplification. Fourth, the dynamic covalent connections should be easily replaceable by permanent covalent bonds to provide sufficient stability for the final drug.

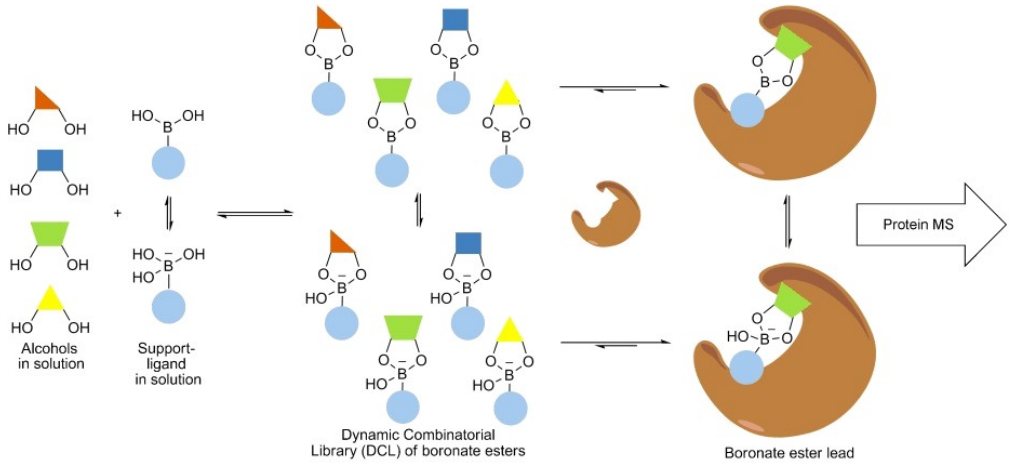


**Figure 38.** Inhibitor screening by dynamic combinatorial mass spectrometry, the boronic acids and diols are converted in-situ into boronic esters which interact with the prolyl hydroxylase domain isoform 2, the blue circles represent a N-oxalylglycine derived moiety that is known to bind to the protein's iron(II) center, the best inhibitor is derived from the mass difference of the single enzyme and the enzyme-inhibitor complex, the formation of boronates facilitates the mass spectrometric detection since the boronic esters are prone to fragmentation under ESI-MS conditions.[70]

Respecting the aforementioned conditions, the group of Schofield investigated the binding properties of multiple in-situ formed boronic esters to the prolyl hydroxylase domain isoform 2, an oxygenase responsible for the hypoxic response in humans, by dynamic combinatorial mass spectrometry (**Figure 38**).[70] The blue circles represent a motif based on N-oxalylglycine, a ligand known to bind to the iron(II) center of the enzyme, while the diols bear the groups to be tested. The compound exhibiting the highest affinity was derived by the difference in mass of the single enzyme and the enzyme-boronic ester complex. The boronate, which formed at the adjusted pH value of 7.5, facilitates the detection by mass spectrometry since the boronic ester undergoes fragmentation during the ionization process (ESI-MS). Additionally, the results were confirmed by

NMR spectroscopy. The successful discovery of several inhibitor structures was completed by the synthesis and analysis of stable analogues with permanent covalent bonds.

A last example is taken form the fields of sensing and pattern recognition. The numerous species that are present at the same time in a dynamic covalent system can be considered a broad library of sensor units. Similar to the drug discovery approach, the structure exhibiting the best binding properties to the analyte is amplified and hence the resultant compound distribution specific to the molecules of interest. The important steps of a sensing event are recognition, transduction, and analysis. The first one describes the nature and extent of the interaction of the analyte with the sensing moieties, that should ideally be selective, sensitive, related to the total amount of analyte, and cover a broad concentration range without saturation. The second step defines the transformation of the recognition event into a measurable signal in which high resolution and sensitivity are desirable. The analysis step refers to the recording and interpretation of the data.

In this context, the group of Bode developed a sensor system based on boronic acids that is capable of detecting various biorelevant carbohydrates (Figure 39).[71]

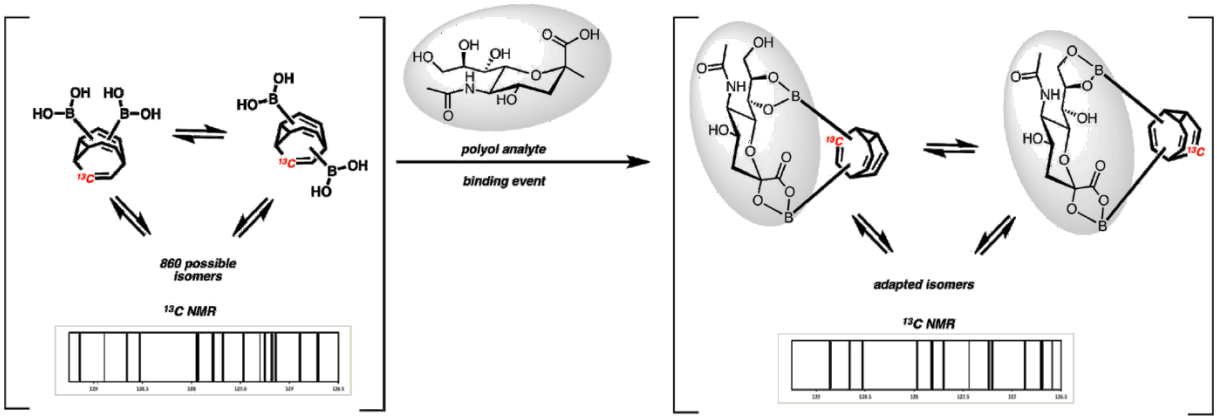


**Figure 39.** Carbohydrate sensor based on the dynamic covalent characteristics of bullvalene which undergoes continuous [3,3] sigmatropic rearrangement (Cope), the substitution pattern and $^{13}C$ labeling of the dynamic core give rise to 860 tautomers, due to the specific distance and orientation of hydroxy groups in different polyols certain bullvalene isomers are favored after conversion into boronic esters, the $^{13}C$-NMR signal pattern is transferred into a an easily readable bar code.[71]

The bullvalene basis of the bisboronic acid undergoes rapid Cope rearrangement which, considering the specific substitution pattern and $^{13}C$ isotopic labeling, gives rise to a total number of 860 possible tautomers. When exposing the dynamic covalent system to polyols, the formation of boronic esters is observed. However, certain bullvalene isomers are favored due to the specific distance and orientation of the hydroxy groups in the analyte molecules. The result is a unique signal pattern in the $^{13}C$ NMR spectrum for each of the investigated carbohydrate-boronic acid pairs which could be simplified and transferred into a barcode by means of the binning technique. Although the simultaneous detection of multiple analytes remains challenging, the technique

provides high selectivity for strongly binding motifs which holds potential for the detection of specific analytes in complex mixtures.

A vast spectrum of other applications for dynamic covalent chemistry is conceivable of which the three given examples intend to provide an impression of how a well-chosen molecular design can create a specific function.

# 3 Molecular Design Considerations

## 3.1 Negatively Charged Species

The first step towards the light-responsive zwitterion is the choice of appropriate charged groups. On the one hand, these moieties have to provide stability in aqueous medium to respect the potential applications in biological environments. On the other hand, the anion as well as the cation must exhibit sufficiently high reactivity as a nucleophile and electrophile, respectively, to form covalent bonds with each other. An overview of common organic anions is depicted in Figure 40.

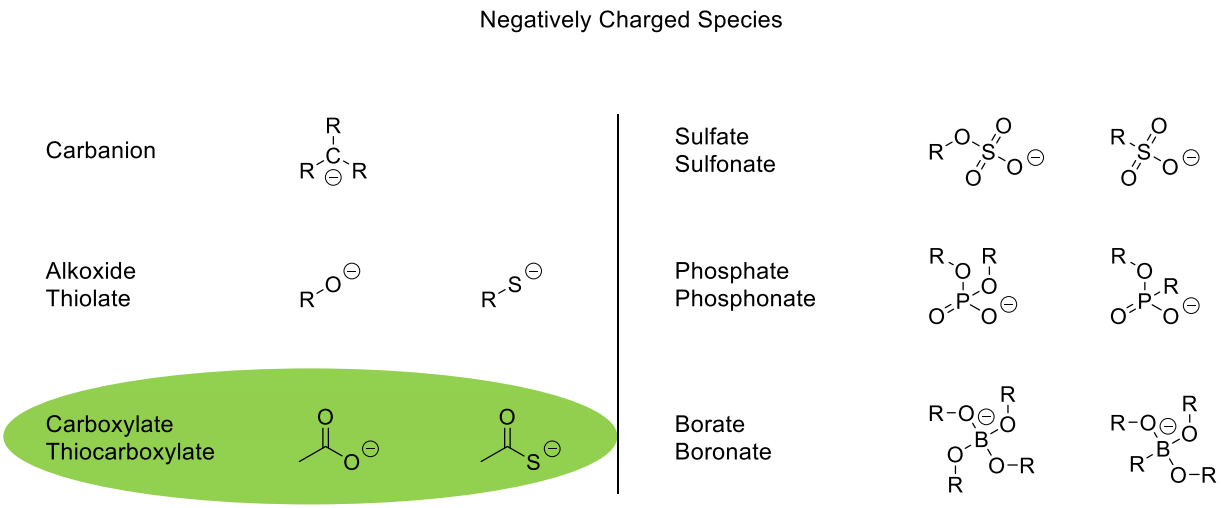


**Figure 40.** Common organic negatively charged groups; carbanions, alkoxides and thiolates, as well as sulfates, sulfonates, phosphates, phosphonates, borate, boronates are not applicable for the zwitterion switch due to their high reactivity, protonation under neutral aqueous conditions, and poor nucleophilic characteristics, respectively; carboxylates and thiocarboxylates (green) are a potential basis for a charged dynamic covalent system since they provide a balanced share of stability and reactivity.

Carbanions are usually highly reactive species which combine the characteristics of strong nucleophiles with high basicity. Their major role in a reaction, base or nucleophile, as well as their overall reactivity can be adjusted by the size and nature of the substituents. However, most anionic carbon derivatives decompose relatively fast under ambient conditions and are not stable in water which excludes them as potential anionic moieties for the zwitterion switch. Similarly, alkoxides and thiolates are unsuitable. Although they provide good nucleophilic characteristics, they mostly exist in their protonated uncharged form in neutral water ($pK_a$ (ethanol) = 16, $pK_a$ (ethanethiol) = 10.6).[72]

In contrast, carboxylates and thiocarboxylates are stable in neutral aqueous medium with $pk_a$ values about 4.8 and 3.4 for acetic acid and thioacetic acid, respectively. Although they are less

nucleophilic due to mesomerism, both functional groups and the sulfur derivative in particular represent a good compromise of stability and reactivity. It must be noted that thiocarboxylic acids exist in an equilibrium of two isomers, i.e. the thiol and the thione form. While the former structure is favored in solid state or in non-polar solvents, the formation of the latter is promoted in polar solvents at low temperatures.[73] However, no literature can be found about different deprotonated states of both isomers, which is most likely attributed to their similarity as a result of electron delocalization. Furthermore, nucleophilic attacks almost exclusively occur from the sulfur center and only a few examples for an attack by oxygen under specific reaction conditions are known.[74]

Sulfates and sulfonates as well as phosphates and phosphonates exhibit excellent stability in water over a long range of pH values. However, their poor nucleophilicity limits their potential use for the zwitterion switch. The last representatives of common negatively charged species are borates and boronates. Due to the stable 8-electron configuration the boron center cannot form another bond which renders a nucleophilic attack impossible. Nevertheless, both species can react in a nucleophile-like fashion by transferring one substituent to an electrophilic target. These transfers, however, are usually limited to carbon substituents and not reversible.

## 3.2 Positively Charges Species

Completing the requirements for zwitterions, an overview of common organic cations including one special case is depicted in Figure 41. Most positively charged organic groups contain nitrogen as electron deficient element. In the cationic state nitrogen forms four covalent bonds, the maximum possible number, and therefore cannot be nucleophilically attacked. However, due to mesomeric and/or inductive effects an adjacent carbon atom is converted into an electrophilic center. In case of ammonium ions, the reaction with a nucleophile is accompanied by the elimination of the corresponding amine which is usually not reversible and hence unfit for a dynamic covalent system. In contrast, the formation of amines from iminium ions is typically reversible, though the latter are often prone to hydrolysis under aqueous conditions. Amidinium and guanidinium ions provide higher stability in water, however, guanidium species are poor electrophiles since the charge is readily delocalized among the three nitrogen atoms. Similarly, charged heterocyclic structures such as imidazolinium, imidazolium, and benzimidazolium ions are stable in aqueous environments. Drawbacks are the longer synthesis of imidazoline derivatives since simple structures are not commercially available, and the very poor electrophilicity of imidazolium compounds due to their aromatic character. Benzimidazolium ions represent a

compromise of both aforementioned species and are therefore a proper basis for the zwitterion switch. The adjacent aromatic benzene ring lowers the stability of the imine double bond in comparison to the imidazole derivative. In either case it must be considered that all cyclic species are able to form carbenes when exposed to strong bases.

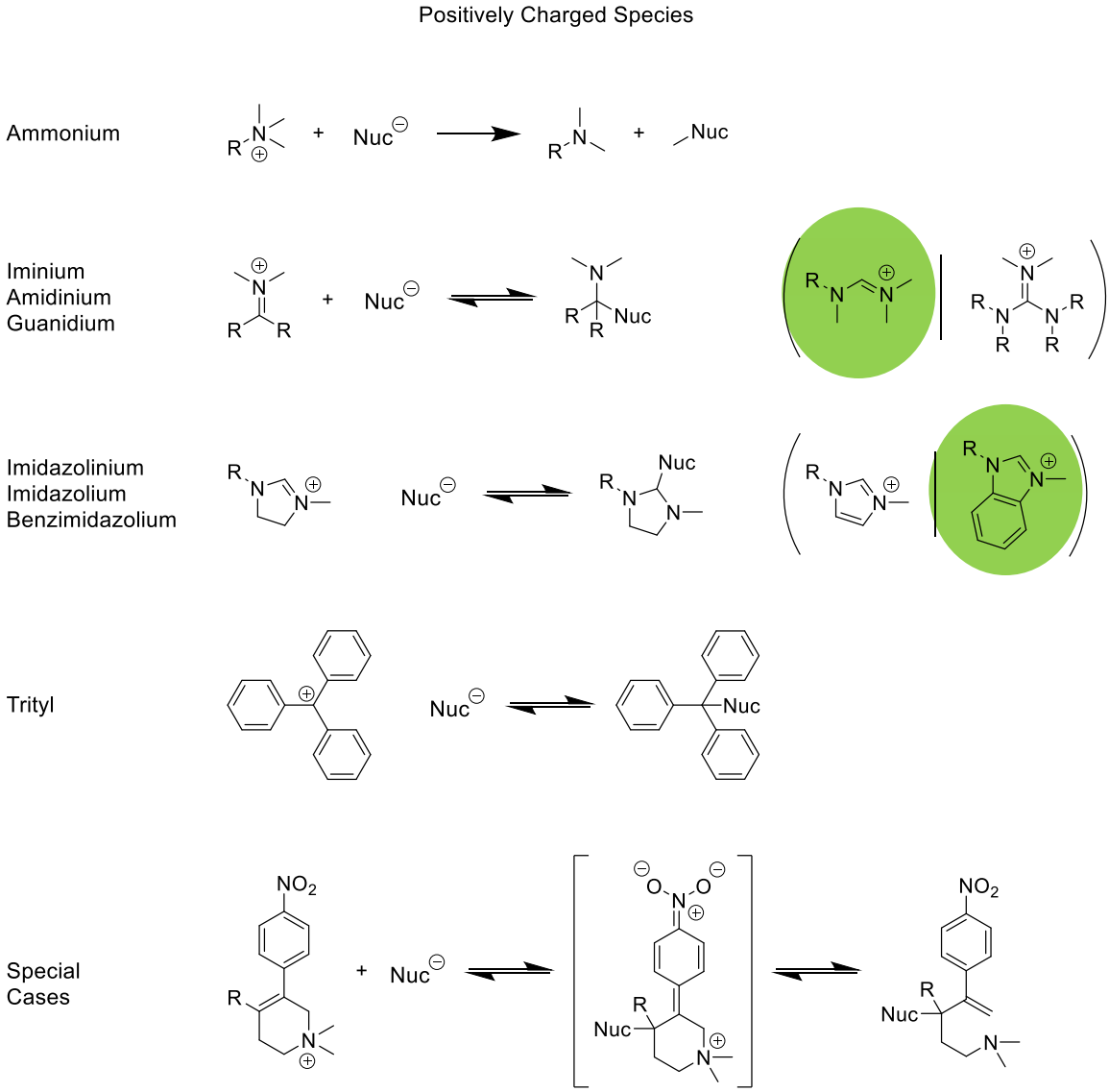


**Figure 41.** Common organic positively charged groups; ammonium and iminium ions do not provide the required reversibility and stability, respectively, for the targeted dynamic covalent system; while guanidinium and imidazolinium derivatives are highly stable in aqueous environments, they lack sufficient electrophilicity for the formation of covalent bonds with moderate nucleophiles; imidazolinium ions as well as the bottom special case are similarly unfit as they require a higher synthetic effort; the spectroscopic properties of trityl ions overlap with the absorption bands of photochromic compounds; aminidinium and benzimidazolium derivatives are suitable candidates in terms of stability and electrophilicity of which the latter is preferred due to the sterically more accessible iminium carbon.

Carbocations usually exhibit low stability under ambient conditions depending on the substituents attached to the carbon atom. One exception is the trityl ion where the positive charge is stabilized by three aromatic rings. However, the absorption bands of the intensely colored trityl derivatives

overlap with the excitation bands of most photoswitches which might have a detrimental effect on the isomerization efficiency of the photochromic system.

A special case of a potentially reversible charged dynamic covalent system is presented at the bottom of Figure 41. The electron-withdrawing effect of the nitrobenzene increases the electrophilicity of the styrene double bond. The ammonium ion is embedded in a ring structure which prevents the complete elimination of the corresponding amine from the system. However, the synthetic effort towards this structure is high and therefore not further considered for the zwitterion switch.

The best targets for the positively charged unit of the presented species in Figure 41 are the amidinium and benzimidazolium ions. Both structures represent a good compromise between stability and electrophilicity. Furthermore, in the latter case the better steric accessibility of the electrophilic benzimidazolium carbon due to the ring structure might be advantageous.

# 4 Results and Discussion

## 4.1 Computational Analysis

Azobenzene photoswitches were chosen as basis for the light-responsive zwitterionic dynamic covalent system. A general overview of the properties, advantages, synthesis, and applications of azobenzenes is presented in the first part of this thesis. The concept envisages the separation of the charges in the elongated *E* state while the contracted Z state allows sufficient proximity of the functional groups for the formation of a covalent bond. Primarily, a simple 3D modelling of different azobenzene structures was performed to investigate molecular motifs that allow proper interaction and proximity of the oppositely charged units in the contracted *Z* state. An overview of all molecules is shown in Figure 42.

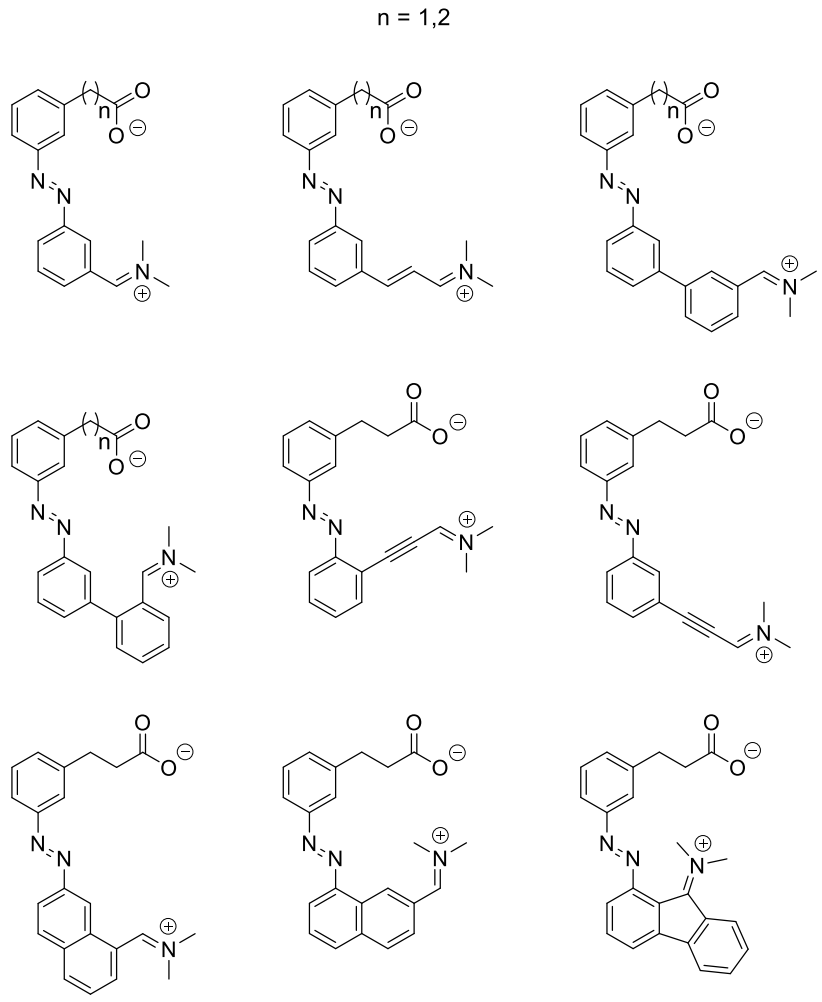


**Figure 42.** Zwitterionic azobenzene derivatives that were screened for the shortest distance between the charged groups in the *Z* configuration, the dihedral angles about the azo bond were fixed according to the data of a *Z* azobenzene crystal structure, MM2 minimization of the remaining parameters revealed two suitable structures (distance of carboxylic oxygen and iminium carbon between 1-2 Å), the C2 carboxylate is generally too short to provide the required proximity.

In order to keep the molecules as simple as possible, an iminium ion was connected to multiple azobenzene cores, which can later be converted into a structurally similar amidinium or benzimidazolium derivate. The charged groups are mostly attached in the *meta* positions of the aromatic rings with respect to the azo bond due to the shorter distance of the 3 and 3' carbon in comparison to 4 and 4' carbon in the *Z* configuration. However, the non-symmetric substitution pattern gives rise to three isomers, one where both groups point towards each other, one where they exhibit opposite directions, and one where they point in the same direction. For simplicity, only the "good" isomer is considered. Nonetheless, even if a "wrong" isomer is the dominant species, it should be continuously removed from the equilibrium as a consequence of covalent bond formation, which can only occur in the proper orientation.

The screening was conducted by fixing the dihedral angles about the *Z* azo bond with values taken from the crystal structure of a *Z* azobenzene. Subsequently, the remaining parameters were minimized by MM2 optimization. In general, the C2 carboxylate attached to the aromatic ring is too short to overcome the distance between the oppositely charged substituents. Finally, two of the investigated molecules were chosen that exhibited the lowest distance between the carboxylic oxygen and the iminium carbon (between 1-2 Å), the atoms where the covalent bond formation should occur (Figure 43).

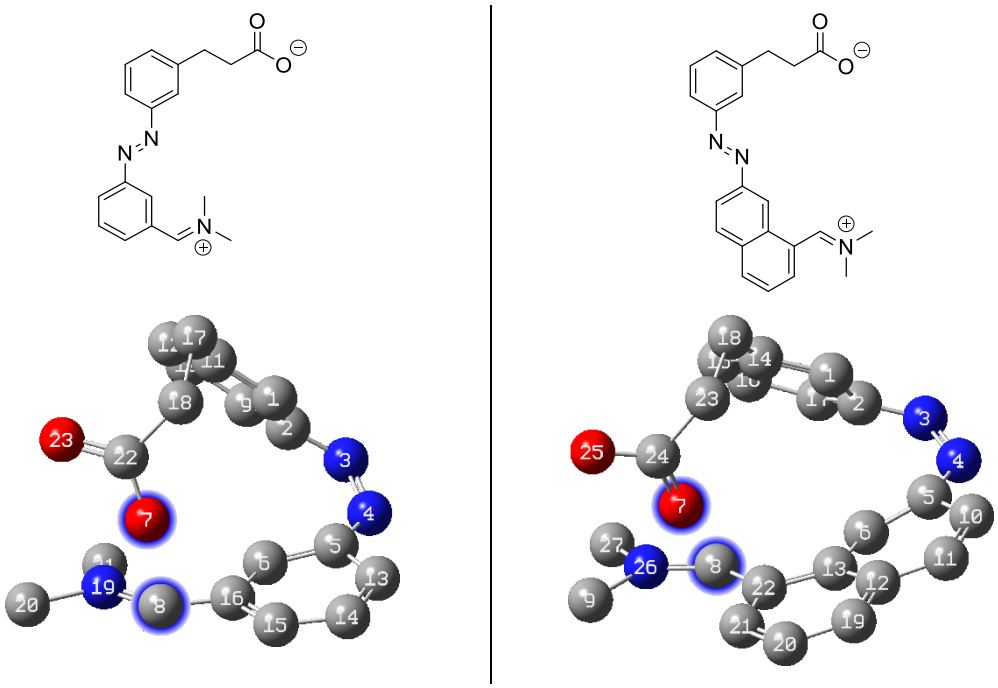

**Figure 43.** The *Z* configuration of the chosen phenyl (left) and naphthyl (right) azobenzene derivative allows close proximity of carboxylate oxygen 7 and iminium carbon 8 (encircled in blue), in the former case a minimum distance of 1.7 Å and in the latter case of 1.5 Å is observed between the charged groups, the dihedral angles about the azo bond are fixed: 1-2-3-4: 57.1°, 2-3-4-5: 7.0°, 3-4-5-6: 42.2° (the values are taken from a *Z* azobenzene crystal structure), hydrogen atoms are not displayed for better clarity.

The phenyl (left) and the naphthyl (right) derivative exhibit a distance of 1.7 Å and 1.5 Å, respectively, between the highlighted oxygen and carbon atom. For comparison, the typical length of a C-O single bond is approximately 1.4 Å.

After the theoretical proof of the concept's steric feasibility, the reactivity of the charged groups with each other was investigated by means of DFT computations. In this regard, Gaussian 09_c01 with the HSEH1PBE method, the 6-311G(d,p) basis set, and the IEFPCM solvent model was employed. The combination of the HSEH1PBE method and the 6-311G(d,p) basis set usually yields better or similar results in terms of enthalpies of formation, geometry optimization, and vibrational frequencies than the B3LYP method.[75] The (d,p) term includes polarization and diffuse functions which are important when dealing with charged species.

For the first screening, three model systems each consisting of a small thiocarboxylate and an amidinium ion were investigated to keep the overall number of atoms low and hence the calculation time as short as possible. The sulfur derivative was chosen due to its higher nucleophilicity in comparison to the normal carboxylate.

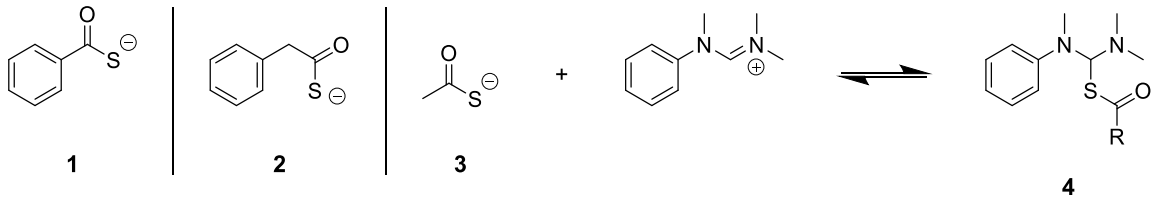


| Solvent | ΔG(4) – ΔG(1) (kJ/mol) | ΔG(4) – ΔG(2) (kJ/mol) | ΔG(4) – ΔG(3) (kJ/mol) |
|---|---|---|---|
| Water | 35.0 | 30.5 | / |
| Acetonitrile | 32.6 | 27.4 | 14.9 |
| Tetrahydrofuran | 21.4 | 15.0 | 3.0 |
| Chloroform | 14.8 | 7.8 | -3.4 |
| Benzene | 2.3 | -7.3 | -18.3 |
| Cyclohexane | 0.3 | -9.5 | - |
| No solvent | -19.1 | - | - |

**Figure 44.** Theoretical investigation of the reaction between three thiocarboxylates and an amidinium ion in different solvents, the position of the equilibrium is dependent on the polarity of the solvent, less polar solvents favor the bound state **4** while more polar solvents favor the unbound states **1**-**3**, no number (-): the unbound state was not accessible since bond formation occurred during the optimization process, the calculations were performed with Gaussian 09_c01, the HSEH1PBE method, the 6-311G(d,p) basis set, and the IEFPCM solvent model.

First, the two molecules of each system were separately optimized. Subsequently, the pre-optimized structures were combined in one system and re-subjected to optimization in order to obtain the free enthalpy of the unbound state **1**-**3**. The identical procedure was applied to the bound state **4**. The difference of the free enthalpy in different solvents is depicted in Figure 44. A negative number (red) indicates a bound state that is more stable than the respective unbound state. According to the computations, the reaction between the charged moieties occurs in solvents of low polarity. Moreover, control over the formation of the theoretical zwitterion and the neutral species seems possible by choosing the appropriate environment. These results are supported by the general trend of stronger stabilization of charged species in polar solvents.

## 4.2 Model System 1: Amidinium and Benzimidazolium Ion

In order to prove the computational results, an aromatic amidinium and benzimidazolium ion was synthesized and the interaction with a (thio)carboxylate in different solvents investigated. The synthesis of compounds **3** and **5** as well as of the nucleophiles **7** and **9** is depicted in Scheme 13.

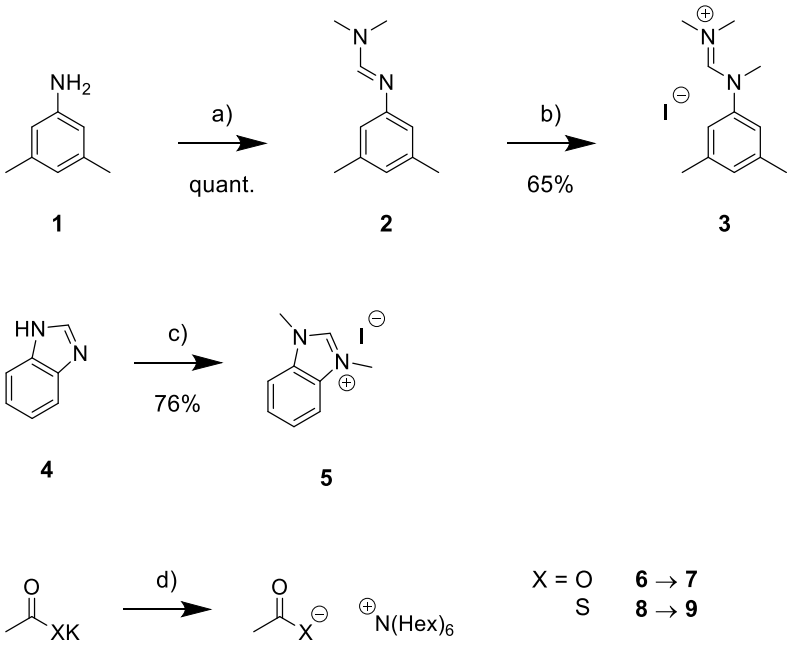


**Scheme 13.** Synthesis of amidinium iodide **3**, benzimidazolium iodide **5**, and tetrahexylammonium (thio)carboxylate **7** and **9** as model compounds for the zwitterionic dynamic covalent system, a) *N,N*-dimethylformamide dimethyl acetal, cat. AcOH, $CHCl_3$, RT, o/n, b) dimethyl sulfate, THF, reflux, o/n, c) methyl iodide, $K_2CO_3$, MeCN, reflux, 5 h d) tetrahexylammonium chloride, organic solvents (benzene, chloroform, dimethylsulfoxide), ultrasound, 30 min.

Dimethylaniline **1** was converted into amidine **2** by N,N-dimethylformamide dimethyl acetal in acidic environment. Since the acetal is prone to hydrolysis, the mixture should be kept under

anhydrous conditions. Furthermore, to increase the overall yield, the reaction can be driven to the product side by removal of methanol, that is formed as a side product. Eventually, amidinium iodide **3** was obtained by methylation with dimethyl sulfate and subsequent anion exchange by means of sodium iodide. The direct methylation employing low-boiling methyl iodide was unsuccessful since higher temperatures and longer reaction times are necessary to achieve a sufficient conversion rate. In contrast, the exhaustive methylation of benzimidazole (**4**) by means of methyl iodide was successful yielding benzimidazolium iodide **5**.

Due to the low solubility of commercially available potassium (thio)carboxylate in common organic solvents, an exchange for the tetrahexylammonium derivatives was performed. However, compound **9** is not stable under ambient conditions in solid or dissolved state. Therefore, a fresh solution was prepared for all experiments.

The first model compound **3** was analyzed by means of NMR spectroscopy in the pure form and in 1:1 mixtures with the carboxylate derivatives. Three solvents of different polarity were employed, i.e. benzene, chloroform, and dimethylsulfoxide. Chloroform was stirred with ground $K_2CO_3$ prior to use to neutralize potential acidic contaminations. In each case, the signals attributed to the amidinium and aromatic protons (Table 4, red) were compared before and after addition of the nucleophile. Especially the amidinium proton should exhibit a significant upfield shift when the charge is neutralized due to addition to the double bond. The remaining aliphatic signals are neglected as they strongly overlap with the ammonium hexyl chains. The results are summarized in Table 4.

**Table 4.** Addition of acetate **5** and thiocarboxylate **7** to amidinium **3**, (+) indicates the appearance of new signals in the $^1$H-NMR spectrum while (-) denotes no change or minor shifts of the aromatic and/or amidinium protons (red), the remaining signals are neglected as they strongly overlap with the signals of ammonium hexyl chains.

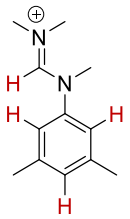

| Solvent | Acetate **5** | Thiocarboxylate **7** |
|---|---|---|
| Benzene | + | + |
| Chloroform | + | - |
| Dimethylsulfoxide | - | - |

While the addition of acetate **7** to amidinium **3** induces a change in the NMR spectrum in both non-polar solvents, regarding thiocarboxylate **9** only in benzene an effect is observed. These results support the computational analysis which indicated no reaction in polar media. However, the nature of the process is unknown since multiple new signals appear in the aromatic and stronger downfield shifted region. Even though the definite assignment of the new signals remains

difficult, it is likely that more than one new species formed. An example spectrum before and after addition of compound **7** to compound **3** in chloroform is depicted in Figure 45. Three new major sets of signals appear in the region between 6.2 to 7.1 ppm. Each set consists of two signals that exhibit an integral ratio of 1 : 2. This ratio matches the aromatic protons in *ortho* (2) and *para* (1) position of amidinium **3**, and suggests the presence of at least three species with an intact aromatic core after the addition of the nucleophile. However, the remaining three signals in the area between 8.3 to 9.5 ppm could not be assigned, as their integrals do not match the expected single amidinium proton.

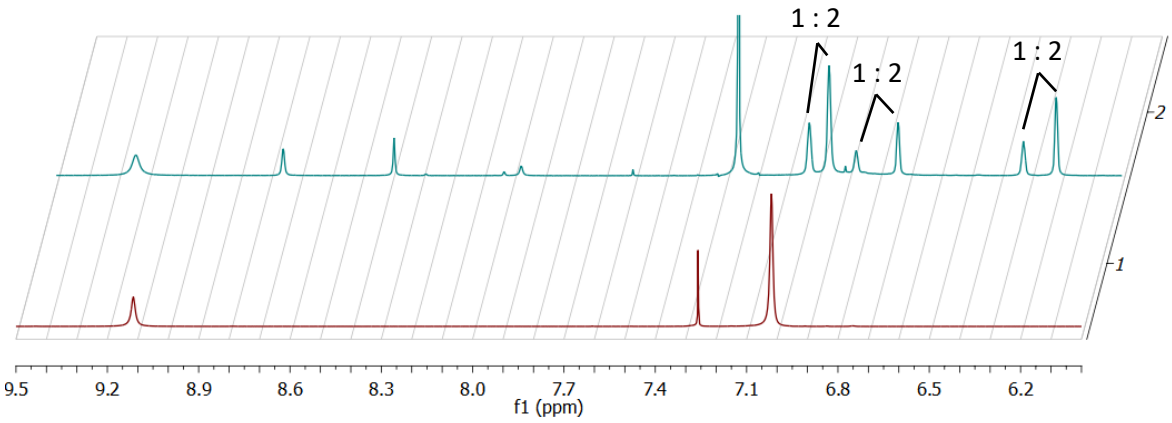


**Figure 45.** $^{1}$H-NMR (300 MHz, $CDCl_3$) spectra of amidinium derivative **3** before (bottom, red) and after (top, blue) addition of **7**, several new signals appear in the aromatic and stronger downfield shifted area indicating processes beyond the single addition of the nucleophile to the amidinium double bond, the displayed integral ratios of 1 : 2 for the three signal sets match the *ortho* and *para* protons of amidinium **3**, which implies the presence of at least three species in the current system; consequently, the reaction was not further investigated as it does not fulfill the requirement of a clean reversible conversion between two species; the NMR solvent was rapidly stirred with ground $K_2CO_3$ and filtered prior to use to neutralize acidic contaminations.

Furthermore, the number, shape, and integrals of the NMR signals are different for every solvent and nucleophile. Hence, it is unlikely that the current system represents a dynamic covalent conversion of two species, but processes beyond the reversible addition of the nucleophile to the amidinium double bond seem to be the reason for the observation. However, deprotonation and formation of carbenes, a typical side reaction of amidinium compounds, can be excluded due to the low basicity of acetate.

The previous experiments were repeated with benzimidazolium derivative **5**. However, due to the very low solubility of **5** in benzene as well as in chloroform, DCM and DMSO were employed for the NMR experiments. In contrast to the amidinium derivative **3** no reaction was observed with acetate **7** or thioacetate **9** in either of the solvents. In order to test the general electrophilic properties of compound **5** two last experiments with a stronger nucleophile, i.e. dimethylamine and benzyl amine, were conducted. Also in this case, no reaction was observed. The corresponding

NMR spectra are depicted in Figure 46. The downfield shift of the benzimidazolium proton in the green spectrum (after addition of acetate **7**) might be attributed to non-covalent interactions. The addition of dimethylamine (blue spectrum) results in no significant change of the NMR spectrum.

The performed experiments do not support the computational data. While no indication for a reaction between benzimidazolium derivative **5** and a nucleophile is observed, amidinium derivative **3** shows a reaction. However, the process was not further investigated since the existence of a dynamic covalent equilibrium consisting of two species can be excluded. In order to avoid side reactions, a system exhibiting both reactive groups in one molecule might be beneficial due to the generally higher rate of intramolecular reactions. Furthermore, regarding the unreactive benzimidazolium compound, the resultant higher effective molarity might induce the targeted conversion to the uncharged state.

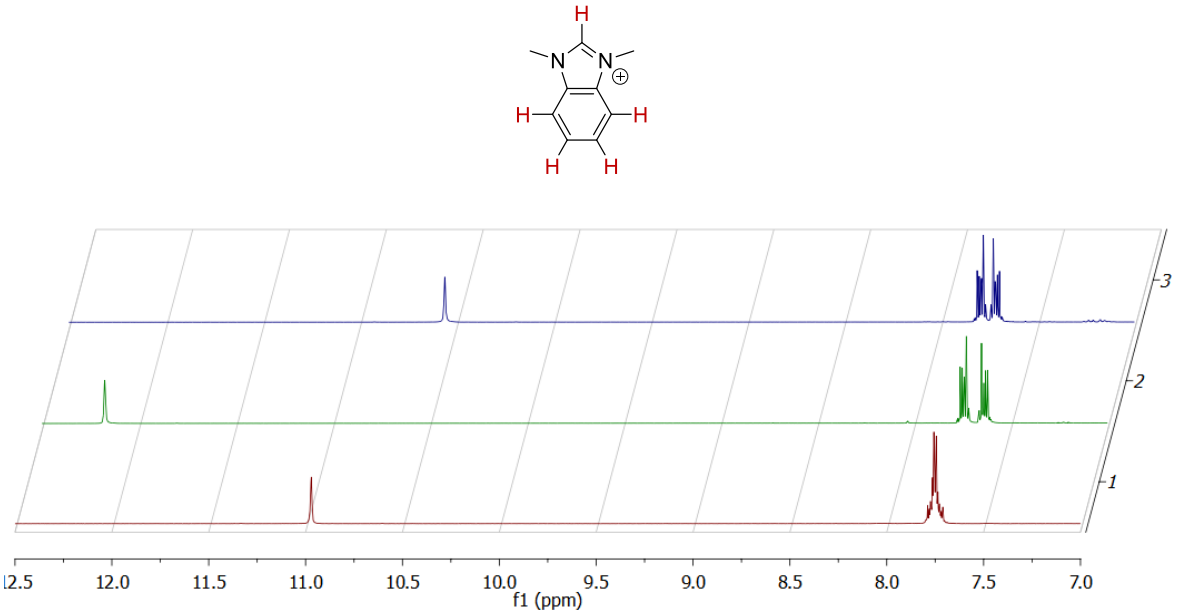


**Figure 46**. $^{1}$H-NMR (300 MHz, DMC) spectra of benzimidazolium derivative **5** before (red) and after addition of acetate **7** (green) and dimethylamine (blue), the spectrum after addition of benzyl amine is not shown as it exhibits only minor changes in comparison to the blue one, no significant change is observed that can be attributed to the addition to the nitrogen double bond, the downfield shift of the benzimidazolium proton in the green spectrum might be attributed to non-covalent interactions.

## 4.3 Model System 2: One Molecule Approach

The synthesis of both target molecules which exhibit a carboxylate and an amidinium (**UT-1**) or benzimidazolium ion (**17**) is depicted in Scheme 14. The thiocarboxylate structures are discarded

because of high synthetic effort. Additionally, the preparation of benzyl amine derivative **18** as a stronger nucleophilic reference compound is shown.

The preparation of amidinium derivative **UT-1** was attempted in two ways. On the first route, methyl anthranilate (**10**) was converted into amidine **11** by *N*,*N*-dimethylformamide dimethyl acetal following the same procedure as for compound **2**. However, the subsequent methylation by either methyl iodide or dimethyl sulfate remained unsuccessful, most likely due to the poor nucleophilicity of the aniline in conjugation to the electron withdrawing ester. The reaction could be accomplished by means of methyl trifluoromethylsulfonate, a stronger methylating agent, with high yields. The hydrolysis of ester **12** to the free carboxylic acid **UT-1** failed under several conditions. Neither diluted acids (AcOH, HCl, $H_2SO_4$) or bases (NaOH, LiOH) nor other reagents such as trimethylsilyl iodide led to the final product, but either no reaction or decomposition of the starting material was observed.

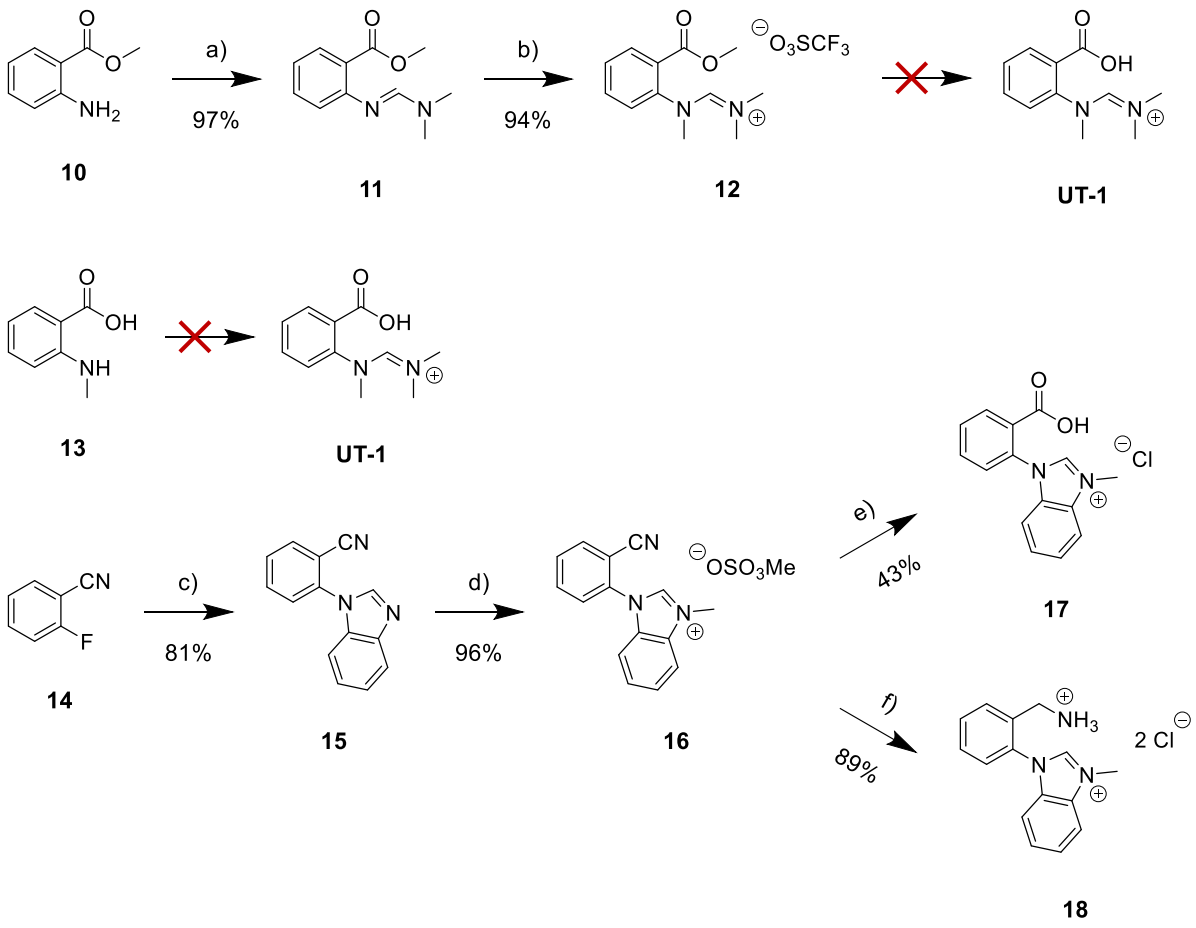


**Scheme 14.** Synthesis of amidinium derivative **UT-1** and benzimidazolium derivatives **17** and **18**, the finals steps towards **UT-1** failed, a) N,N-dimethylformamide dimethyl acetal, cat. AcOH, $CHCl_3$, RT, o/n, b) methyl trifluoromethylsulfonate, $K_2CO_3$, DCM, 0 °C → RT, 4 h, c) benzimidazole, $K_2CO_3$, DMSO, 80 °C, o/n, d) dimethyl sulfate, MeCN, 80 °C, o/n, e) $AcOH/H_2O/H_2SO_4$ (2/1/1), 120 °C, o/n, f) $H_2$, Pd/C, HCl, MeOH, 24 h, RT.

An alternative route towards **UT-1** starts from N-methylanthranilic acid (**13**), which allows the use of the free carboxylic acid as starting material as no methylation is needed. However, the formation of the amidinium group remains challenging. Typical procedures such as the conversion with *N*,*N*-dimethylformamide dimethyl acetal in acetic environment, with the Vilsmeier reagent, or the tosylated equivalent of the Vilsmeier reagent were unsuccessful. Further optimization of the reaction conditions might provide better results since traces of product **UT-1** could be identified by UPLC analysis. However, due to time limitations at this point of the project, the synthesis of the second model compound was prioritized.

Benzonitrile derivative **15** was prepared by a nucleophilic aromatic substitution of *2*-fluoro-benzonitrile (**14**) and benzimidazole. Subsequently, methylation by dimethyl sulfate yielded benzimidazolium derivative **16** which was hydrolyzed in a mixture of acetic acid, sulfuric acid, and water to the corresponding free carboxylic acid **17**. Due to the high polarity of the product, the removal of sulfuric acid from the reaction mixture could not be performed by standard methods such as a liquid-liquid extraction. Hence, the sulfate was precipitated by barium acetate, filtered, and the remaining acetic acid evaporated under reduced pressure. The low yield of the last step can be explained by the thin amorphous $BaSO_4$ slurry, that complicated filtration and proper rinsing of the residue. Reference compound **18** was readily prepared by reduction of the nitrile group with hydrogen under Pd/C catalysis.

Similar to the two-molecule approach, compound **17** was analyzed by NMR spectroscopy in the protonated and deprotonated (nucleophilic) state (Figure 47). The red spectrum represents the pure carboxylic acid in DMSO while the blue spectrum was recorded after the addition of triethylamine. Minor shifts of the signals attributed to the aromatic and benzimidazolium protons are observed which can be explained by the formation of the benzoate. However, there is no indication for an intramolecular covalent bond between the nucleophilic oxygen and the electrophilic carbon, which supports the computational data for polar solvents. The same experiment in non-polar solvents could not be performed due to the insolubility of the highly polar benzimidazolium derivative **17** therein.

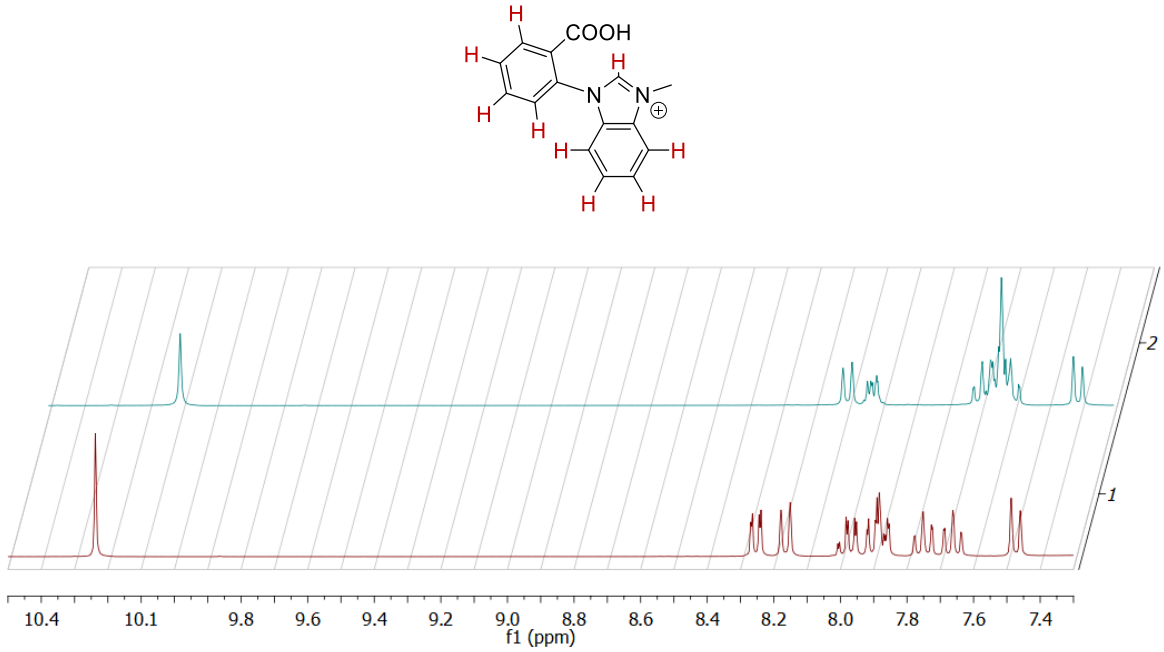


**Figure 47.** $^{1}$H-NMR (300 MHz, DMSO) spectra of benzimidazolium derivative **17** before (red) and after addition of triethylamine (blue), minor shifts of the aromatic and benzimidazolium protons due to deprotonation of the benzoic acid are observed, a strong upfield shift of the benzimidazolium proton due to the formation of an intramolecular covalent bond is missing.

Alternatively, **17** was dissolved in basic water, a non-polar solvent (benzene, chloroform, DCM) was added, the mixture rapidly stirred, and a sample of the organic layer taken after 1 h, 5 h, and 24 h. Analysis by UPLC reveals no transfer of a potentially uncharged species from the aqueous to the organic phase. Hence, the zwitterionic structure is the major species under these conditions considering that the ring-closed structure should not be soluble in water.

In order to test the electrophilicity of the benzimidazolium moiety, the same experiment was performed with benzyl amine derivative **18**. In this regard, the benzyl ammonium ion **18** was dissolved in water and potassium carbonate was added. Rapid precipitation of an off-white solid was observed, which was dried and analyzed by $^{1}$H-NMR spectroscopy in DCM. The spectra of the protonated initial state **18** (red), of the potential intermediate **18a** (green), and of the final structure **18b** (blue) are depicted in Figure 48. The nucleophilic attack of the free amine at the charged benzimidazolium moiety is accompanied by the disappearance of the strongest downfield shifted benzimidazolium proton. Furthermore, the methyl group attached to one of the benzimidazolium nitrogens is equally shifted to higher field and a specific coupling of the benzyl protons typical of cyclohexyl-like ring structures arises.

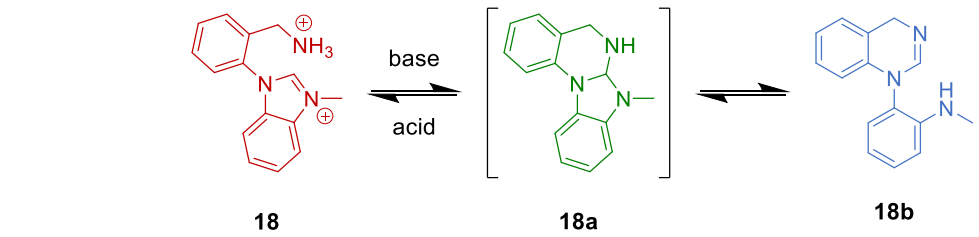


**18** **18a** **18b**

a)

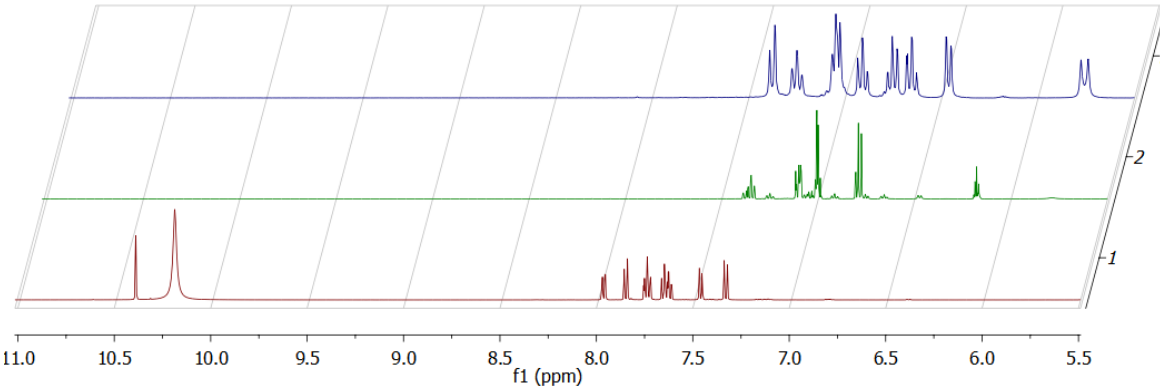


b)

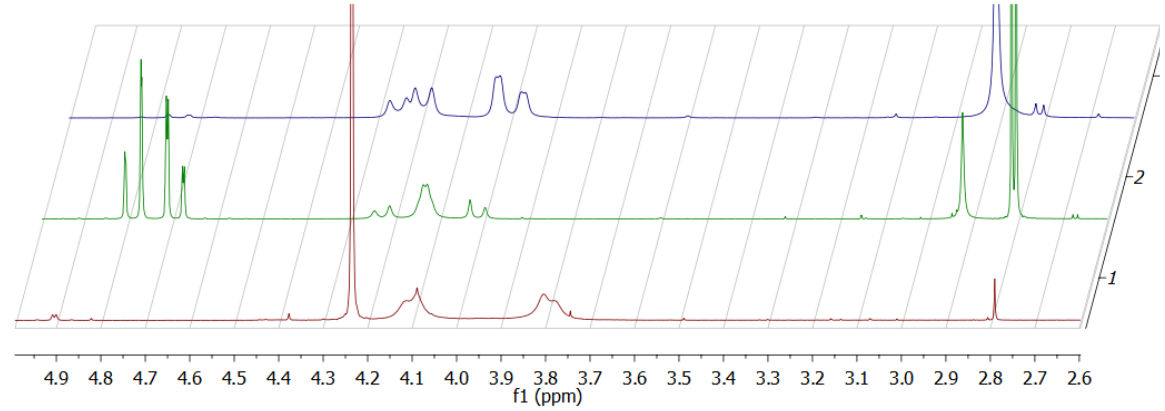


**Figure 48.** $^{1}$H-NMR spectra (500 MHz, DCM) of the a) aromatic and b) aliphatic region of pure compound **18** (red), after precipitation in basic water and re-dissolution in DCM (green), and after slight heating of the precipitate solution (blue), the heating increases the conversion rate to the final state, the broad signals at 10.2 ppm in the red spectrum is attributed to acetic acid which blocks the nucleophilic properties of benzyl amine by protonation, the process is fully reversible depending on the proton concentration and can be also observed in solution without prior precipitation, the structure of intermediate **18a** is an assumption based on compound **18** and **18b**, the structure of **18b** was confirmed by 2D-NMR analysis and recording of a crystal structure.

The intermediate **18a** and the aniline structure **18b** remain in an equilibrium state in basic or neutral medium, which lies almost completely on the side of **18b**. Slight heating increases the conversion rate towards the amidine, though no complete conversion even after prolonged thermal treatment was observed. In fact, the addition of acid induces the complete conversion back to the benzyl ammonium state **18**, reproducing the initial spectrum. In this case, at least two equivalents of acid are required, one to activate the amidine and facilitate the nucleophilic attack of the aniline, and one to block the benzyl amine and prevent the back reaction.

While the nature of the intermediate state is an assumption based on the starting and the end structure, amidine **18b** is supported by standard 2D-NMR spectroscopic analysis (COSY, HMBC, HSQC) and $^{1}H$-$^{14}N$ long range coupling. In the latter case, no proton was observed that interacts with all three nitrogen atoms, which would be required for the triaminomethane derivative **18a**. Furthermore, a crystal structure of compound **18b** was recorded confirming the open benzimidazole ring and the amidine double bond (Figure 49). The bond length between carbon C7 and nitrogen N3 is 1.27 Å which is a typical value for C-N double bonds.

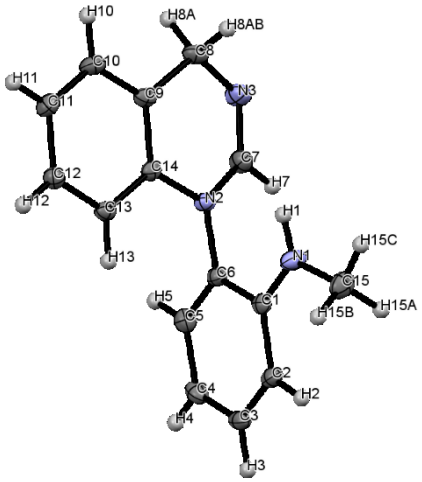


**Figure 49.** Crystal structure of compound **18b** crystallized from a MeCN solution, the amidine indicated by the bond length between N3 and C7 of 1.27 Å (typical value of C-N double bonds) and the opened 5-membered ring of the former benzimidazole confirm the results obtained by NMR analysis.

The current data implies sufficient electrophilicity and reversibility of the benzimidazolium moiety for the preparation of a charged dynamic covalent system. However, the carboxylate does not provide the required nucleophilic characteristics to attack the electrophilic carbon. A stronger nucleophile, i.e. a benzyl amine, induces the ring-opening of the benzimidazole under formation of a phenylenediamine derivative. The process is fully reversible giving rise to an equilibrium that can be controlled by means of acid and base.

## 4.4 Summary and Outlook

The development of a zwitterionic dynamic covalent system that can be integrated in an azobenzene photoswitch was started. Potential cationic and anionic groups were chosen and screened by computational methods. In this regard, amidinium and benzimidazolium ions were suitable candidates. Experimental investigations revealed an undefined reaction of amidinium derivative **3** with acetate and thioacetate in non-polar solvents, supporting the theoretical data

from the reactivity point of view. The benzimidazolium derivative **5** did not show any reaction even when stronger nucleophiles such as dimethylamine were applied. In either case, no indication for the targeted equilibrium between a charged and neutral state was found.
Subsequently, a second model system was synthesized which combines both functional groups in one molecule. Even though the amidinium derivatives were not accessible, the benzimidazolium compounds **17** and **18** could be made. While the benzoate did not provide sufficient nucleophilicity, the benzyl amine induced the conversion of the benzimidazole moiety into the phenylenediamine structure **18b**. The latter could be confirmed by NMR and X-ray crystal structure analysis. The process is fully reversible and can be controlled by means of acid and base. This result represents a first proof of the concept. A stronger, charged nucleophile such as thiobenzoate or an aliphatic carboxylate might be sufficient to induce the targeted reaction.

Due to time limitation, the synthesis of another model system with a stronger nucleophile as well as the preparation of the final azobenzene could not be accomplished. However, even the investigated cationic model compound **18** can be integrated in an azobenzene as basis for a light-controlled pH switch. A proposed structure based on the models from Chapter 4.1 is depicted in Scheme 15.

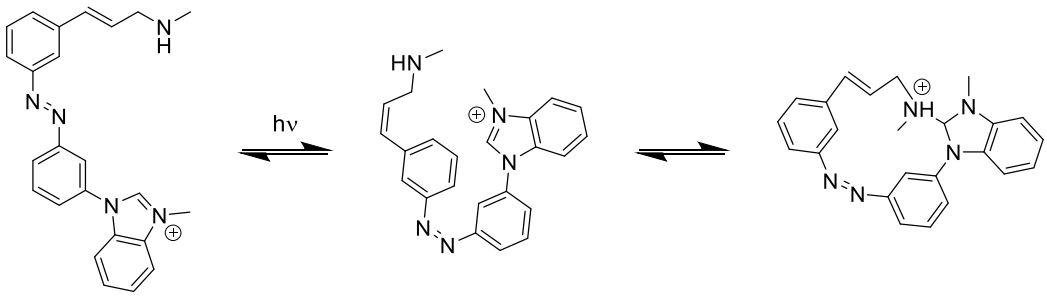


**Scheme 15.** Proposed structure for an azobenzene $pk_a$ switch, in the *E* configuration both functional groups are spatially separated while the *Z* isomer allows the addition to the benzimidazolium double bond, the additional methyl group at the amine prevents the formation of the phenylenediamine species, the double bond limits the flexibility of the alkyl chain which might facilitate the proper orientation of the nucleophile, the system, switches between a free amine and an ammonium ion which is accompanied by a $pk_a$ change of more than 20 orders of magnitude.

The nucleophilic attack of the amine at the benzimidazolium moiety generates a protonated ammonium ion with a $pk_a$ value in the range of 10. Considering the $pk_a$ values of secondary amine of over 30, a change of more than 20 orders of magnitude could be theoretically achieved.[76]
The additional methyl group at the amine prevents the ring-opening of benzimidazole and the formation of the phenylenediamine species. Furthermore, a double bond to restrict the flexibility of the alkyl chains might be beneficial for proper orientation in the *Z* isomer. The control over the

equilibrium by means of acid and base is substituted by the spatial separation of the electrophilic and nucleophilic group as a consequence of azobenzene isomerization. In case of the model compound, protonation of the amine in close proximity to the benzimidazolium ion was required to stabilize and access the initial state.

# 5 Experimental Part

Remarks about materials and instrumentation can be found in chapter 5.1 of the first part of this thesis.

## 5.1 Synthethic Procedures

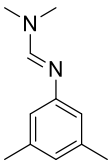

***N,N*-dimethyl-*N'*-(3,5-dimethylphenyl)formamidine (2)**: *3,5*-Dimethylaniline (**1**) (10.0 mmol, 1.21 g, 1.0 eq.) was dissolved in dry chloroform and *N*,*N*-dimethylformamide dimethyl acetal (15.0 mmol, 2.01 g, 1.5 eq.) as well as acetic acid (0.5 mmol, 0.03 g, 0.05 eq.) were added. The mixture was stirred at room temperature overnight, diluted with ethyl acetate, and washed with 1 M aqueous NaOH (3x) and brine. The organic layer was dried over $Na_2SO_4$, filtered, and evaporated under reduced pressure yielding compound **2** which was used without further purification (1.75 g, quant.).

**$^1$H-NMR** (300 MHz, $CDCl_3$): δ (ppm) = 7.52 (s, 1H), 6.67 (s, 1H), 6.60 (s, 2H), 3.00 (s, 6H), 2.28 (s, 6H). **$^{13}$C-NMR** (75 MHz, $CDCl_3$): δ (ppm) = 153.4, 152.1, 138.6, 124.3, 119.1, 21.4. **MS-ESI**: m/z = 177.1385 (calc. for [M + $H^+$]: 177.1392).

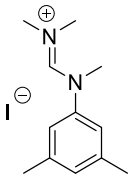

**Formamidinium iodide 3**: Formamidine **2** (9.5 mmol, 1.67 g, 1.0 eq.) was dissolved in THF and dimethyl sulfate (1.2 mmol, 1.44 g, 1.2 eq.) was added. The mixture was heated at reflux overnight. After cooling down, the mixture was diluted with water and washed with hexanes (3x). Sodium iodide (1.2 mmol, 1.71 g, 1.2 eq.) was added to the aqueous phase and the yellow solution extracted with DCM (3x). The combined organic layers were dried over $MgSO_4$, filtered, and evaporated under reduced pressure. The solid residue was recrystallized from *2*-propanol yielding compound **3** as a white solid (1.95 g, 65%).

**$^1$H-NMR** (300 MHz, $CDCl_3$): δ (ppm) = 9.11 (s, 1H), 7.02 (s, 3H), 3.70 (s, 3H), 3.49 (s, 3H), 2.48 (s, 3H), 2.31 (s, 6H). **$^{13}$C-NMR** (75 MHz, $CDCl_3$): δ (ppm) = 155.1, 140.3, 139.4, 131.5, 123.6, 47.5, 46.5, 39.4, 21.2. **MS-ESI**: m/z = 191.1535 (calc. for $[M^+]$: 191.1548).

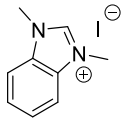

***N,N'*-dimethylbenzimidazolium iodide 5**: Benzimidazole (**4**) (10.0 mmol, 1.18 g, 1.0 eq.) was dissolved in acetonitrile, methyl iodide (30.0 mmol, 1.87 g, 3.0 eq.), and ground $K_2CO_3$ (11.0 mmol, 1.52 g, 1.1 eq.) were added. The mixture was heated at reflux for 5 h. After cooling down, the solvent was distilled and the solid residue extracted with DCM (3x). The combined organic phases were evaporated under reduced pressure yielding compound **5** as a white solid that was used without further purification (2.09 g, 76%).

**$^1$H-NMR** (500 MHz, DMSO-$d_6$): δ (ppm) = 9.68 (s, 1H), 8.06 – 7.98 (m, 2H), 7.74 – 7.66 (m, 2H), 4.09 (d, J = 0.5 Hz, 6H). **$^{13}$C-NMR** (125 MHz, DMSO-$d_6$): δ (ppm) = 143.1, 131.6, 126.4, 113.4, 33.3. **MS-ESI**: m/z = 147.0897 (calc. for $[M^+]$: 147.0922).

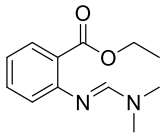

**Formamidine 11**: Following the procedure of *N,N*-dimethyl-*N'*-(3,5-dimethylphenyl)formamidine (2), methyl anthranilate (**10**) (9.0 mmol, 1.49 g, 1.0 eq.), *N,N*-dimethylformamide dimethyl acetal (13.5 mmol, 1.61 g, 1.5 eq.), acetic acid (0.5 mmol, 0.03 g, 0.05 eq.), yield: 1.92 g (97%).

**$^1$H-NMR** (300 MHz, $CDCl_3$): δ (ppm) = 7.77 – 7.68 (m, 1H), 7.39 – 7.29 (m, 2H), 7.00 (ddd, J = 7.7, 7.3, 1.2 Hz, 1H), 6.90 – 6.81 (m, 1H), 4.30 (q, J = 7.1 Hz, 2H), 3.01 (s, 6H), 1.34 (t, J = 7.1 Hz, 3H). **$^{13}$C-NMR** (75 MHz, $CDCl_3$): δ (ppm) = 168.2, 153.0, 152.7, 132.3, 130.6, 124.8, 122.6, 121.9, 60.6, 14.4. **MS-ESI**: m/z = 221.1292 (calc. for $[M + H^+]$: 221.1290).

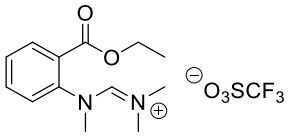

**Formamidinium trifluoromethylsulfonate 12**: Formamidine **11** (9.5 mmol, 1.67 g, 1.0 eq.) was dissolved in dry DCM under argon and ground dry $K_2CO_3$ (10.2 mmol, 1.41 g, 3.0 eq.) was added. The mixture was cooled down to 0 °C and methyl trifluoromethylsulfonate (10.2 mmol, 1.67 g, 3.0 eq.) was added slowly. The suspension was stirred for 4 h at room temperature after which

excess methylating agent was carefully quenched by slow addition of methanol. The mixture was filtered, washed with 1 M aqueous $K_2CO_3$ and brine, dried over $MgSO_4$, filtered and evaporated under reduced pressure yielding compound **12** as a light-brown oil which was used without further purification (1.27 g, 97%).

**$^1$H-NMR** (300 MHz, $CDCl_3$): δ (ppm) = 9.11 (s, 1H), 7.02 (s, 3H), 3.70 (s, 3H), 3.49 (s, 3H), 2.48 (s, 3H), 2.31 (s, 6H). **$^{13}$C-NMR** (75 MHz, $CDCl_3$): δ (ppm) = 155.1, 140.3, 139.4, 131.5, 123.6, 47.5, 46.5, 39.4, 21.2. **MS-ESI**: m/z = 235.1426 (calc. for [$M^+$]: 235.1447).

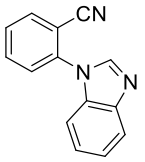


***2*-(*1H*-benzo[*d*]imidazol-*1*-yl)benzonitrile (15)**: *2*-Fluorobenzonitrile (**1**) (20.0 mmol, 2.42 g, 1 eq.) was dissolved in DMSO and benzimidazole (21.0 mmol, 2.48 g, 1.05 eq.) as well as ground $K_2CO_3$ (21.0 mmol, 2.90 g, 1.05 eq.) were added. The mixture was stirred at 80 °C for 15 h. After cooling down, the mixture was diluted with sat. aqueous $NH_4Cl$ solution and extracted with EA three times. The combined organic layers were washed with brine (3x), dried over $MgSO_4$, filtered, and evaporated. The crude material was purified by flash column chromatography (hexanes/EA) yielding the title compound as an off-white solid (3.53 g, 81%).

**$^1$H-NMR** (500 MHz, DMSO-$d_6$): δ (ppm) = 8.63 (s, 1H), 8.20 – 8.13 (m, 1H), 8.02 – 7.94 (m, 1H), 7.87 – 7.80 (m, 2H), 7.77 (td, J = 7.7, 1.1 Hz, 1H), 7.42 – 7.37 (m, 1H), 7.37 – 7.32 (m, 2H). **$^{13}$C-NMR** (125 MHz, DMSO-$d_6$): δ (ppm) = 143.8, 143.2, 137.7, 135.1, 134.6, 133.8, 129.6, 128.0, 123.9, 123.0, 120.1, 116.1, 110.6, 109.5. **MS-ESI**: m/z = 220.0900 (calc. for [M + $H^+$]: 220.0875).

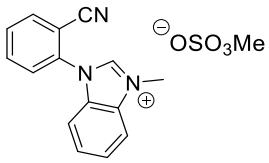


**Cyanophenyl-benzimidazolium methylsulfate 16**: *2*-(*1H*-Benzo[*d*]imidazol-*1*-yl)benzonitrile (**2**): (5.7 mmol, 1.24 g, 1 eq.) was dissolved in MeCN and dimethyl sulfate (6.8 mmol, 0.65 g, 1.2 eq.) was added. The mixture was stirred at 80 °C for 15 h. After cooling down, the product was precipitated by addition of EA. The white solid was filtered, washed with EA, and dried under vacuum yielding 1.84 g (94%) of benzimidazolium salt **3**.

**$^1$H-NMR** (500 MHz, DMSO-$d_6$): δ (ppm) = 10.27 (s, 1H), 8.32 (dd, J = 7.8, 1.2 Hz, 1H), 8.22 (dt, J = 8.4, 0.6 Hz, 1H), 8.16 – 8.11 (m, 1H), 8.06 (dd, J = 8.1, 0.9 Hz, 1H), 7.98 (td, J = 7.7, 1.2 Hz, 1H), 7.83 (ddd, J = 8.3, 6.7, 1.6 Hz, 1H), 7.80 – 7.73 (m, 2H), 4.26 (s, 3H). **$^{13}$C-NMR** (125 MHz, DMSO-$d_6$): δ

(ppm) = 143.9, 135.5, 134.9, 134.4, 131.9, 131.4, 131.1, 128.9, 127.7, 127.3, 115.1, 114.3, 113.5, 110.0, 34.0. **MS-ESI**: m/z = 234.1051 (calc. for [$M^+$]: 234.1031).

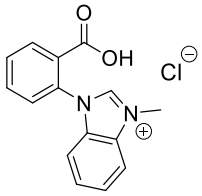

**Carboxyphenyl-benzimidazolium chloride 17**: Cyanophenyl-benzimidazolium methylsulfate **3** (3.0 mmol, 1.04 g, 1 eq.) was dissolved in a mixture of $H_2O$/AcOH/$H_2SO_4$ (2/4/4) and stirred at 120 °C for 15 h. After cooling down, the reaction mixture was poured into an aqueous $BaCl_2$ solution. The white precipitate ($BaSO_4$) was filtered off, washed with water, and the filtrate, that contains the product, evaporated. The solid residue was suspended in MeCN/$H_2O$ (1/1), and the suspension centrifuged. The clear liquid layer was decanted, evaporated, and the remaining glassy solid dried under vacuum yielding 0.78 g (90%) of the title compound.

**$^1$H-NMR** (500 MHz, DMSO-$d_6$): δ (ppm) = 10.32 (s, 1H), 8.29 – 8.21 (m, 1H), 8.16 (d, J = 8.3 Hz, 1H), 8.02 – 7.83 (m, 3H), 7.79 – 7.71 (m, 1H), 7.66 (t, J = 7.3 Hz, 1H), 7.47 (d, J = 8.2 Hz, 1H), 4.24 (s, 3H). **MS-ESI**: m/z = 253.0997 (calc. for [$M^+$]: 253.0977).

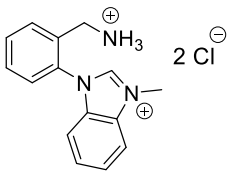

**Benzammonium-benzimidazolium chloride 18**: Cyanophenyl-benzimidazolium methylsulfate **3** (5.0 mmol, 1.72 g, 1 eq.) was suspended in MeOH and HCl (37.5 mmol, 1.37 g, 7.5 eq., equals 3.1 mL of a 37% aqueous solution) as well as Pd/C (0.25 mmol, 0.03 g, 0.05 eq.) were added. The mixture was rapidly stirred under a hydrogen atmosphere at room temperature for 24 h. The mixture was filtered through Celite, the filtrate concentrated, and the remaining solution diluted with MeOH. A white precipitate formed that was filtered off and discarded. The filtrate was evaporated and the remaining wax dried under vacuum yielding 1.70 g (97%) of a light-purple solid.

**$^1$H-NMR** (500 MHz, DMSO-$d_6$): δ (ppm) = 10.13 (s, 1H), 8.63 (s, 3H), 8.15 (d, J = 8.3Hz, 1H), 7.99 (d, J = 7.7Hz, 1H), 7.72 (m, 5H), 7.50 (d, J = 8.3Hz, 1H), 4.17 (s, 3H), 3.86 (d, J = 52.3Hz, 2H). **$^{13}$C-NMR** (125 MHz, DMSO-$d_6$): δ (ppm) = 144.4, 131.9, 131.6, 131.4, 131.31, 131.26, 131.0, 130.3, 128.3, 127.4, 126.8, 114.0, 113.1, 37.0, 33.6. **MS-ESI**: m/z = 238.1342 (calc. for [$M^+$]: 238.1344).

# 6 References


[1] K. Palczewski, *Annu Rev Biochem* **2006**, *75*, 743-767.

[2] a) H. Priya James, R. John, A. Alex, K. R. Anoop, *Acta Pharm Sin B* **2014**, *4*, 120-127; b) *Targeted Delivery of Small and Macromolecular Drugs*, CRC Press, **2010**; c) R. Langer, *Nature* **1998**, *392*, 5-10.

[3] a) J. Mayr, C. Saldias, D. Diaz Diaz, *Chem Soc Rev* **2018**, *47*, 1484-1515; b) F. Seidi, R. Jenjob, D. Crespy, *Chem Rev* **2018**, *118*, 3965-4036.

[4] J. Andréasson, U. Pischel, *Isr J Chem* **2013**, *53*, 236-246.

[5] a) A. Campanella, D. Dohler, W. H. Binder, *Macromol Rapid Commun* **2018**, *39*, e1700739; b) J. Dahlke, S. Zechel, M. D. Hager, U. S. Schubert, *Adv Mater Interfaces* **2018**, *5*; c) Y. Yang, M. W. Urban, *Adv Mater Interfaces* **2018**, *5*.

[6] a) L. Bromberg, *Adv Drug Deliv Rev* **1998**, *31*, 197-221; b) S. Chatterjee, P. Hui, C.-w. Kan, *Polymers* **2018**, *10*, 480; c) C. Zhou, M. A. Abdel-Rahman, W. Li, K. Liu, A. Zhang, *Chin Chem Lett* **2017**, *28*, 832-838.

[7] a) X. Guo, J. You, *J Pharm Investig* **2017**, *47*, 297-316; b) M. D. J. Quinn, T. Wang, M. Al Kobaisi, V. S. J. Craig, S. M. Notley, *Mater Chem Phys* **2018**, *205*, 154-163; c) G. Liu, W. Liu, C.-M. Dong, *Polym Chem* **2013**, *4*, 3431-3443.

[8] a) Y. Gao, G. P. Zago, Z. Jia, M. J. Serpe, *ACS Appl Mater Interfaces* **2013**, *5*, 9803-9808; b) C.-H. Whang, H. K. Lee, S. Kundu, S. N. Murthy, S. Jo, *J Appl Polymer Sci* **2018**, *135*, 46552; c) A. Kumar, C. Montemagno, H. J. Choi, *Sci Rep* **2017**, *7*, 3059.

[9] a) J. Ge, E. Neofytou, T. J. Cahill, 3rd, R. E. Beygui, R. N. Zare, *ACS Nano* **2012**, *6*, 227-233; b) D. Uppalapati, M. Sharma, Z. Aqrawe, F. Coutinho, I. D. Rupenthal, B. J. Boyd, J. Travas-Sejdic, D. Svirskis, *Int J Pharm* **2018**, *543*, 38-45.

[10] a) S. Kennedy, C. Roco, A. Deleris, P. Spoerri, C. Cezar, J. Weaver, H. Vandenburgh, D. Mooney, *Biomaterials* **2018**, *161*, 179-189; b) C. R. Thomas, D. P. Ferris, J. H. Lee, E. Choi, M. H. Cho, E. S. Kim, J. F. Stoddart, J. S. Shin, J. Cheon, J. I. Zink, *J Am Chem Soc* **2010**, *132*, 10623-10625.

[11] D. Bleger, Z. Yu, S. Hecht, *Chem Comm* **2011**, *47*, 12260-12266.

[12] a) H. M. Bandara, S. C. Burdette, *Chem Soc Rev* **2012**, *41*, 1809-1825; b) S. Helmy, F. A. Leibfarth, S. Oh, J. E. Poelma, C. J. Hawker, J. Read de Alaniz, *J Am Chem Soc* **2014**, *136*, 8169-8172; c) C. Y. Huang, A. Bonasera, L. Hristov, Y. Garmshausen, B. M. Schmidt, D.

Jacquemin, S. Hecht, *J Am Chem Soc* **2017**, *139*, 15205-15211; d) D. J. van Dijken, P. Kovaricek, S. P. Ihrig, S. Hecht, *J Am Chem Soc* **2015**, *137*, 14982-14991.

[13] H. Dürr, H. Bouas-Laurent, *Photochromism: Molecules and Systems*, Elsevier Inc., **2003**.

[14] M. Irie, *Chem Rev* **2000**, *100*, 1683-1684.

[15] a) S. Helmy, S. Oh, F. A. Leibfarth, C. J. Hawker, J. Read de Alaniz, *J Org Chem* **2014**, *79*, 11316-11329; b) J. R. Hemmer, S. O. Poelma, N. Treat, Z. A. Page, N. Dolinski, Y. J. Diaz, W. Tomlinson, K. D. Clark, J. P. Hooper, C. J. Hawker, J. Read de Alaniz, *J Am Chem Soc* **2016**; c) M. M. Lerch, S. J. Wezenberg, W. Szymanski, B. L. Feringa, *J Am Chem Soc* **2016**, *138*, 6344-6347.

[16] R. Klajn, *Chem Soc Rev* **2014**, *43*, 148-184.

[17] a) M. Irie, *Proc Jpn Acad B Phys Biol Sci* **2010**, *86*, 472-483; b) M. Irie, M. Mohri, *J Org Chem* **1988**, *53*, 803-808; c) K. Matsuda, M. Irie, *J Photochem Photobiol C Photochem Rev* **2004**, *5*, 169-182.

[18] a) M. Seibold, M. Handschuh, H. Port, H. C. Wolf, *J Lumin* **1997**, *72-74*, 454-456; b) F. Strübe, S. Rath, J. Mattay, *Eur J Org Chem* **2011**, *2011*, 4645-4653; c) B. Yao, Y. Wang, N. Menke, M. Lei, Y. Zheng, L. Ren, G. Chen, Y. Chen, M. Fan, *Mol Cryst Liq Cryst* **2005**, *430*, 211-219; d) Y. Yokoyama, *Chem Rev* **2000**, *100*, 1717-1740.

[19] a) H. Knoll, *ChemInform* **2004**, *35*; b) H. Rau, in *Photochromism: Molecules and Systems* (Eds.: H. Dürr, H. Bouas-Laurent), Elsevier **2003**.

[20] a) A. P. Demchenko, V. I. Tomin, P. T. Chou, *Chem Rev* **2017**, *117*, 13353-13381; b) A. Nenov, R. Borrego-Varillas, A. Oriana, L. Ganzer, F. Segatta, I. Conti, J. Segarra-Marti, J. Omachi, M. Dapor, S. Taioli, C. Manzoni, S. Mukamel, G. Cerullo, M. Garavelli, *J Phys Chem Lett* **2018**, *9*, 1534-1541.

[21] a) C. W. Chang, Y. C. Lu, T. T. Wang, E. W. Diau, *J Am Chem Soc* **2004**, *126*, 10109-10118; b) C. R. Crecca, A. E. Roitberg, *J Phys Chem A* **2006**, *110*, 8188-8203; c) T. Fujino, S. Y. Arzhantsev, T. Tahara, *J Phys Chem* **2001**, *105*, 8123-8129; d) M. Quick, A. L. Dobryakov, M. Gerecke, C. Richter, F. Berndt, I. N. Ioffe, A. A. Granovsky, R. Mahrwald, N. P. Ernsting, S. A. Kovalenko, *J Phys Chem B* **2014**, *118*, 8756-8771.

[22] a) P. Bortolus, S. Monti, *J Phys Chem* **1979**, *83*, 648-652; b) A. Cembran, F. Bernardi, M. Garavelli, L. Gagliardi, G. Orlandi, *J Am Chem Soc* **2004**, *126*, 3234-3243; c) A. Muzdalo, P. Saalfrank, J. Vreede, M. Santer, *J Chem Theory Comput* **2018**, *14*, 2042-2051; d) C. Rietze, E. Titov, S. Lindner, P. Saalfrank, *J Phys Condens Matter* **2017**, *29*, 314002.

[23] a) A. A. Beharry, O. Sadovski, G. A. Woolley, *J Am Chem Soc* **2011**, *133*, 19684-19687; b) S. Samanta, A. A. Beharry, O. Sadovski, T. M. McCormick, A. Babalhavaeji, V. Tropepe, G. A. Woolley, *J Am Chem Soc* **2013**, *135*, 9777-9784.

[24] a) D. Bleger, J. Schwarz, A. M. Brouwer, S. Hecht, *J Am Chem Soc* **2012**, *134*, 20597-20600; b) C. Knie, M. Utecht, F. Zhao, H. Kulla, S. Kovalenko, A. M. Brouwer, P. Saalfrank, S. Hecht, D. Bleger, *Chemistry* **2014**, *20*, 16492-16501.

[25] R. Siewertsen, H. Neumann, B. Buchheim-Stehn, R. Herges, C. Nather, F. Renth, F. Temps, *J Am Chem Soc* **2009**, *131*, 15594-15595.

[26] a) Y. Yang, R. P. Hughes, I. Aprahamian, *J Am Chem Soc* **2012**, *134*, 15221-15224; b) Y. Yang, R. P. Hughes, I. Aprahamian, *J Am Chem Soc* **2014**, *136*, 13190-13193.

[27] a) C. García-Iriepa, M. Marazzi, L. M. Frutos, D. Sampedro, *RSC Adv* **2013**, *3*; b) F. Hamon, F. Djedaini-Pilard, F. Barbot, C. Len, *Tetrahedron* **2009**, *65*, 10105-10123; c) E. Merino, *Chem Soc Rev* **2011**, *40*, 3835-3853.

[28] S. Okumura, C. H. Lin, Y. Takeda, S. Minakata, *J Org Chem* **2013**, *78*, 12090-12105.

[29] a) D. C. Barman, P. Saikia, D. Prajapati, J. S. Sandhu, *Synthetic Comm* **2009**, *32*, 3407-3412; b) J. M. Birchall, R. N. Haszeldine, J. E. G. Kemp, *J Chem Soc C* **1970**; c) N. A. Noureldin, *Synthesis* **1999**, *1999*, 939-942.

[30] C. Zhang, N. Jiao, *Angew Chem Int Ed Engl* **2010**, *49*, 6174-6177.

[31] a) S. Gowda, K. Abiraj, D. C. Gowda, *Tetrahedron Lett* **2002**, *43*, 1329-1331; b) M. G. Pamar, P. Govender, K. Muthusamy, R. W. M. Krause, H. M. Nanjundaswamy, *Orient J Chem* **2013**, *29*, 969-974.

[32] a) Y. K. Lim, K. S. Lee, C. G. Cho, *Org Lett* **2003**, *5*, 979-982; b) Z. Wang, R. T. Skerlj, G. J. Bridger, *Tetrahedron Lett* **1999**, *40*, 3543-3546; c) Z. Zhang, F.-F. Ma, Z.-Y. Peng, W.-F. Li, X.-M. Xie, *Synlett* **2011**, *2011*, 2555-2558.

[33] a) M. Banghart, K. Borges, E. Isacoff, D. Trauner, R. H. Kramer, *Nat Neurosci* **2004**, *7*, 1381-1386; b) M. Borowiak, W. Nahaboo, M. Reynders, K. Nekolla, P. Jalinot, J. Hasserodt, M. Rehberg, M. Delattre, S. Zahler, A. Vollmar, D. Trauner, O. Thorn-Seshold, *Cell* **2015**, *162*, 403-411; c) L. Guerrero, O. S. Smart, C. J. Weston, D. C. Burns, G. A. Woolley, R. K. Allemann, *Angew Chem Int Ed Engl* **2005**, *44*, 7778-7782; d) R. J. Mart, R. K. Allemann, *Chem Comm* **2016**, *52*, 12262-12277; e) S. Samanta, C. Qin, A. J. Lough, G. A. Woolley, *Angew Chem Int Ed Engl* **2012**, *51*, 6452-6455.

[34] W. A. Velema, W. Szymanski, B. L. Feringa, *J Am Chem Soc* **2014**, *136*, 2178-2191.

[35] a) S. Geng, Y. Wang, L. Wang, T. Kouyama, T. Gotoh, S. Wada, J. Y. Wang, *Sci Rep* **2017**, *7*, 39202; b) S. Wang, N. Zhang, X. Ge, Y. Wan, X. Li, L. Yan, Y. Xia, B. Song, *Soft Matter* **2014**,

*10*, 4833-4839; c) H.-Z. Yu, Y.-Q. Wang, J.-Z. Cheng, J.-W. Zhao, S.-M. Cai, H. Inokuchi, A. Fujishima, Z.-F. Liu, *Langmuir* **1996**, *12*, 2843-2848.

[36] a) B. Adhikari, Y. Yamada, M. Yamauchi, K. Wakita, X. Lin, K. Aratsu, T. Ohba, T. Karatsu, M. J. Hollamby, N. Shimizu, H. Takagi, R. Haruki, S. I. Adachi, S. Yagai, *Nat Commun* **2017**, *8*, 15254; b) D. Chen, H. Liu, T. Kobayashi, H. Yu, *J Mater Chem* **2010**, *20*; c) N. Hosono, M. Yoshikawa, H. Furukawa, K. Totani, K. Yamada, T. Watanabe, K. Horie, *Macromolecules* **2013**, *46*, 1017-1026; d) X. Mei, S. Yang, D. Chen, N. Li, H. Li, Q. Xu, J. Ge, J. Lu, *Chem Comm* **2012**, *48*, 10010-10012; e) X. Wang, Y. Yang, Y. Liao, Z. Yang, M. Jiang, X. Xie, *Eur Polymer J* **2012**, *48*, 41-48; f) P. Weis, W. Tian, S. Wu, *Chemistry* **2018**, *24*, 6494-6505.

[37] S. Schimka, S. Santer, N. M. Mujkic-Ninnemann, D. Bleger, L. Hartmann, M. Wehle, R. Lipowsky, M. Santer, *Biomacromolecules* **2016**, *17*, 1959-1968.

[38] K. Kumar, C. Knie, D. Bleger, M. A. Peletier, H. Friedrich, S. Hecht, D. J. Broer, M. G. Debije, A. P. Schenning, *Nat Commun* **2016**, *7*, 11975.

[39] S.-K. Oh, M. Nakagawa, K. Ichimura, *J Mater Chem* **2002**, *12*, 2262-2269.

[40] J. A. Delaire, K. Nakatani, *Chem Rev* **2000**, *100*, 1817-1846.

[41] a) T. T. Nguyen, D. Turp, D. Wang, B. Nolscher, F. Laquai, K. Mullen, *J Am Chem Soc* **2011**, *133*, 11194-11204; b) S. Patnaik, A. K. Sharma, B. S. Garg, R. P. Gandhi, K. C. Gupta, *Int J Pharm* **2007**, *342*, 184-193.

[42] a) H. Chen, X. Ma, S. Wu, H. Tian, *Angew Chem Int Ed Engl* **2014**, *53*, 14149-14152; b) Y. Kawata, T. Yamamoto, H. Kihara, K. Ohno, *ACS Appl Mater Interfaces* **2015**, *7*, 4185-4191; c) M. Moniruzzaman, P. Christogianni, G. Kister, *Procedia Eng* **2016**, *148*, 114-121.

[43] W. Schärtl, *Light Scattering from Polymer Solutions and Nanoparticle Dispersions*, Springer-Verlag Berlin Heidelberg, **2007**.

[44] S. Iamsaard, S. J. Asshoff, B. Matt, T. Kudernac, J. J. Cornelissen, S. P. Fletcher, N. Katsonis, *Nat Chem* **2014**, *6*, 229-235.

[45] J. Chen, F. K. Leung, M. C. A. Stuart, T. Kajitani, T. Fukushima, E. van der Giessen, B. L. Feringa, *Nat Chem* **2018**, *10*, 132-138.

[46] L. X. Liao, F. Stellacci, D. V. McGrath, *J Am Chem Soc* **2004**, *126*, 2181-2185.

[47] a) D. M. Junge, D. V. McGrath, *Chem Comm* **1997**, 857-858; b) D. M. Junge, D. V. McGrath, *J Am Chem Soc* **1999**, *121*, 4912-4913; c) S. Li, D. V. McGrath, *J Am Chem Soc* **2000**, *122*, 6795-6796.

[48] M. Jin, R. Lu, C. Bao, T. Xu, Y. Zhao, *Polymer* **2004**, *45*, 1125-1131.

[49] F. Cisnetti, R. Ballardini, A. Credi, M. T. Gandolfi, S. Masiero, F. Negri, S. Pieraccini, G. P. Spada, *Chemistry* **2004**, *10*, 2011-2021.

[50] D. Bleger, J. Dokic, M. V. Peters, L. Grubert, P. Saalfrank, S. Hecht, *J Phys Chem B* **2011**, *115*, 9930-9940.

[51] D. Bleger, T. Liebig, R. Thiermann, M. Maskos, J. P. Rabe, S. Hecht, *Angew Chem Int Ed Engl* **2011**, *50*, 12559-12563.

[52] S. Wiktorowicz, V. Aseyev, H. Tenhu, *Polym Chem* **2012**, *3*.

[53] N. Sakai, K. Fujii, S. Nabeshima, R. Ikeda, T. Konakahara, *Chem Comm* **2010**, *46*, 3173-3175.

[54] A. Bergmann, D. Orthaber, G. Scherf, O. Glatter, *Journal of Applied Crystallography* **2000**, *33*, 869-875.

[55] I. Bressler, J. Kohlbrecher, A. F. Thunemann, *J Appl Crystallogr* **2015**, *48*, 1587-1598.

[56] a) O. Glatter, O. Kratky, *Small angle x-ray scattering*, Academic Press: London, **1982**; b) G. Porod, *Z. Naturforsch., A* **1949**, *4*, 401-414.

[57] a) J. A. Beto, *Clin Nutr Res* **2015**, *4*, 1-8; b) W. B. Farquhar, D. G. Edwards, C. T. Jurkovitz, W. S. Weintraub, *J Am Coll Cardiol* **2015**, *65*, 1042-1050; c) M. R. Picciotto, M. J. Higley, Y. S. Mineur, *Neuron* **2012**, *76*, 116-129; d) C. M. Weaver, *Adv Nutr* **2013**, *4*, 368S-377S.

[58] M. Bonora, S. Patergnani, A. Rimessi, E. De Marchi, J. M. Suski, A. Bononi, C. Giorgi, S. Marchi, S. Missiroli, F. Poletti, M. R. Wieckowski, P. Pinton, *Purinergic Signalling* **2012**, *8*, 343-357.

[59] M. P. Johnson, *Essays Biochem* **2016**, *60*, 255-273.

[60] R. Liu, H. Ochman, *Proc Natl Acad Sci Unit States Am* **2007**, *104*, 7116-7121.

[61] a) X. Liu, H. Li, Q. Jin, J. Ji, *Small* **2014**, *10*, 4230-4242; b) L. Mi, S. Jiang, *Angew Chem Int Ed Engl* **2014**, *53*, 1746-1754; c) T. Wei, Z. Tang, Q. Yu, H. Chen, *ACS Appl Mater Interfaces* **2017**, *9*, 37511-37523; d) Z. K. Zander, M. L. Becker, *ACS Macro Lett* **2017**, *7*, 16-25.

[62] a) F. Schaufelberger, B. J. J. Timmer, O. Ramström, in *Dynamic Covalent Chemistry* (Eds.: W. Zhang, Y. Jin), Wiley, **2017**, pp. 1-30; b) D. Komáromy, P. Nowak, S. Otto, in *Dynamic Covalent Chemistry* (Eds.: W. Zhang, Y. Jin), Wiley, **2017**, pp. 31-119.

[63] T. Liu, Y. Wang, X. Luo, J. Li, S. A. Reed, H. Xiao, T. S. Young, P. G. Schultz, *Proc Natl Acad Sci Unit States Am* **2016**, *113*, 5910-5915.

[64] L. R. Tuck, K. Altenbach, T. F. Ang, A. D. Crawshaw, D. J. Campopiano, D. J. Clarke, J. Marles-Wright, *Sci Rep* **2016**, *6*, 22108.

[65] P. T. Corbett, J. Leclaire, L. Vial, K. R. West, J. L. Wietor, J. K. Sanders, S. Otto, *Chem Rev* **2006**, *106*, 3652-3711.

[66] P. J. Boul, P. Reutenauer, J. M. Lehn, *Org Lett* **2005**, *7*, 15-18.

[67] R. C. Brachvogel, F. Hampel, M. von Delius, *Nat Commun* **2015**, *6*, 7129.

[68] V. T. Bhat, A. M. Caniard, T. Luksch, R. Brenk, D. J. Campopiano, M. F. Greaney, *Nat Chem* **2010**, *2*, 490-497.

[69] P. Kovaricek, J. M. Lehn, *Chemistry* **2015**, *21*, 9380-9384.

[70] M. Demetriades, I. K. Leung, R. Chowdhury, M. C. Chan, M. A. McDonough, K. K. Yeoh, Y. M. Tian, T. D. Claridge, P. J. Ratcliffe, E. C. Woon, C. J. Schofield, *Angew Chem Int Ed Engl* **2012**, *51*, 6672-6675.

[71] J. F. Teichert, D. Mazunin, J. W. Bode, *J Am Chem Soc* **2013**, *135*, 11314-11321.

[72] The pka numbers are taken from the ChemIDplus database of the US National Library of Medicine.

[73] a) S. Kato, Y. Kawahara, H. Kageyama, R. Yamada, O. Niyomura, T. Murai, T. Kanda, *J Am Chem Soc* **1996**, *118*, 1262-1267; b) D. Delaere, G. Raspoet, M. T. Nguyen, *J Phys Chem A* **1999**, *103*, 171-177; c) O. Niyomura, S. Kato, in *Chalcogenocarboxylic Acid Derivatives* (Ed.: S. Kato), Springer-Verlag Berlin Heidelberg, **2005**; d) S. Kato, O. Niyomura, M. Ebihara, J.-D. Guo, S. Nagase, *Bull Chem Soc Jpn* **2016**, *89*, 361-368.

[74] W. Yao, M. Liao, X. Zhang, H. Xu, J. Wang, *Eur J Org Chem* **2003**, 1784-1788.

[75] a) D. Avcı, S. Bahçeli, Ö. Tamer, Y. Atalay, *Can J Chem* **2015**, *93*, 1147-1156; b) T. M. Henderson, A. F. Izmaylov, G. Scalmani, G. E. Scuseria, *J Chem Phys* **2009**, *131*, 044108; c) J. Heyd, G. E. Scuseria, *J Chem Phys* **2004**, *120*, 7274-7280; d) A. F. Izmaylov, G. E. Scuseria, M. J. Frisch, *J Chem Phys* **2006**, *125*, 104103; e) A. V. Krukau, O. A. Vydrov, A. F. Izmaylov, G. E. Scuseria, *J Chem Phys* **2006**, *125*, 224106.

[76] pka values in DMSO were taken from the Bordwell pka table; corresponding review: F. G. Bordwel,l Acc. Chem. Res. 1988, 21, 456, 463.

# 7 Abbreviations

| | |
|---|---|
| AcOH | Acetic acid |
| $Af_n$ | Normalized amplification factor |
| ATP | Adenosine triphosphate |
| Boc | *tert*-Butyloxycarbonyl |
| CMC | Critical micelle concentration |
| cryo TEM | Cryogenic transmission electron microscopy |
| Đ | Number of repeating units |
| DASA | Donor-acceptor Stenhouse adduct |
| DBPO | Dibenzoyl peroxide |
| DCC | Dynamic covalent chemistry |
| DFT | Density functional theory |
| DLS | Dynamic light scattering |
| DMAc | *N*,*N*-Dimethylacetamide |
| DMF | *N*,*N*-Dimethylformamide |
| DMSO | Dimethylsulfoxide |
| DNA | Deoxyribonucleic acid |
| dppf | *1,1'*-Bis(diphenylphosphino)ferrocene |
| Et | Ethyl |
| EtOAc | Ethayl acetate |
| EtOH | Ethanol |
| GPC | Gel permeation chromatography |
| HCOOH | Formic acid |
| HOMO | Highest occupied molecular orbital |
| K | Equilibrium constant |
| Me | Methyl |
| MeCN | Acetonitrile |
| MeOH | Methanol |
| $M_n$ | Number-average molecular weight |
| $M_w$ | Weight-averagy molecular weight |
| NBS | *N*-Bromosuccinimide |
| $^n$Bu | *n*-Butyl |
| NMR | Nuclear magnetic resonance |

| | |
|---|---|
| o/n | Overnight |
| PDI | Polydispersity index |
| PS | Polystyrene |
| PSS | Photostationary State |
| *p*TSA | *para*-Toluenesulfonic acid |
| Red-Al | Sodium bis(*2*-methoxyethoxy)aluminium hydride |
| RNA | Ribonucleic acid |
| RT | Room temperature |
| SAXS | Small-angle X-ray scattering |
| SLS | Static light scattering |
| SPhos | *2*-Dicyclohexylphosphino-*2'*,*6'*-dimethoxybiphenyl |
| $^{t}$Bu | *tert*-Butyl |
| THF | Tetrahydrofuran |
| THP | Tetrahydropyranyl |
| TOF | Time of flight |
| TsOTg | 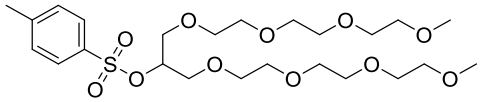 |
| UPLC | Ultra-high performance liquid chromatography |
| $V_h$ | Hydrodynamic volume |
| ΔH | Standard enthalpy |

**<u>For Light Scattering</u>**

| | |
|---|---|
| $A_2$ | Second virial coefficient |
| D | Diffusion coeffcient |
| $g_1$ | Amplitude correlation function |
| $g_2$ | Intensity correlation function |
| I | Scattering intensity |
| K | Contrast factor |
| $n_D$, $n_a$, $n_s$ | Refractive index |
| P(a) | Structure factor |
| q | Scattering vector |
| R | Rayleigh ratio |
| $R_g$ | Radius of gyration |
| $R_h$ | Hydrodynamic radius |

| | |
|---|---|
| Si | Sine integral function |
| η | Viscosity |
| θ | Scattering angle |
| $\kappa_1$, $\kappa_2$, … | First, second, … cumulant |
| λ | Wavelength |
| ρ-ratio | $R_g/R_h$ |
| T | Correlation time |

**For NMR**

| | |
|---|---|
| br | Broad |
| d | Doublet |
| dd | Doublet of doublets |
| ddd | Doublet of doublet of doublets |
| m | Multiplet |
| s | Singlet |
| t | Triplet |

Selbstständigkeitserklärung

Hiermit versichere ich, dass ich die vorliegende Arbeit selbstständig und nur unter Verwendung der angegebenen Literatur und Hilfsmittel angefertigt habe.

Berlin, 20.12.2018

Christopher Knie